Cyclodextrin-Based Rotaxanes for Material Science Applications

A thesis submitted for admission to the degree of

Doctor of Philosophy

By

Hwi Young Lee

Australian National University

Research School of Chemistry
Canberra, Australia

April, 2014

Author's Statement

This is to declare that the work in this thesis represents original work that I have undertaken during my PhD degree at the Research School of Chemistry, the Australian National University from 2010 to 2014, except the synthesis and X-ray crystal analysis of the compounds **4.1** and **4.2**, and the synthesis of compounds **4.4** and **4.5**, which was carried out as part of my PhB Honours degree.

To my best of knowledge, the thesis does not contain material that has been published or written by another person or accepted for the award of any other degree of diploma in any other university or tertiary institution, unless due reference has been made in the text.

I give consent to this copy of my thesis, when deposited in the University library, being available for loan or photocopying.

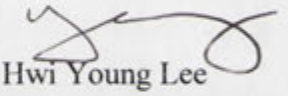

Hwi Young Lee

April 2014

Acknowledgements

I would like to express my most sincere gratitude to my supervisor, Prof. Christopher J. Easton. This work would not have been possible without his guidance, patience and understanding. I appreciate the time and energy you put into students' academic excellence and personal welfare. I am also grateful that you have never stopped providing me with challenges and inspiration.

I am extremely grateful to Dr Hideki Onagi for introducing me to cyclodextrin chemistry. I appreciate your willingness to sacrifice your lunch breaks, late evenings and even weekends to share your expertise.

I am fortunate to have gone through this journey with two very talented chemists, Shenglin and Kaheng. I feel that we make a great team and have learnt from each other throughout our PhDs. Your thoughts and suggestions are greatly appreciated and I have enjoyed attending conferences and traveling with you.

I wish to thank Roger for getting me interested in cyclodextrin chemistry and Daniel for his technical support and friendship. I also wish to thank the past and present members of the Easton group, especially Ryan, Suba, Karen, Allan, Nicole, Hye-Kyung, Amy, Melissa, Dan, Alex, Zac, Karine, Mantas, Sue and Carol. Many thanks to Hideki, Ryan, Kaheng, Jeff, Jim, Melissa and Shenglin for being great office mates.

I would like to acknowledge Dr Chris Blake for training and assistance with NMR spectroscopy, Dr Anthony C. Willis and Dr Rowan Young for collecting X-ray crystal data, Prof. Peter J. Steel for solving the crystal structures, Dr Frank Brink and Dr Hua Chen for training and assistance with SEM and Prof. Steven E. Bottle for valuable discussions.

Special thanks to my friends Lisa, Gordon, Ben, Stef, Sangeeta and Vivek for making Canberra my second home. Your friendship means the world to me.

Finally, I wish to thank my family for their unconditional love and support.

Presentations

LEE, H-Y.; Onagi, H.; Maniam, S.; Cieslinski, M. M.; Steel, P. J.; Lincoln, S. F.; Easton, C. J. 'Crystal Engineering with Cyclodextrin Based Rotaxanes for Material Science Applications.'

- Poster presentation. *16th International Cyclodextrin Symposium (ICS16).* May **2012**. Tianjin, China.
- Oral presentation. *Gordon Research Conference on Physical Organic Chemistry (GRC)*. June **2011**. New Hampshire, America.
- Poster presentation. *Gordon Research Conference on Physical Organic Chemistry (GRC)*. June **2011**. New Hampshire, America.
- Poster presentation. *6th International Symposium on Macrocyclic and Supramolecular Chemistry (ISMSC)*. July **2011**. Brighton, England.
- Oral presentation. *6th Asian Cyclodextrin Conference (ACC2011).* Aug **2011**. Canberra, Australia.

LEE, H-Y.; Maniam, S.; Fairfull-Smith, K. E.; Bottle, S. E.; Easton, C. J. 'Photostable Stilbenylnitroxide Rotaxanes'

- Poster presentation. *Free Radical Carnival.* Nov **2011**. Wollongong, Australia.
- Poster presentation. *Free Radical Carnival.* Oct **2011**. Sydney, Australia.

LEE, H-Y.; Onagi, H.; Maniam, S.; Norén, L.; Sterns, M.; Willis, T.; Steel, P. J.; Lincoln, S. F.; Easton, C. J. 'Cyclodextrin Based Rotaxane Crystals, Amorphous Solids and Lyotropic Liquid Crystals in Aqueous Solution'

- Poster presentation. *15th International Cyclodextrin Symposium (ICS15).* May **2010**. Vienna, Austria.

Abstract

In the work described in this thesis, CD-based rotaxanes were prepared and their solid-state structures/packing, morphology and crystal growth behaviour were explored. Encapsulation of profluorescent nitroxides through rotaxane formation demonstrated the use of CD-based rotaxanes to change the reactivity of CD guests and therefore preserve their properties.

In Chapter 2, the rotaxane **1.17** having a stilbene-based axle and 3,5-dimethylaniline blocking groups, as well as the rotaxane **1.18** having an azobenzene-based axle and 2,6-dimethylaniline blocking groups were prepared to complete the set of rotaxanes **1.9**, **1.10**, **1.17** and **1.18** with 2,6-dimethylaniline and 3,5-dimethylaniline blocking groups, with azobenzene- and stilbene-based axles.

Chapter 3 describes the solid-state structures/packing, morphology and crystal growth of the set of rotaxanes **1.9**, **1.10**, **1.17** and **1.18**. Observation of crystal morphology using SEM and microscope images, suggests not only that crystal shape and size can be controlled depending on the choice of blocking groups and varying the conditions of crystal growth, but also that crystal packing is reflected in the crystal growth and the final shape of the crystals. Thus, crystal engineering can be bottomed-up to make nano-molecular architecture to micrometre scale or beyond.

In Chapter 4, the unsymmetrically capped rotaxanes **4.1** and **4.2** were purposely designed and prepared using a crystal engineering approach such that they can be used to regulate the crystal growth of the self-assembling rotaxane **1.9** through co-crystallisation. 2D NMR spectroscopy was used to determine the orientation of the CDs with respect to the dumbbells and assign the structures of the rotaxane isomers **4.1** and **4.2**. Co-crystallisation experiments showed that the rotaxanes **4.1** and **4.2** act as crystal growth inhibitors of the rotaxane **1.9**. In addition, a method to prepare supersaturated solutions from a mixture of amorphous and crystalline rotaxane was developed for crystal growth studies.

The unsymmetrically capped rotaxane **5.5** with 3,5-dimethylaniline and trinitrophenyl blocking groups on either end that can form π–π interactions was prepared in Chapter

5. Co-crystallisation experiments with the rotaxanes **1.9** and **5.5** illustrate that blocking groups of rotaxanes can be used as synthons to guide intermolecular self-assembly to regulate the formation of fibrous structures. Therefore crystal engineering using CD-based rotaxanes is a versatile approach towards regulating self-assembly and understanding molecular level interactions in the solid-state. These interactions may be used to fine-tune physical, chemical, photochemical or electrical properties of the end product that is fabricated through a bottom-up approach.

New paramagnetic profluorescent nitroxides, the rotaxanes **1.33**, **1.35** and **1.36**, as well as the previously reported rotaxane **1.34** were prepared and their photoisomerisation and decomposition behaviour in comparison to the corresponding dumbbells **1.37** and **1.38** were examined in Chapters 6 and 7. UV/visible spectroscopy and HPLC analysis illustrated that the profluorescent probes of the dumbbells **1.37** and **1.38** were preserved through formation of the CD-rotaxanes **1.33**, **1.34**, **1.35** and **1.36** making them advantageous for fluorescence detection.

Glossary

Å	angstrom
Abs.	absorbance
ACN	acetonitrile
AU	arbitary units
Azo	azobenzene
BOP	benzotiazol-1-yloxy-tris(dimethylamino)phosphonium hexafluorophosphate (Castro's reagent)
Br	broad
°C	degrees Celcius
CD	cyclodextrin
$CDCl_3$	deuterated chloroform
CD_2Cl_2	deuterated dichloromethane
CD_3OD	deuterated methanol
CD-CX-H	cyclodextrin protons, X=1-6
cm	centimetre
DCM	dichloromethane
dec.	decomposition
DMF	*N,N'*-dimethylformamide
DMSO	dimethylsulfoxide
DMT-MM	4-(4,6-dimethoxy-1,3,5-triazin-2-yl)-4-methylmorpholinium chloride
DQF-COSY	double quantum filter correlation spectroscopy
EI	electron impact
EPR	electron paramagnetic resonance
equiv.	equivalence
ESI	electrospray ionisation
et al.	*et alia*
Et_2O	diethyl either
EtOAc	ethyl acetate
g	gram
h	hour(s)
HPLC	high performance liquid chromatography

HR	high resolution
Hz	hertz
J	coupling constant (Hz)
lit.	literature
LR	low resolution
M	moles per litre
$M^{+\cdot}$	molecular ion
MALDI	matrix assisted laser desorption ionisation
Me	methyl
MeOH	methanol
min	minute(s)
mm	milimetre
m/z	mass-to-charge ratio
nm	nanometre
NMR	nuclear magnetic resonance
NOE	nuclear Overhauser effect
ppm	parts per million
R_f	retention factor
ROESY	rotating-frame Overhauser effect spectroscopy
SEM	scanning electron microscope
STM	scanning tunneling microscope
TEA	triethylamine
TEM	transmission electron microscope
TFA	trifluoroacetic acid
THF	tetrahydrofuran
TLC	thin layer chromatography
TOF	time of flight
t_R	retention time
t-BuOH	tertiary butanol
UV	ultraviolet
v	volume
δ	chemical shift (ppm)
λ_{max}	wavelength absorption maximum

CONTENTS

CHAPTER 8 – Experimental

CHAPTER 1 - Introduction

1.1 Supramolecular Chemistry

The capability to generate very small structures is important in modern science and technology. The physical approach to miniaturisation has limitations that can be overcome by a synthetic chemical approach, known as the 'bottom-up' approach,[1] to construct from a molecular-level.[2,3] This approach involves engineering molecular components that are able to assemble into a supramolecular structure capable of performing a specific function. This falls into the discipline of supramolecular chemistry, defined as 'chemistry beyond the molecule'. It concerns two or more chemical species held together by intermolecular forces such as electrostatic interactions, hydrogen bonding and van der Waals forces.[4] These types of non-covalent interactions are important in understanding natural biological systems such as DNA, where two strands of nucleotides are held together *via* hydrogen bonding.[5] Furthermore, molecular machines and devices have been designed to mimic natural systems or perform specific functions such as rotational movement,[6,7] shuttling,[8,9] switching,[10,11] and entrapment.[12,13]

1.2 Cyclodextrins

Cyclodextrins (CDs) are widely used as building blocks for supramolecular chemistry. They are 1,4-α-linked cyclic oligomers of six or more D-glucopyranose subunits in a toroidal structure (**Figure 1.1**).[14] The most widely occurring CDs have six to eight glucopyranose subunits.[15] α-CD **1.1** is the smallest CD with six glucopyranose subunits, while β-CD **1.2** and γ-CD **1.3** consist of seven and eight subunits respectively. The primary hydroxyl groups of the CD are located on the narrower end of the cavity, while secondary hydroxyl groups are on the wider end of the CD cavity. This feature provides CDs with a hydrophilic exterior, which accounts for their aqueous solubility.[16] The inside of the CD cavity on the other hand, is hydrophobic due to CD-C3 and C5 hydrogens and the ether-like oxygens.[16] Hence the formation of CD inclusion complexes with hydrophobic guests is favoured in aqueous media through the displacement of water molecules from the hydrophobic CD cavity.[14,17]

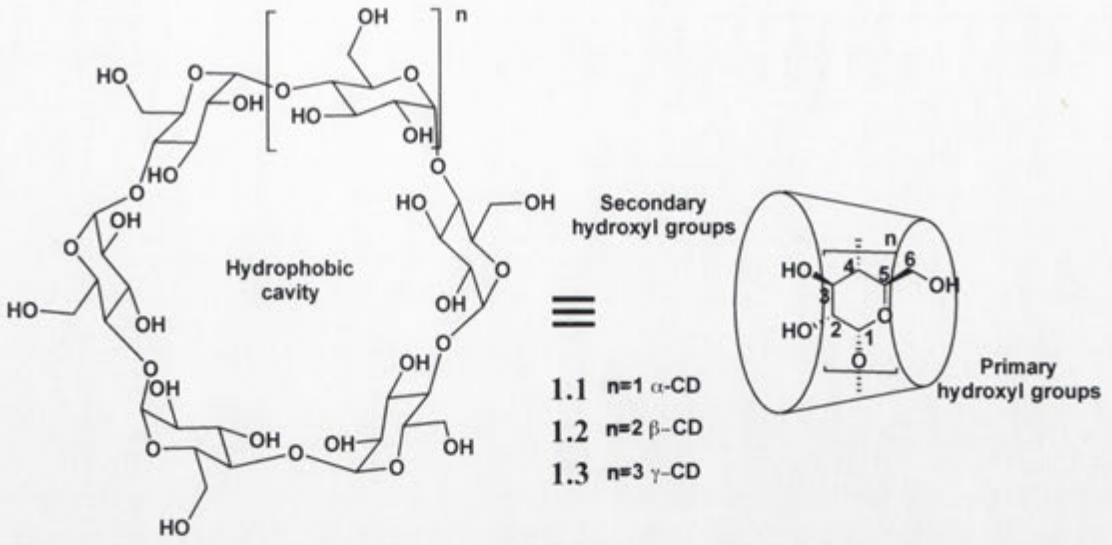

Figure 1.1. Structure of α-CD **1.1**, β-CD **1.2** and γ-CD **1.3** (left) and a schematic representation as a truncated cone (right). The narrower end of the cone is lined by the CD-C6 primary hydroxyl groups while the wider end of the cone is lined by the CD-C2 and C3 secondary hydroxyl groups.

The ability of CDs to form inclusion complexes with hydrophobic guests, and therefore increase the solubility of molecules that are otherwise poorly soluble in water, is widely utilised in areas including the pharmaceutical, food, cosmetics, toiletries, chemical and biotechnological industries.[17,18] CDs are also used in analytical chemistry[17] to separate chiral and other molecules, and as catalysts[15,19] and molecular reactors[20] in chemical reactions. CDs can be chemically modified to improve their solubility and complexation behaviour, or to introduce groups with specific functions.[21,22] Modified CDs are most frequently prepared through functionalisation at their primary or secondary hydroxyl groups.[22] Supramolecular structures are derived from non-covalent interactions of CDs with guest molecules.[22]

1.3 Rotaxanes

Rotaxanes are supramolecular species comprising macrocycles surrounding axles that are bonded to bulky blocking groups so as to prevent the macrocycles and axles from dissociating (**Figure 1.2**).[23,24] Unlike typical molecular structures, rotaxanes consist of two or more distinct molecules which are not joined by covalent bonds. These molecules are mechanically interlocked, and the supramolecular species have chemical and physical properties that are different from their non-interlocked components. Furthermore, the interlocked structures cannot dissociate without cleavage of one or more covalent bonds.

Figure 1.2. A schematic representation of a molecular axle, macrocycle and blocking groups forming a rotaxane.

CDs are ideal for use as macrocycles in rotaxane synthesis since, in aqueous solution, they spontaneously form host-guest complexes with hydrophobic species that can then be the axles.[14,25] Accordingly, CD host-guest complexes are being used to produce rotaxanes and related supramolecular species that can potentially form working molecular sensors and machines, and microelectronic devices.[26-29]

1.4 Cyclodextrin Based Rotaxanes

The first crystal packing of a CD-based rotaxane, the stilbene **1.4**, was reported by Onagi *et al.*[30] X-Ray crystallographic analysis of the rotaxane **1.4** showed molecular strands aligned along a single axis through π–π stacking of the blocking groups that were twisted out of the plane of the axle and insulated by the CDs (**Figure 1.3**). The dumbbell of the rotaxane **1.4**, lacking the CD macrocycle, formed a complex network of molecules aligned along multiple axes and showing diverse intermolecular interactions.

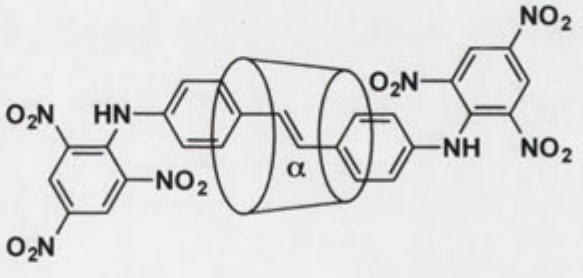

1.4

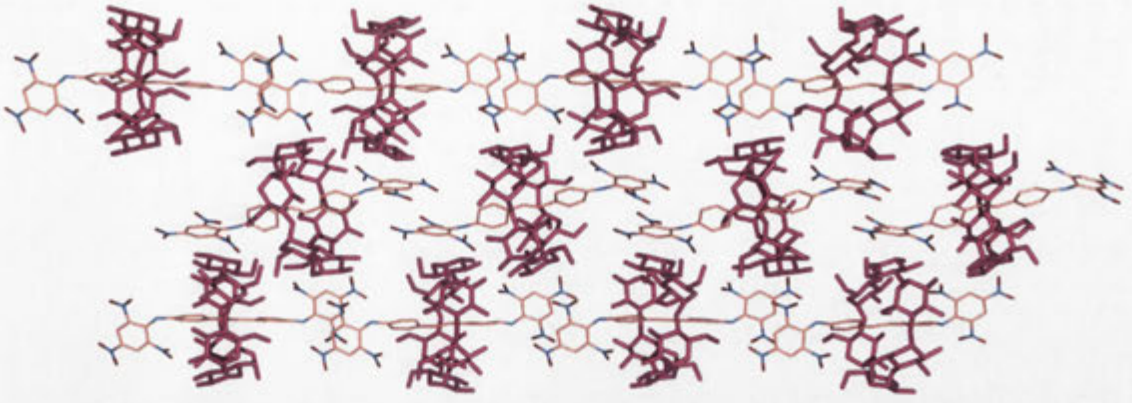

Figure 1.3. Crystal packing of the rotaxane **1.4** showing insulated strands along a single axis.[30]

The crystal structure of a CD-based rotaxane, the tetraacid **1.5**, had been reported earlier by Stanier *et al.*,[31] but it was only later that Terao *et al.*,[32] analysed the crystal packing of this material to find that it also displayed insulated molecular wires with π–π stacking[33-35] of the isophthalic acid blocking groups, with those being co-planar with the stilbene moiety (**Figure 1.4**). In this case, the CDs are aligned head-to-tail in one direction interspersed by others at right angles, notably different from the crystal packing of the rotaxane **1.4**, where the CDs are aligned faithfully along a single axis, but the lack of co-planarity of the blocking groups with the axle with the rotaxane **1.4** prevents extended π-electron delocalisation through π-stacking to produce an insulated molecular wire.

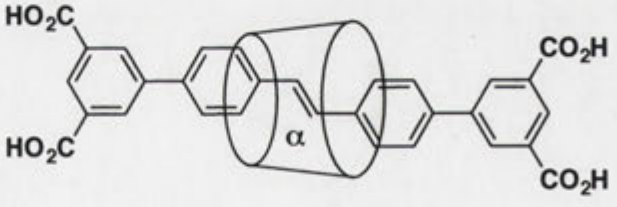

1.5

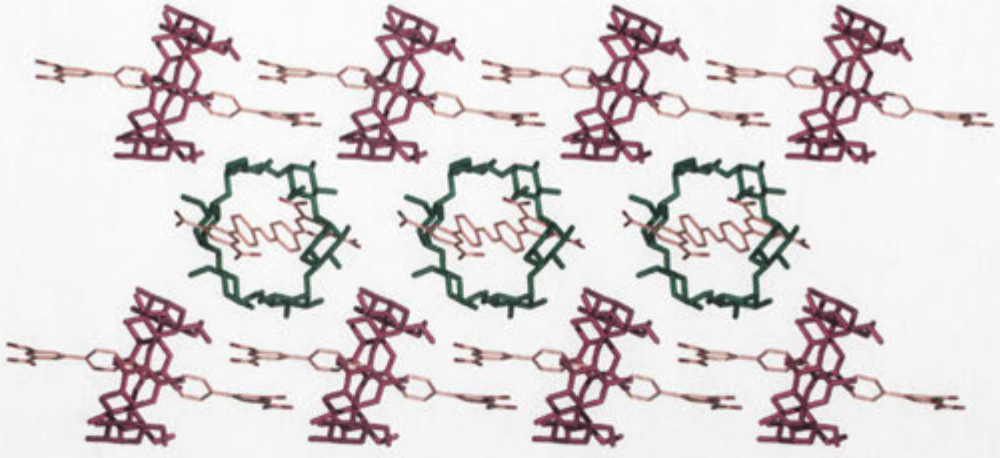

Figure 1.4. Crystal packing of the rotaxane **1.5**.[32]

When oriented along a single axis, CDs can align in head-to-head, tail-to-tail and head-to-tail fashions. Head-to-head and tail-to-tail alignment leads to centrosymmetric packing while head-to-tail packing can lead to either centrosymmetric or non-centrosymmetric packing depending on the rows of CDs all facing the same direction (non-centrosymmetric packing) or different directions (centrosymmetric packing) (**Figure 1.5**).[36] The latter results in non-polar crystals, while non-centrosymmetric packing leads to the formation of polar crystals, due to the dipole of the CDs.[14] Polar crystals can form as a result of other interactions overcoming the energetically unfavourable dipolar interactions of unidirectionally aligned CDs.

(a)

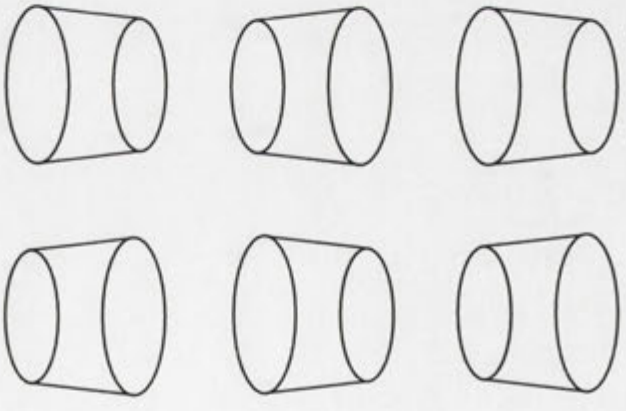

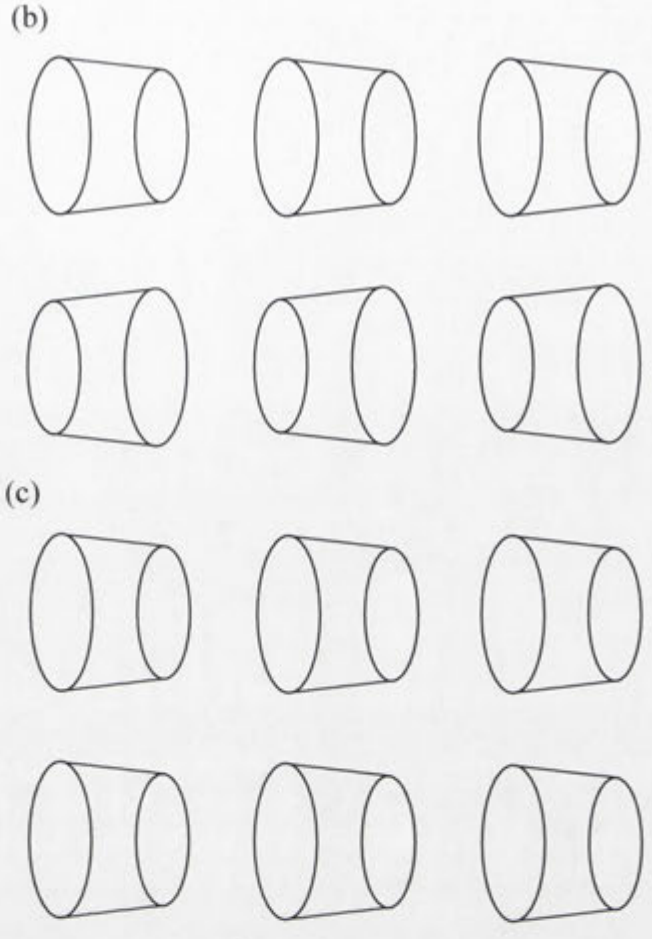

Figure 1.5. Schematic representations of CD alignments showing (a) head-to-head and tail-to-tail centrosymmetric, (b) head-to-tail centrosymmetric and (c) head-to-tail non-centrosymmetric packing.

CD-based rotaxanes inherit the dipole of the CDs.[14] Thus unidirectionally aligned dipoles of rotaxanes form non-centrosymmetric crystals.[36] The crystal packing of the series of rotaxanes **1.6-1.8**, analogous to the rotaxane **1.4**, modified with substituents at the 3- and 3'-positions of the stilbene moiety were reported by Onagi *et al.*,[30] and Cieslinski *et al.*[37] The crystal structures showed the substituents provide slight changes in the conformations of the dumbbells, which are sufficient to change the directionality of the CDs in the crystal packing.[30,37] Each of the rotaxanes **1.4** and **1.6-1.8** showed the CDs aligned along a single axis. The rotaxane **1.4** (**Figure 1.3**) and the difluoride **1.7** (**Figure 1.6** (b)) showed head-to-head and tail-to-tail alignment of the CDs, forming centrosymmetric, non-polar crystals. The dimethoxystilbene **1.6** showed head-to-tail alignment of the CDs, where alternating rows have the CDs facing opposite directions, also forming centrosymmetric, non-polar crystals (**Figure 1.6** (a)). On the other hand, the dichloride **1.8** showed rows of CDs all aligned head-

to-tail in the same direction to give a non-centrosymmetric, polar crystal (**Figure 1.6** (c)).

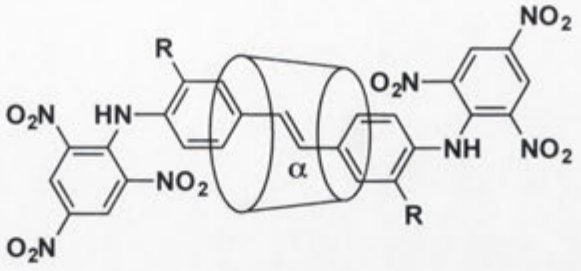

1.6 R = OMe
1.7 R = F
1.8 R = Cl

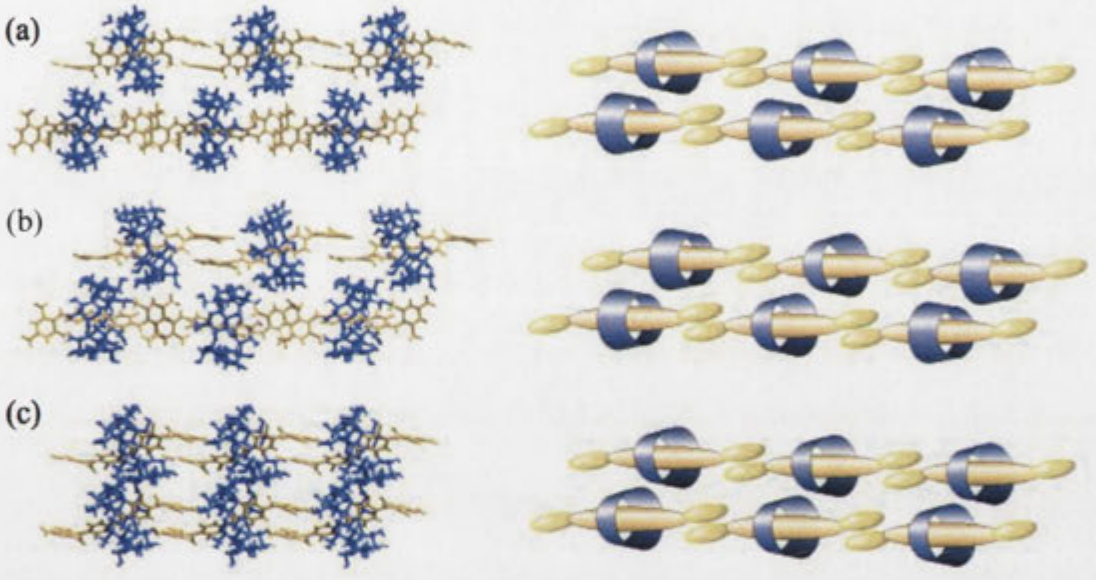

Figure 1.6. Crystal packing (left) and schematic representation of the alignment of the CDs (right) of two adjacent molecular fibres in (a) the dimethoxystilbene **1.6**, (b) the difluoride **1.7** and (c) the dichloride **1.8**.[37] Reproduced with permission from Taylor & Francis.

Recently, Maniam *et al.*,[38] reported the synthesis of the rotaxane **1.9**, where α-CD, an azobenzenedicarboxylic acid and 3,5-dimethylaniline were assembled through amide bond formation. X-Ray crystallographic analysis showed that in the solid-state the axles form linearly aligned molecular fibres along a single axis, with π–π stacking of the blocking groups associated with adjacent molecules, while the fibres are insulated by the CDs (**Figure 1.7**). Extended conjugation within each rotaxane through co-planarity between the axle and the blocking groups is also evident.

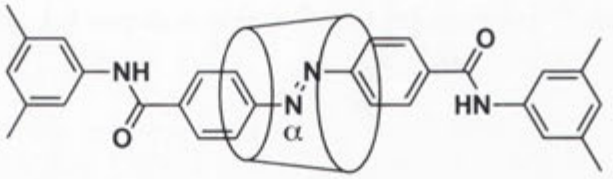

1.9

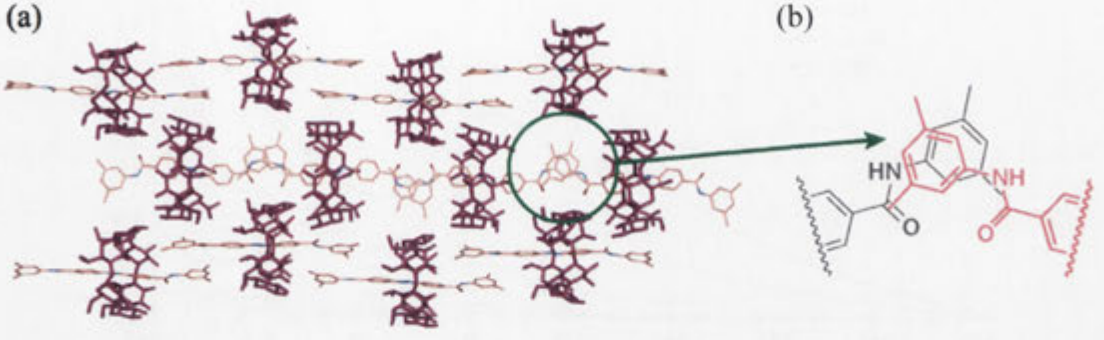

Figure 1.7. Crystal packing of the rotaxane **1.9** showing (a) alignment into insulated molecular fibres, and (b) π–π stacking between the blocking groups.[38]

In solution, the absorption of the rotaxane **1.9** in MeOH and DMSO was found to obey Beer's law, but in water, when the absorbance was measured at various concentrations, unusual spectroscopic behaviour was observed (**Figure 1.8**).[38] For example, at 350 nm where an azobenzene moiety absorbs,[39] the absorbance of a 100 μM solution was significantly less than the expected value of twice the absorbance of a 50 μM solution. When absorbance at 350 nm was plotted against the concentration, the deviation from Beer's law was found to occur at about 16 μM concentration and above. In addition, when the deviation occurred, absorbance at wavelengths higher than 350 nm was also observed, which is characteristic of formation of aggregates with extended conjugation.[40] This was attributed to the rotaxane **1.9** assembling through π–π stacking of the blocking groups to form polymeric aggregates in aqueous solution.

The CD insulates the axle, so only the blocking groups are exposed to form π–π interactions. These must be intermolecular in such a way that the rotaxane **1.9** forms molecular wires. The π–π interactions between the blocking groups of adjacent rotaxanes affect the spectral characteristics of the azobenzene moiety, so the axles must be fully conjugated with the blocking groups. These features are evidence that in

solution the rotaxane **1.9** aggregates in a liquid crystal-like[41,42] fashion as organised molecular wires.

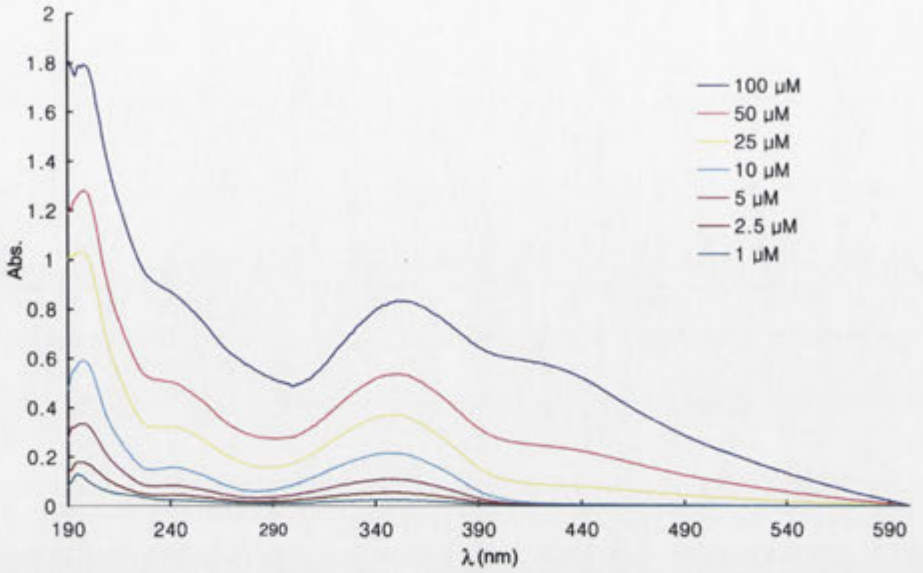

Figure 1.8. Absorbance spectrum of the rotaxane **1.9** in water at the concentrations indicated.

An azobenzene is generally non-fluorescent in solution.[39] However, irradiation of solutions of the rotaxane **1.9** at 480 nm, which is near the wavelength where atypical absorbance is observed, resulted in fluorescence at 520 nm. This unusual fluorescence behaviour supports the self-assembly of the rotaxane **1.9** into molecular wires in aqueous solution through intermolecular π–π interactions.

The analogous rotaxane **1.10** was also made, where a stilbene-based axle was used instead of an azobenzene-based axle, and 2,6- instead of 3,5-dimethylaniline blocking groups were used.[38] The absence of conjugation along the axle in this case is seen in the solid-state where the plane of the dimethylaniline blocking groups is twisted approximately 90° from that of the stilbene moiety (**Figure 1.9**).[38] This conformation prevents the overlap of adjacent blocking groups necessary for π–π stacking of the type seen with the rotaxane **1.9**. This prevents close-packing of the CDs along one axis. Instead, CDs oriented in one direction alternate with others aligned at right angles (**Figure 1.10**).

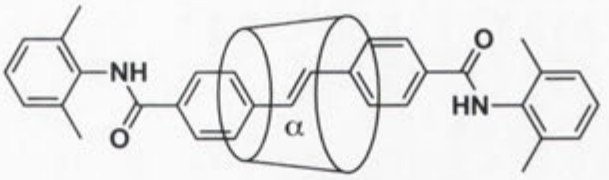

1.10

(a) (b)

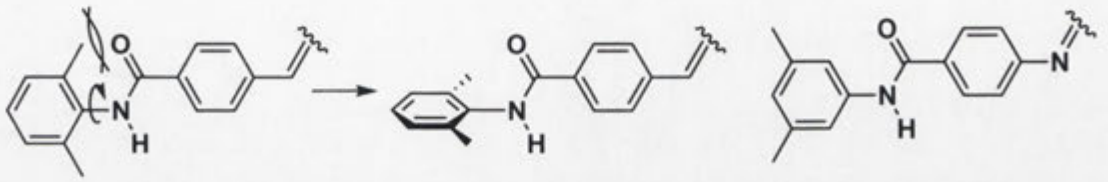

Figure 1.9. (a) Steric interactions prevent co-planarity of the blocking groups with the axle in the rotaxane **1.10**, and (b) the absence of such steric interactions with the rotaxane **1.9**.[38]

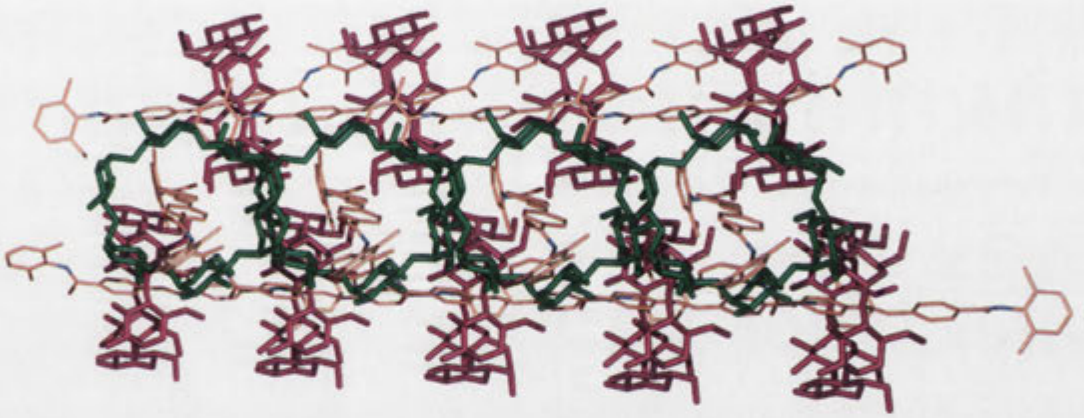

Figure 1.10. Crystal packing of the rotaxane **1.10** showing orientation of CDs in one direction (purple) interspersed by others aligned at right angles (green).[38]

1.5 Crystal Engineering

Having observed this interesting crystal packing behaviour of CD-based rotaxanes, it was decided to explore them using a crystal engineering approach. Desiraju[43] defined crystal engineering as 'the understanding of intermolecular interactions in the context of crystal packing and the utilisation of such understanding in design of new solids with desired physical and chemical properties.' An approach to designing crystals with predicable structure is to use supramolecular 'synthons' that represent molecular building blocks and determine the features of crystal packing though molecular recognition.[44] For example, the crystal structure of hydrogen cyanide **1.11** consists of linear chains all pointing in the same direction based on C-H···N hydrogen bonds (**Figure 1.11** (a)).[45] Crystal packing of cyanoacetylene **1.12**, 4-ethynylcyanobenzene

1.13, and 4-cyano-4'-ethynylbiphenyl **1.14**[46] also show linear chains with C-H···N hydrogen bonds conserved (**Figure 1.11** (b), (c) and (d)). Hence regardless of the nature of the hydrocarbon fragment that comes between the CH and N, the C-H···N hydrogen bonds exemplified by hydrogen cyanide **1.11** result in linear chains.

(a)

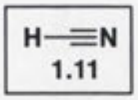

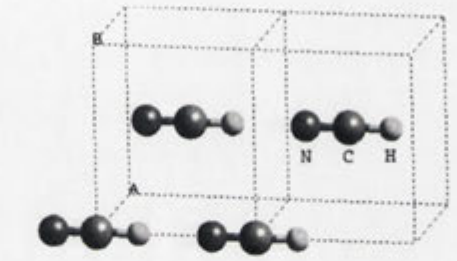

(b)

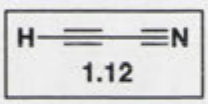

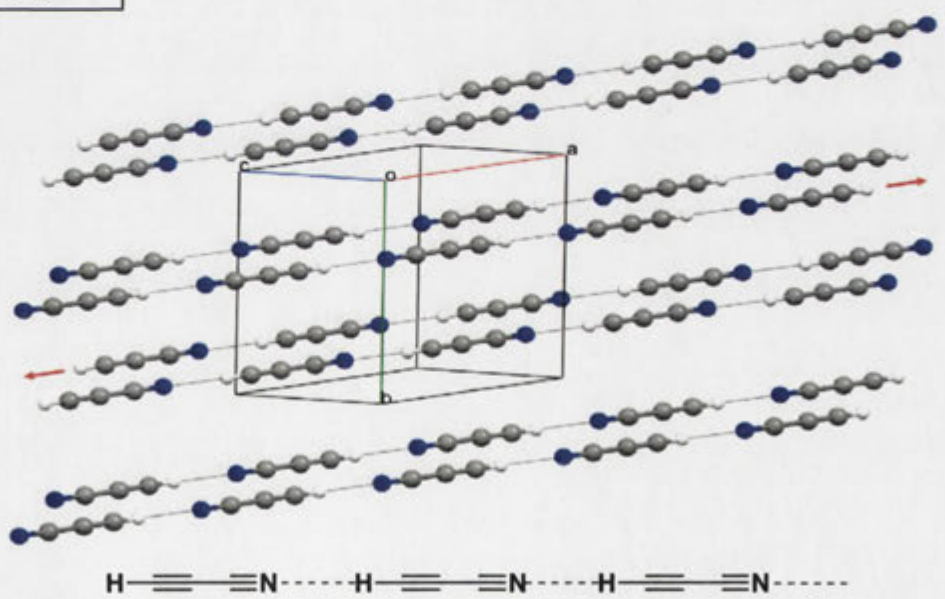

(c)

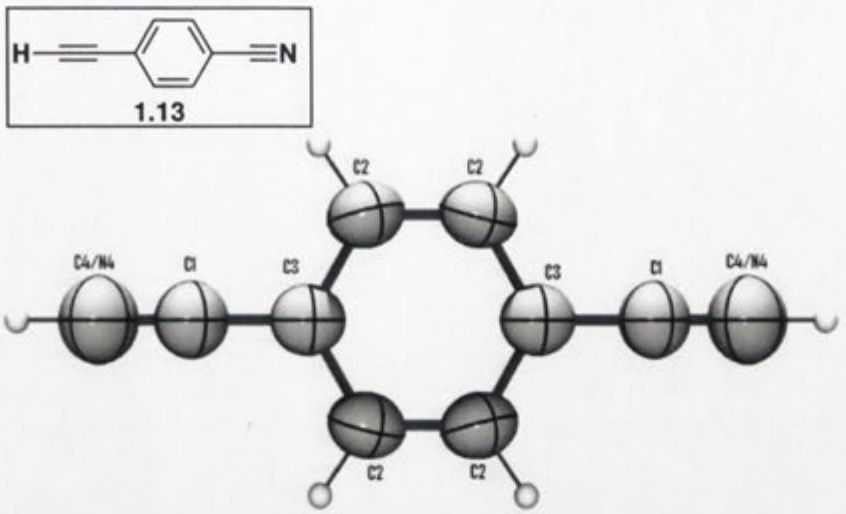

ORTEP diagram of 4-ethynylcyanobenzene with thermal ellipsoids at 50% probability.

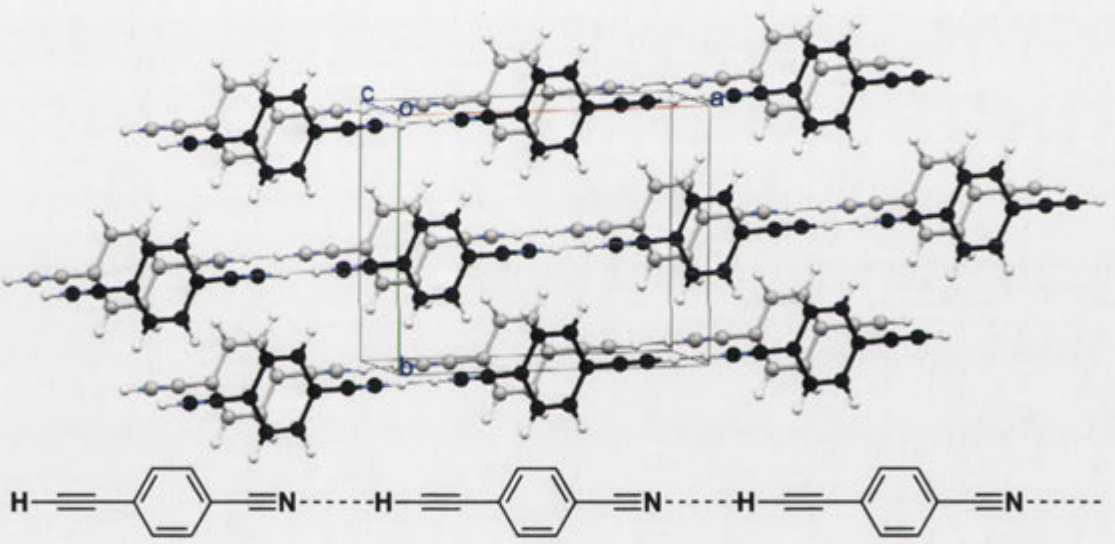

(d)

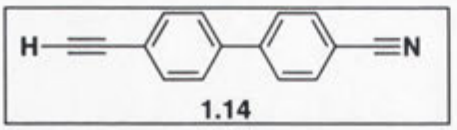

1.14

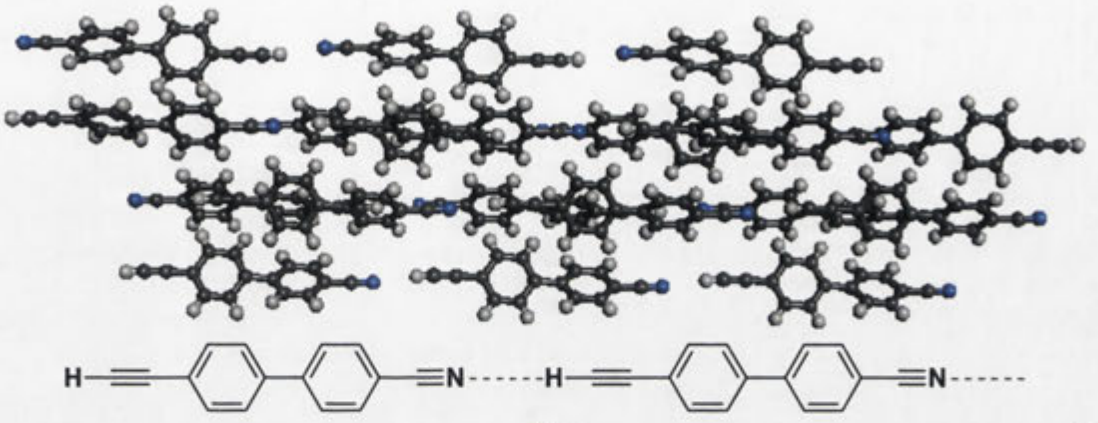

Figure 1.11. Crystal packing diagrams[43,44] (top) and schematic representations[47] (bottom) of (a) hydrogen cyanide **1.11**, (b) cyanoacetylene **1.12**, (c) 4-ethynylcyanobenzene **1.13** (shown in thermal ellipsoids at 50% probability as there is 50% occupancy of cyano and ethynyl groups at each end of the molecule) and (d) 4-cyano-4'-ethynylbiphenyl **1.14** showing C-H···N hydrogen bonding interactions. Crystal packing diagram reproduced with permission from Elsevier.

Whilst molecular similarity also leads to packing similarity, leading to predictable crystal structures,[48] Thakur *et al.*,[49] demonstrated that crystal packing depends not only on the nature of the functional groups, but also the positioning of the functional groups in the molecule. Fluorobenzene **1.15** and benzonitrile, pyridine, pyridine-*N*-oxide and cyanobenzene represent a structure type that forms tetragonal packing. Fluorobenzene **1.15** forms tetragonal packing through two principal types of interaction. The first is the C-H···F interaction between the hydrogens that are *ortho* to the fluorine and the fluorine of neighbouring fluorobenzene. The second is the CH-π interaction between the hydrogens that are *meta* to the fluorine and the neighbouring phenyl ring acceptor as shown in **Figure 1.12**.[49] Despite the similar shape and size of 1,2,3,5-tetrafluorobenzene **1.16** to those of the molecules that adopt the tetragonal fluorobenzene **1.15** structure, the lack of hydrogens in the 3- and 5-positions means that tetragonal packing would require unfavourable C-F···π interactions. Instead, π–π stacking of 1,2,3,5-tetrafluorobenzene **1.16** results, as shown in **Figure 1.13**. This illustrates that crystal engineering requires understanding of the dominating interactions for the self-assembly.

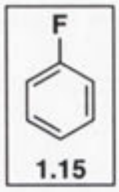

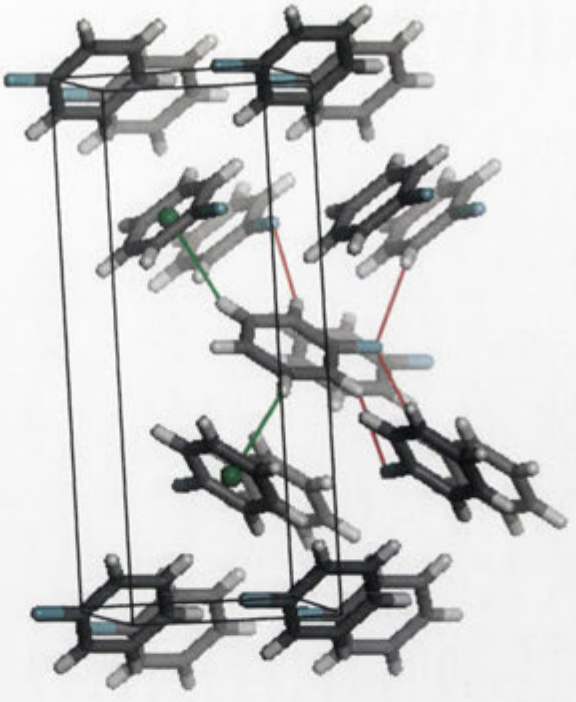

Figure 1.12. Crystal packing of fluorobenzene **1.15** showing tetragonal interactions, with C-H···F interaction between the hydrogens that are *ortho* to the fluorine and the fluorine of neighbouring fluorobenzene (red), as well as CH–π interaction between the hydrogens that are *meta* to the fluorine and the neighbouring fluorobenzene rings (green).

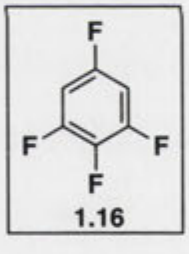

Figure 1.13. Crystal packing of 1,2,3,5-tetrafluorobenzene **1.16** showing π–π interactions.

Crystallisation occurs not only when molecules self-assemble but also when supermolecules further self-assemble.[50] Crystal structure and packing of native CDs has been studied extensively.[51] The crystal structures collectively show intramolecular hydrogen bonds between the O(2)H and O(3)H hydroxyl groups of adjacent glucopyranose units, which contribute to the stable conformation of CDs.[16] α-CD **1.1**, β-CD **1.2** and γ-CD **1.3** crystallise from water as hydrates. α-CD **1.1** crystallises with

$6^{51,52}$ or 7.57^{53} water molecules, while β-CD **1.2** crystallises with 12^{52} and γ-CD **1.3** crystallises with 17 water molecules.[54] The water molecules fill the CD cavity and external interstices between molecules either in fixed positions (**Figure 1.14**) or statistically distributed over a number of disordered sites (**Figure 1.15**). CDs also crystallise from mixtures of water and other solvents including methanol,[55,56] ethanol,[57] 2-propanol[58] and DMF.[59]

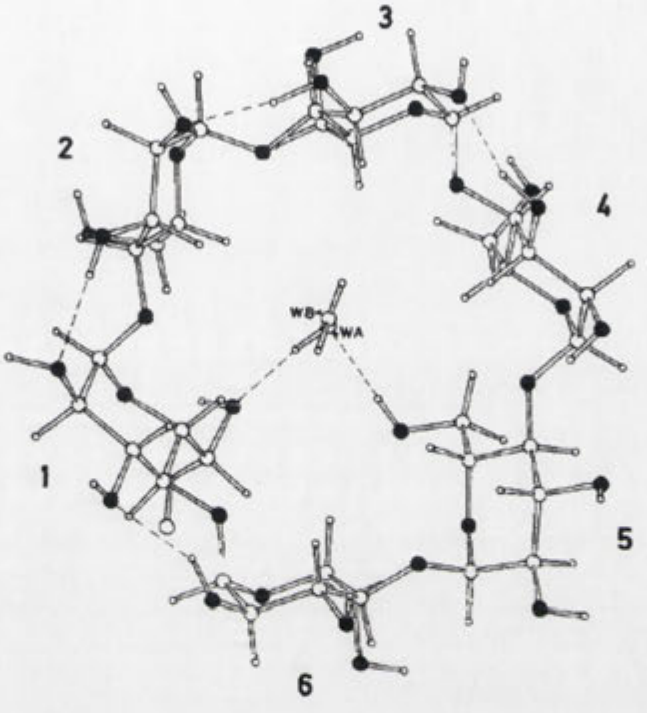

Figure 1.14. Crystal structure of the α-CD **1.1** hexahydrate,[16,18] containing two included molecules of water (WA and WB). Four molecules of water which are not included in the CD cavity are not shown. Hydrogen bonding interactions are indicated by dashed lines. Reproduced with permission from Academic Press, London.

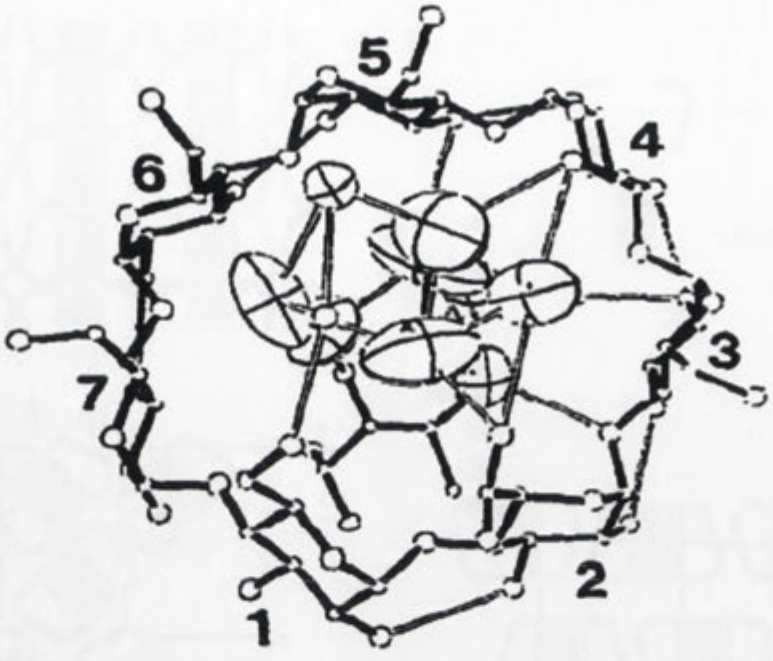

Figure 1.15. Crystal structure of the β-CD **1.2** dodecahydrate.[60] The 6.5 water molecules distributed statistically over 9 sites inside the CD cavity are shown as ellipsoids. Water molecules which are not included in the CD cavity are not shown. Reproduced with permission from Elsevier.

When a molar excess of guest is added, the inclusion complex may be isolated in crystalline form. Crystal structures of CD inclusion complexes provide information on host-guest interactions as well as the geometry of the host and guest molecules.[16] CD complexes can crystallise in a channel-type or cage-type structure depending on the size and ionic character of the guest molecule.[61] The channel-type structure has the CDs packed on top of each other to form continuous channels occupied by the guests (**Figure 1.16** (a)). The cage-type structure has both ends of the CD cavity blocked by neighbouring CDs in a herringbone arrangement (**Figure 1.16** (b)) or a brick arrangement where the CDs are packed in layers of sheets, offset from each other (**Figure 1.16** (c)).[16,61] Channel-type complexes generally show disorder of guest molecules.[62,63] Cage-type complexes, on the other hand, generally show disorder when guest molecules are smaller than the cavity,[58,60,64] but order when the guest molecules are of compatible size.[65,66]

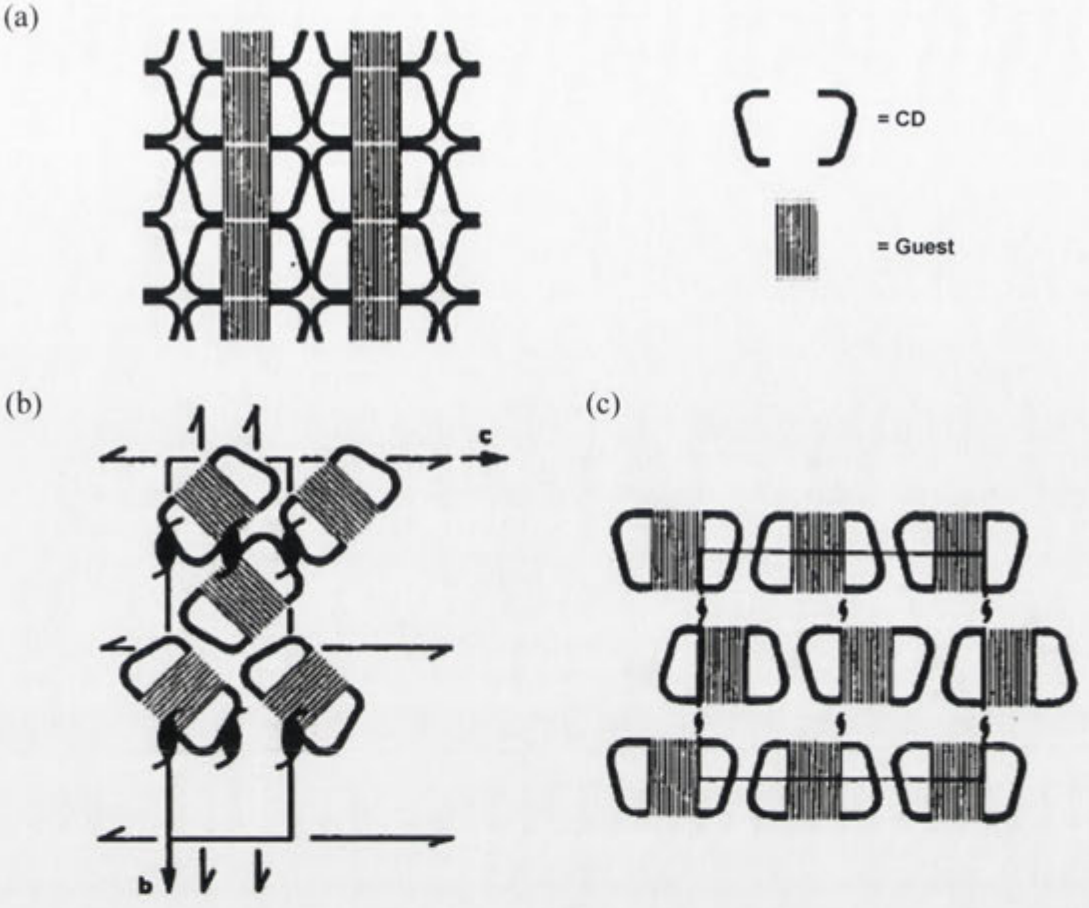

Figure 1.16. Schematic representation of (a) the channel-type, (b) the herringbone-type cage and (c) the brick-type cage crystal packing of CD inclusion complexes.[16] Reproduced with permission from Academic Press, London.

Crystal structures and packing of modified CDs have also been extensively studied. Methylated CDs show increased cavity size due to methyl groups aligned in rings at both ends, resulting in guest molecules including differently to native CDs.[67-69] Monosubstituted CDs may include a substituent group of an adjacent molecule. For example, 6-deoxy-6-(phenylthio)-β-CD shows the phenylthio substituent included in the cavity of an adjacent CD to form an extended polymeric structure (**Figure 1.17**).[70] Alternatively, self-inclusion complexes may form where the substituent group is included in the cavity of the attached CD. A 6-deoxy-6-cyclo($_L$-histidyl-$_L$-leucyl)-β-CD forms a self-inclusion complex where the cyclo(($_L$-histidyl-$_L$-leucyl) moiety bends to include in the CD cavity as shown in **Figure 1.18**.[71]

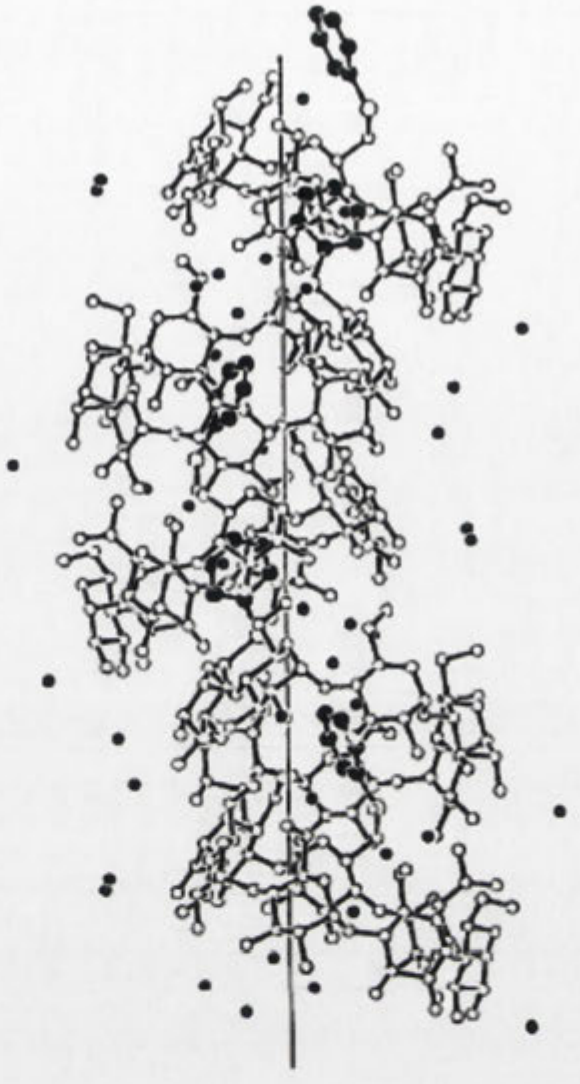

Figure 1.17. Crystal packing of 6-deoxy-6-(phenylthio)-β-CD.[70] The phenyl moiety and water molecules are shown in filled circles. The molecules are arranged along a 4-fold screw axis represented by the vertical line. The phenyl group is inserted in the cavity of an adjacent molecule. Reproduced with permission from The Royal Society of Chemistry.

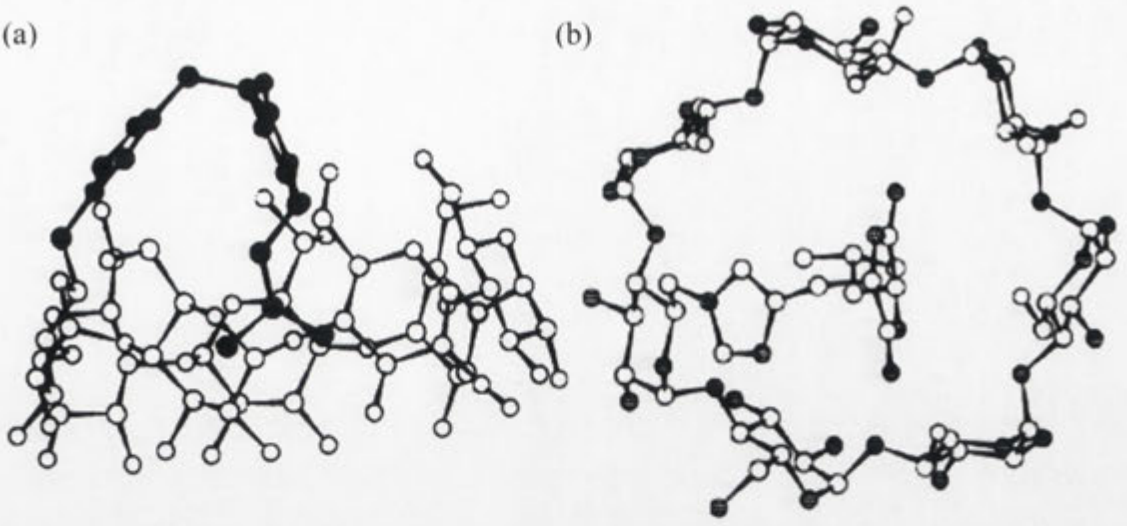

Figure 1.18. Crystal structure of a 6-deoxy-6-cyclo($_L$-histidyl-$_L$-leucyl)-β-CD.[71] (a) View along the side of the CD. The cyclo($_L$-histidyl-$_L$-leucyl) moiety shown in filled circles includes in the CD cavity. (b) View from the narrower end of the CD cavity showing attachment of the cyclo($_L$-histidyl-$_L$-leucyl) moiety at the CD-C6 position. Reproduced with permission from The National Academy of Sciences, USA.

Obtaining crystals of CD-based rotaxanes is of interest as they have guest molecules that do not dissociate and show more ordered geometry inside the cavity. As seen with the rotaxane **1.9**, solid-state studies may be a starting point to understanding molecular level interactions in solids and in solution. The solid-state studies may be used to fine-tune physical, chemical, photochemical or electrical properties of the end product that is fabricated through a bottom-up approach.

Given the solid-state behaviour of the rotaxanes **1.9** and **1.10** with different blocking groups and axles, one of the aims of this project was to prepare the complementary rotaxane **1.17** having a stilbene-based axle and 3,5-dimethylaniline blocking groups, as well as the rotaxane **1.18** having an azobenzene-based axle and 2,6-dimethylaniline blocking groups. Subject to their successful synthesis, the intention was to explore the crystal structure and the crystal packing behaviour of the rotaxanes **1.17** and **1.18** in comparison to those of the rotaxanes **1.9** and **1.10**. In particular, through the study of crystal packing and morphology of rotaxanes, it was of interest to see if the blocking groups of rotaxanes could be used as synthons to guide intermolecular self-assembly to regulate the formation of fibrous structures. Based on this work, examining the crystal growth behaviour, and furthermore, interfering with crystal growth using unsymmetrically capped rotaxanes was to be investigated. Gaining insight into the

molecular level interactions is necessary to design supramolecular assemblies that can be bottomed-up to control the morphology and size of rotaxane crystals.

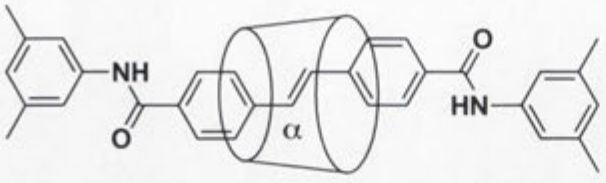

1.17

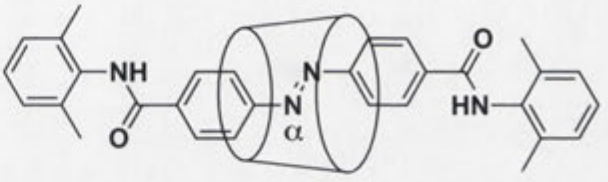

1.18

1.6 Rotaxanes to Preserve the Fluorescence of Profluorescent Nitroxides

As discussed above, CD-based rotaxanes are of interest for crystal engineering studies. In addition, CD-based rotaxanes can be used to change the properties of guest molecules.[29,72-77] In the second part of this thesis, preventing photoisomerisation of profluorescent nitroxide guest molecules, and consequently preserving the profluorescent properties through formation of CD-based rotaxanes was of interest.

Aminyl oxides, aminoxyl radicals, nitroxyl radicals, or more commonly, nitroxides, are free radicals that have the general formula R(NO$^{\bullet}$)R'. The persistency of nitroxides results from electron delocalisation between the two heteroatoms through resonance as shown in **Scheme 1.1**.[78,79] Owing to the persistent nature of the free radicals, nitroxides are commonly used as spin labels,[80,81] spin traps,[82] antioxidants[83] and in radical polymerisations.[84,85]

Scheme 1.1. Resonance structures of nitroxides.

Nitroxides have also been recognised as effective profluorescent probes for oxidative change and free radical generation.[86-91] When a nitroxide is attached to a fluorophore,

the electronic interaction of the unpaired electron with the fluorophore enhances intersystem crossing, causing fluorescence from the first excited singlet state to decrease, and hence quench the fluorescence signal. Despite the persistency of nitroxides towards other nitroxides, they can readily abstract hydrogen or react with alkyl radicals to form hydroxylamines or alkoxyamines. The species then becomes diamagnetic and is now fluorescent and can be detected through fluorescence spectroscopy (**Scheme 1.2**).[89,90] Therefore nitroxides that are attached to fluorophores can be exploited as profluorescent probes as the fluorescence of the fluorophores is quenched until it gets restored through the nitroxides reacting with free radicals.

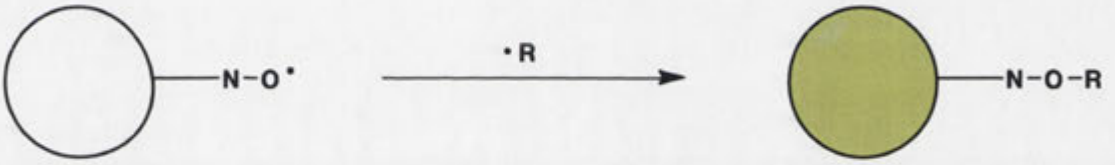

Scheme 1.2. Reduction of a profluorescent nitroxide to give a fluorescent species.

Earlier studies of profluorescent nitroxides consisted of nitroxides covalently linked to fluorophores *via* ester,[86-88] amine,[92] amide[93] and sulfonamide[94] linkages. More recently, the Bottle group[95,96] has investigated the chemistry of profluorescent 1,1,3,3-tetramethylisoindoline-2-yloxyl **1.19** where the nitroxide is directly fused to the fluorophore. In the fused system, the close proximity of the nitroso radical and the fluorophore allows effective quenching of the fluorescence which can be restored upon trapping free radicals to form diamagnetic species.[97] The aromatic ring of 1,1,3,3-tetramethylisoindoline-2-yloxyl **1.19** allows further functionalisation,[90,98-100] and the narrower linewidth and simpler EPR spectra of isoindoline nitroxides compared to other nitroxides makes them ideal for detection. In addition, isoindoline nitroxides are more robust under harsh conditions[101] such as extreme heat or pH, relative to the earlier profluorescent nitroxides reported in the literature, where the fluorophore is linked to the nitroxide *via* more labile linkages.[86-88,92-94] These properties make profluorescent isoindoline nitroxides ideal for detection of free radicals in cells[102,103] and in pollution,[104-106] and for monitoring material degradation.[99,107-109] Profluorescent isoindoline nitroxides in the literature include the fluorescamine **1.20**, the phenanthrene **1.21** and the naphthalene **1.22**.

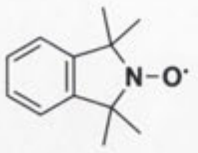

1.19

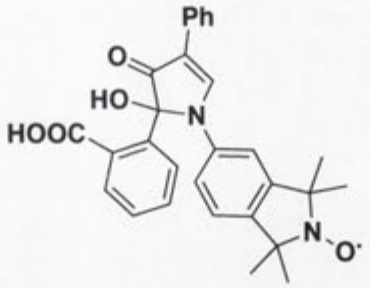

1.20

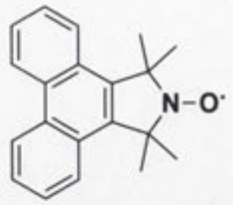

1.21

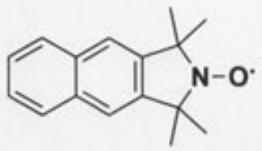

1.22

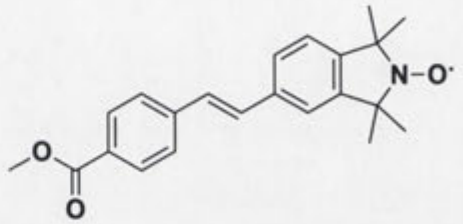

1.23

Compounds that contain the stilbene functionality are often used as fluorescent probes due to their high quantum yields and short excited states.[110] For this reason, the stilbene-based nitroxide **1.23** has also been developed as a versatile fluorescent probe,[90] however, the *trans*-stilbene **1.23** can undergo *trans-cis* isomerisation when exposed to light. The extinction coefficient of a *cis*-stilbene is less than 14% of the *trans*-isomer around the λ_{max} of the *trans*-stilbene, and the fluorescence of the *cis*-stilbene is less than 1% of that from the *trans*-stilbene.[111] Hence *trans-cis* isomerisation causes loss of fluorescence.[111-113]

To sustain the profluorescent properties of fluorescent probes that contain the stilbene functionality, the aim of the work discussed in the latter parts of this thesis was to prevent the stilbene moiety of a compound related to the stilbene **1.23** from undergoing isomerisation by preparing rotaxanes where the stilbene-based axle is mechanically entrapped in α-CD **1.1**. In the study of photochemistry of stilbene-based CD rotaxanes by Stainer *et al.*,[26] the *trans*-stilbene moiety of the rotaxane **1.24** undergoes photoisomerisation resulting in the α-CD macrocycle shifting away from the centre of the stilbene moiety as the cavity of the α-CD is not wide enough to include a *cis*-stilbene moiety (**Scheme 1.3**). In the case of the stilbene-based rotaxane **1.26**, *trans-cis* isomerisation is prevented, again, as the cavity of the α-CD is not wide enough to include a *cis*-stilbene moiety and the CD cannot shuttle away from the

stilbene moiety towards the bulky blocking groups. By comparison, the analogous rotaxane **1.27** with β-CD in the place of α-CD shows *trans-cis* isomerisation as the wider cavity of the β-CD can include a *cis*-stilbene moiety. Hence based on these reports, the objective was to prepare rotaxanes of a stilbene based nitroxide, related to the stilbene **1.23**, to hinder *trans-cis* isomerisation due to the combination of the limited size of the α-CD cavity, and the length of the dumbbell being insufficient for the CD to shift away from the stilbene moiety. Another aim was to improve the solubility in aqueous media through encapsulation of the stilbene moiety by CD such that the fluorescence probe could be used under physiological conditions and *in vivo* studies.

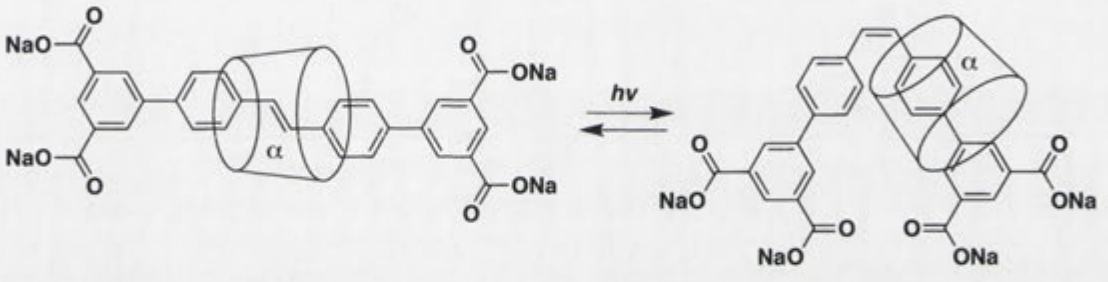

1.24 **1.25**

Scheme 1.3. The rotaxane **1.24** showing shuttling of the CD for *trans-cis* isomerisation to occur.

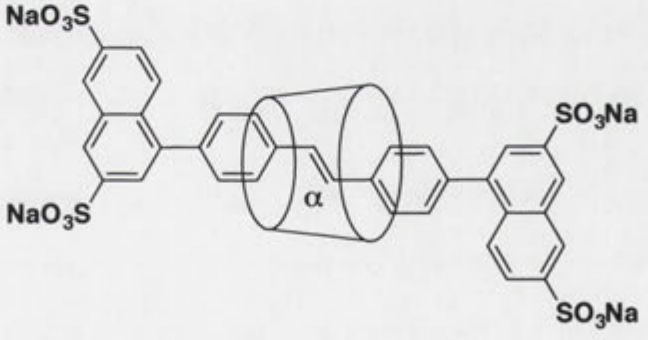

1.26

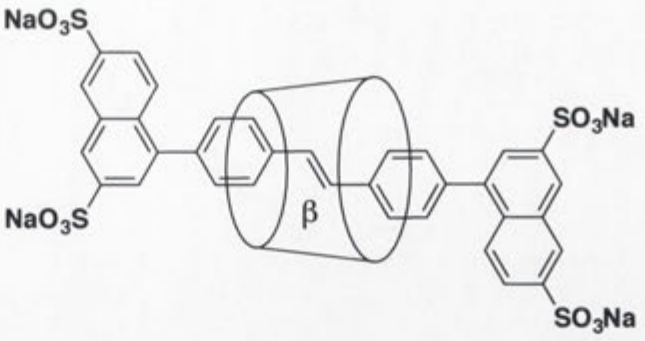

1.27

Nitroxides show increased EPR spectroscopic signals when included in the cavity of a CD.[114-117] CD inclusion complexes with nitroxides[118-125] and nitroxide labeled CDs,[126-131] where the nitroxide is covalently attached to the CD, have been reported in the literature. They are used to monitor supramolecular assemblies,[128,131] host-guest complexations[118-121,123,125,127,128] and aggregation of CDs.[122,130] Nevertheless, only a few nitroxide based CD rotaxanes have been reported.

Mezzina *et al.*,[132] reported the synthesis of the first nitroxide based CD rotaxane **1.28**. The rotaxane **1.28** was prepared using α-CD **1.1** as the macrocycle, sebacoylchloride as the axle and 4-amino-2,2,6,6-tetramethylpiperidine-*N*-oxyl (4-amino-TEMPO) as the blocking group. Thermal lability studies using EPR spectroscopy indicated that the rotaxane **1.28** was non-labile when heated at 60 °C for 14 days.

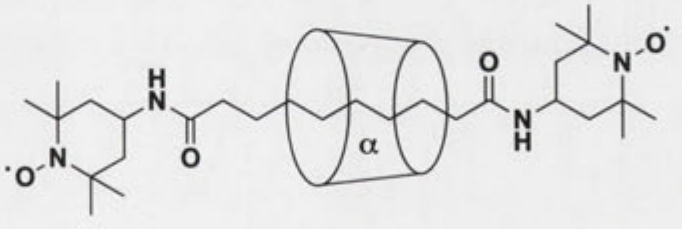

1.28

Another example of a nitroxide based CD rotaxane is the [1]rotaxane **1.29** reported by Franchi *et al.*[133] The nitroxide moiety is mechanically trapped inside the cavity of the CD through a covalent link to the primary end of the CD. The trapping of the 2,2,6,6-tetramethylpiperidine-*N*-oxyl (TEMPO) moiety leads to EPR signal enhancement and increased persistency against reductive conditions compared to unprotected TEMPO.

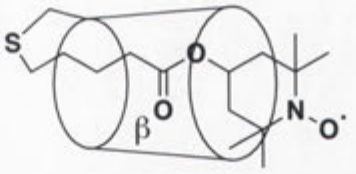

1.29

More recently, Casati *et al.*,[134] prepared α-CD **1.1** based rotaxanes, the nitroxides **1.30** and **1.31**, having 4-oxy-TEMPO as the blocking group on one end of the axle. The unsymmetrically capped dumbbell gave the isomeric rotaxanes **1.30** and **1.31** differing by virtue of the orientation of the CD on the dumbbell. Furthermore, the double spin labeled [2]rotaxane **1.32** was reported, where the dumbbell as well as the α-CD is substituted with the TEMPO moiety.

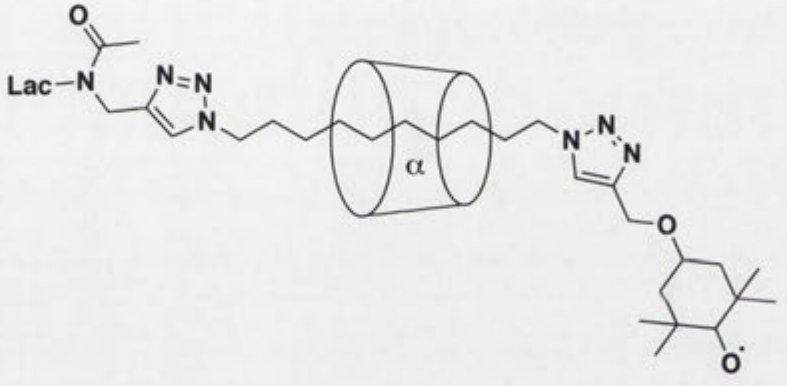

1.30

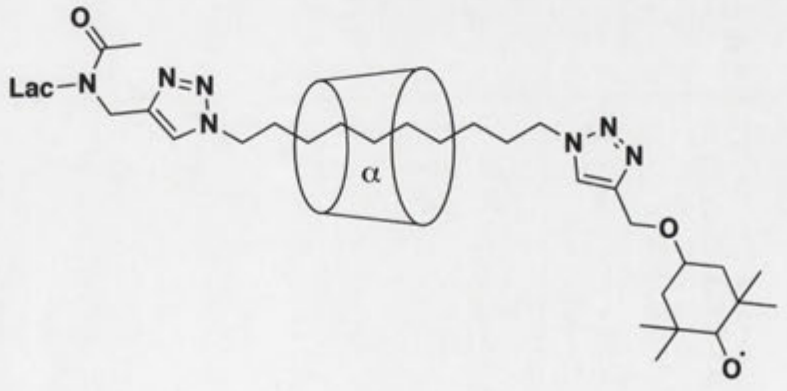

1.31

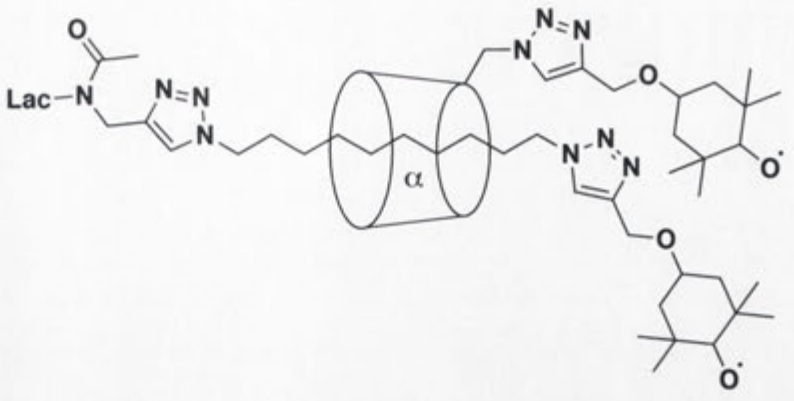

1.32

Maniam[135] reported the synthesis of the water-soluble and stable profluorescent paramagnetic rotaxane **1.34** and the corresponding dumbbell **1.37**. Compared to the dumbbell **1.37** that is virtually insoluble in water, the rotaxane **1.34** has increased water solubility. NMR spectroscopic studies indicated that the rotaxane **1.34** has enhanced resistance against degradation compared to the dumbbell **1.37**. Therefore continuing on from earlier work done by Maniam,[135] the compounds **1.33**, **1.34**, **1.35**, **1.36**, **1.37** and **1.38** were prepared in this work. The photoisomerisation behaviour of the compounds **1.33**, **1.34**, **1.35**, **1.36**, **1.37** and **1.38** was studied to compare the effects on photoisomerisation behaviour of the dumbbells **1.37** and **1.38** alone, and when they are included in α-CD in the form of the rotaxanes **1.33**, **1.34**, **1.35** and **1.36**. The photoisomerisation behaviour depending on 2,6- or 3,5-dimethylaniline blocking groups as well as the orientation of the CD macrocycle was also compared.

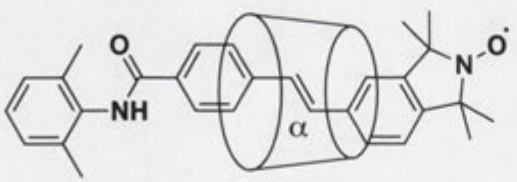

1.33

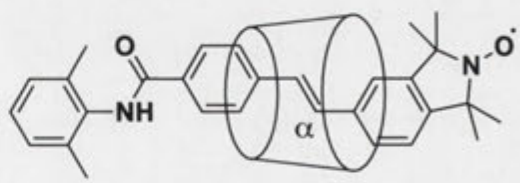

1.34

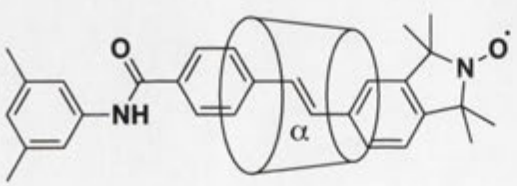

1.35

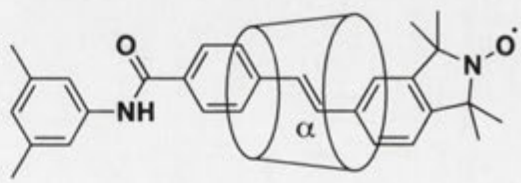

1.36

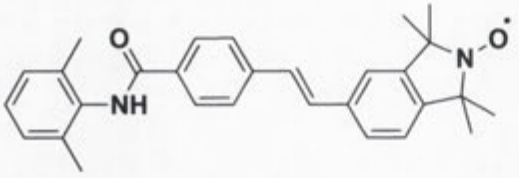

1.37

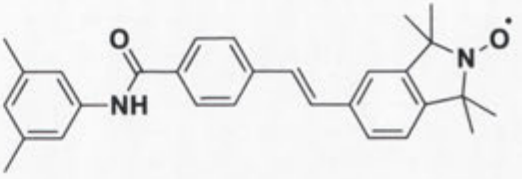

1.38

CHAPTER 2 - Results and Discussion
Synthesis of α-Cyclodextrin [2]Rotaxanes with Aniline-based Blocking Groups

2.1 Introduction

As described in the Introduction, the aim of the work described in this Chapter was to prepare the rotaxanes **1.17** and **1.18**, analogous to the rotaxanes **1.9** and **1.10**. Maniam[135] used 4-(4,6-dimethoxy-1,3,5-triazin-2-yl)-4-methylmorpholinium chloride (DMT-MM)[136,137] as the amide coupling reagent for the synthesis of the CD-based [2]rotaxanes **1.9** and **1.10**. The synthesis of the rotaxane **1.9** involved forming the inclusion complex of the azobenzene **2.1** with α-CD **1.1**, followed by the addition of DMT-MM and the aniline **2.2** as shown in **Scheme 2.1**.[38] The synthesis of the rotaxane **1.10** involved forming the inclusion complex of the stilbene **2.3** with α-CD **1.1**, followed by the addition of DMT-MM and the aniline **2.4** as shown in **Scheme 2.2**.[38] In the present work, this methodology using the inexpensive, water-soluble amide coupling agent, DMT-MM was further employed.

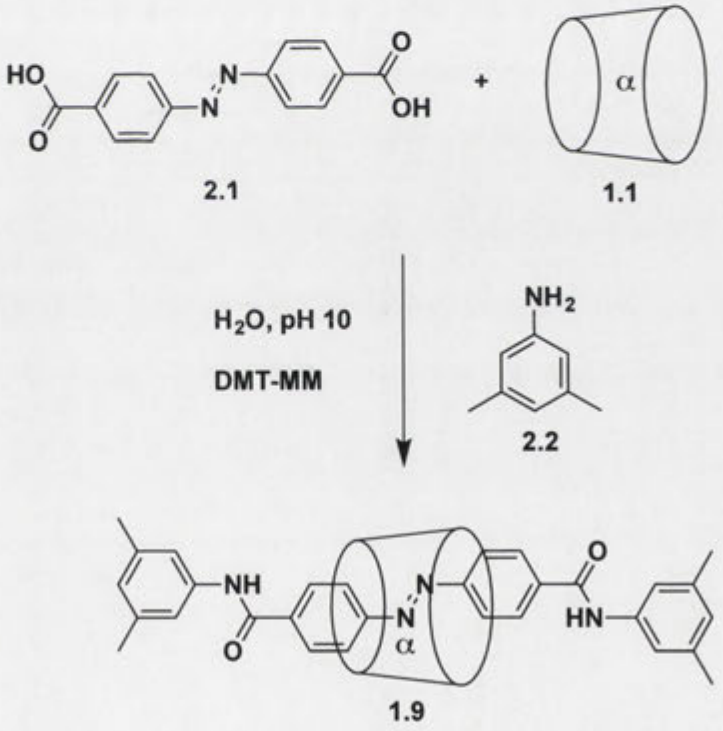

Scheme 2.1. Synthesis of the rotaxane **1.9**.[38]

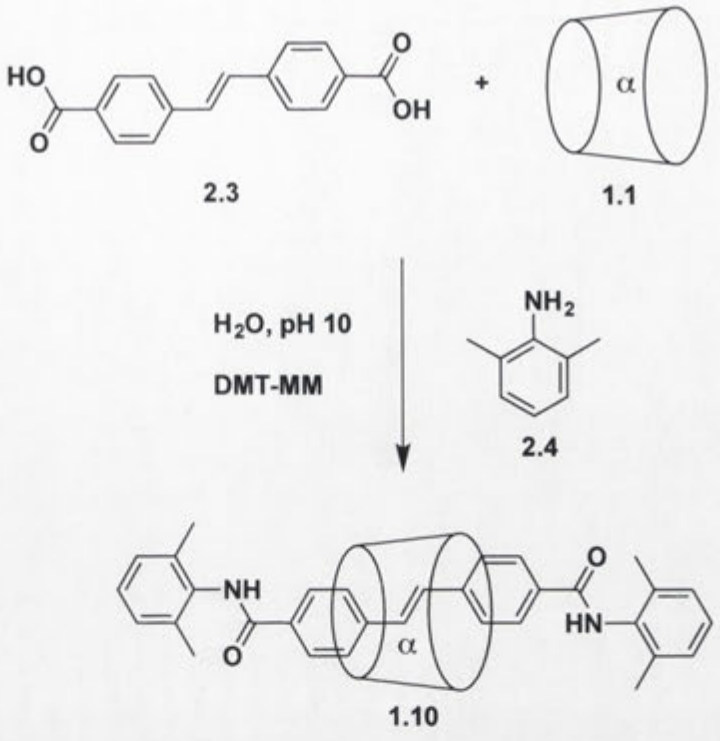

Scheme 2.2. Synthesis of the rotaxane **1.10**.[38]

2.2 Synthesis and Conformational Analysis

Initially, the synthesis of the rotaxane **1.17** was attempted by adapting the procedure of Maniam *et al*.,[38] by equilibrating the stilbene **2.3** in carbonate buffer (pH 10) with excess α-CD **1.1**. The stilbene **2.3**, however, was found to be insoluble in the buffer, unlike the azobenzene **2.1**. Hence the rotaxane **1.17** was prepared according to **Scheme 2.3**. The stilbene **2.3** was equilibrated with excess α-CD **1.1** and three molar equivalents of TEA in water for the inclusion complex **2.5** to form. The TEA provides the basic conditions required to maintain the nucleophilicity of the aniline **2.2** as well as the formation of the stilbene bis(triethyl)ammonium salt, which has enhanced solubility compared to the disodium salt in ionic solution. The bis(triethyl)ammonium salt was not fully soluble. Then, the aniline **2.3** and a large excess of DMT-MM were added. Formation of the product **1.17** was monitored by TLC. The TLC of the reaction mixture showed a component with a different R_f value to α-CD **1.1**, yet showing both the UV absorbance of an aromatic compound and the pink colouration characteristic of a CD on exposure to acidic naphthalene-1,3-diol.[138] The rotaxane **1.17** was isolated in 2% yield through reverse phase HPLC and its ESI mass spectrum showed an $(M\text{-}H)^-$ ion of *m/z* 1446. A low yield was obtained in comparison to the 27% yield of the azobenzene analogue **1.9**[38] despite the large excess of DMT-MM for

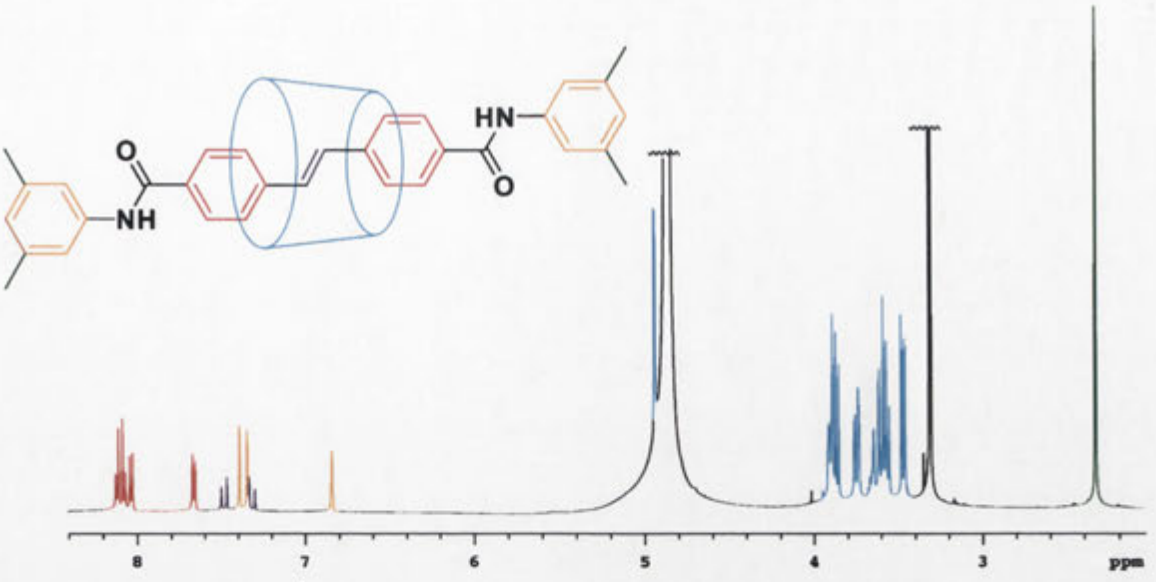

Figure 2.1. 500 MHz ^{1}H NMR spectrum of the rotaxane **1.17** in CD_3OD.

Methodology employed by Inoue and co-workers[139,140] was applied to determine the position of the CD along the axle and the conformation of the rotaxane **1.17**. **Figure 2.2** shows a section of the DQF-COSY NMR spectrum of the rotaxane **1.17**, where the CD proton cross-peaks are found. The C1 anomeric protons resonate the most downfield, and those resonances are well separated from the resonances of the C2-C6 protons. Characteristically the C1 protons' resonance is observed at about δ4.8.[141] While this region of the spectrum is partially obscured by the OH signal, a signal at δ4.94 is observed, and therefore assigned to the CD-C1 protons. A ^{1}H-^{1}H correlation between these protons and those giving rise to the signal at δ3.47 is seen, and the latter is therefore assigned to the CD-C2 protons. Likewise, there is a cross-peak between the resonance at δ3.47 (CD-C2) and the resonance at δ3.87 which is therefore attributed to the CD-C3 protons. This resonance at δ3.87 (CD-C3) also shows a cross-peak with the resonance at δ3.57 which is therefore assigned to the CD-C4 protons. Again, the resonance at δ3.57 (CD-C4) also shows a cross-peak with the resonance at δ3.90 which is therefore assigned to the CD-C5 protons. Finally, the resonances at δ3.75 and 3.60 corresponding to the CD-C6 protons show cross-peaks with each other.

optimisation. This is presumably due to the relatively low solubility of the stilbene **2.3** that does not fully dissolve even when the bis(triethyl)ammonium salt is formed. Rotaxane formation using these types of reactions also leads to side products as discussed later with the rotaxane **1.18**, contributing to the low yield.

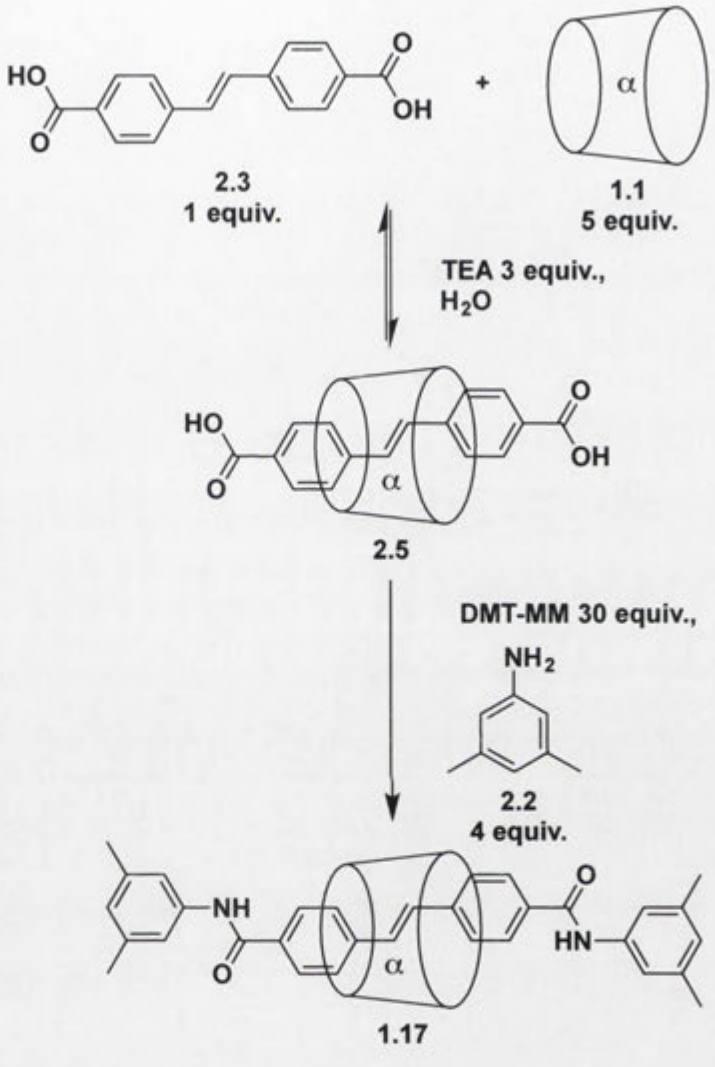

Scheme 2.3. Synthesis of the rotaxane **1.17**.

The 1D ^{1}H NMR spectrum of the rotaxane **1.17** confirms the presence of the components, showing resonances of CD, stilbene and arylamino protons (**Figure 2.1**). The signals at δ7.39 and 7.34 which each integrate for two protons correspond to the 2- and 6-protons of each arylamino group. The 2- and 6-protons of each arylamino group are chemically equivalent due to rotation around the aryl group to nitrogen bond, but the arylamino groups are non-equivalent because of the asymmetry of the CD. Accordingly, the methyl substituents of the blocking groups are observed as two partially resolved apparent singlets at δ2.34 and 2.33.

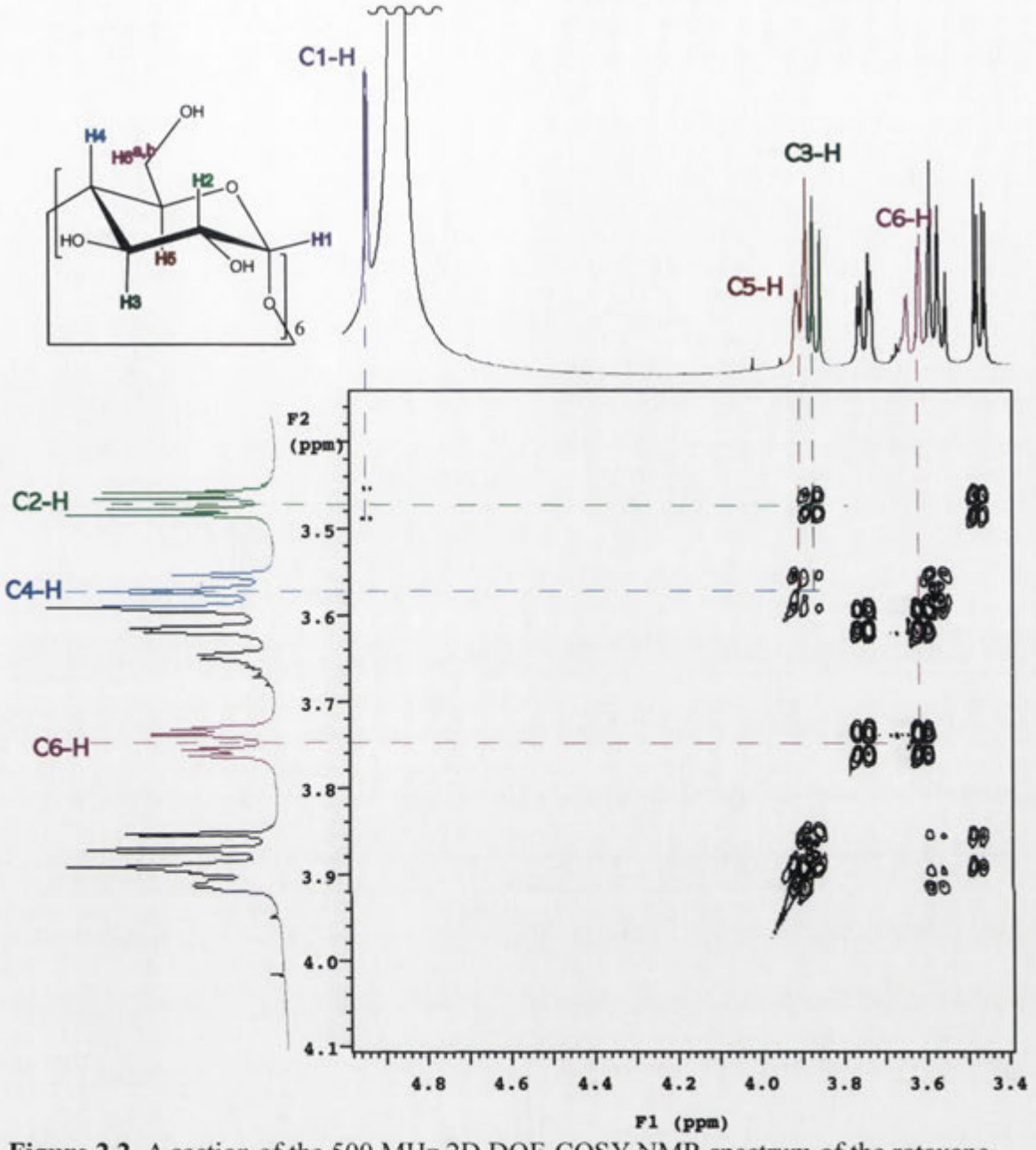

Figure 2.2. A section of the 500 MHz 2D DQF-COSY NMR spectrum of the rotaxane **1.17** in CD_3OD showing cross-peaks between CD proton signals.

The structural assignment can then be completed by analysis of the nuclear Overhauser effect (NOE) interactions in the ROESY NMR spectrum. **Figure 2.3** shows a section of the 2D ROESY NMR spectrum with cross-peaks for the stilbene protons. Since cross-peaks are observed between the resonances of olefinic protons F and G, and proton resonances at δ7.67 and 8.12, these resonances are assigned to protons H and E adjacent to the olefinic protons.

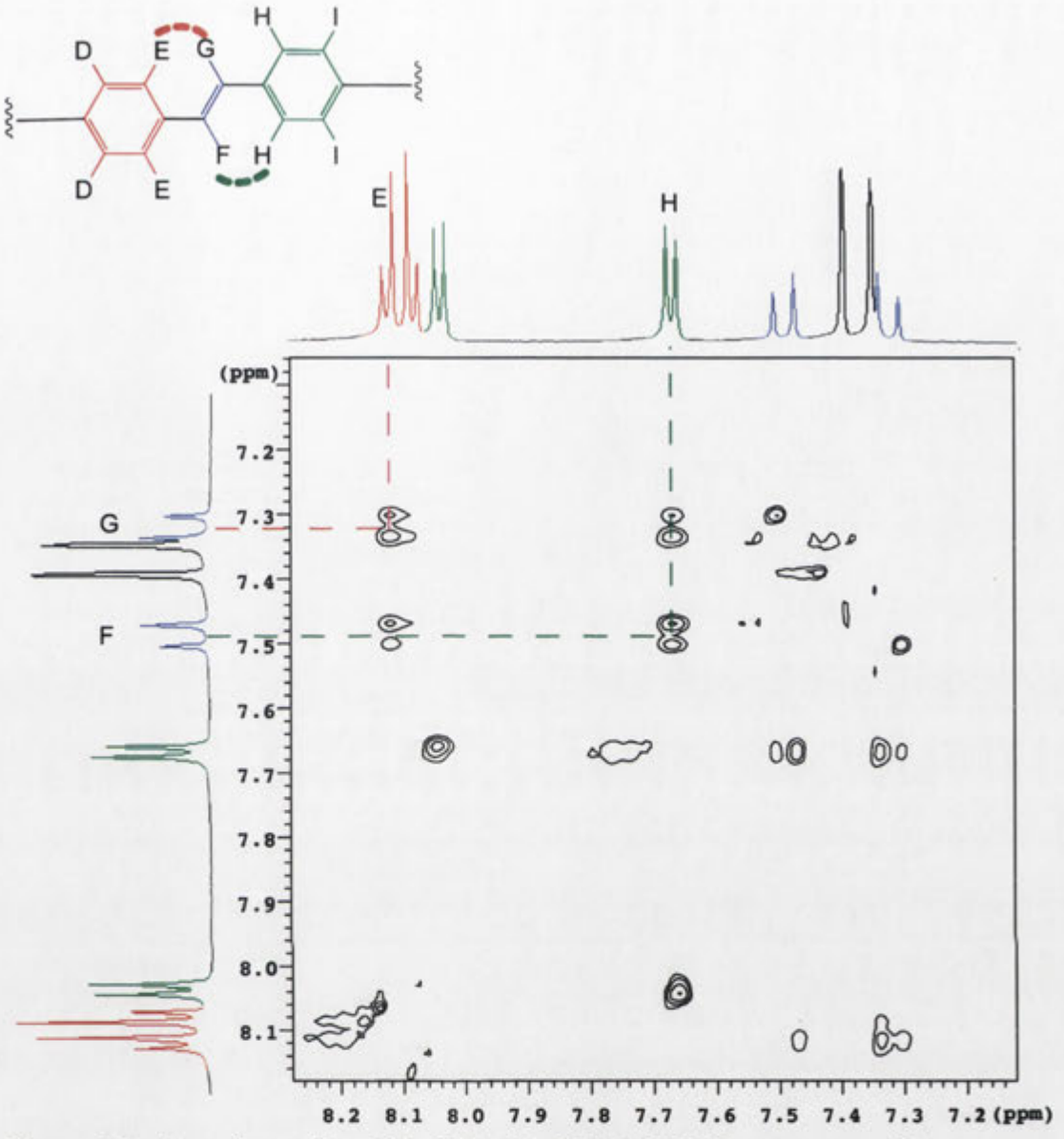

Figure 2.3. A section of the 500 MHz 2D ROESY NMR spectrum of the rotaxane **1.17** in CD_3OD showing cross-peaks between stilbene proton resonances.

Figure 2.4 shows a section of the 2D ROESY NMR spectrum with axle and aniline aromatic proton resonance cross-peaks with those of methyl and CD protons. The presence of the NOE cross-peaks labelled NOE1, NOE2 and NOE3 indicate the resonances at δ7.39, 7.34 and 6.84 correspond to the aniline protons C, J, A and L. Looking at the cross-peaks between the aromatic and CD protons, the CD conformation can be assigned. Protons D and E show NOEs with the CD-C3 protons, hence they are next to the wider end of the CD. The olefinic protons F and G show NOEs with CD-C5 protons. While protons I show an NOE with one of the CD-C6 protons, protons H show NOEs with the CD-C5 and both the CD-C6 protons, hence

they are next to the narrow end of the CD. Overall the CD is located on the middle of the stilbene moiety as shown in **Figure 2.4**.

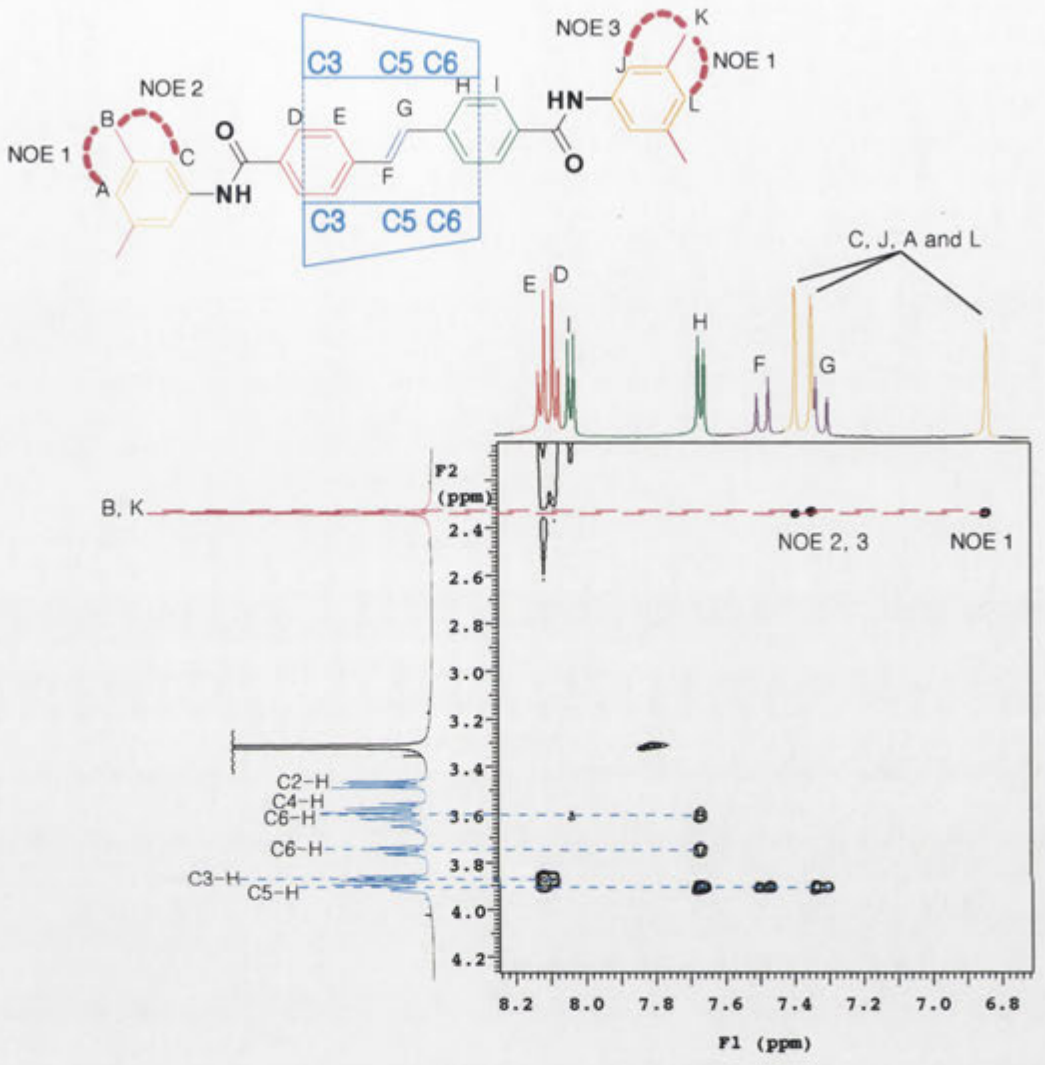

Figure 2.4. A section of the 500 MHz 2D ROESY NMR spectrum of the rotaxane **1.17** in CD_3OD showing stilbene and aniline aromatic proton resonance cross-peaks with those of methyl and CD protons.

The procedure used to prepare the rotaxane **1.18** is shown in **Scheme 2.4**. Initially, the synthesis was attempted using TEA, due to the successful synthesis of the rotaxane **1.17** using TEA. **Figure 2.5** shows the chromatogram obtained through reverse phase HPLC of the crude reaction mixture using TEA. Fractions were isolated and analysed using ESI mass spectrometry. The material corresponding to the peak indicated by the pink asterisk showed an ion at *m/z* 1472, which corresponds to the sodiated ion of the rotaxane **1.18**. The sample corresponding to the peak indicated by the blue asterisk showed an ion at *m/z* 1417 which corresponds to α-CD substituted with three dimethoxytriazinyl groups from the DMT-MM. Finally, the material giving rise to the

peak indicated by the yellow asterisk showed an ion at *m/z* 1590 which corresponds to the rotaxane **1.18** substituted with one dimethoxytriazinyl group. The pK_a of the secondary hydroxyl groups of a CD is around 12, while the pK_a of the primary hydroxyl groups is around 15-16.[17,142,143] Hence under basic conditions using TEA, secondary hydroxyl groups are more likely to become deprotonated and act as nucleophiles, initiating side reactions. Therefore, although the exact structures of reaction side products have not been fully determined, they can be attributed to substitution on the secondary side of the CD.

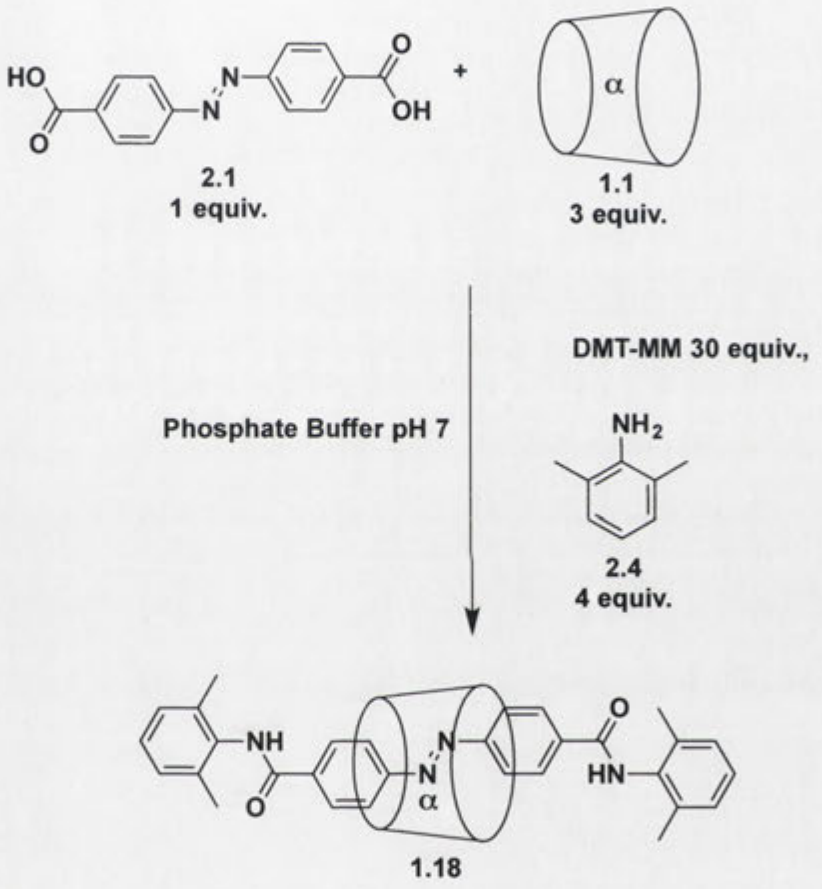

Scheme 2.4. Synthesis of the rotaxane **1.18**.

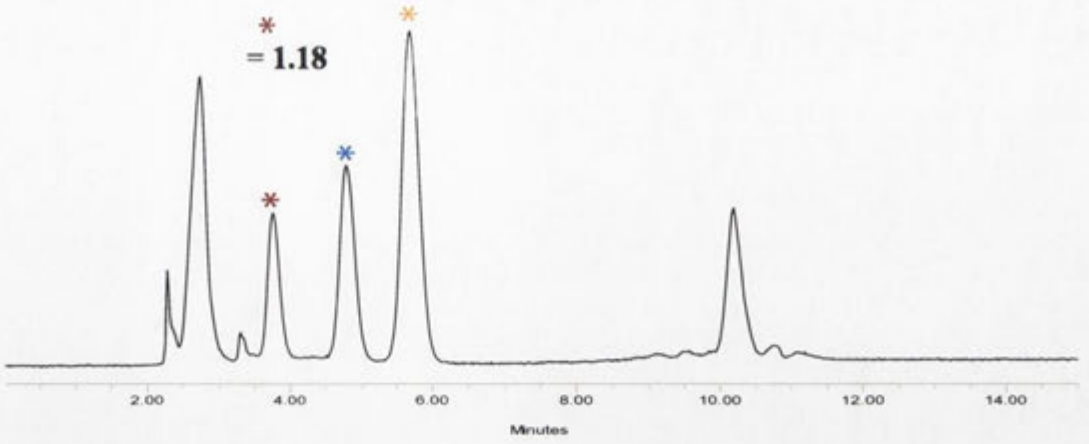

Figure 2.5. Chromatogram obtained through reverse phase HPLC of the crude product mixture when TEA was used to prepare the rotaxane **1.18**.

In a second attempt to prepare the rotaxane **1.18**, nucleophilic substitution of the CD was to be avoided. Hence the reaction mixture was maintained at pH 7 using a buffer system. Unwanted side products such as tri-substituted α-CD and mono-substituted rotaxane, observed when TEA was used, were no longer observed at pH 7. In order to optimise the reaction conditions, the formation of the desired product **1.18** was monitored every hour using reverse phase HPLC as shown in **Figure 2.6**. As time progressed, an increase in peak area of the desired product **1.18** was seen up to four hours, after which time no further increase was observed.

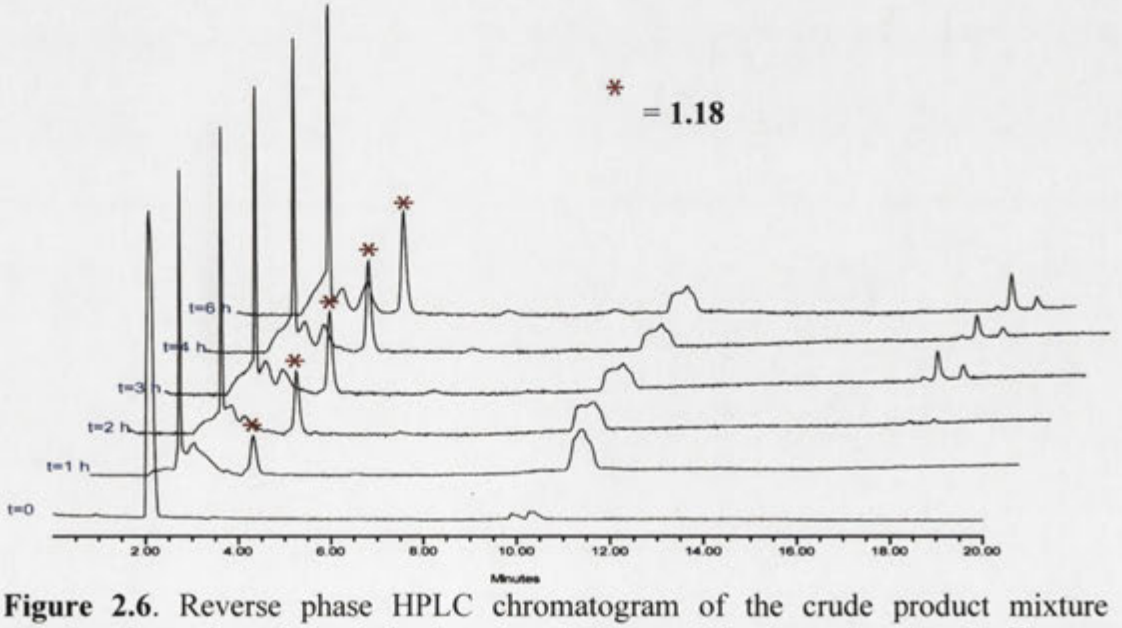

Figure 2.6. Reverse phase HPLC chromatogram of the crude product mixture showing formation of the desired product **1.18** over 6 h when phosphate buffer was used.

Next, the optimal amount of the coupling agent DMT-MM was tested. The formation of the desired product **1.18** was monitored every hour using reverse phase HPLC and plotted against time when varying amounts of DMT-MM were used (**Figure 2.7**). The rate of reaction was the fastest when forty equivalents of DMT-MM were used (shown by the red line) as suggested by the steepest slope on the graph. However, forty equivalents made the reaction mixture go cloudy. Hence thirty equivalents of DMT-MM were used to keep the solution homogeneous.

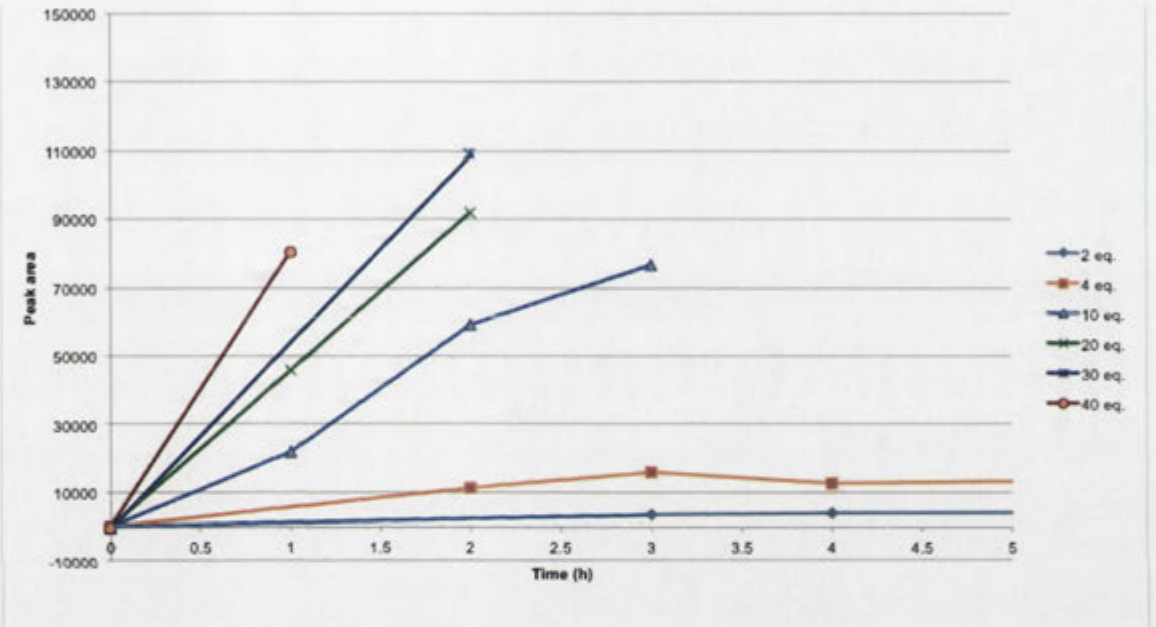

Figure 2.7. Plot of the product **1.18** peak area on the reverse phase HPLC chromatogram versus time when 2, 4, 10, 20, 30 and 40 equivalents of DMT-MM were added to the reaction mixture.

Finally, the optimal amount of the aniline **2.4** was determined. The formation of the desired product **1.18** indicated with a pink asterisk was monitored using reverse phase HPLC when four, eight and twelve equivalents of the aniline **2.4** were used (**Figure 2.8**). Four equivalents of the aniline **2.4** was found to give the optimal formation of the rotaxane **1.18** (shown in green), while larger amounts of the aniline **2.4** resulted in less of this product.

Hence the rotaxane **1.18** was prepared using these optimised conditions according to **Scheme 2.4**. The azobenzene **2.1** was equilibrated with excess α-CD **1.1** in phosphate buffer at pH 7. Then, four equivalents of the aniline **2.4** and thirty equivalents of DMT-MM were added. The formation of the product **1.18** was monitored by TLC.

The TLC of the reaction mixture showed a component with a different R_f value to α-CD **1.1**, yet showing both the UV absorbance of an aromatic compound and the pink colouration of a CD on exposure to acidic naphthalene-1,3-diol.[138] The rotaxane **1.18** was isolated in 8% yield through reverse phase HPLC and its ESI mass spectrum showed an ion at *m/z* 1472 which corresponds to the sodiated molecular ion.

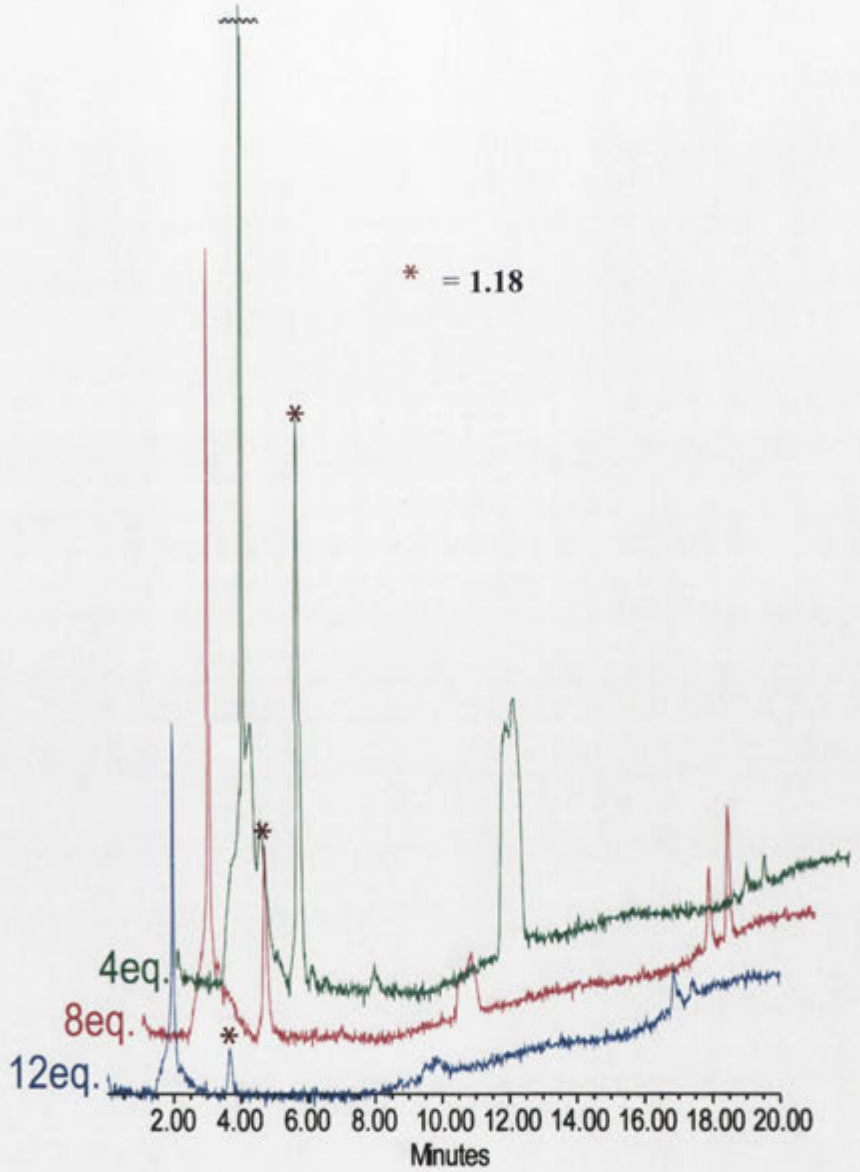

Figure 2.8. Reverse phase HPLC chromatogram showing formation of the desired product **1.18** when 4, 8 and 12 equivalents of the aniline **2.4** were added to the reaction mixture.

The 1D ^{1}H NMR spectrum of the rotaxane **1.18** confirms the presence of the components, showing resonances of CD, azobenzene and arylamino protons (**Figure 2.9**).

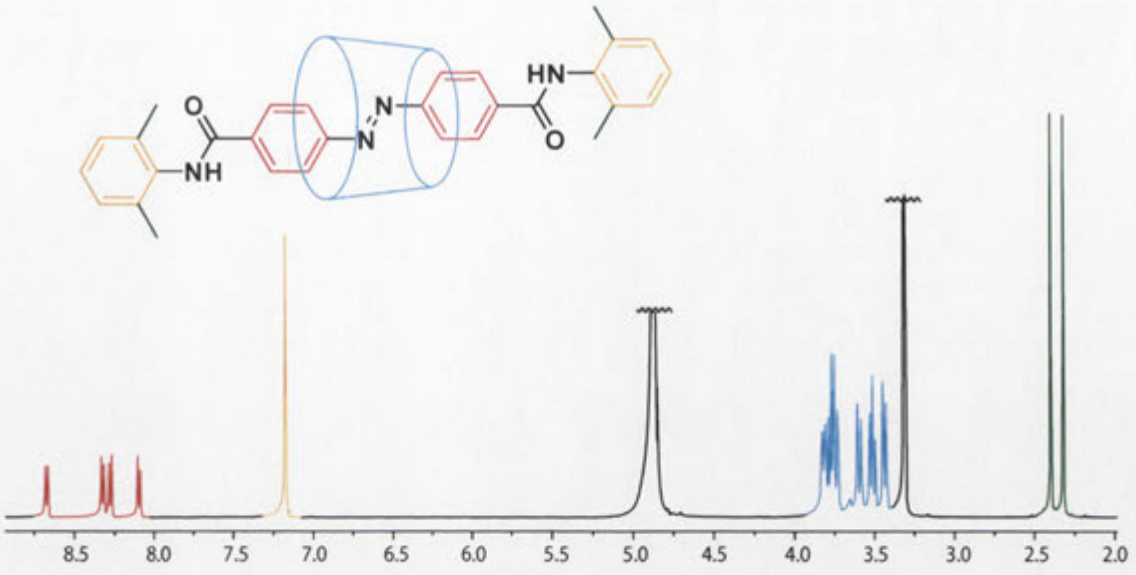

Figure 2.9. 500 MHz ^{1}H NMR spectrum of the rotaxane **1.18** in CD_3OD.

The general protocol to determine the position of the CD along the axle and the conformation of CD-based [2]rotaxanes was followed for the rotaxane **1.18**. **Figure 2.10** shows a section of the DQF-COSY NMR spectrum of the rotaxane **1.18**, where the CD proton cross-peaks are found. The most down field CD resonance at δ4.91 is assigned to the CD-C1 anomeric protons. A ^{1}H-^{1}H correlation between these protons and those giving rise to the signal at δ3.43 is seen, and the latter is therefore assigned to the CD-C2 protons. Likewise, there is a cross-peak between the resonance at δ3.43 (CD-C2) and the resonance at δ3.77 which is therefore attributed to the CD-C3 protons. This resonance at δ3.77 (CD-C3) also shows a cross-peak with the resonance at δ3.51 which is therefore assigned to the CD-C4 protons. Again, the resonance at δ3.51 (CD-C4) also shows a cross-peak with the resonance at δ3.82 which is therefore assigned to the CD-C5 protons. Finally, the resonances at δ3.74 and 3.60 corresponding to the CD-C6 protons show cross-peaks with each other.

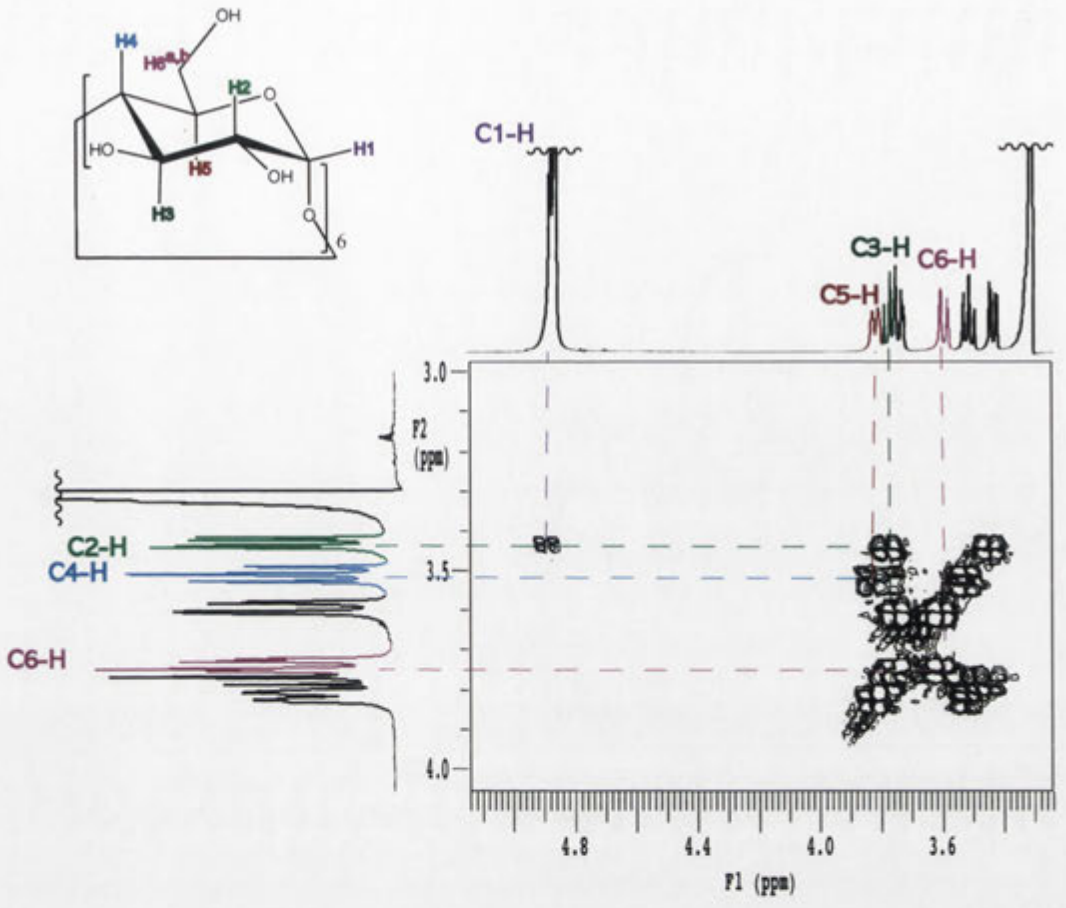

Figure 2.10. A section of the 500 MHz 2D DQF-COSY NMR spectrum of the rotaxane **1.18** in CD_3OD showing cross-peaks between CD proton signals.

Figure 2.11 shows a section of the 2D ROESY NMR spectrum with axle and aniline aromatic proton resonance cross-peaks with those of methyl and CD protons. The presence of the NOE cross-peak labelled NOE1 indicates that the resonance at δ8.32 corresponds to the azobenzene protons D in proximity to the methyl protons C. Likewise, the NOE cross-peak labelled NOE2 indicates the resonance at δ8.27 corresponds to the azobenzene protons G in proximity to the methyl protons H. Looking at the cross-peaks between the aromatic and CD protons, the location of the CD along the azobenzene axle can be assigned. Protons D show an NOE with the CD-C3 protons, hence they are next to the wider end of the CD. Protons E show NOEs with the CD-C3 and CD-C5 protons. Hence protons D and protons E are assigned to one phenyl group. The azobenzene protons F and G show NOEs with the CD-C5 and CD-C6 protons, hence they are assigned to the other phenyl group that is next to the narrow end of the CD. Protons F show stronger NOEs with the CD-C5 and CD-C6 protons compared to protons G. Over all, the CD is located around the middle of the azobenzene moiety as shown in **Figure 2.11**.

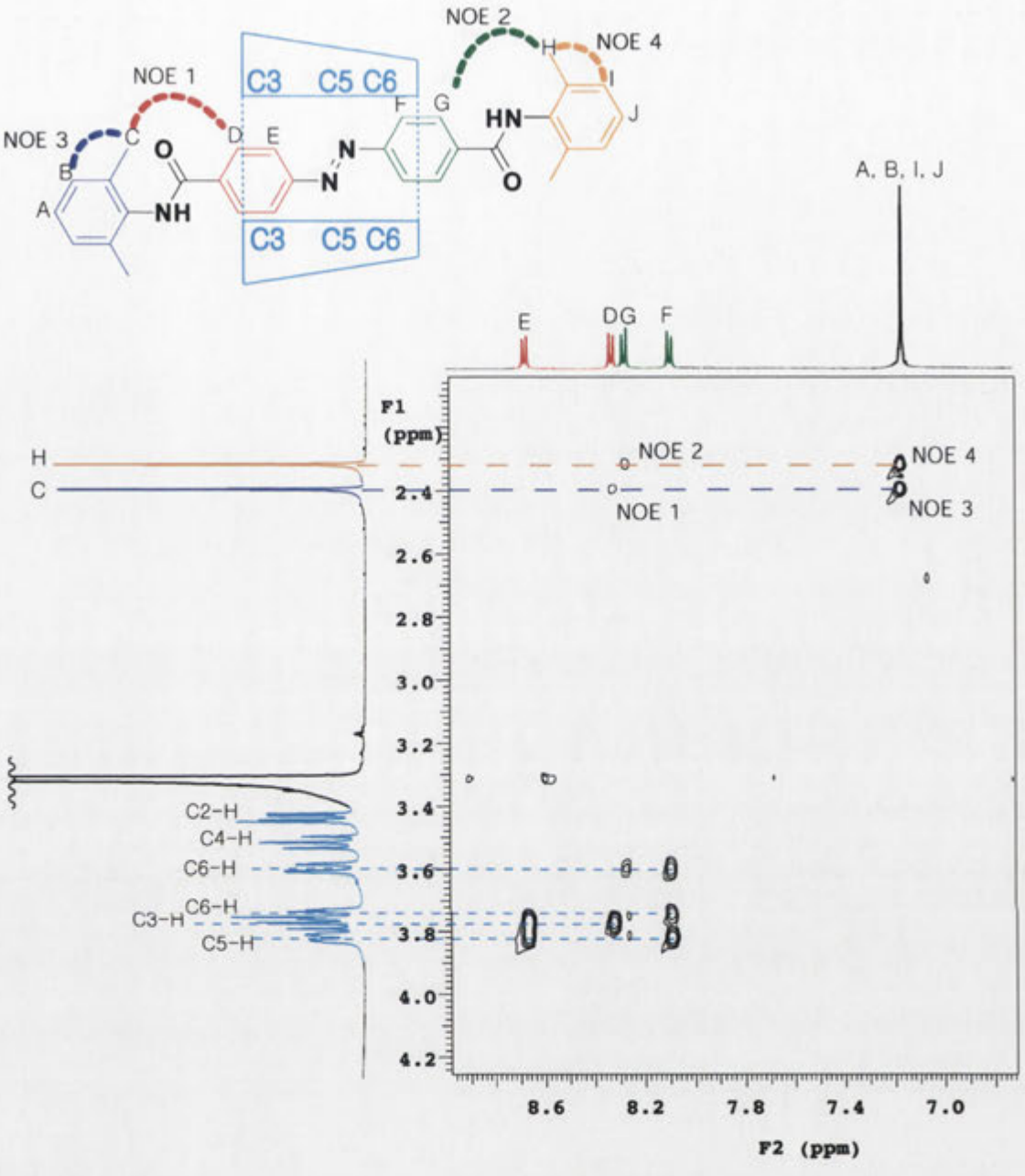

Figure 2.11. A section of the 500 MHz 2D ROESY NMR spectrum of the rotaxane **1.12** in CD_3OD showing azobenzene and aniline aromatic proton resonance cross-peaks with those of methyl and CD protons.

Having prepared the rotaxanes **1.17** and **1.18**, this completed the set **1.9**, **1.10**, **1.17** and **1.18** with 2,6-dimethylaniline and 3,5-dimethylaniline blocking groups, with azobenzene- and stilbene-based axles. Growing crystals of the rotaxanes **1.17** and **1.18** to obtain X-ray crystal packing data, and investigating relationships between the crystal growth and the crystal packing of the rotaxanes **1.9**, **1.10**, **1.17** and **1.18** was the next objective.

CHAPTER 3 - Results and Discussion
Solid-state Structure, Morphology and Crystal Growth of α-Cyclodextrin [2]Rotaxanes

3.1 Self-assembly in the Solid-state

Having prepared the rotaxanes **1.17** and **1.18**, crystals were grown to compare and contrast with the crystal packing of the rotaxanes **1.9** and **1.10**. Crystals of the rotaxanes **1.17** and **1.18** were obtained through slow evaporation of MeOH/water over a period of several days or weeks. The rotaxanes **1.17** and **1.18** are more soluble in MeOH than water, hence, crystallisation occurred as MeOH selectively evaporated and a supersaturated solution resulted. The X-ray crystallographic analysis of the rotaxanes **1.9** and **1.10** has been reported previously as discussed in Chapter 1.[38] The solid-state structures of the rotaxanes **1.17** and **1.18** were examined using X-ray crystallography. The crystallographic data of the rotaxanes **1.17** and **1.18** are presented in Appendix 1.

The crystal structure of the rotaxane **1.10** was reported by Maniam *et al.*[38] (**Figure 3.1**). The crystal belongs to the orthorhombic space group, and there are four rotaxane molecules in the unit cell. The stilbene is planar, and as discussed in the Introduction, the planes of the dimethylaniline blocking groups are twisted approximately 90° from that of the stilbene moiety. In comparison, the rotaxane **1.18** crystal also belongs to the orthorhombic space group, and has four rotaxane molecules in the unit cell. The crystal structure shows that the azobenzene is planar and the planes of the dimethylaniline blocking groups are twisted approximately 90° from that of the azobenzene moiety (**Figure 3.2**). The crystal packing of the rotaxane **1.18** shows that the CDs oriented in one direction (green) alternate with others aligned at right angles (red) as shown in **Figure 3.3**, remarkably similar to the crystal packing seen with the rotaxane **1.10** (**Figure 1.10**).[38] There is no overlap between the dumbbells of the rotaxanes that are aligned in the same direction, and the rotaxanes do not form fibres. In **Figure 3.3**, the rotaxanes that appear to form fibres with CDs (green) aligning in a head-to-tail direction, horizontal to the page, are in fact offset on planes going into the page. Overall, the very similar conformations and crystal packing indicate that changing the axle from a stilbene moiety to an azobenzene moiety does not significantly affect the crystal packing of the rotaxanes **1.10** and **1.18** with 2,6-dimethylaniline blocking groups.

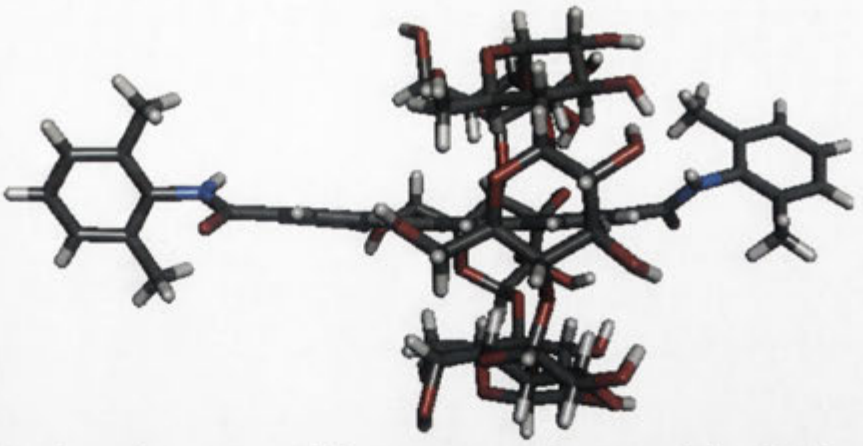

Figure 3.1. Crystal structure of the rotaxane **1.10** reported by Maniam *et al.*,[38] displayed in stick style. Solvent molecules are removed for clarity. Black = carbon, white = hydrogen, blue = nitrogen and red = oxygen.

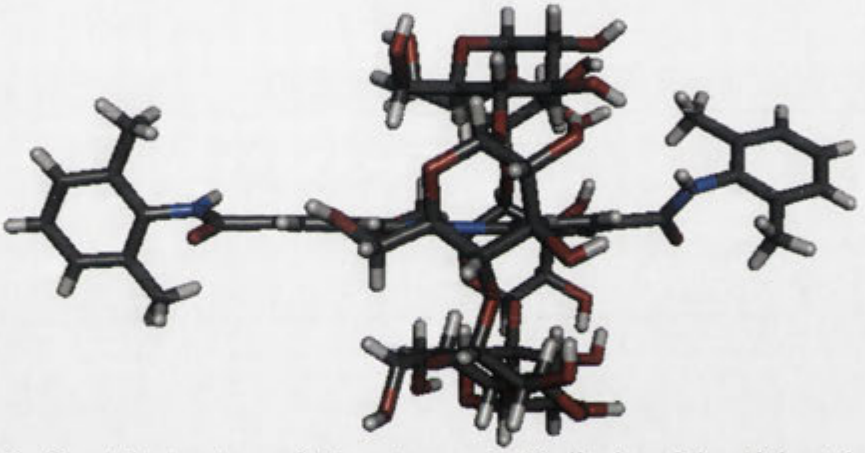

Figure 3.2. Crystal structure of the rotaxane **1.18** displayed in stick style. Solvent molecules are removed for clarity. Black = carbon, white = hydrogen, blue = nitrogen and red = oxygen.

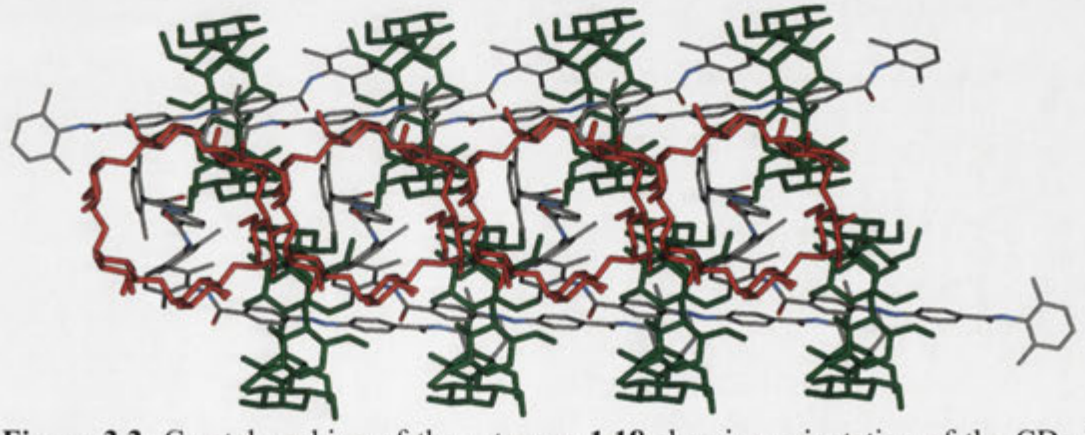

Figure 3.3. Crystal packing of the rotaxane **1.18** showing orientation of the CDs in one direction (green) interspersed by others aligned at right angles (red). Displayed in stick style. Hydrogen atoms and solvent molecules are removed for clarity.

The crystal structure of the rotaxane **1.9** was reported by Maniam *et al.*[38] (**Figure 3.4**). The crystal belongs to the orthorhombic space group, and there are four rotaxane molecules in the unit cell. The azobenzene is planar, and as discussed in the Introduction, the planes of the dimethylaniline blocking groups are co-planar to the azobenzene axle. In contrast, the crystal of the rotaxane **1.17** belongs to the monoclinic space group. There are two rotaxane molecules in the unit cell. The crystal structure shows that the planes of the two phenyl rings of the stilbene moiety are twisted at approximately 30° from each other (**Figure 3.5**). The plane of the aniline moiety on the wider end of the CD cavity is twisted approximately 90° from that of the adjacent phenyl ring, thus it is not conjugated with the stilbene axle. The plane of the aniline moiety at the narrower end of the CD cavity is twisted at approximately 30° from its adjacent phenyl ring. This is in contrast to the strictly co-planar azobenzene axle and blocking groups seen in the crystal structure of the rotaxane **1.9** (**Figure 1.7**). The crystal packing of the rotaxane **1.17** shows a herringbone type packing of the dumbbells (**Figure 3.6** (a)), which allows π–π stacking of the blocking group on the narrower end of the CD cavity and one stilbene phenyl ring of the adjacent dumbbell to be accommodated (**Figure 3.6** (b)). The degree of extended conjugation along the molecular fibre is reduced, however, due to the deviation from strict co-planarity. The CDs display a head-to-tail alignment along a single axis. While the rotaxane **1.9**, which is also aligned head-to-tail, shows alternating rows having the CDs facing opposite directions, making it centrosymmetric around the 2-fold axis of the crystal, the rotaxane **1.17** has the CDs all facing the same direction. This results in the formation of a non-centrosymmetric polar crystal,[36] as per the rotaxane **1.8** crystal observed by Cieslinski *et al.*[37] Overall, using the stilbene axle in place of the azobenzene axle, which is insulated in the cavity of the CD, changes the solid-state structural configuration and crystal packing behaviour of the rotaxanes **1.9** and **1.17** with 3,5-dimethylaniline blocking groups. Despite the change in space group and the solid-state structural configuration, the linear alignment of the rotaxanes **1.9** and **1.17** is retained.

Figure 3.4. Crystal structure of the rotaxane **1.9** reported by Maniam *et al.*,[38] displayed in stick style. Solvent molecules are removed for clarity. Black = carbon, white = hydrogen, blue = nitrogen and red = oxygen.

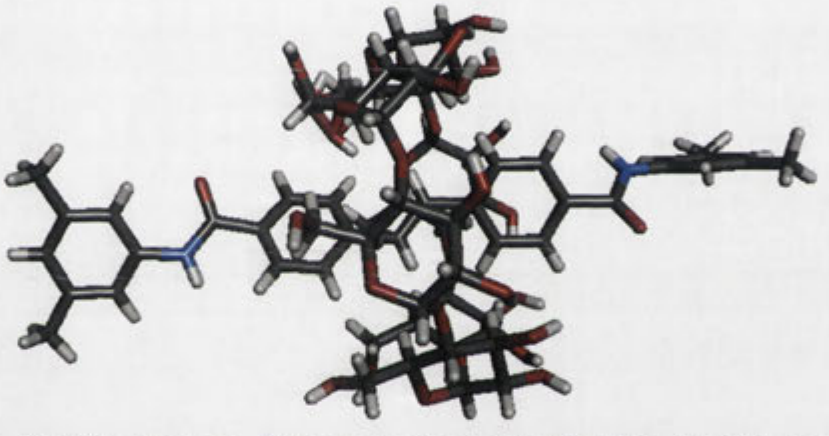

Figure 3.5. Crystal structure of the rotaxane **1.17** displayed in stick style. Solvent molecules are removed for clarity. Black = carbon, white = hydrogen, blue = nitrogen and red = oxygen.

(a)

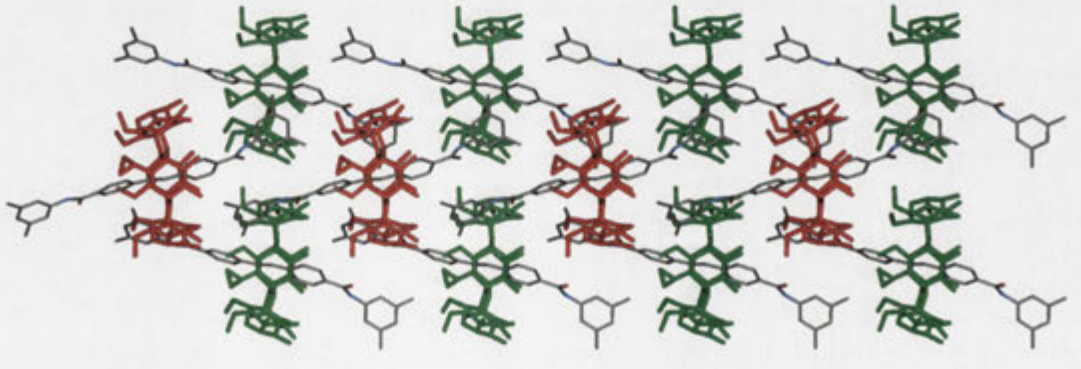

(b)

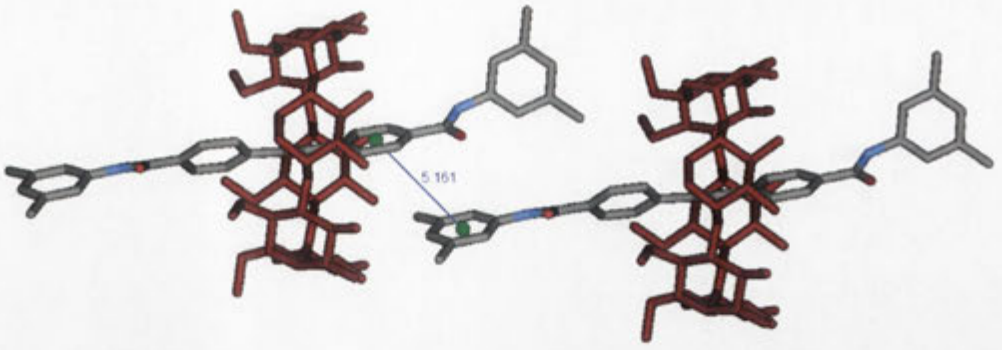

Figure 3.6. Crystal packing of the rotaxane **1.17** showing (a) alignment into insulated molecular fibres, and (b) π–π stacking between the blocking group and the adjacent stilbene phenyl ring of the dumbbell. Displayed in stick style. Hydrogen atoms and solvent molecules are removed for clarity.

The rotaxanes **1.9** and **1.17** are different only in the linkage (-N=N- or -C=C-) that bridges the two phenyl rings of the axle moiety that is included inside the CD cavity. This slight difference results in a different crystal structure. Some molecules can form crystals that have different crystal structures and packing, known as polymorphs.[144,145] Hence a possible explanation for the different crystal structures and packing of the rotaxanes **1.9** and **1.17** is formation of polymorphs. To examine whether the structure and packing seen in **Figure 1.7** is representative of the structure and packing of the rotaxane **1.9**, or if others are possible, crystals of the rotaxane **1.9** were prepared again through slow evaporation of MeOH/water over a period of several weeks. A grown crystal was examined using X-ray crystallography. The X-ray diffraction data showed the same crystal diffraction pattern and the crystals grown from two different solutions belong to the same space group. To unambiguously identify whether the different crystal structure and packing of the rotaxanes **1.9** and **1.17** is a consequence of polymorph formation, a more thorough investigation involving examination of numerous crystals with different sizes and shapes of the rotaxanes **1.9** and **1.17** in various growth conditions would be required. Hence this study is not conclusive, but, examination of two different crystals of the rotaxane **1.9** at least suggests that the difference in solid-state behaviour of the rotaxanes **1.9** and **1.17** is not due to formation of polymorphs.

An alternative explanation for the different crystal structures and packing of the rotaxanes **1.9** and **1.17** could be related to the energy required for the blocking group

to twist out of the plane of the axle being greater for the azobenzene based dumbbell compared to the stilbene analogue. Stilbenes and azobenzenes have different isomerisation behaviours. As described in the Introduction, stilbenes undergo photochemical *trans-cis* and *cis-trans* isomerisation, where irreversible side reactions can cause decomposition of the material.[146,147] Azobenzenes, on the other hand, undergo clean, fully reversible isomerisation. In addition, the *cis*-azobenzene can also thermally relax back to the *trans* state.[148,149] Therefore it can be speculated that a lower energy is required to twist the azobenzene from a planar, conjugated structure. As a result of weak conjugation within the azobenzene moiety, the conjugation between the azobenzene and the blocking groups may be increased. It could be that because the blocking groups are strongly conjugated to the azobenzene, the energy required to rotate the plane of the blocking group out of the plane of the azobenzene axle is greater compared to the stilbene analogue. Therefore, the rotaxane **1.17** with a stilbene based axle has one blocking group twisted out of the plane of the axle, while it is energetically unfavourable to have the blocking group of the azobenzene based rotaxane **1.9** similarly twisted out of the plane of the axle. This different twisting of the planes of the blocking groups in the crystal structures might determine the intermolecular interactions between adjacent rotaxanes, resulting in different crystal packing.

3.2 SEM and Optical Microscope Images

Having examined the crystal structures and packing of the rotaxanes **1.9**, **1.10**, **1.17** and **1.18**, the morphology of the crystals was observed using SEM and optical microscopy to examine whether there would be any relationship between crystal packing and morphology. The rotaxanes **1.17** and **1.18** were available through synthesis discussed in Chapter 2. The rotaxanes **1.9** and **1.10** were prepared according to the procedure of Maniam *et al.*,[38] for comparison of the set of all four rotaxanes. Crystals for X-ray crystallography had been grown through slow evaporation of MeOH/water. MeOH aids to dissolve rotaxanes to produce supersaturated solutions as they selectively evaporate. Hence it was thought that the crystals were effectively grown from water, however, depending on the amount of MeOH used, the speed of evaporation and crystallisation varies, resulting in crystal growth in an uncontrolled manner. Consequently, crystals for microscopy were grown from water to obtain reproducibility.

Crystals obtained by evaporating aliquots of solutions of the rotaxanes **1.9**, **1.10**, **1.17** and **1.18** were mounted on carbon tape to observe using SEM. **Figure 3.7** shows the morphology of the rotaxanes **1.9**, **1.10**, **1.17** and **1.18**. The solution of the rotaxane **1.9** gave needle shaped crystals as shown in **Figure 3.7** (a). The shapes of crystals can be determined by preferential growth along certain axes, which is governed by the kinetics of the molecular growth process through which assembly occurs.[150] Therefore, observation of needle shaped crystals suggests that there is a preferential growth along one axis of the crystal. This preferential growth can be attributed to the kinetic π–π interaction between 3,5-dimethylaniline blocking groups of the linearly aligned rotaxanes observed in the crystal packing (**Figure 1.7**). The kinetically driven π–π interaction in water is due to hydrophobic interactions of the hydrophobic blocking groups. Therefore, needle shaped crystals grown from water are reflective of the crystal packing of the rotaxane **1.9**.

The rotaxane **1.17** also results in needle shaped crystals (**Figure 3.7** (c)). Observation of needle shaped crystals again suggests that there is a preferential growth along one axis of the crystal. This preferential growth can be attributed to the linear alignment of the rotaxanes through the kinetic π–π interaction between the blocking group and a stilbene phenyl ring on the adjacent rotaxane observed in the crystal packing (**Figure 3.6**). The kinetically driven π–π interaction in water is again attributable to hydrophobic interactions of the hydrophobic blocking group and axle. Therefore, as per the rotaxane **1.9**, needle shaped crystals of the rotaxane **1.17** grown from water are consistent with its crystal packing behaviour.

Non-needle shaped crystals were obtained from the solutions of the rotaxanes **1.10** and **1.18** (**Figure 3.7** (b) and (d)). Observation of non-needle shaped crystals suggests that there is no preferential growth along one axis of the crystals. In the crystals, the rotaxanes **1.10** and **1.18**, with 2,6-dimethylaniline blocking groups, do not align along a single axis, but align in one direction, interspersed by others at right angles (**Figure 1.10** and **Figure 3.3**). Therefore, when rotaxanes do not align along a single axis, it appears that they do not adopt needle shaped morphology. Overall, observation of SEM images of crystals suggests a correlation between the linearly aligned crystal

packing of the rotaxanes **1.9** and **1.17** though π–π stacking and the morphology of needle shaped crystals. On the contrary, the rotaxanes **1.10** and **1.18** that do not show crystal packing aligned along a single axis, do not adopt needle shaped morphology. Thus, a correlation between non-linear crystal packing and non-needle shaped crystal morphology is also evident.

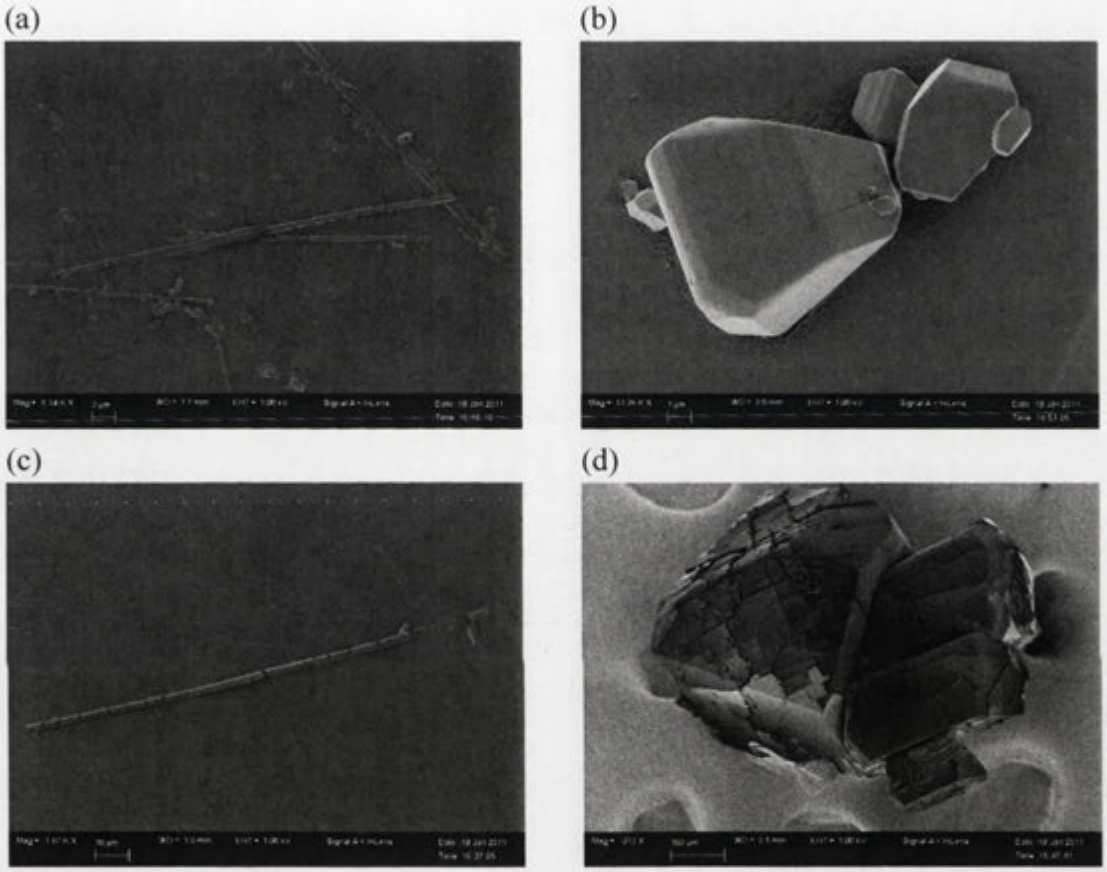

Figure 3.7. SEM images of crystals grown from solutions of (a) the rotaxane **1.9**, (b) the rotaxane **1.10**, (c) the rotaxane **1.17**, and (d) the rotaxane **1.18**.

Having observed that the needle shaped morphology seems to be related to the kinetic process of π–π interactions between adjacent rotaxanes that are linearly aligned in the solid-state, it was of interest to examine whether this initial needle shaped morphology results in continued preferential growth along one axis. Hence, the relative rates of crystal growth along the axes of the crystals of the rotaxanes **1.9** and **1.17** grown from water was monitored using an optical microscope. To prepare supersaturated solutions, each of the rotaxanes **1.9** and **1.17** was added to water, and each mixture was heated and filtered before the solutions were left to stand for days at 25 °C while being monitored under an optical microscope fitted with a polarising

lens. The polarising lens prevents unpolarised light from passing. As crystals polarise light, they are more clearly observed, as the polarised light contrasts the black background. Images of crystals from the supersaturated solutions are shown in **Figure 3.8**. In each image, an individual crystal is circled to compare the changes in crystal dimensions with time.

Over time, the solution of the rotaxane **1.9** formed yellow, needle shaped crystals. The image taken after 24 h shows a crystal circled that is 1.3 mm in length and 0.14 mm in width (**Figure 3.8** (a) left). After 54 h the crystals did not grow further. The fully grown crystal was 2.5 mm in length and 0.18 mm in width (**Figure 3.8** (a) right). The microscope view is limited to two dimensions, however, needle shaped crystals would have approximately the same height and width, as plates would not all stand on their sides. From the two dimensional view, the length of the crystal almost doubled while the width increased by less than a third. Hence, the growth is predominantly along a single axis. Therefore, the kinetic process of π–π interactions between adjacent rotaxanes that are linearly aligned in the solid-state, which determined the initial needle shaped morphology, also results in continued preferential growth along an axis.

The solution of the rotaxane **1.17** also formed yellow, needle shaped crystals. The image taken after 47 h shows a crystal circled that is 1.3 mm in length and 0.22 mm in width (**Figure 3.8** (c) left). At this point, the crystals were already almost fully grown. After 72 h the fully grown crystal was 1.4 mm in length and 0.22 mm in width (**Figure 3.8** (c) right). While the length of the crystals grew marginally, there was no apparent change in the width. However, a corresponding growth along the width is within error range and not practical to measure. Therefore, it cannot be unambiguously determined whether there is continued preference in growth along a single axis. This is not inconsistent with needle shaped crystals continuing to grow along a single axis, however, as the final shape of the crystals remained as needles.

Given that non-needle shaped morphology was observed for the rotaxanes **1.10** and **1.18** that are non-linearly aligned in the solid-state, it seemed unlikely that the non-needle shaped crystals would develop further selectively along one axis. To examine

the relative rates of crystal growth along the axes of the crystals of the rotaxanes **1.10** and **1.18**, solutions were prepared and monitored as per the rotaxanes **1.9** and **1.17**. The solution of the rotaxane **1.10** formed yellow, non-uniform shaped crystals. The shapes of the crystals varied from trapezoidal to rectangular. The image taken after 7 h shows a trapezoid shaped crystal circled that is 1.0 and 0.7 mm in length on the parallel sides, and 0.5 mm in height (**Figure 3.8** (b) left). After 50 h the crystal grew to 2.5 and 1.7 mm on the parallel sides, and 1.2 mm in height, and did not grow further (**Figure 3.8** (b) right). It was not practical to determine whether the crystals were increasing in depth, as the microscope view is limited to two dimensions. From the two dimensional view, crystal dimensions increased by approximately 2.5 times in all directions. Hence, the non-needle shaped crystal continued to show proportional growth rather than preferential growth along one axis. This is consistent with the crystal packing, where the rotaxanes align in one direction, interspersed by others at right angles (**Figure 1.10**).

The solution of the rotaxane **1.18** formed orange, non-needle shaped crystals. The shapes of the crystals varied from trapezoidal to hexagonal and triangular, amongst others. The image taken after 20 h shows a trapezoid shaped crystal that is 0.8 and 0.6 mm in length on the parallel sides, and 1.0 mm in height (**Figure 3.8** (d) left). After 45 h the crystal grew to 1.1 and 0.8 mm on the parallel sides, and 1.4 mm in height (**Figure 3.8** (d) right). Each of the crystal dimension increased by approximately 1.4 times over time. Hence, the non-needle shaped crystal also continued to show proportional growth in this case. Again, this is consistent with the crystal packing, where rotaxanes align in one direction, interspersed by others at right angles (**Figure 3.3**). Overall, when rotaxanes show alignment along a single axis in the crystal packing as per the rotaxanes **1.9** and **1.17**, needle shaped crystals form, and the crystal growth is predominantly along a single axis. When rotaxanes show alignment along two axes in the crystal packing as per the rotaxanes **1.10** and **1.18**, non-needle shaped crystals form and the crystals grow proportionally along several dimensions.

(a)

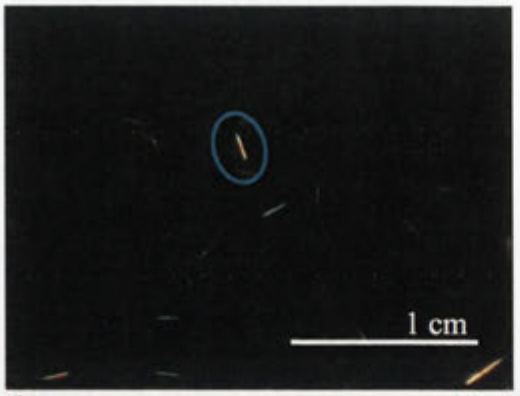

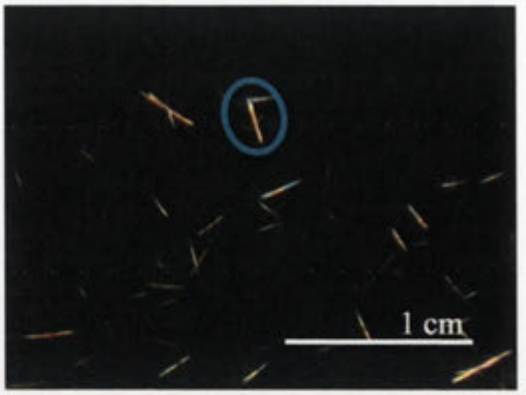

(b)

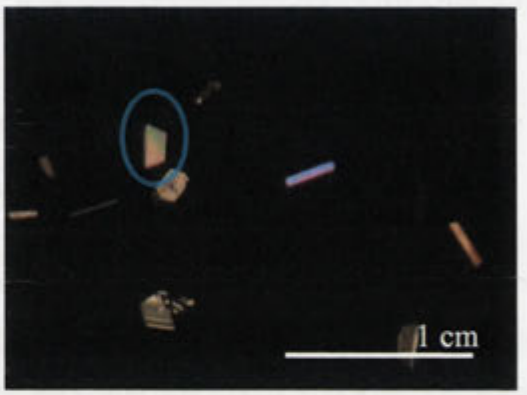

(c)

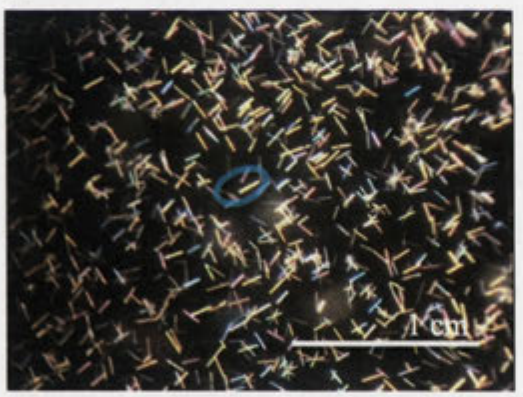

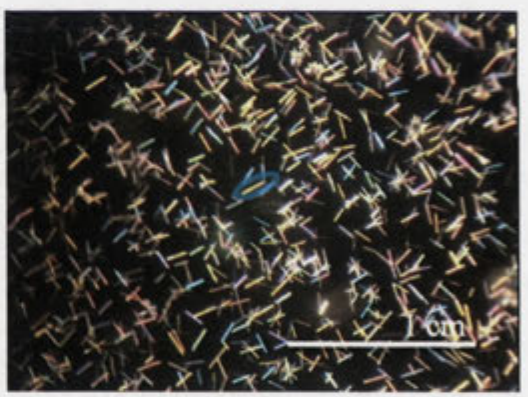

(d)

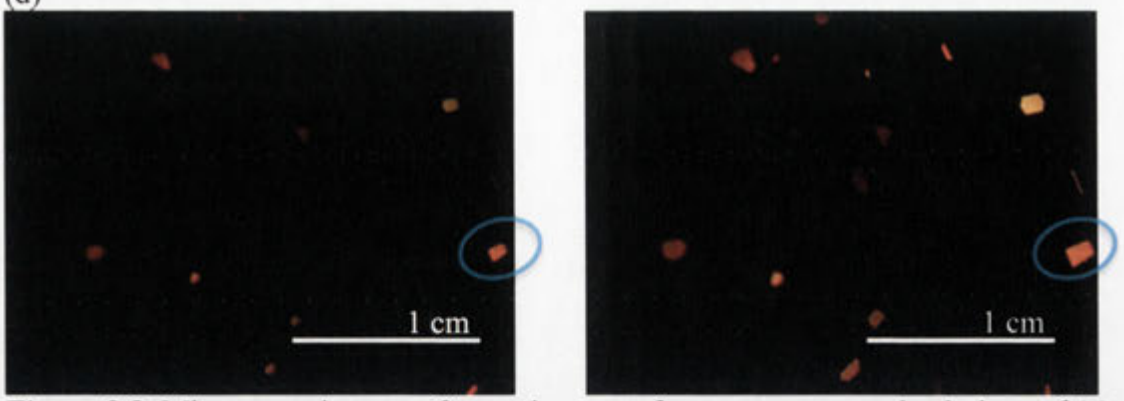

Figure 3.8. Microscope images of crystals grown from supersaturated solutions of (a) the rotaxane **1.9** after 24 h (left) and after 54 h (right), (b) the rotaxane **1.10** after 7 h (left) and after 50 h (right), (c) the rotaxane **1.17** after 47 h (left) and after 72 h (right), and (d) the rotaxane **1.18** after 20 h (left) and after 45 h (right).

3.3 Crystal Growth Behaviour

Having monitored the crystal growth in the preliminary experiments described above, the effects of varying time, temperature and concentration on crystal growth were then studied in more detail. The rotaxane **1.9** was chosen for these studies, as it shows alignment and preferential growth along one axis, and the crystal packing shows a clear correlation with the morphology and growth. These experiments were monitored using an optical microscope fitted with a polarising lens.

Firstly, the rotaxane **1.9** was added to water, and the mixture was heated below boiling point to prepare a 250 μM solution, and the solution was left to stand for days at 25 °C. In the preliminary experiments, the concentration of the supersaturated solution was unknown as the rotaxane **1.9** had been added to water, and any undissolved material after the mixture was heated had been filtered. In this study, the concentration of the supersaturated solution was known as the mixture was heated to give a clear solution, to ensure that all of the rotaxane **1.9** added was dissolved. **Figure 3.9** shows crystals of the rotaxane **1.9** grown from a 250 μM solution after 2 and 90 h respectively. At each time frame, grown crystals were uniform in size. Hence, a crystal that does not distinctively deviate from the mean size was arbitrarily chosen at both time frames and the crystal dimensions were measured. The image taken after 2 h shows crystals that are 0.23 mm in width and 0.96 mm in length (**Figure 3.9** (a)). After 90 h the crystal grew to 1.60 mm in length while the width did not grow further (**Figure 3.9** (b)). Comparing the dimensions of the crystals over

time, the length of the crystal has almost doubled while the width showed no significant growth, resulting in needle shaped crystals. Hence, this is consistent with the preliminary growth experiment, which suggests that when rotaxanes align along a single axis in the crystal packing, crystals grow preferentially along a single axis. As crystals grow longer over time, the crystal length of the rotaxane **1.9** can be manipulated by changing the duration of crystal growth.

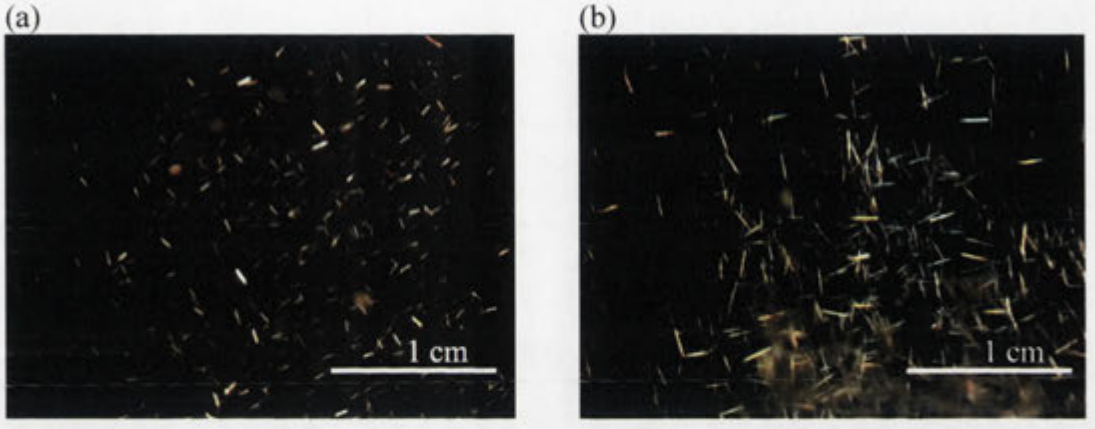

Figure 3.9. Optical microscope images of crystals grown from a 250 μM solution of the rotaxane **1.9** after (a) 2 h and (b) 90 h at 25 °C.

To investigate the effect of varying the concentration of the rotaxane **1.9** in solution on crystal growth, the rotaxane **1.9** was added to water, and the mixture was heated below boiling point to prepare a 25 μM solution, before the solution was left to stand for days at 25 °C. Crystals grown from a 25 μM solution of the rotaxane **1.9** over 90 h were compared with those grown from a 250 μM solution over 90 h (**Figure 3.10**). The crystals that are out of focus under the microscope appear thicker than those that are in focus. However, at each concentration, uniform size needles were obtained. More crystals come out of solution at higher concentration. At 25 μM, crystals come out of solution, as the solution is above saturation concentration. Therefore, the 250 μM solution has significantly more material dissolved above saturation compared to the 25 μM solution, accounting for more crystals coming out of solution. The crystals grown from the 25 μM solution of the rotaxane **1.9** are 0.23 mm in width and 0.52 mm in length (**Figure 3.10** (a)). The crystals grown from the 250 μM solution of the rotaxane **1.9** grew to 1.60 mm in length while the width did not increase (**Figure 3.10** (b)). Comparing the dimension of the crystals at two different concentrations, the widths show no significant difference, while the lengths of the crystals grown from a

250 μM solution are more than triple the length of those grown from a 25 μM solution. This suggests that at higher concentrations, crystal growth is faster and the crystals grow further. Crystals growing longer at higher concentrations is consistent with the time dependent crystal growth experiment above that shows that crystals grow longer as they grow further. Hence, the crystal length of the rotaxane **1.9** can be manipulated not only by changing the duration of crystal growth, but also by changing the concentration of the rotaxane solution.

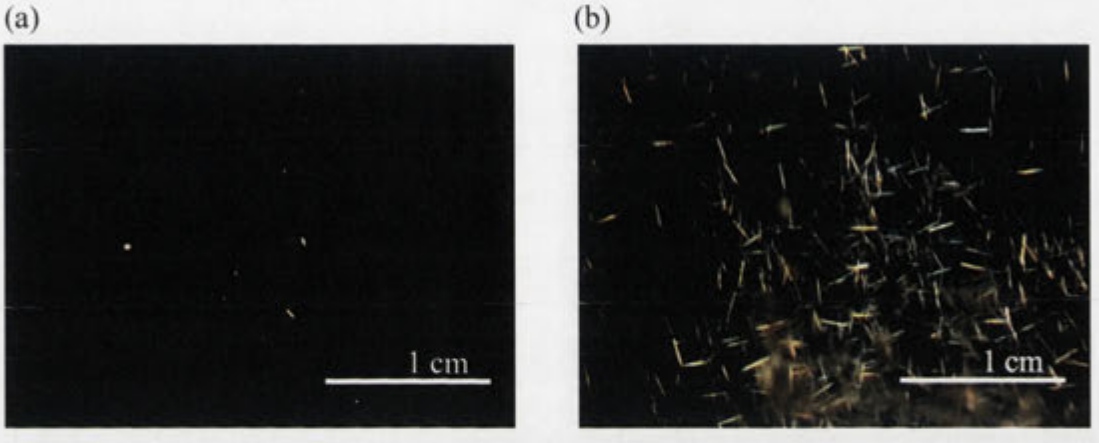

Figure 3.10. Optical microscope images of crystals grown from (a) 25 μM and (b) 250 μM solutions of the rotaxane **1.9** after 90 h at 25 °C.

To investigate the effect of varying the temperature on crystal growth, crystals were also grown from solutions of the rotaxane **1.9** (250 μM) at 4 and 18 °C. **Figure 3.11** shows microscope images of the crystals grown at 4 and 18 °C after 72 h. Crystals grown at 4 °C were monitored without a polarising lens as the crystals are too fine to be observed otherwise. The lengths of the crystals cannot be measured from the image, as the crystals are too long to see the ends. Crystals grown at 18 °C can be monitored with a polarising lens and the ends of the crystal were observed. Thus, visual inspection of the crystals shows that longer and thinner crystals are grown at the lower temperature. The crystals grown from a solution of the rotaxane **1.9** (250 μM) at 25 °C are not directly comparable to those grown at 4 and 18 °C, as at 25 °C, the solution was monitored after 90 h instead of 72 h. Nevertheless, crystals grown at 25 °C show the thickest and shortest needles, consistent with longer and thinner crystals growing at lower temperatures (**Figure 3.11** (c)). Crystals grow faster at lower temperatures resulting in kinetically favoured crystal growth. Therefore, crystals that grow longer and thinner at lower temperatures indicate that kinetically

favoured π–π interactions of the rotaxanes result in preferential growth along one axis, also seen in the time and concentration dependent crystal growth experiments above. The thickness and the length of the crystals can be controlled by varying the temperature at which the crystals are grown.

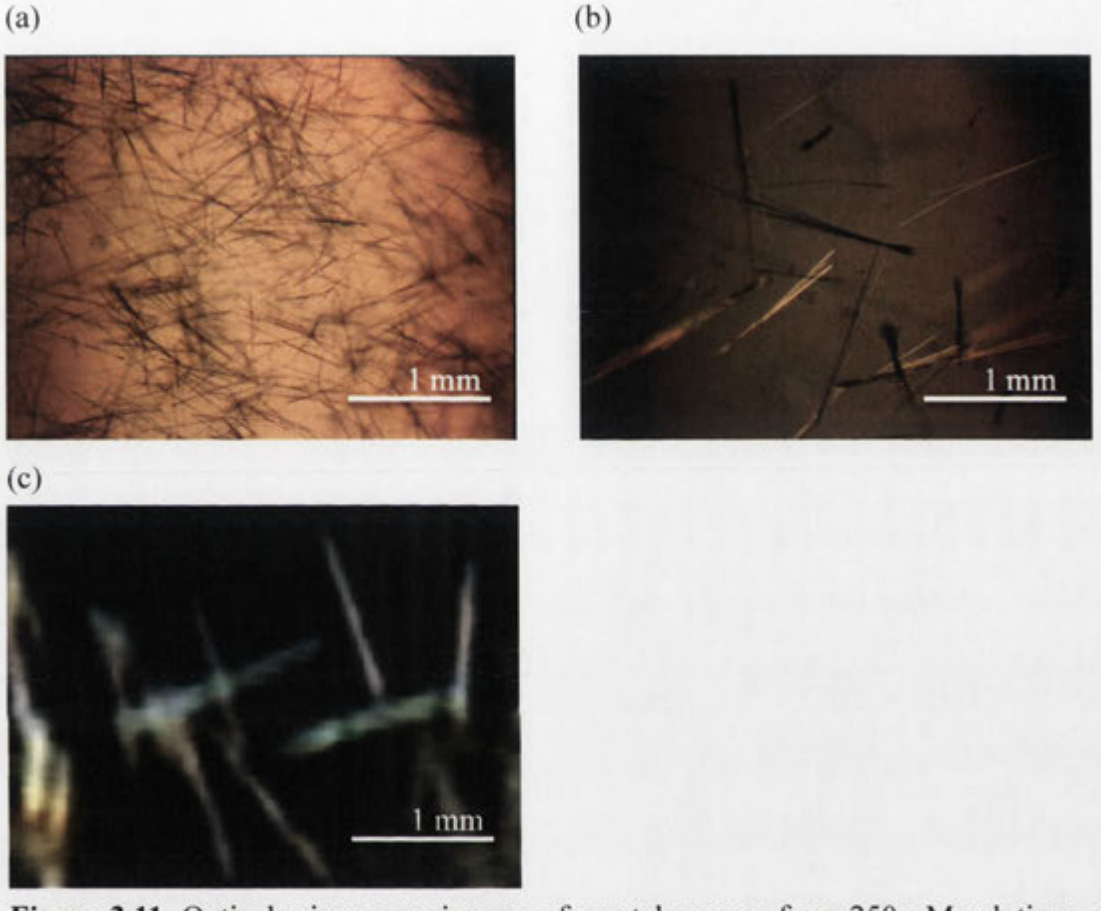

Figure 3.11. Optical microscope images of crystals grown from 250 μM solutions of the rotaxane **1.9** at (a) 4 °C (72 h), (b) 18 °C (72 h) and (c) 25 °C (90 h).

To investigate whether needle shaped crystal formation is not only kinetically favourable, but also thermodynamically favourable, needle shaped crystals of the rotaxane **1.9** were sonicated. The needle shaped crystals broke into blocks where the lengths and widths are similar and did not break further (**Figure 3.12** (b)). The mechanical vibration from sonication creates stress on the needle shaped crystals. As a result, shearing of the crystals occurs when the stress is stronger than the strength of the crystal in the direction of shearing. When shearing force is applied to long needles, the needles break along the weakest cross sections, which are initially perpendicular to the length of the crystals. The final shape of the resulting crystals reflects the thermodynamic stability of the intermolecular interactions along the

various axes of the crystals. Shearing is more likely if the interactions are weaker, and if the axis is longer and therefore, the sheer stress is larger. Shearing of the needle shaped crystals into blocks where the lengths and widths are similar indicates that the interactions between molecules are similar in strength in all directions. Accordingly, obtaining block shaped crystals suggests that crystal growth along a single axis is a kinetic process, where there is no thermodynamic preference for the crystals to grow this way. Thus, to regulate the shape and size of the crystals of the rotaxane **1.9**, regulating the conditions that affect the kinetics of the crystal growth is required.

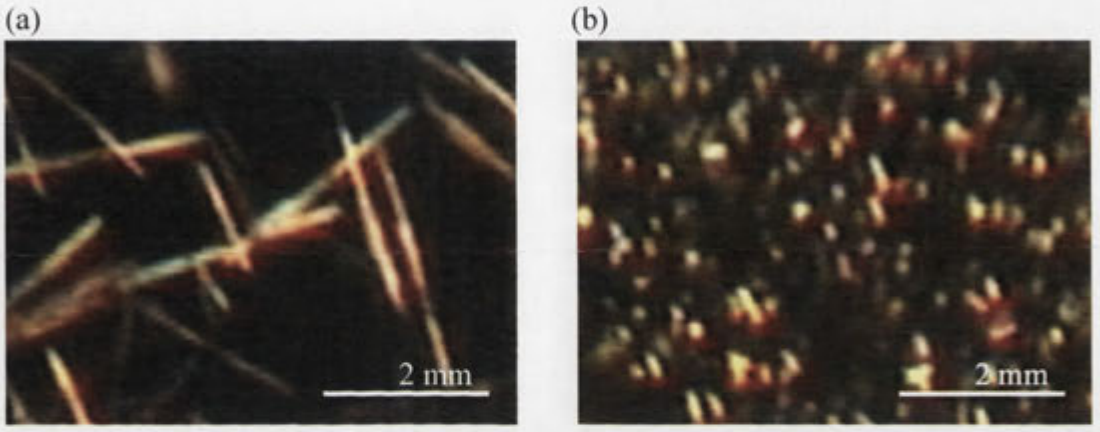

Figure 3.12. Optical microscope images of crystals grown from a solution of the rotaxane **1.9** (a) before and (b) after sonication.

3.4 Conclusion

X-Ray crystal packing of the rotaxanes **1.9**, **1.10**, **1.17** and **1.18** suggests that the blocking groups of the rotaxanes guide the self-assembly, resulting in different alignment in the solid-state depending on the choice of 2,6- or 3,5-dimethylaniline blocking groups. From SEM and optical microscope images, it can be inferred that the crystal packing of the rotaxanes **1.9**, **1.10**, **1.17** and **1.18** is reflected in the crystal growth and morphology of the crystals. Hence, crystals can be engineered to give needle or non-needle shaped crystals depending on the choice of 2,6- or 3,5-dimethylaniline blocking groups. Furthermore, the shape and size of the needle shaped crystals of the rotaxane **1.9** can be manipulated by varying the time, temperature and concentration in which the crystals are grown. Therefore, crystal engineering can be bottomed-up to make nano-molecular architectures of micrometre scale or beyond.

CHAPTER 4 - Results and Discussion
Regulation of Crystal Growth of an α-Cyclodextrin [2]Rotaxane

4.1 Introduction

Having established ways to control crystal shape and size depending on the choice of blocking groups of rotaxanes or varying the conditions of crystal growth, regulation of crystal growth was of interest. For this reason, the two unsymmetrically capped rotaxanes **4.1** and **4.2** that are structurally similar to the rotaxanes **1.9** and **1.18** were designed as crystal growth inhibitors. Each is capped with a 3,5-dimethylaniline blocking group on one end and a 2,6-dimethylaniline blocking group on the other end. From the crystal structure and packing of the rotaxane **1.9**, it was envisaged that the 3,5-dimethylaniline blocking group of the rotaxanes **4.1** and **4.2** would be co-planar to the axle, allowing incorporation to the growing chains of molecular fibres of the rotaxane **1.9** though π–π interactions. On the other hand, from the crystal structure and packing of the rotaxane **1.18**, it was envisaged that the 2,6-dimethylaniline blocking group of the rotaxanes **4.1** and **4.2** would be out-of-plane to the axle, and consequently not form π–π interactions. Hence, if one of the rotaxanes **4.1** and **4.2** was incorporated at the end of the growing molecular fibres of the rotaxane **1.9** through the 3,5-dimethylaniline blocking group, crystals might not be able to grow further as the 2,6-dimethylaniline blocking group exposed might prohibit further growth. Through co-crystallisation[151] of the rotaxanes **4.1** and/or **4.2** with the rotaxane **1.9**, the growth of the molecular fibres might therefore be regulated.

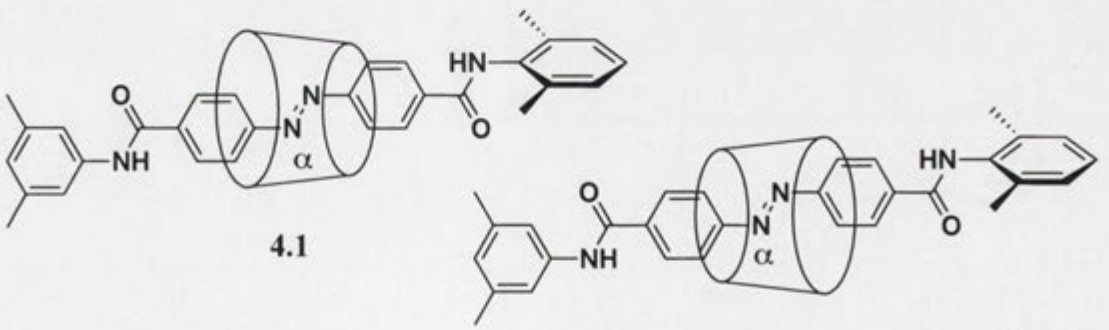

4.1

4.2

4.2 Synthesis and Conformational Analysis

In Chapter 2, a typical threading approach[152] shown in **Figure 4.1** (a) was used to prepare the rotaxanes **1.17** and **1.18**. In order to synthesise the unsymmetrically capped rotaxanes **4.1** and **4.2**, a variation of the threading approach was employed

(**Figure 4.1** (b)). Unlike the typical threading approach where the axle is threaded into the macrocycle and capped with bulky blocking groups on both ends of the axle, the variation of the threading approach involved threading a monocapped axle into the macrocycle and capping the other end of the monocapped axle with a blocking group. Depending on the reactivity of 2,6-dimethylaniline **2.4** relative to 3,5-dimethylaniline **2.2**, the synthesis of rotaxanes using a typical threading approach would result in formation of a mixture of compounds including the symmetric rotaxanes **1.9** and **1.18**. Hence the strategy was to first make a monocapped axle and then couple this with the other blocking group in the presence of α-CD **1.1** to form the unsymmetrically capped rotaxanes **4.1** and **4.2** selectively and obtain better yields. It was decided to introduce 2,6-dimethylaniline **2.4** first, as amide coupling with this more hindered aniline was expected to be less favourable in the final step. Reaction with the reactive azobenzene-4,4'-dicarbonyl dichloride **4.3** was performed in organic solvent, avoiding water which is required for association of an axle with a CD to make a rotaxane but would also hydrolyse the dicarbonyl dichloride **4.3**. 3,5-Dimethylaniline **2.2** was to be introduced to the hydrolysed monocapped axle **4.4** in water to cap the axle that had been threaded through the CD.

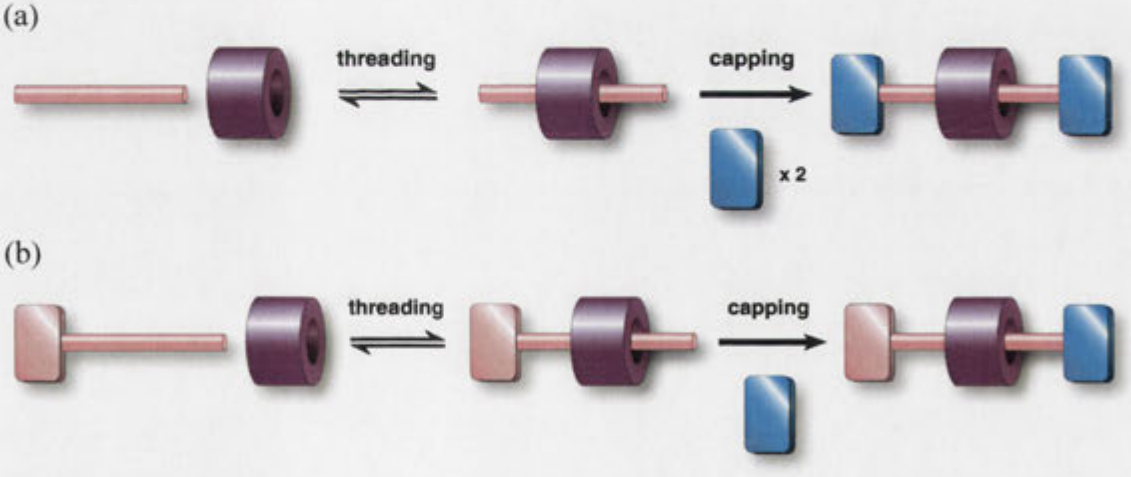

Figure 4.1. Schematic representation of (a) the typical assembly of a rotaxane *via* the threading approach and (b) a variation of the threading approach used to prepare unsymmetrically capped rotaxanes.

The monocapped axle **4.4** was therefore prepared by treating the dicarbonyl dichloride **4.3** with slightly more than one equivalent of 2,6-dimethylaniline **2.4**, followed by hydrolysis, which resulted in a mixture of azobenzene-4,4'-dicarboxylic acid **2.1**, the desired monocapped axle **4.4**, and the dicapped axle **4.5** (**Scheme 4.1**). The

monoamide **4.4** was isolated using column chromatography on silica gel in 42% yield and its mass spectrum showed a molecular ion with *m/z* 373. The ^{1}H NMR spectrum showed the presence of aniline protons and protons corresponding to an unsymmetrically substituted azobenzene, confirming the formation of the desired product **4.4**.

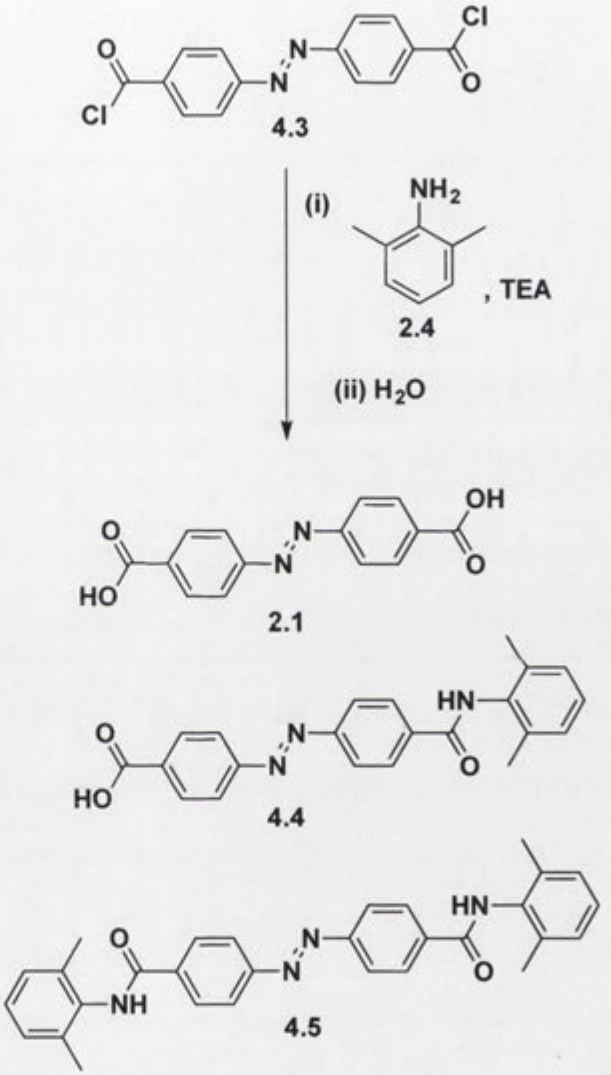

Scheme 4.1. Synthesis of the monocapped azobenzene **4.4**.

With the monocapped azobenzene **4.4** in hand, the unsymmetrically capped rotaxanes **4.1** and **4.2** were prepared according to **Scheme 4.2**. The monocapped azobenzene **4.4** was equilibrated with excess α-CD **1.1** and slightly more than one equivalent of TEA in water for the inclusion complexes **4.6** and **4.7** to form. Four molar equivalents of DMT-MM and three molar equivalents of 3,5-dimethylaniline **2.2** were then added and the progress of the reaction was monitored using TLC. A new spot was detected

that showed both the characteristic UV absorbance of the axle component and the pink colouration of a CD when treated with acidic naphthalene-1,3-diol.[138] Another four molar equivalents of DMT-MM and three molar equivalents of 3,5-dimethylaniline **2.2** were then added as the TLC showed the reaction was incomplete, presumably due to DMT-MM hydrolysis. Although only one new spot was detected by TLC, two components that presumably co-eluted on TLC were separated by HPLC in yields of 34% and 22%. MALDI-TOF mass spectrometry of each component showed an ion at *m/z* 1450 which corresponds to the protonated ion of the rotaxanes **4.1** and **4.2**. The rotaxanes **4.1** and **4.2** are isomers due to the orientation of the CD annulus, thus a single synthetic procedure yields two rotaxanes at the same time.

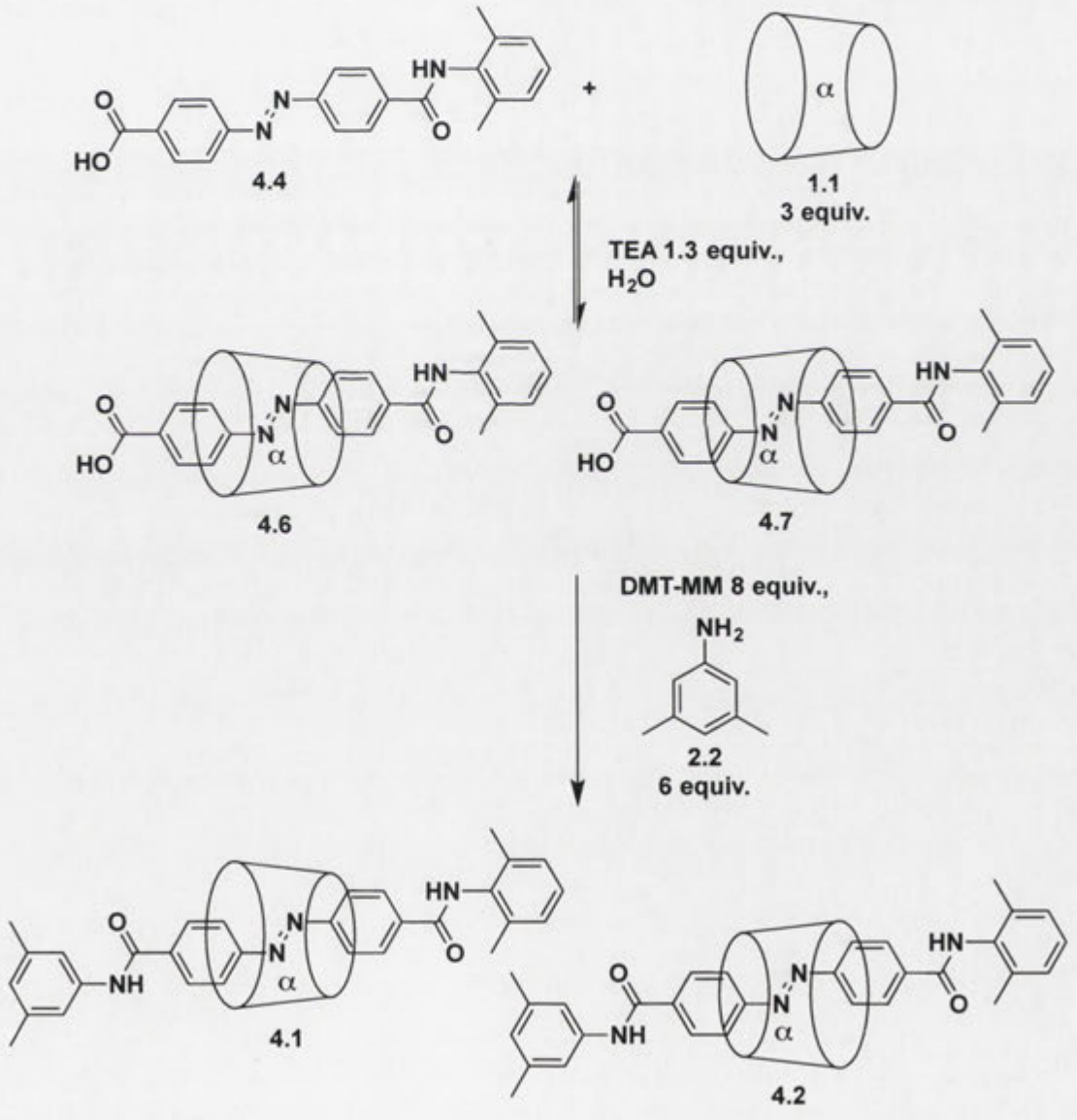

Scheme 4.2. Synthesis of the unsymmetrically capped [2]rotaxanes **4.1** and **4.2**.

Two fractions, each containing an unsymmetrically capped rotaxane isomer, were

collected through HPLC. The first eluting fraction was assigned as the rotaxane **4.1** and the later fraction as the rotaxane **4.2** by NMR analysis described below. The 1D ^{1}H NMR spectrum of the first eluting fraction confirms the presence of the components of an unsymmetrically capped rotaxane, showing resonances of CD, unsymmetrically substituted azobenzene and arylamino protons (**Figure 4.2**). The apparent singlet at δ7.17 which integrates for three protons indicates that the protons in the 3-, 4- and 5-positions of the 2,6-dimethylaniline group resonate at the same frequency, not giving rise to coupling, as observed in the ^{1}H NMR spectrum of the monocapped axle **4.4**. The singlet observed at δ6.87 integrates for one proton and corresponds to the *para*-proton of the 3,5-dimethylaniline group. The singlet observed at δ7.45 which integrates for two protons indicates that the 2- and 6-positions of the 3,5-dimethylaniline group are chemically equivalent, presumably due to rotation around the aryl group to nitrogen bond on the NMR time scale at 25 °C. Accordingly, the two sets of singlets at δ2.35 and 2.31 can be assigned one each to the methyl groups of the 2,6- and 3,5-dimethylaniline groups, as the methyl groups within the same blocking group are likely to be chemically equivalent.

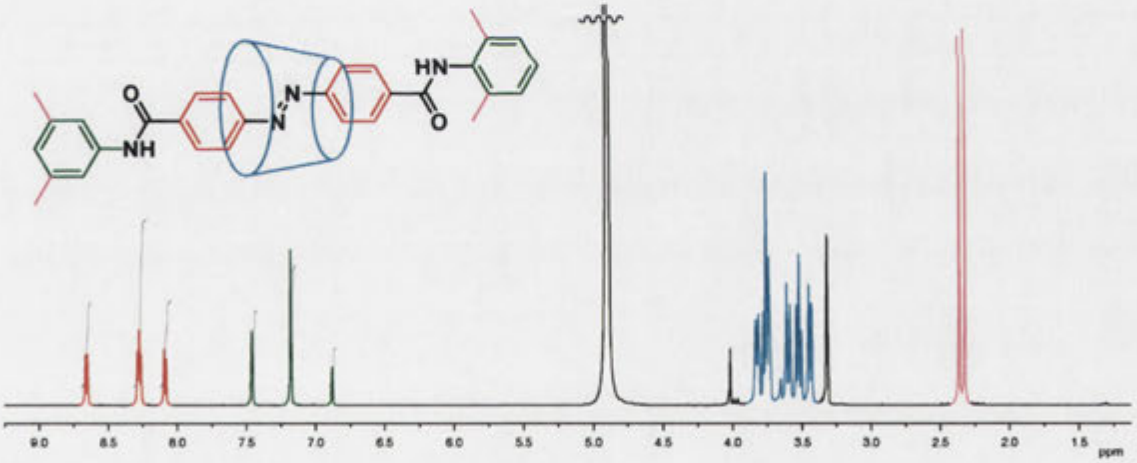

Figure 4.2. 500 MHz ^{1}H NMR spectrum of the rotaxane **4.1** in CD_3OD.

To unambiguously determine the orientation of the CDs with respect to the dumbbells and assign the structures of the rotaxane isomers, 2D NMR analysis was carried out following the general protocol used in Chapter 2. **Figure 4.3** shows a section of the DQF-COSY NMR spectrum of the first eluting isomer, where CD proton cross-peaks are found. While the region of the spectrum where the C1 protons' resonance is typically found is obscured by the OH signal, a ^{1}H-^{1}H correlation between these

protons and those giving rise to the signal at δ3.42 is seen, and the latter is therefore assigned to the CD-C2 protons. Likewise, there is a cross-peak between the resonance at δ3.42 (CD-C2) and the resonance at δ3.77 which is therefore attributed to the CD-C3 protons. This resonance at δ3.77 (CD-C3) also shows a cross-peak with the resonance at δ3.50, which is therefore assigned to the CD-C4 protons. Again, the resonance at δ3.50 (CD-C4) also shows a cross-peak with the resonance at δ3.83 which is therefore assigned to the CD-C5 protons. Finally, the resonances at both δ3.72 and 3.59 corresponding to the CD-C6 protons show cross-peaks with each other.

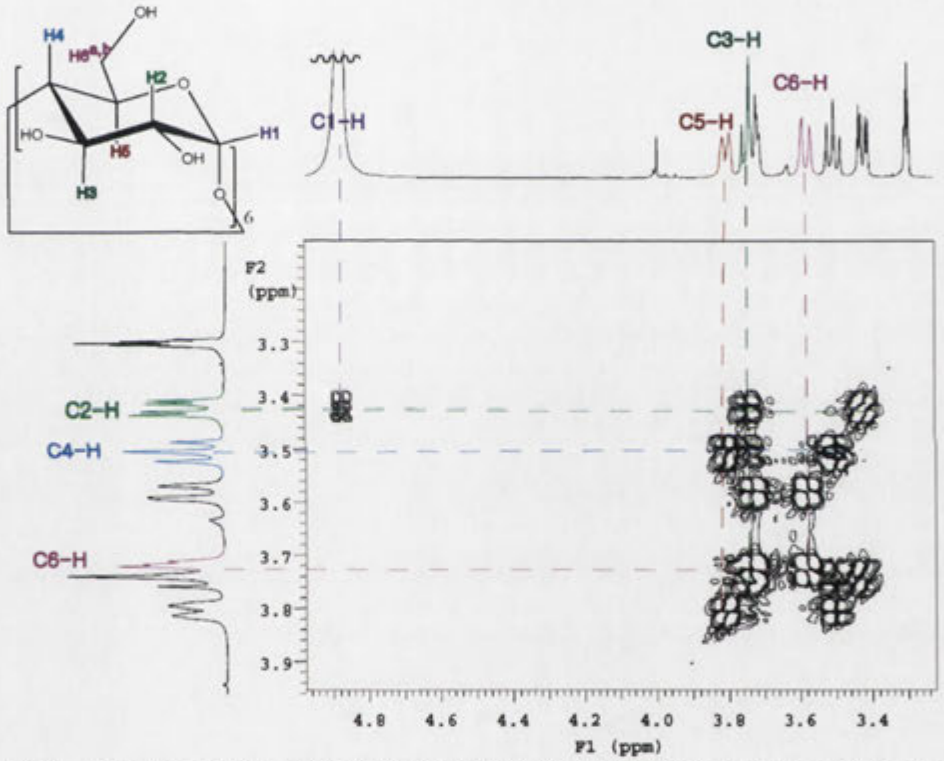

Figure 4.3. A section of the 500 MHz 2D DQF-COSY NMR spectrum of the rotaxane **4.1** in CD_3OD showing cross-peaks between CD proton signals.

Figure 4.4 shows a section of the 2D ROESY NMR spectrum with axle and aniline aromatic proton resonance cross-peaks with those of methyl and CD protons. The presence of the NOE cross-peak labelled NOE1 between the resonance of the 2,6-dimethylaniline aromatic protons and the resonance at δ2.31 shows that the latter corresponds to the methyls of the 2,6-dimethylaniline group (protons H). Likewise, the NOE cross-peaks labelled NOE2 and NOE3 between the resonances of the 3,5-dimethylaniline aromatic protons and the resonance at δ2.35 indicate that the latter corresponds to the methyls of the 3,5-dimethylaniline moiety (protons B). The NOE

cross-peak labelled NOE4 indicates that the azobenzene protons G are in proximity to the 2,6-dimethylaniline methyl protons H. Protons G show coupling with protons F, and protons D and E with each other. Hence protons G and F are assigned to one phenyl group of the azobenzene and protons D and E to the other. Protons E and F are located next to the centre of the azobenzene moiety as they both show extensive NOEs with the CD-C5 protons. Protons E also show an NOE with the CD-C3 protons while protons F show NOEs with both of the CD-C6 protons. Thus, localisation of the CD over the middle of the azobenzene is observed where the narrow end of the CD corresponding to the CD-C6 OH groups is closest to the 2,6-dimethylaniline blocking group. This structure is therefore assigned as the rotaxane **4.1**.

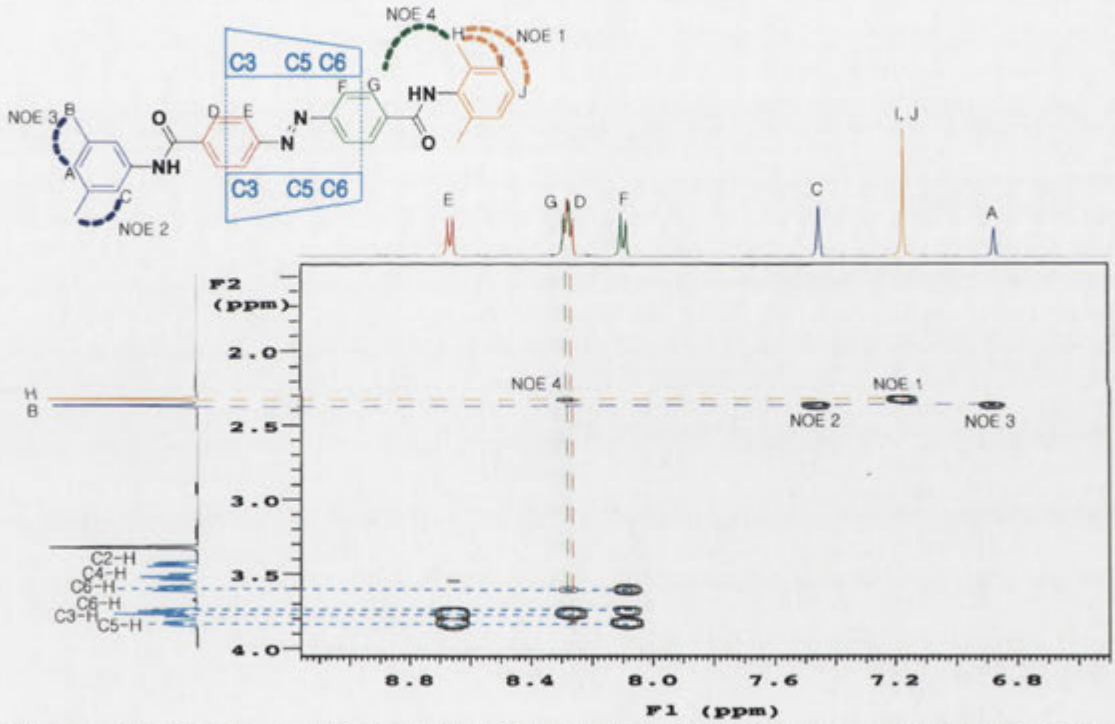

Figure 4.4. A section of the 500 MHz 2D ROESY NMR spectrum of the rotaxane **4.1** in CD_3OD showing azobenzene and aniline aromatic proton resonance cross-peaks with those of methyl and CD protons.

Figure 4.5 shows the ^1H NMR spectrum of the second eluting fraction collected from the HPLC. Similar to the case of the rotaxane **4.1**, the NMR spectrum confirmed the presence of the rotaxane components, showing resonances of CD, azobenzene and aniline protons. Also as per the rotaxane **4.1**, the general protocol was followed to determine the orientation of the CD and the conformation of this rotaxane.

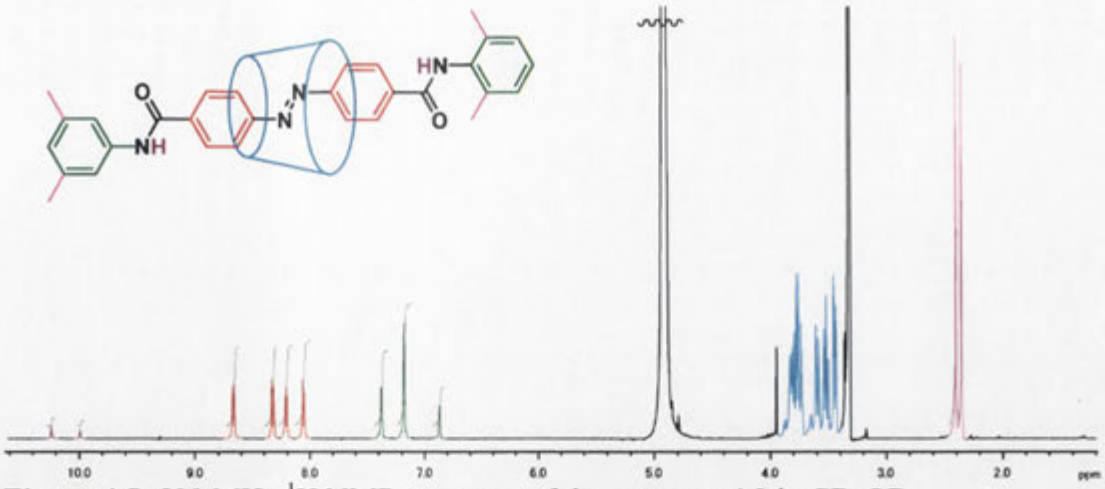

Figure 4.5. 500 MHz ^{1}H NMR spectrum of the rotaxane **4.2** in CD_3OD.

The CD proton resonances were assigned in the same manner as per the rotaxane **4.1**. **Figure 4.6** shows a section of the DQF-COSY NMR spectrum, where CD proton cross-peaks are found. While the region of the spectrum where the C1 protons' resonance is typically observed is obscured by the OH signal, a ^{1}H-^{1}H correlation between protons in this region and those giving rise to the signal at δ3.43 is seen, and the latter is therefore assigned to the CD-C2 protons. Likewise, there is a cross-peak between the resonance at δ3.43 (CD-C2) and a resonance at δ3.77 which is therefore attributed to the CD-C3 protons. This resonance at δ3.77 (CD-C3) also shows a cross-peak with the resonance at δ3.51, which is therefore assigned to the CD-C4 protons. Again, the resonance at δ3.51 (CD-C4) also shows a cross-peak with the resonance at δ3.81 which is therefore assigned to the CD-C5 protons. Finally, the resonances at both δ3.74 and 3.59 corresponding to the CD-C6 protons show cross-peaks with each other.

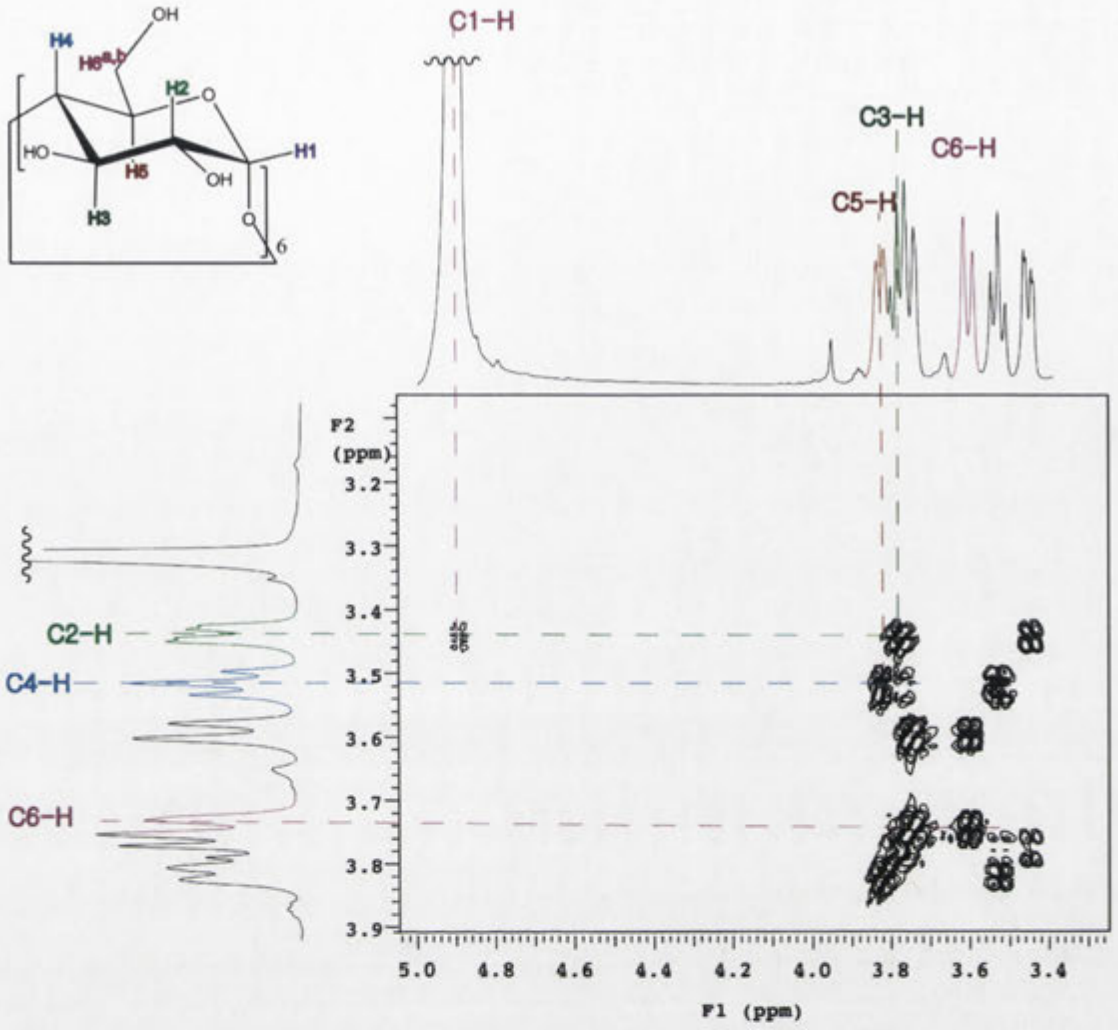

Figure 4.6. A section of the 500 MHz 2D DQF-COSY NMR spectrum of the rotaxane **4.2** in CD_3OD showing cross-peaks between CD proton signals.

Figure 4.7 shows a section of the 2D ROESY NMR spectrum with axle and aniline aromatic proton resonance cross-peaks with those of methyl and CD protons. The presence of the NOE cross-peak labelled NOE1 between the resonance of the 2,6-dimethylaniline aromatic protons and the resonance at δ2.39 shows that the latter corresponds to the methyls of the 2,6-dimethylaniline group (protons H). Likewise, the NOE cross-peaks labelled NOE2 and NOE3 between the resonances of the 3,5-dimethylaniline aromatic protons and the resonance at δ2.34 indicate that the latter corresponds to the methyls of the 3,5-dimethylaniline group (protons B). Protons G show coupling with protons F, and protons D and E with each other. Hence protons G and F are assigned to one phenyl group of the azobenzene and protons D and E to another. Looking at the cross-peaks between the aromatic and CD protons, the location of the CD along the azobenzene axle can be assigned. Protons E show NOEs

with both the CD-C6 protons, hence they are next to the narrow end of the CD. Protons F and G both have strong NOE interactions with the CD-C3 protons, located on the wider end of the CD. Azobenzene protons G are in proximity to the 2,6-dimethylaniline methyl protons H as shown by the cross-peak labelled NOE4. There is no NOE interaction between CD protons and protons D. Thus, localisation of the CD towards one end of the azobenzene dumbbell unit is observed where the wider end of the CD is closest to the 2,6-dimethylaniline blocking group as shown in **Figure 4.7**. This confirms that the structure corresponds to the rotaxane **4.2**.

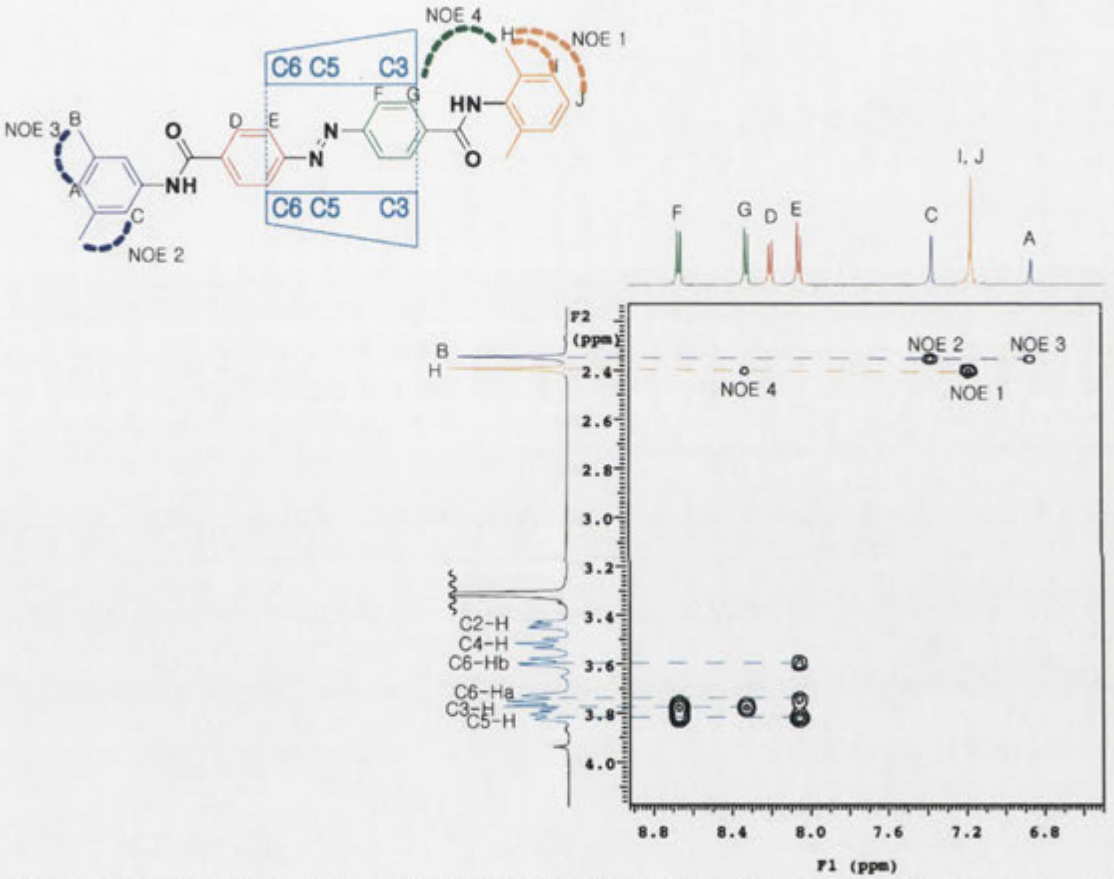

Figure 4.7. A section of the 500 MHz 2D ROESY NMR spectrum of the rotaxane **4.2** in CD_3OD showing azobenzene and aniline aromatic proton resonance cross-peaks with those of methyl and CD protons.

4.3 X-Ray Crystallographic Analysis of Unsymmetrically Capped [2]Rotaxanes

Having obtained the purposely designed rotaxanes **4.1** and **4.2**, the crystal structures were studied to examine whether the planarity of the blocking groups with respect to the azobenzene axles was as predicted. Crystallisation of the rotaxanes **4.1** and **4.2** required longer times and was found to be significantly more difficult compared to that of the rotaxane **1.9**. After a number of attempts, crystals of the rotaxanes **4.1** and **4.2** were obtained through slow evaporation of MeOH/water over a period of several

weeks. The solid-state structures of the rotaxanes **4.1** and **4.2** were examined using X-ray crystallography. The crystallographic data of the rotaxanes **4.1** and **4.2** are presented in Appendix 1.

Crystals of the rotaxane **4.1** belong to the orthorhombic space group and have four molecules per unit cell. The crystal structure shows that the 3,5-dimethylaniline blocking group is twisted roughly 45° to the closest ring of the azobenzene moiety, whereas the 2,6-dimethylaniline blocking group is twisted approximately 90° to the closest ring of the azobenzene moiety (**Figure 4.8**). The crystal packing of the rotaxane **4.1** reveals a highly ordered structure where the CDs are all aligned head-to-tail along a single axis (**Figure 4.9**). Alternating pairs of rows of the CDs face opposite directions giving rise to centrosymmetric, non-polar crystals. Hydrogen bonding interactions of CDs in the neighbouring rows are observed. Twisting of the 3,5-dimethylaniline blocking group 45° out-of-plane of the azobenzene suggests that unlike the rotaxane **1.9**, the crystal packing interactions do not allow the 3,5-dimethylaniline blocking group to be in the same plane as the azobenzene. As this geometry may be caused by crystal packing, studying the conformation in solution was required to determine whether the expected planarity of the blocking groups with respect to the azobenzene axle of the rotaxane **4.1** was likely to be suitable for the rotaxane **4.1** to co-crystallise with the rotaxane **1.9**, and consequently inhibit the crystal growth of the rotaxane **1.9**.

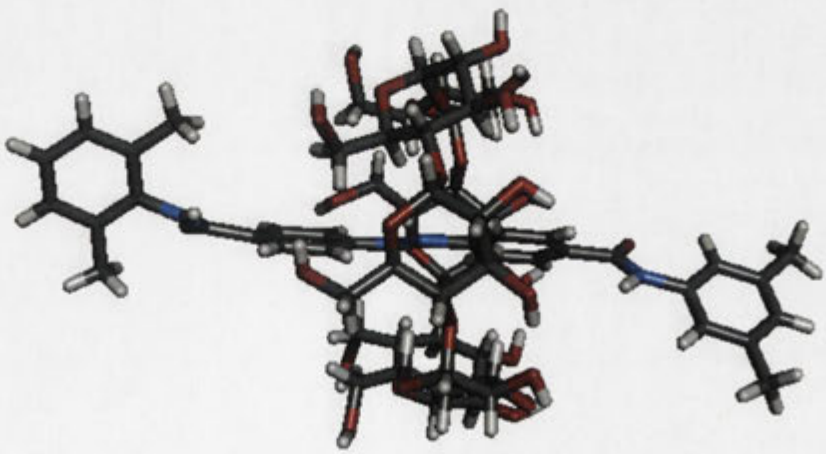

Figure 4.8. Crystal structure of the rotaxane **4.1** displayed in stick style. Solvent molecules are removed for clarity. Black = carbon, white = hydrogen, blue = nitrogen and red = oxygen.

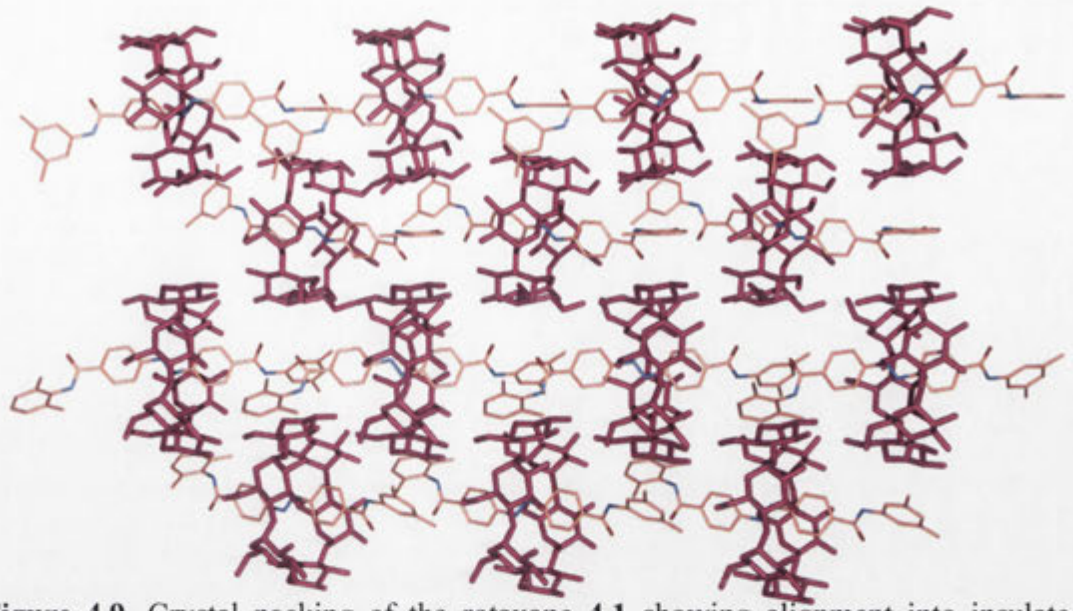

Figure 4.9. Crystal packing of the rotaxane **4.1** showing alignment into insulated molecular fibres. Displayed in stick style. Hydrogen atoms and solvent molecules are removed for clarity.

In contrast to those of the rotaxane **4.1**, crystals of the rotaxane **4.2** belong to the monoclinic space group and have two molecules per unit cell. The crystal structure shows an unusual bend in the dumbbell (**Figure 4.10**). The 3,5-dimethylaniline blocking group is twisted roughly 30° from the plane of the azobenzene moiety, whereas, the 2,6-dimethylaniline blocking group is twisted approximately 90° from the plane of the azobenzene moiety, comparable to the features of the rotaxane **4.1**. The crystal packing of the rotaxane **4.2** also shows the CDs aligned head-to-tail along each row (**Figure 4.11**). Every alternating row of the CDs faces the opposite direction, giving rise to centrosymmetric, non-polar crystals. Hydrogen bonding interactions of CDs in the neighbouring rows are observed. Twisting of the 3,5-dimethylaniline blocking group 30° out-of-plane of the azobenzene suggests that like the rotaxane **4.1**, the crystal packing interactions do not allow the 3,5-dimethylaniline blocking group to be in the same plane as the azobenzene in the solid-state. The solid-state conformation is not necessarily the same as that in solution. Therefore, studying the conformation in solution was also required to determine whether the expected planarity of the blocking groups with respect to the azobenzene axle of the rotaxane **4.2** was again likely to be suitable for the rotaxane **4.2** to co-crystallise with the rotaxane **1.9**, and consequently inhibit the crystal growth of the rotaxane **1.9**.

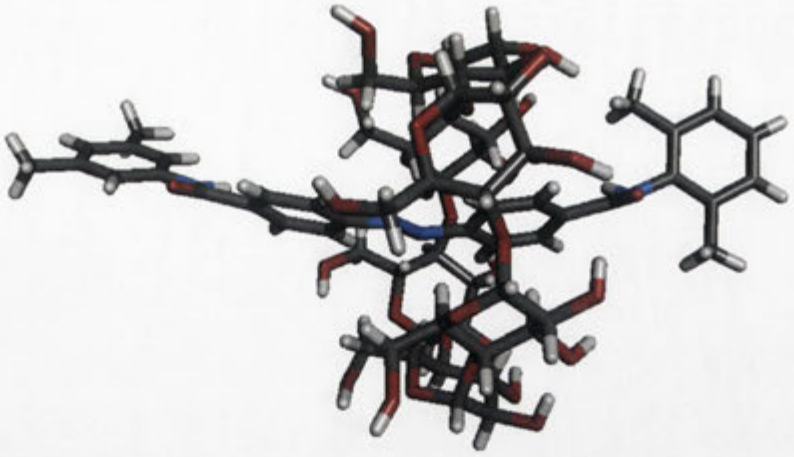

Figure 4.10. Crystal structure of the rotaxane **4.2** displayed in stick style. Solvent molecules are removed for clarity. Black = carbon, white = hydrogen, blue = nitrogen and red = oxygen.

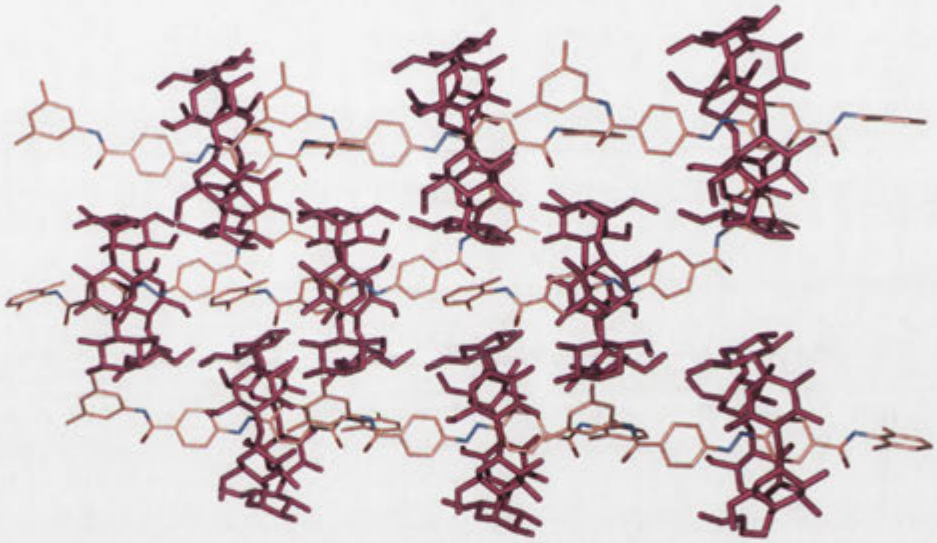

Figure 4.11. Crystal packing of the rotaxane **4.2** showing alignment into insulated molecular fibres. Displayed in stick style. Hydrogen atoms and solvent molecules are removed for clarity.

4.4 Conformational Analysis of Unsymmetrically Capped [2]Rotaxanes in Solution

Having examined the solid-state structures of the rotaxanes **1.9** and **1.18** in the work reported in Chapter 3 and the rotaxanes **4.1** and **4.2** as described above, it was apparent that unlike the rotaxane **1.9**, the crystal packing interactions of the rotaxanes **4.1** and **4.2** do not allow the 3,5-dimethylaniline blocking group to be in the same plane as the axle. However, whether co-crystallisation can occur or not is more dependent on the conformation of rotaxanes in solution rather than the solid-state. The solution conformations are the lowest energy conformations the rotaxanes would prefer to adopt in the absence of any long range structural order. Therefore, to study

the conformations of the unsymmetrically capped rotaxanes **4.1** and **4.2** in comparison to those of the analogous symmetrically capped rotaxanes **1.9** and **1.18** in solution, the absorbance spectra of the set of rotaxanes **1.9**, **1.18**, **4.1** and **4.2** in solution were obtained. Each of the rotaxanes **1.9**, **1.18**, **4.1** and **4.2** was dissolved in water and the absorbance of each solution was measured using a UV/visible spectrometer. The molar extinction coefficients of the rotaxanes **1.9**, **1.18**, **4.1** and **4.2** are similar. Nevertheless, concentrations of the rotaxanes **1.9**, **1.18**, **4.1** and **4.2** were not measured accurately given the small quantities that were weighed. Hence the UV/visible spectra were adjusted to about the same absorbance near 350 nm and overlaid for the convenience of comparison (**Figure 4.12**). The rotaxane **1.9** has the longest absorption wavelength with a λ_{max} at 352 nm. The absorbance spectra of the unsymmetrically capped rotaxanes **4.1** and **4.2** are blue shifted to a shorter wavelength (λ_{max} = 346 nm). Finally, the absorbance spectrum of the rotaxane **1.18** is further blue shifted (λ_{max} = 340 nm). The longest absorption wavelength of the rotaxane **1.9** suggests that this rotaxane has the highest degree of conjugation and that the dumbbell is therefore fully co-planar, while the rotaxanes **4.1** and **4.2** are less conjugated with one of the blocking groups twisted out of the plane of the azobenzene. Finally, the spectrum of the rotaxane **1.18**, which is most blue shifted, suggests that the rotaxane **1.18** has the lowest degree of conjugation and that the blocking groups on both ends are twisted out of the plane of the azobenzene.

Although the solid-state structures of the rotaxanes **4.1** and **4.2** have the 3,5-dimethylaniline blocking group twisted out-of-plane of the azobenzene, the conformational analysis of the rotaxanes **4.1** and **4.2** in solution suggests that the 3,5-dimethylaniline blocking group is co-planar to the azobenzene in this phase. This supports the suggestion made above that the solid-state conformations are likely to be affected by crystal packing interactions, and are not a reflection of the conformations in solution. Given the apparent planarity of the 3,5-dimethylaniline blocking groups with respect to the azobenzene axles of the rotaxanes **4.1** and **4.2** in solution, the rotaxanes **4.1** and **4.2** met the design criteria to test the hypothesis outlined at the beginning of this Chapter that co-crystallisation of the rotaxanes **4.1** and/or **4.2** with the rotaxane **1.9** might result in inhibition of crystal growth.

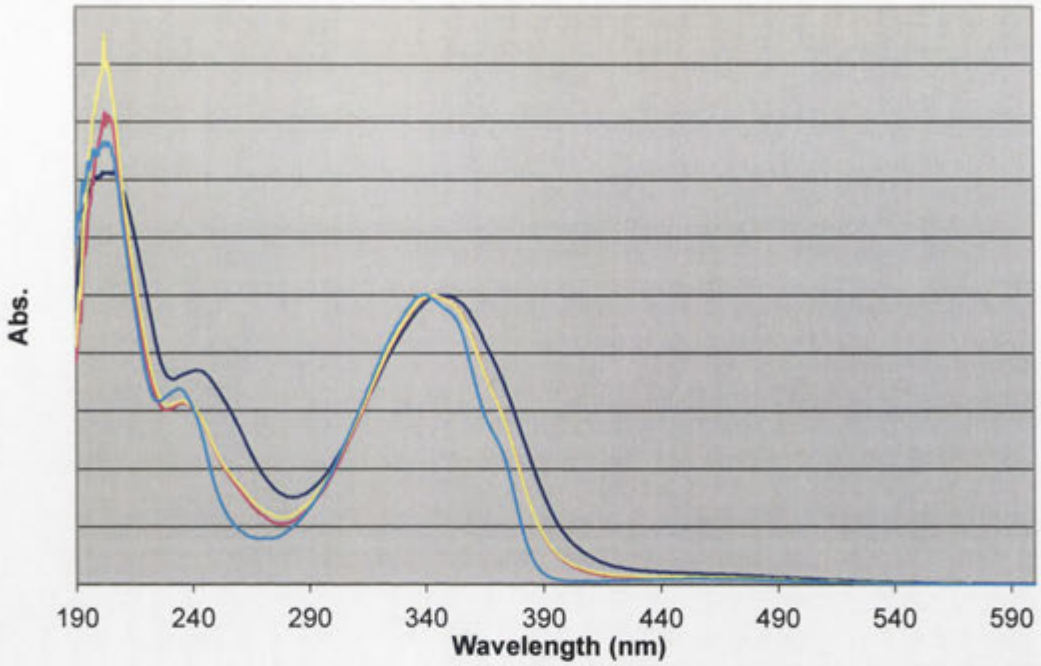

Figure 4.12. Overlay of UV/visible spectra of solutions of the rotaxane **1.9** (dark blue), the rotaxane **4.1** (pink), the rotaxane **4.2** (yellow) and the rotaxane **1.18** (skyblue) in water.

4.5 Attempted Preparation of Amorphous Solids of α-Cyclodextrin [2]Rotaxanes

For co-crystallisation of the rotaxane **1.9** with the rotaxanes **4.1** and/or **4.2**, preparation of supersaturated solutions of these compounds was required. In the work described in Chapter 3, solutions of the rotaxanes **1.9**, **1.10**, **1.17** and **1.18** were prepared by adding each compound to water and heating the mixtures, then leaving them to stand. Crystals came out of solution indicating that the solutions were saturated, however, more of the rotaxanes **1.9**, **1.10**, **1.17** and **1.18** dissolved, as observed by UV/visible spectroscopy in each case, when more solid compound was added. Amorphous solids are potentially more soluble than their crystalline forms, forming metastable highly supersaturated solutions, which can cause precipitation or nucleation followed by growth of crystals with higher crystal lattice energies.[153,154] Hence the rotaxanes **1.9**, **1.10**, **1.17** and **1.18** were thought to be mixtures of crystalline and amorphous forms, and the amorphous forms continued to dissolve in solutions already saturated with respect to the crystalline forms. Using amorphous materials is a useful way to prepare solutions supersaturated with respect to the crystalline forms of those materials. However, when a mixture of crystalline and amorphous solids dissolves, seed crystals that are invisible to the naked eye may remain, affecting crystallisation in an unpredictable and irregular

manner. Consequently, a method to prepare completely amorphous solids was sought in order to prepare homogeneous supersaturated solutions, required for reliable and reproducible crystal growth regulation studies. Experiments were carried out with the rotaxanes **1.9**, **1.10**, **1.17** and **1.18**. Those using the rotaxane **1.9** are described below but similar results were obtained with the other compounds.

In an attempt to prepare amorphous material, the rotaxane **1.9** was dissolved in MeOH and the solvent was removed using a rotary evaporator. Although the solvent was removed rapidly, crystallisation during evaporation of the solvent was not eliminated. Subsequently, the rotaxane **1.9** was added to water to make up a 5 μM solution, which was then lyophilised. As shown on the following pages, a 5 μM solution is below saturation with respect to the crystalline form, so it is reasonable to expect all the rotaxane **1.9** dissolved. Even so, SEM images showed that this attempt gave a solid that was a mixture of crystalline and amorphous material as shown in **Figure 4.13** (a). Lyophilisation involves freezing the solution and applying vacuum such that sublimation occurs. Sublimation proceeds without the solution phase where material can dissolve and re-orient for crystallisation to occur. Observation of a mixture of crystalline and amorphous solids suggests that perfect sublimation does not occur during lyophilisation, but that the frozen mixture partially melts at least locally, allowing crystallisation to occur.

In a further attempt, the rotaxane **1.9** was added to a MeOH/water solution to make up a 5 μM solution. MeOH was removed using a rotary evaporator, and the resulting solution was lyophilised. This attempt also gave a solid that was a mixture of crystalline and amorphous forms as shown in **Figure 4.13** (b). The rotaxane **1.9** is significantly more soluble in MeOH compared to water. However, preparation of an amorphous solid by dissolving the rotaxane **1.9** in a MeOH/water mixture initially to ensure dissolution of any crystals was unsuccessful.

In another attempt to ensure that the rotaxane **1.9** was fully dissolved in solution before lyophilisation, the rotaxane **1.9** dissolved in MeOH was added dropwise to water to make up a 5 μM solution. As a precaution, that solution was filtered through a 0.45 μm pore membrane filter. The resulting solution was reduced to remove MeOH

using a rotary evaporator and lyophilised, but again, the solid obtained was partially crystalline (**Figure 4.13** (c)). The SEM image shows that the crystals have a width of around 0.36 μm, which means that they would pass through a 0.45 μm membrane filter. Hence even filtration does not guarantee the absence of seed crystals.

In yet a further attempt to prepare amorphous material, the rotaxane **1.9** was added to *t*-BuOH/water co-solvent systems (3% *t*-BuOH, 10% *t*-BuOH) to make up 5 μM solutions, and each solution was lyophilised. Preparation of amorphous complexes of hydroxypropyl-β-CD by lyophilisation from a *t*-BuOH system has been reported previously.[155,156] *t*-BuOH is known to be an ideal freeze-drying medium as it is an organic solvent that is miscible with water, has a high freezing point and vapour pressure, and alters the crystal habit of ice to aid the sublimation process.[157] Accordingly a *t*-BuOH/water co-solvent system has been reported to produce porous powder forms.[158,159] Even so, this process did not eliminate crystals, as a mixture of amorphous and crystalline material was obtained as shown in **Figure 4.13** (d). As obtaining purely amorphous materials was found to be difficult, an alternative method to prepare supersaturated solutions was required.

(a)

(b)

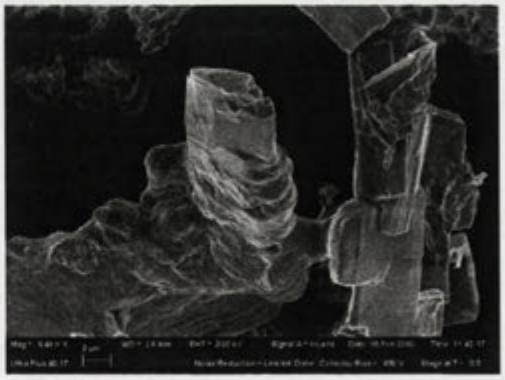

(c)

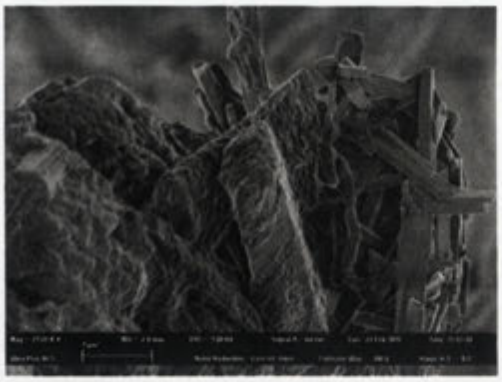

(d)

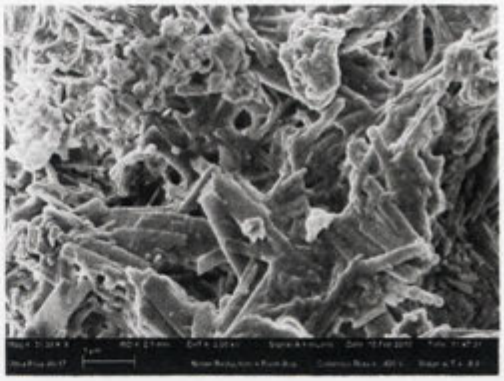

Figure 4.13. SEM images of samples of the rotaxane **1.9** showing mixtures of crystalline and amorphous forms obtained by lyophilisation of (a) a 5 μM aqueous solution, (b) a 5 μM MeOH/water solution after MeOH had evaporated, (c) a filtered 5 μM MeOH/water solution after MeOH had evaporated and (d) a 5 μM 3% *t*-BuOH/water solution.

4.6 Determination of the Solubility of α-Cyclodextrin [2]Rotaxanes

Due to the difficulty in preparing amorphous solids, a more conventional method was used to prepare supersaturated solutions, which involved heating, for reliablity and reproduciblity in crystal growth regulation studies. First, in order to obtain solutions of the rotaxane **1.9**, determining the solubility at different temperatures was required. A 100 μM solution of the rotaxane **1.9** in water was prepared at 80 °C. Maintaining the initial temperature, the stock solution was then diluted to 5, 10, 20 and 50 μM. The UV/visible spectrum of each solution was recorded and the absorbance of each solution was plotted against concentration as shown in **Figure 4.14**. Initially, all solutions were clear and the absorbance shows linear increase with increasing concentration drawn in black line. The UV/visible spectrum of each solution was recorded again after incubation at 80 °C for 7 days. There is no change in absorbance before and after incubation. On that basis, material was fully dissolved at 80 °C and the saturation concentration is at least 100 μM at that temperature. Solubility studies were also done at 50 °C and 10 °C. After incubation for 7 days the absorbance of the supernatant of each solution did not change further. Comparing the absorbance before and after equilibration at 50 °C, the absorbance of a 100 μM mixture has decreased as shown by the red asterisk. The absorbance can be extrapolated to the black line and shows a concentration of 66 μM. Therefore, the saturation concentration at 50 °C was determined to be 66 μM. Similarly, at 10 °C, the saturation concentration was

determined to be 16 μM shown by the red circles. Similar studies were also carried out to determine the solubilities of the rotaxanes **4.1** and **4.2**. The saturation concentrations with respect to the crystalline forms of the rotaxanes **4.1** and **4.2** at room temperature were found to be 70 and 190 μM respectively. Therefore, the rotaxanes **4.1** and **4.2** are more soluble in water compared to the rotaxane **1.9**.

On the basis that a 100 μM solution of the rotaxane **1.9** was determined to be completely dissolved at 80 °C, but supersaturated at 30 °C, a 100 μM solution was prepared at 80 °C. This solution was left to stand at 30 °C and the UV/visible spectra were recorded at intervals as shown in **Figure 4.15**. The initial solution showed a narrow absorbance band at 350 nm that did not change for 5 days. After 5 days, crystals came out of solution, and the absorbance at 350 nm decreased over time. No further change in absorbance was observed after 11 days. This indicates that the supersaturated solution equilibrated to saturation concentration, causing the absorbance at 350 nm to decrease over time. The delay in the onset of this crystallisation indicates that heating is an effective way of removing seed crystals and preparing supersaturated solutions such that a typical crystallisation process occurs as these solutions are equilibrated to saturation concentration.

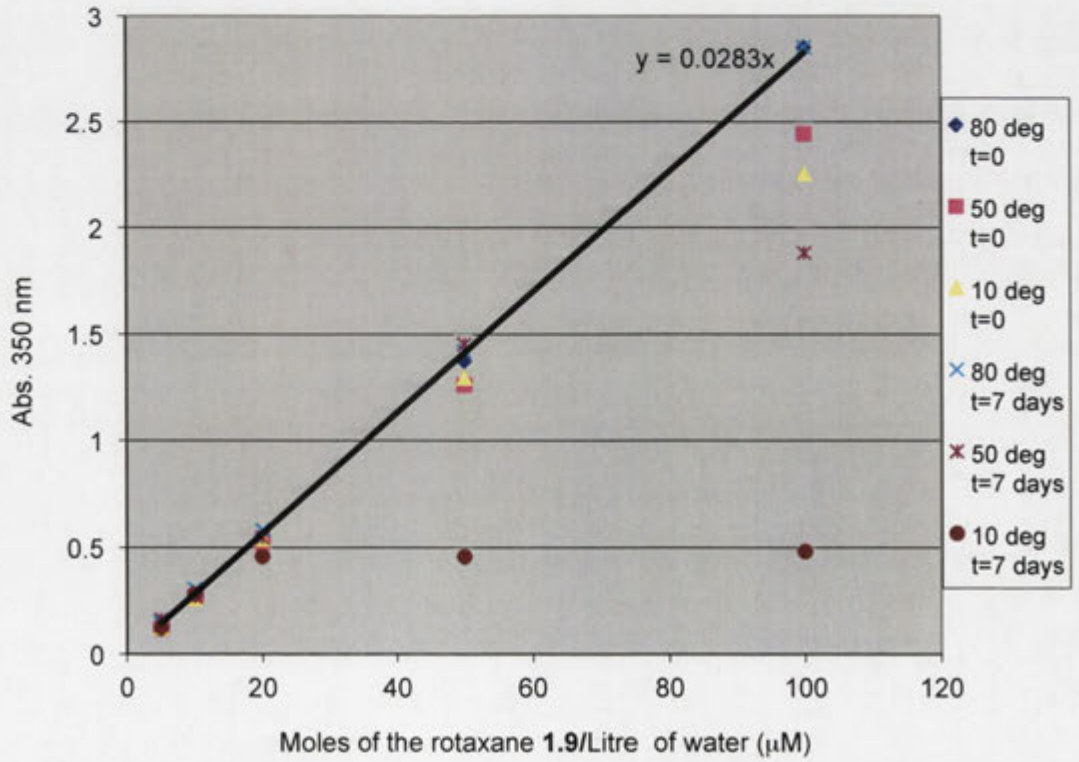

Figure 4.14. Solubility plot of the rotaxane **1.9** in water at 10, 50 and 80 °C.

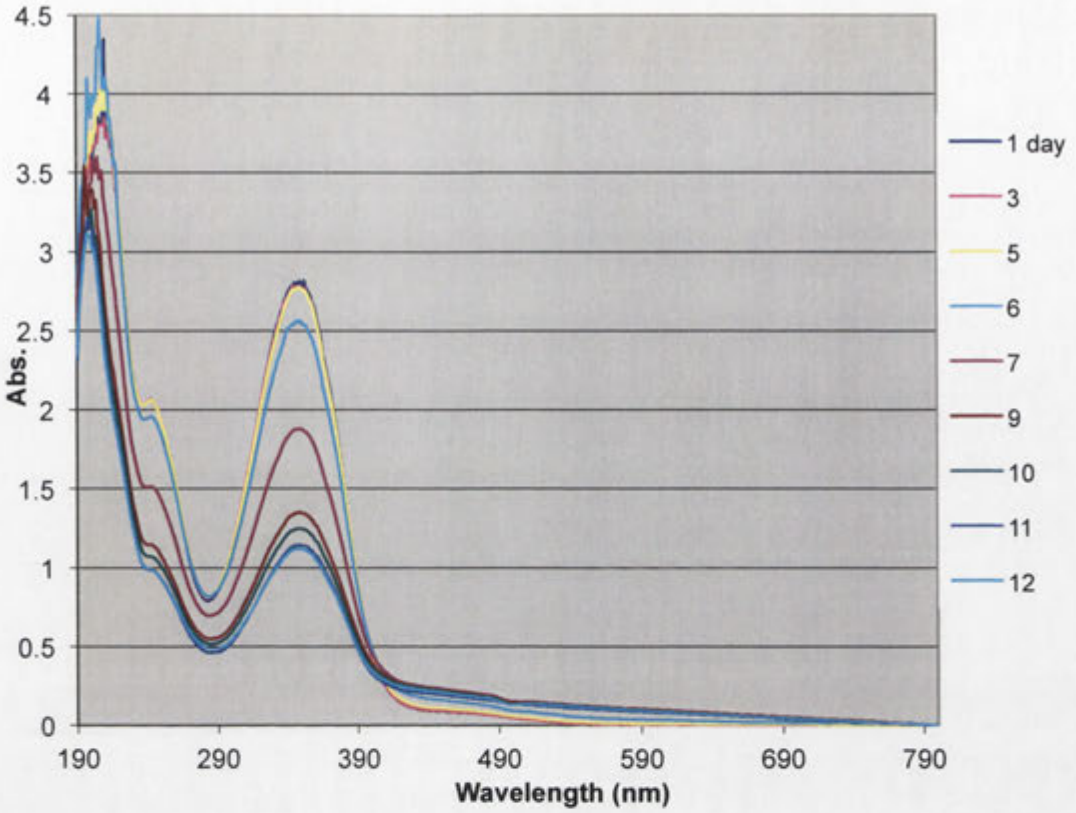

Figure 4.15. UV/visible spectra of a 100 μM mixture of the rotaxane **1.9** in water, monitored at time intervals during incubation at 30 °C.

4.7 Crystal Growth Inhibition Study

Having established that the saturation concentration of the rotaxane **1.9** is 16 μM at 10 °C, 66 μM at 50 °C, and 100 μM or higher at 80 °C, it is clear that the rotaxane **1.9** can completely dissolve up to at least 100 μM at 80 °C. Therefore, this method of heating at higher temperatures and equilibrating at lower temperatures was used to prepare supersaturated solutions required for experiments to regulate crystal growth. Four solutions containing 0, 10, 50 or 100 μM of the rotaxane **4.1** and 100 μM of the rotaxane **1.9** were prepared. As described in the previous section, the solubility of the rotaxane **4.1** is higher than that of the rotaxane **1.9**, hence, solutions of the rotaxane **4.1** at 100 μM or lower were also able to be prepared through heating above 80 °C and cooling at lower temperature. The resulting clear solutions were left to stand for 3.5 days while being monitored using an optical microscope fitted with a polarising lens (**Figure 4.16**). Inspection of the crystals grown from a solution of the rotaxane **1.9** (100 μM) gave long needles that are on average 1.17 mm in length (**Table 4.1** Entry 1). The length of the crystals grown decreased with increasing concentration of

the rotaxane **4.1**. When crystals were grown from a solution of the rotaxane **1.9** (100 μM) and the rotaxane **4.1** (100 μM), the length of the needles decreased to 0.28 mm on average. Furthermore, when a solution that had an even higher concentration of the rotaxane **4.1** (200 μM) and 100 μM of the rotaxane **1.9** was left to stand, crystallisation did not occur over a month. Inverse correlation between the crystal length and the concentration of the rotaxane **4.1** indicates that the rotaxane **4.1** terminates needle elongation.

In order to investigate whether the rotaxane **4.1** interferes with crystal growth by simply associating and disassociating with the growing fibres of the rotaxane **1.9** or by incorporating in the crystal lattice, and if the latter to determine the level of incorporation, crystals were collected by centrifugation, dissolved in MeOH and analysed using HPLC to measure the relative proportions of the rotaxanes **1.9** and **4.1** (**Table 4.1**). The molar extinction coefficients of the rotaxanes **1.9** and **4.1** are similar, hence the areas under the peaks in the HPLC chromatogram were integrated to estimate the percentage compositions. When 10 μM of the rotaxane **4.1** was present in the mixture that was left to stand, the area under the peak corresponding to the rotaxane **4.1** was 0.9% of the total peak area (**Table 4.1** Entry 2). When 100 μM of the rotaxane **4.1** was present in the mixture that was left to stand, the area under the peak corresponding to the rotaxane **4.1** increased to 3.4% of the total (**Table 4.1** Entry 4). This shows that the rotaxane **4.1** is incorporated into the crystals of the rotaxane **1.9**. The percentage composition of the rotaxane **4.1** is inversely proportional to crystal length. Therefore, the amount of crystal length truncation depends on the amount of the rotaxane **4.1** incorporated. A solution containing 10 μM of the rotaxane **4.1** yielded crystals which are on average 0.59 mm in length. The length of a single unit of the rotaxane **1.9** being approximately 2.2 nm, roughly 270,000 units of the rotaxane **1.9** are aligned linearly to constitute a single molecular fibre with that length. If the rotaxane **4.1** only incorporated to the ends of the growing chains of the rotaxane **1.9**, the incorporation frequency of the rotaxane **4.1** would only be 2 in 270,000. Incorporation of 2 in 270,000 units equates to roughly 0.0007% of the total crystal composition. A much higher incorporation rate of the rotaxane **4.1** (0.9%) suggests that the crystal of the rotaxane **1.9** continues to grow around incorporated molecules of the rotaxane **4.1** as shown in **Figure 4.17**. Presumably, when the number of crystal

lattice defects becomes large enough, the crystals do not grow further and therefore become truncated. Overall, the rotaxane **4.1** acts as a crystal growth inhibitor of the rotaxane **1.9**, as designed.

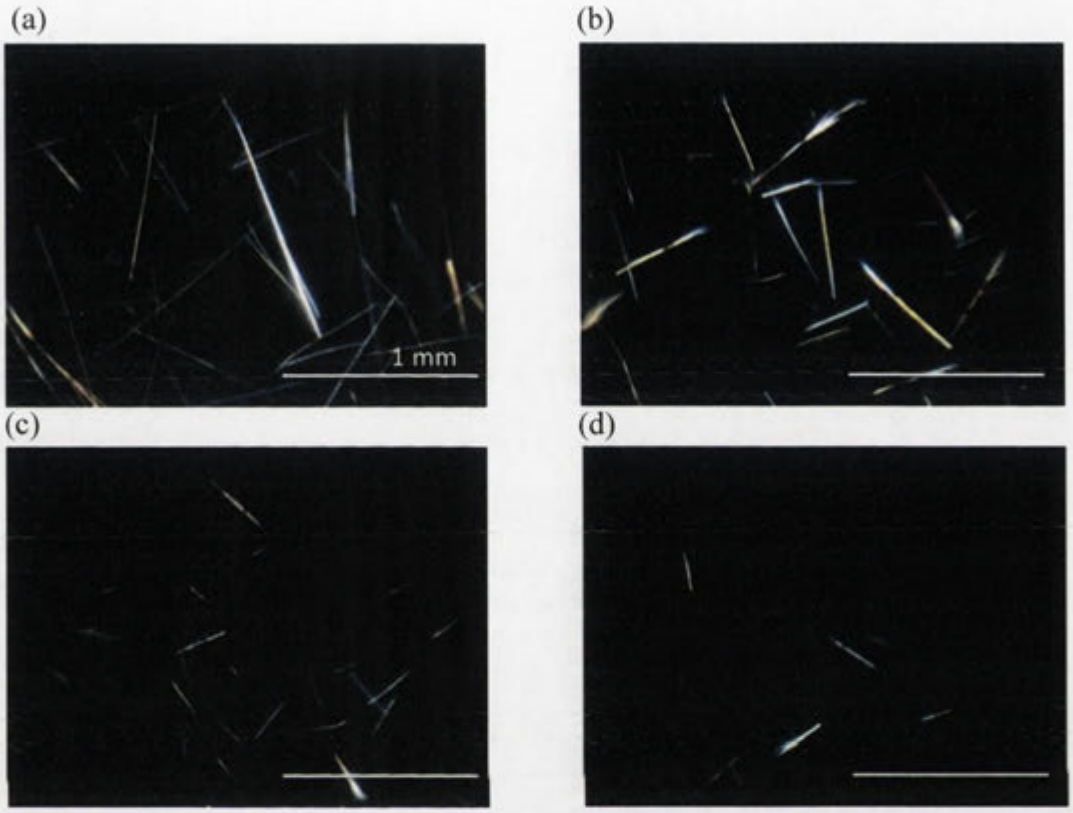

Figure 4.16. Optical microscope images of crystals grown after 3.5 days from solutions of (a) 100 μM of the rotaxane **1.9**, (b) 100 μM of the rotaxane **1.9** and 10 μM of the rotaxane **4.1**, (c) 100 μM of the rotaxane **1.9** and 50 μM of the rotaxane **4.1** and (d) 100 μM of the rotaxane **1.9** and 100 μM of the rotaxane **4.1**.

Entry	Concentration of the rotaxane **1.9** (μM)	Concentration of the rotaxane **4.1** (μM)	Average length of crystals (mm)	Number of rotaxanes aligned along the molecular fibre of the grown crystals	Composition of the rotaxane **4.1** in the grown crystals (%)
1	100	0	1.17	530000	0
2	100	10	0.59	270000	0.9
3	100	50	0.30	140000	2.5
4	100	100	0.28	130000	3.4

Table 4.1. Analysis of lengths and compositions of crystals shown in **Figure 4.16**.

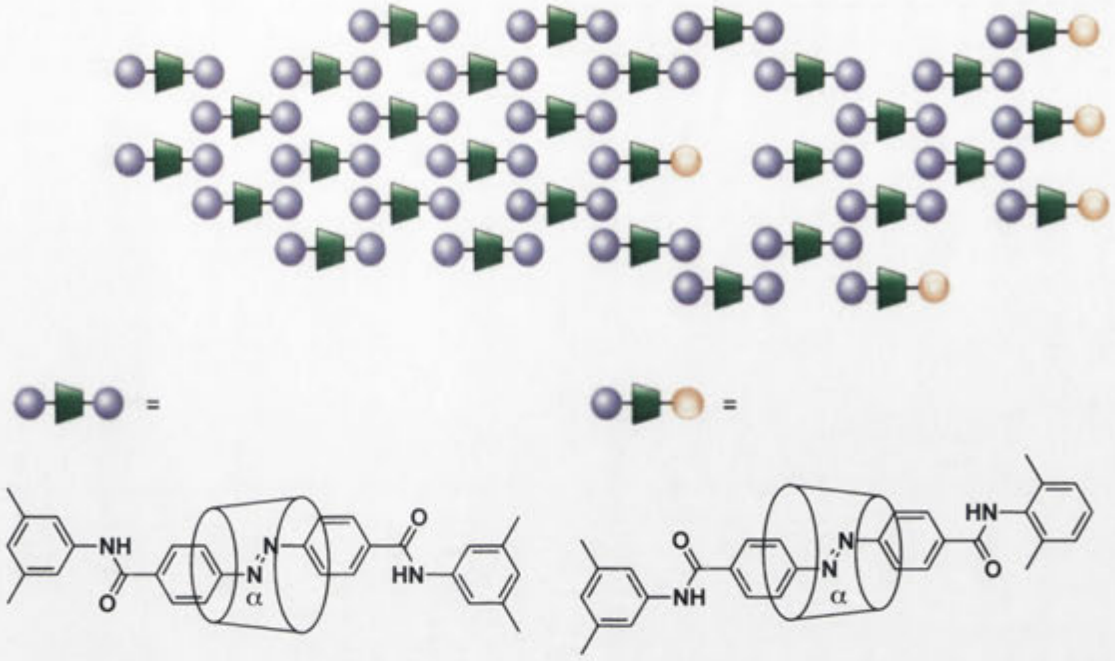

Figure 4.17. A model illustration of the rotaxane **1.9** crystal growing around an incorporated molecule of the rotaxane **4.1** and further incorporation of the rotaxane **4.1** eventually terminating crystal growth.

Given that the rotaxane **4.1** shows crystal growth regulation through co-crystallisation, the ability to regulate crystal growth using the orientational isomer, the rotaxane **4.2**, was examined for comparison using the conditions described above. Inspection of the crystals grown from four solutions containing 0, 10, 50 or 100 μM of the rotaxane **4.2** and 100 μM of the rotaxane **1.9** did not show large differences in crystal length. Therefore, crystal growth studies were repeated using solutions with higher concentrations (0, 100, 150 or 200 μM) of the rotaxane **4.2** with 100 μM of the rotaxane **1.9**, that were left to stand for 36 days (**Figure 4.18**). Inspection of the crystals grown from a solution of the rotaxane **1.9** (100 μM) gave long needles that are on average 1.76 mm in length (**Table 4.2** Entry 1). The length of the crystals grown decreased with increasing concentration of the rotaxane **4.2**. When crystals were grown from a solution of the rotaxane **1.9** (100 μM) and the rotaxane **4.2** (200 μM), the length of the needles decreased to 0.82 mm on average (**Table 4.2** Entry 4). As per the rotaxane **4.1**, an inverse correlation between the crystal length and the concentration of the rotaxane **4.2** is indicates that the rotaxane **4.2** terminates needle elongation.

In order to investigate whether the rotaxane **4.2** interferes with crystal growth by simply associating and disassociating with the growing fibres of the rotaxane **1.9** or by incorporating in the crystal lattice, and if the latter to determine the level of incorporation, crystals were collected by centrifugation, dissolved in MeOH and analysed using HPLC to measure the relative proportions of the rotaxanes **1.9** and **4.2** (**Table 4.2**). The molar extinction coefficients of the rotaxanes **1.9** and **4.2** are also similar, hence the areas under the peaks in the HPLC chromatogram were integrated to estimate the percentage compositions. When 100 μM of the rotaxane **4.2** was present in the mixture that was left to stand, the area under the peak corresponding to the rotaxane **4.2** was 2.5% of the total peak area (**Table 4.2** Entry 2). When 200 μM of the rotaxane **4.2** was present in the mixture that was left to stand, the area under the peak corresponding to the rotaxane **4.2** increased to 7.2% of the total (**Table 4.2** Entry 4). This shows that the rotaxane **4.2** is incorporated into the crystals of the rotaxane **1.9**. As per the rotaxane **4.1**, the amount of crystal length truncation is proportional to the amount of the rotaxane **4.2** incorporated.

In contrast to crystals being fully grown after 3.5 days and not growing further when the rotaxane **4.1** was added, the crystal growth was much slower when the rotaxane **4.2** was added (36 days). Crystals were grown from different stock solutions of the rotaxane **1.9** in these experiments, and therefore the lengths of the crystals grown from the control experiment with 100 μM of the rotaxane **1.9** are not identical in each experiment (**Table 4.1** Entry 1 and **Table 4.2** Entry 1). Comparing the crystal growth inhibition of the rotaxanes **4.1** and **4.2**, an addition of 10 μM of the rotaxane **4.1** was required to truncate the crystal length by approximately half. On the other hand, even an addition of 150 μM of the rotaxane **4.2** was insufficient to truncate the crystal length by a half (**Table 4.1** Entry 2 and **Table 4.2** Entry 3). When 10 μM of the rotaxane **4.1** was added, 0.9% of the crystal composition corresponded to the rotaxane **4.1**, compared to 4.4% of the crystal composition corresponding to the rotaxane **4.2** when 150 μM of the rotaxane **4.2** was added. The smaller percentage composition of the rotaxane **4.1** required to truncate the crystal length by approximately a half suggests that the rotaxane **4.1** terminates crystal growth more effectively. Higher degree of incorporation of the rotaxane **4.2** may delay needle elongation as the

rotaxane **1.9** needs to grow around the defects in the crystal lattice. This may cause the crystals to grow over a longer period of time with the rotaxane **4.2**.

A possible rationalisation for why the effectiveness to truncate crystal growth is different for the rotaxanes **4.1** and **4.2** is described below, although the factors affecting the process of crystal growth truncation are complex and difficult to fully rationalise. CD-based rotaxanes typically show head-to-tail alignment of the CDs in the crystal packing, presumably due to the dipole of the CDs. The 3,5-dimethylaniline blocking group is next to the tail end of the CD for the rotaxane **4.1**, while the 3,5-dimethylaniline blocking group is next to the head end of the CD for the rotaxane **4.2**. If the incorporation of the rotaxanes **4.1** and **4.2** to the crystals of the rotaxane **1.9** also occurs in a head-to-tail fashion, the rotaxane **4.1** would be expected to incorporate only on the head end of the rotaxane **1.9** while the rotaxane **4.2** would be expected to incorporate only on the tail end. Consequently, the different interactions involved by incorporation into either the head or the tail end of the rotaxane **1.9** may contribute to the effectiveness of the rotaxanes **4.1** and **4.2** to terminate crystal growth being different.

(a)

(b)

(c) (d)

Figure 4.18. Optical microscope images of crystals grown after 36 days from solutions of (a) 100 μM of the rotaxane **1.9**, (b) 100 μM of the rotaxane **1.9** and 100 μM of the rotaxane **4.2**, (c) 100 μM of the rotaxane **1.9** and 150 μM of the rotaxane **4.2** and (d) 100 μM of the rotaxane **1.9** and 200 μM of the rotaxane **4.2**.

Entry	Concentration of the rotaxane **1.9** (μM)	Concentration of the rotaxane **4.2** (μM)	Average length of crystals (mm)	Number of rotaxanes aligned along the molecular fibre of the grown crystals	Composition of the rotaxane **4.2** in the grown crystals (%)
1	100	0	1.76	800000	0
2	100	100	1.57	710000	2.5
3	100	150	1.02	460000	4.4
4	100	200	0.82	370000	7.2

Table 4.2. Analysis of lengths and compositions of crystals shown in **Figure 4.18**.

It appears that the rotaxanes **4.1** and **4.2** act as crystal growth inhibitors by incorporating into the growing chains of molecular fibres of the rotaxane **1.9**. This is presumably due to the conformation of the 3,5-dimethylaniline blocking group being co-planar to the axle and therefore being able to form π–π interactions with the structurally similar rotaxane **1.9**, while the conformation of the 2,6-dimethylaniline blocking group is out-of-plane of the axle and cannot form π–π interactions to continue crystal growth. For this to be correct, the rotaxane **1.18** with 2,6-dimethylaniline blocking groups on both ends would not be expected to form π–π interactions with the rotaxane **1.9** and thus would not affect the crystal growth of the rotaxane **1.9**. To examine this hypothesis, crystal growth was monitored using four solutions that contained 0, 10, 50 or 100 μM of the rotaxane **1.18** and 100 μM of the

rotaxane **1.9**. **Figure 4.19** shows optical microscope images of crystals formed after 10 days. Visual inspection shows that the length of the crystals grown from all four solutions is unaffected, and HPLC analysis of the crystals collected from each solution showed only a single peak corresponding to the rotaxane **1.9**, which shows that there is no incorporation of the rotaxanes **1.18** in the crystal lattice of the rotaxane **1.9**. This is consistent with the expectation that as the rotaxane **1.18** has blocking groups on both ends that are unable to form the appropriate π–π interactions, consequent incorporation into the molecular fibres of the rotaxane **1.9** does not occur. Thus, crystal growth of the rotaxane **1.9** is not inhibited by the rotaxane **1.18**.

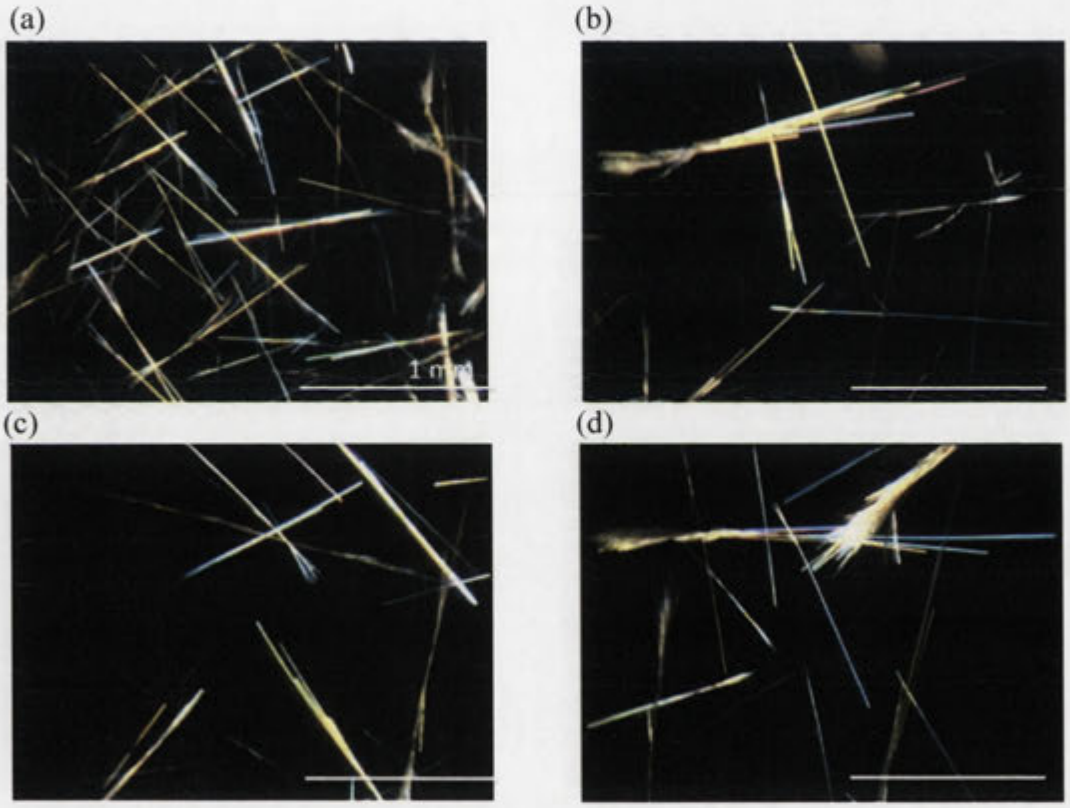

Figure 4.19. Optical microscope images of crystals grown after 10 days from solutions of (a) 100 μM of the rotaxane **1.9**, (b) 100 μM of the rotaxane **1.9** and 10 μM of the rotaxane **1.18**, (c) 100 μM of the rotaxane **1.9** and 50 μM of the rotaxane **1.18** and (d) 100 μM of the rotaxane **1.9** and 100 μM of the rotaxane **1.18**.

4.8 Conclusion

In conclusion, the purposely designed rotaxanes **4.1** and **4.2** showed crystal growth inhibition of the rotaxane **1.9**. It appears that when the rotaxanes **4.1** and **4.2** incorporate into the growing crystals of the rotaxane **1.9**, the rotaxane **1.9** grows around the incorporated molecules until the number of the crystal lattice defects

increases to the point that crystal growth eventually terminates. If this is the case, microscopy techniques such as TEM or STM could be used to investigate the crystal lattice defects to see, for example, whether they are concentrated on the ends of the crystals. Furthermore, as the crystal packing of the rotaxane **1.9** shows molecules aligned head-to-tail with alternating rows facing opposite directions,[38] the mis-incorporated rotaxanes **4.1** and **4.2** which are expected to interact with either the head or tail end are likely to be observed on the ends of alternating rows of the rotaxane **1.9**. The rotaxane **4.1** shows more effective inhibition of crystal growth. Therefore, more irregularity in the crystal lattice of the rotaxane **1.9** would expected to be observed by microscopy when the rotaxane **4.2** is incorporated compared to the rotaxane **4.1**, as the rotaxane **1.9** appears to grow around the incorporated molecules of the rotaxane **4.2** better without terminating crystal growth.

During the crystal growth inhibition studies, an interesting liquid-phase behavior was observed. When a large amount of the rotaxane **4.1** was added to a supersaturated solution of the rotaxane **1.9**, crystallisation did not occur, but instead the rotaxane **1.9** remained in solution. The focus of this Chapter was to regulate the growth of molecular fibres in the solid-state. The process of manipulating the self-assembly of CD-based rotaxanes in solution is likely to be similar in some ways to the process in the solid-state. Therefore, this technology may not be limited to the application in the solid-state but also applicable to aggregates in solution and lyotropic liquid crystalline materials.[160,161] Future work could therefore be directed to regulating self-assembly of rotaxanes in the solution phase.

CHAPTER 5 – Conclusions and Future Directions for Crystal Engineering with α-Cyclodextrin Based Rotaxanes

In the work described in the previous Chapters of this thesis, CD-based rotaxanes were prepared and their solid-state structures/packing, morphology and crystal growth behaviour were explored. The rotaxane **1.17** having a stilbene-based axle and 3,5-dimethylaniline blocking groups, as well as the rotaxane **1.18** having an azobenzene-based axle and 2,6-dimethylaniline blocking groups were prepared to complete the set of rotaxanes **1.9**, **1.10**, **1.17** and **1.18** with 2,6-dimethylaniline and 3,5-dimethylaniline blocking groups, with azobenzene- and stilbene-based axles. Observation of crystal morphology and growth using SEM and microscope images suggests not only that crystal shape and size can be controlled depending on the choice of blocking groups and varying the conditions of crystal growth, but also that crystal packing is reflected in the crystal growth and the final shape of the crystals. Thus crystal engineering can be bottomed-up to make nano-molecular architectures to micrometre scale or beyond.

Crystal engineering may be used to fine-tune physical, chemical, photochemical or electronic properties of molecular and supramolecular devices and machines that are fabricated through a bottom-up approach. Another way to regulate the degree of conjugation in molecular fibres would be to build a conjugated system where the backbones of rotaxanes are polyconjugated. The resultant conjugated polyrotaxane system would have a higher degree of conjugation compared to extended conjugation through π–π interactions shown in the crystal packing of the rotaxane **1.9**. It is conceivable that conjugated polyrotaxanes could be prepared using building blocks such as the rotaxane **5.1**. If the 2,5-dimethylaniline blocking groups maintained co-planarity with the axle, the rotaxane **5.1** would be fully conjugated. Conjugated polyrotaxanes might then be accessible if the dumbbells of the rotaxane **5.1** were coupled with conjugated linkers through Heck reaction[162] as shown in **Scheme 5.1**. This type of polyrotaxane could potentially be developed into molecular wires for electronic communication, or into materials that expand and shrink on exposure to external stimuli due to linkers that can undergo isomerisation.

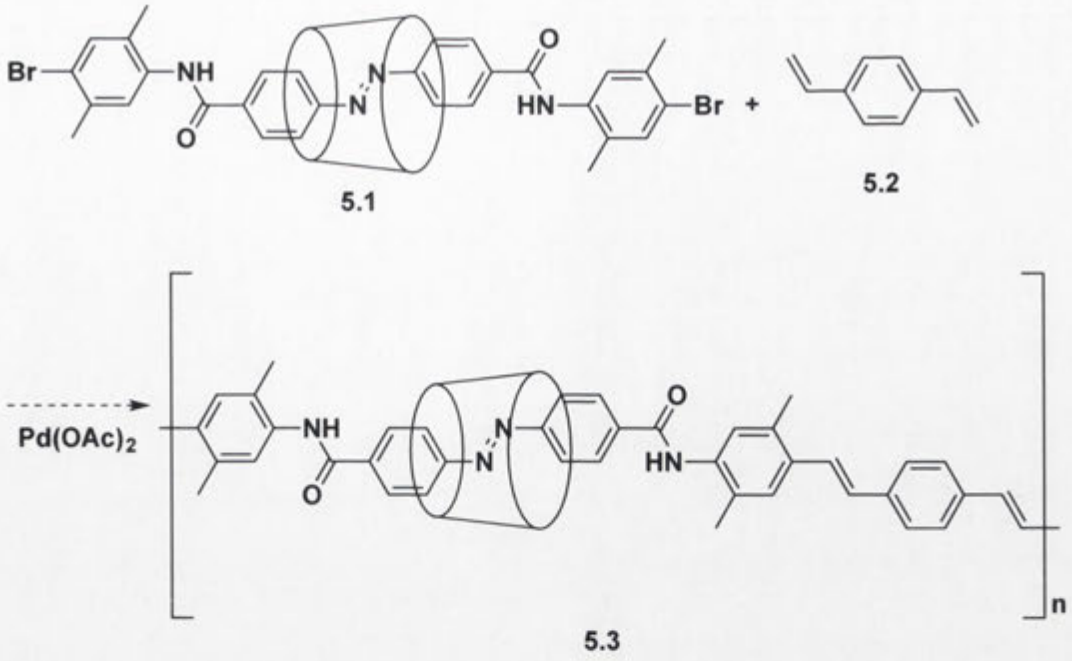

Scheme 5.1. Proposed synthesis of the polyrotaxane **5.3**.

Alternatively, a much wider range of rotaxanes including unsymmetrically capped rotaxanes might be designed using a crystal engineering approach where the blocking groups act as synthons to guide intermolecular self-assembly and regulate the degree of conjugation in molecular fibres of aligned rotaxanes. In Chapter 4, the unsymmetrically capped rotaxanes **4.1** and **4.2** were used to regulate the crystal growth of the self-assembling rotaxane **1.9** through co-crystallisation. This type of crystal growth regulation is unlikely to be restricted to rotaxanes with 3,5-dimethylaniline blocking groups but to be extendable to other types of blocking groups and rotaxanes that form fibres through π–π interactions. The possibilities for regulating crystal growth using different rotaxanes with different blocking groups that can be used as crystal synthons are vast. While it was not practical to examine all possibilities, preliminary crystal engineering experiments were carried out with another CD-based rotaxane. The rotaxane **1.4** with trinitrophenyl blocking groups also forms linearly aligned fibres through π–π interactions of the blocking groups that are twisted out of the plane of the axle as described in the Introduction.[163] Given their two different blocking groups having potential to form π–π interactions, the two unsymmetrically capped rotaxanes **5.4** and **5.5** that are structurally similar to the rotaxanes **1.4** and **1.9** were designed. Each is capped with a 3,5-dimethylaniline blocking group on one end and a trinitrophenyl blocking group on the other end. From

the crystal structure and packing of the rotaxane **1.9**, it was envisaged that the 3,5-dimethylaniline blocking group of the rotaxanes **5.4** and **5.5** would allow π–π interactions between 3,5-dimethylaniline blocking groups of adjacent rotaxanes. Likewise, from the crystal structure and packing of the rotaxane **1.4**, it was envisaged that the rotaxanes **5.4** and **5.5** could form π–π interactions between trinitrophenyl blocking groups of adjacent rotaxanes. Alternatively, π–π interactions between the 3,5-dimethylaniline blocking groups and the trinitrophenyl blocking groups of adjacent rotaxanes might occur.

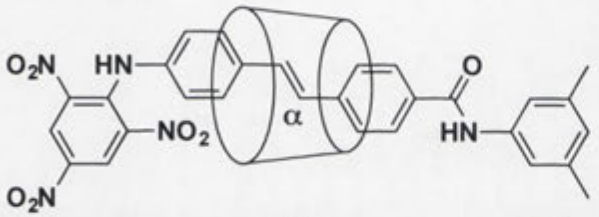

5.4

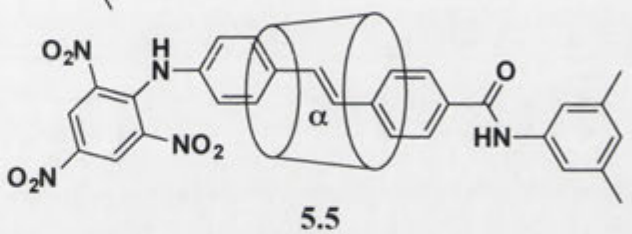

5.5

5.1 Synthesis

The synthesis of the rotaxanes **5.4** and **5.5** was attempted using a variation of the threading approach described in Chapter 4. First, the stilbene axle **5.8** was prepared by palladium-catalysed Heck coupling of 4-vinylaniline **5.6** and 4-iodobenzoic acid **5.7** according to literature procedures.[164] The stilbene **5.8** was capped with the aniline **2.2** using the amide coupling agent, BOP (**Scheme 5.2**). The aniline **2.2** was used as both the capping reagent and solvent. Having an excess of the aniline **2.2** ensured that the amino group of the stilbene **5.8** did not act as a nucleophile, without having to protect and deprotect it.

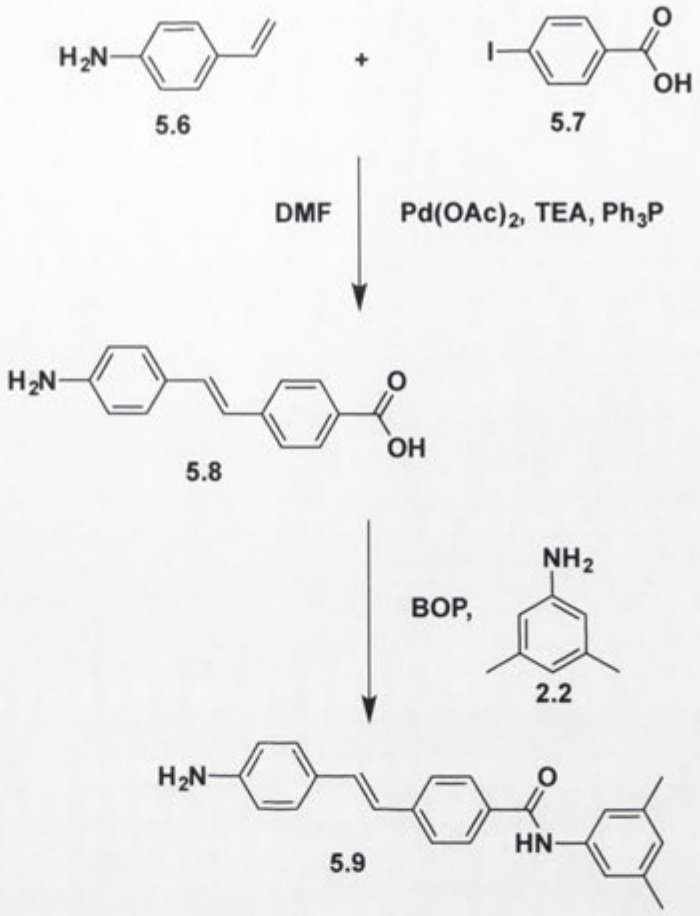

Scheme 5.2. Synthesis of the amide **5.9**.

With the monocapped axle **5.9** in hand, the rotaxane **5.5** was prepared following the procedure adapted from Easton *et al.*[163] The synthesis involved equilibrating the aminostilbene **5.9** in sodium carbonate buffer (pH 10) with a large excess of α-CD **1.1** (**Scheme 5.3**). An increased amount of buffer and α-CD **1.1** was used compared to the literature conditions to solubilise the aminostilbene **5.9**. Then, the dihydrate of 2,4,6-trinitrobenzene-1-sulfonic acid sodium salt **5.10** was added. The ESI mass spectrum of the reaction mixture showed an ion at *m/z* 1549, which corresponds to the sodiated ion of the rotaxane **5.5**. The product **5.5** was not observed on TLC, however, as only small amounts were formed. Instead, the reaction mixture was analysed by HPLC. The HPLC trace of the reaction mixture showed a peak that had the absorbance of both the stilbene and the 2,4,6-trinitrophenyl blocking group. This peak was isolated through reverse phase HPLC to give the rotaxane **5.5** in 2% yield. The low yield is presumably due to the low solubility of the monocapped axle **5.9** in water, or a low tendency for the CD **1.1** forming an inclusion complex with the axle **5.9**. In theory,

both of the rotaxanes **5.4** and **5.5** could have formed. However, formation of only the one was detected by HPLC and this was determined to be the rotaxane **5.5** through structural analysis as discussed below.

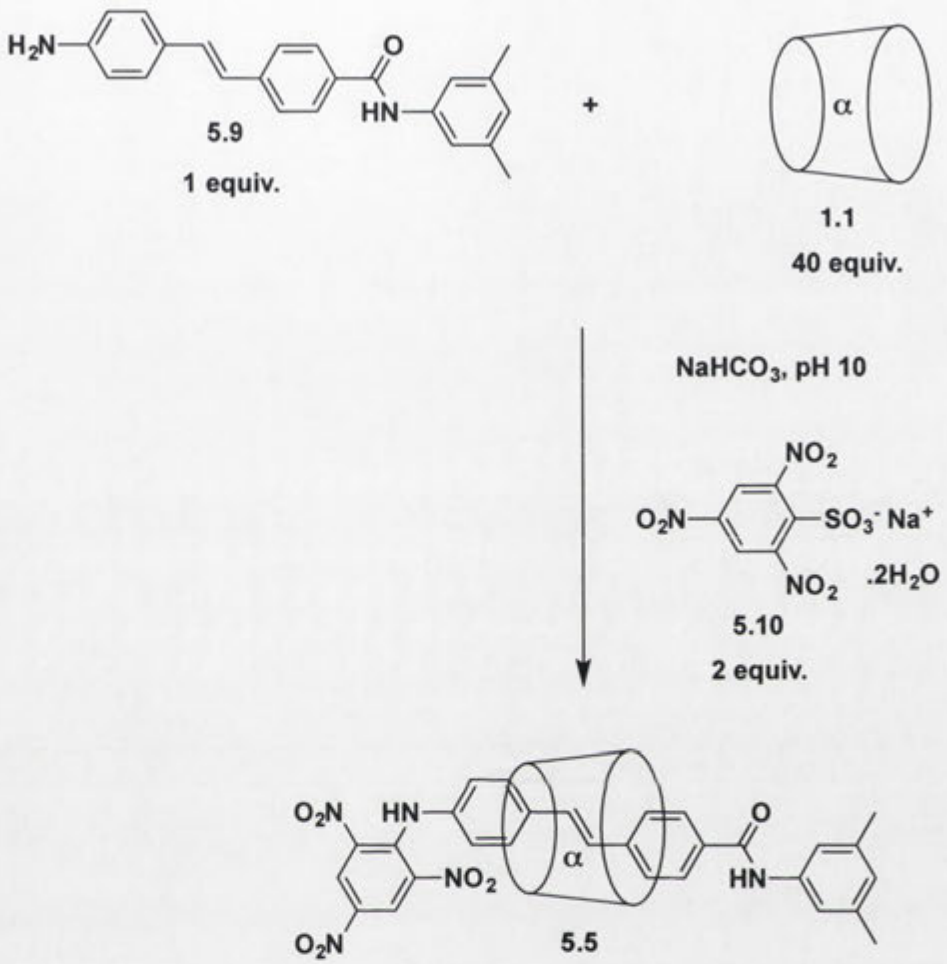

Scheme 5.3. Synthesis of the rotaxane **5.5**

5.2 Conformational Analysis Using NMR Spectroscopy and X-Ray Crystallography

The 1D ^{1}H NMR spectrum of the rotaxane **5.5** confirms the presence of the components, showing resonances of CD, stilbene, dimethylphenyl and trinitrophenyl protons (**Figure 5.1**).

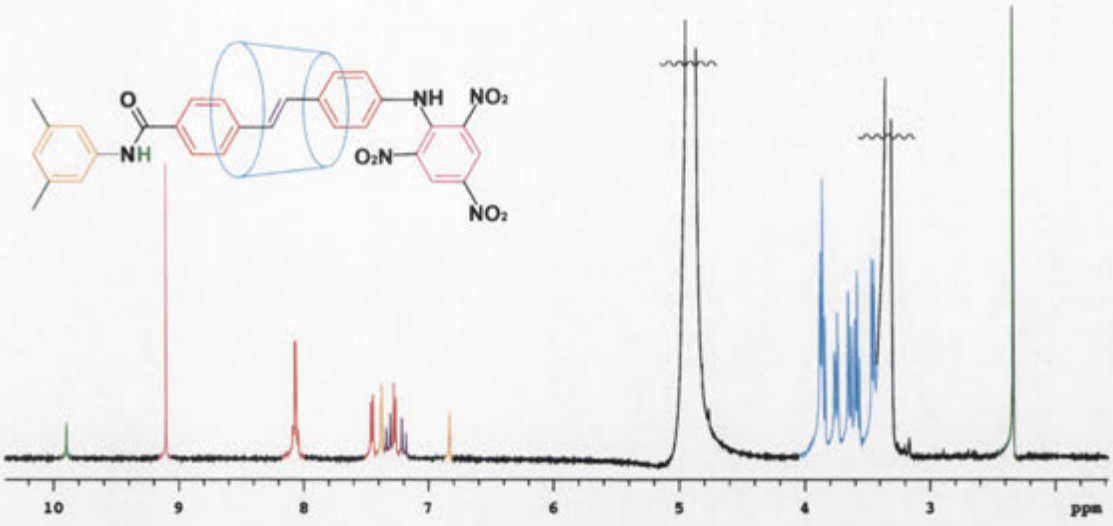

Figure 5.1. 500 MHz ^{1}H NMR spectrum of the rotaxane **5.5** in CD_3OD.

The general protocol used in Chapter 2 to assign structures of CD-based [2]rotaxanes was followed for the rotaxane **5.5** in an attempt to assign the structure using 2D NMR experiments. **Figure 5.2** shows a section of the DQF-COSY NMR spectrum of the rotaxane **5.5**, where the CD proton cross-peaks are found. The most down field CD resonance at δ4.93 is assigned to the CD-C1 anomeric protons. A ^{1}H-^{1}H correlation between these protons and those giving rise to the signal at δ3.45 is seen, and the latter is therefore assigned to the CD-C2 protons. Likewise, there is a cross-peak between the resonance at δ3.45 (CD-C2) and the resonance at δ3.86 which is therefore attributed to the CD-C3 protons. This resonance at δ3.86 (CD-C3) also shows a cross-peak with the resonance at δ3.58 which is therefore assigned to the CD-C4 protons. Again, the resonance at δ3.58 (CD-C4) also shows a cross-peak with the resonance at δ3.87 which is therefore assigned to the CD-C5 protons. Finally, the resonances at δ3.75 and 3.64 corresponding to the CD-C6 protons show cross-peaks with each other.

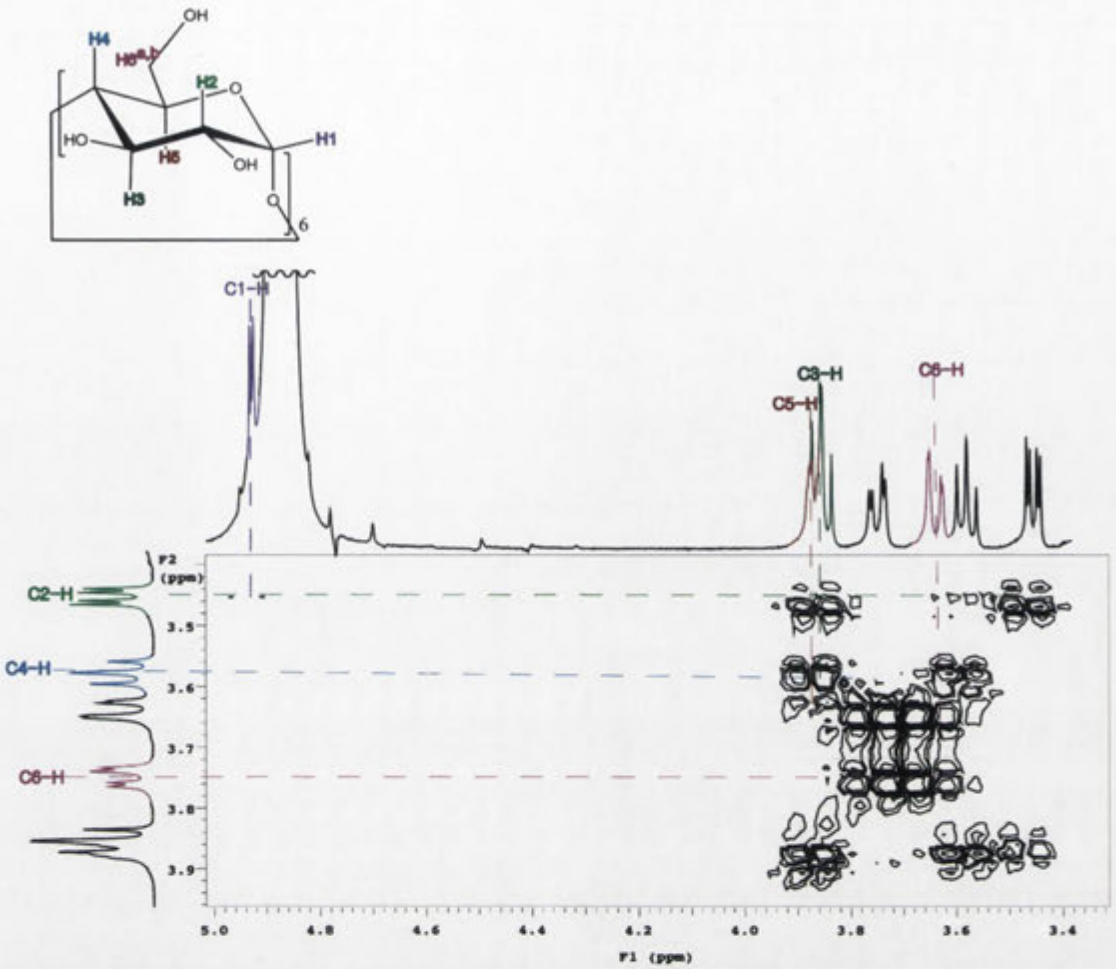

Figure 5.2. A section of the 500 MHz 2D DQF-COSY NMR spectrum of the rotaxane **5.5** in CD_3OD showing cross-peaks between CD proton signals.

The structural assignment can then be continued by analysis of the nuclear Overhauser effect (NOE) interactions in the ROESY NMR spectrum. **Figure 5.3** shows a section of the 2D ROESY NMR spectrum with cross-peaks for the stilbene protons. Since cross-peaks are observed between the resonances of olefinic protons C and D, and proton resonances at δ7.45 and 8.08, these resonances are assigned to protons E and B in proximity to the olefinic protons.

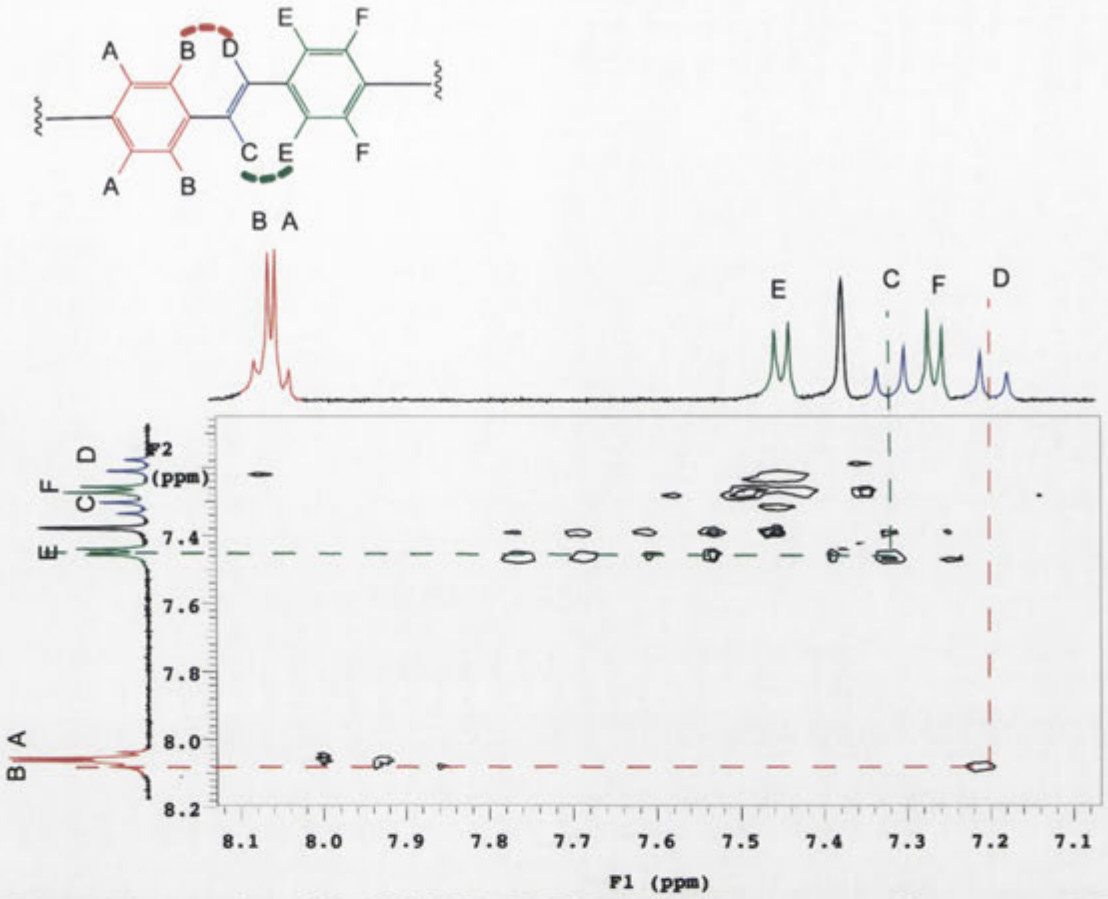

Figure 5.3. A section of the 500 MHz 2D ROESY NMR spectrum of the rotaxane **5.5** in CD_3OD showing cross-peaks between stilbene proton resonances.

Figure 5.4 shows a section of the 2D ROESY NMR spectrum with axle and aniline aromatic proton resonance cross-peaks with those of methyl and CD protons. The presence of the NOE cross-peak labelled NOE1 shows the resonance at δ7.38 corresponds to the aniline aromatic protons. Assignment of the CD conformation was attempted looking at the cross-peaks between the aromatic and CD protons. Protons A and B show strong NOEs with the CD-C3 protons, hence they are next to the wider end of the CD. The olefinic protons C and D show NOEs with CD-C5 protons. Protons E show NOEs with both the CD-C5 and CD-C6 protons, hence they are next to the narrow end of the CD. There is no NOE interaction seen between CD protons and protons F. Thus, the CD is localised over one end of the stilbene as shown in **Figure 5.4**. Due to the lack of NOE interaction between protons of the blocking groups and CD protons or axle protons, the orientation of the CD with respect to the dumbbell cannot be assigned using 2D ROESY NMR spectroscopy. Hence the structural assignment of the rotaxane **5.5** was completed using X-ray crystallography.

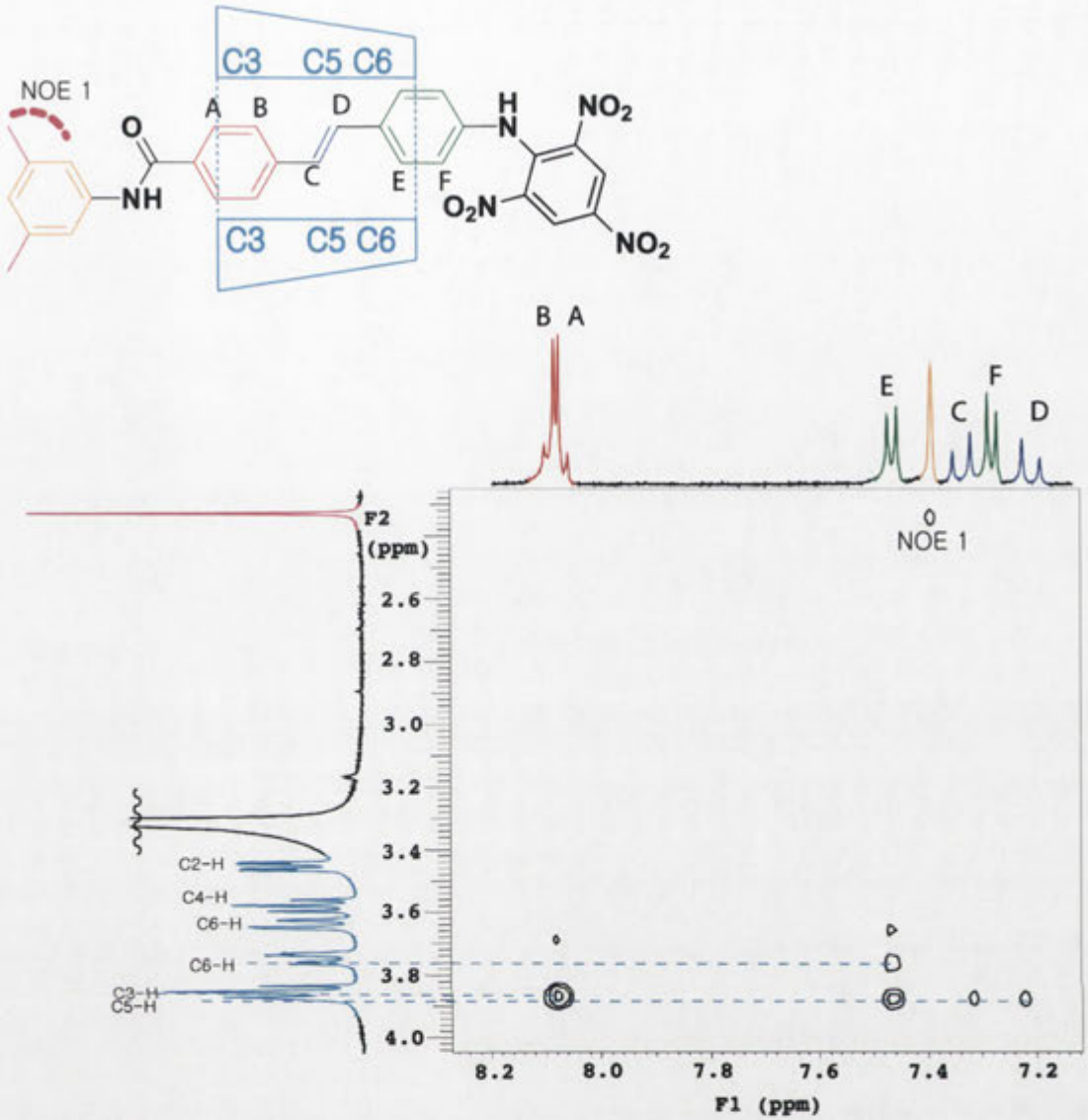

Figure 5.4. A section of the 500 MHz 2D ROESY NMR spectrum of the rotaxane **5.5** in CD_3OD showing stilbene and aniline aromatic proton resonance cross-peaks with those of methyl and CD protons.

Crystals of the rotaxane **5.5** were obtained through slow evaporation of MeOH/water over a period of several weeks. The solid-state structure was examined using X-ray crystallography. The crystallographic data are presented in Appendix 1. The rotaxane **5.5** belongs to the monoclinic space group and there are two molecules per unit cell. The stilbene axle is planar. The plane of the trinitrophenyl blocking group is twisted approximately 45° from that of the stilbene moiety. Meanwhile, the plane of the 3,5-dimethylaniline blocking group is twisted approximately 30° from that of the stilbene moiety.

X-Ray crystallography shows the orientation of the rotaxane **5.5** with the wider end of the CD nearest to the 3,5-dimethylaniline blocking group (**Figure 5.5**). The formation of the rotaxane **5.5** occurs through threading of the CD **1.1** from the wider end of the cavity to form an inclusion complex, followed by capping with the 2,4,6-trinitrobenzene-1-sulfonic acid **5.10**. It may be that threading only occurs in this direction as the dipoles of the monocapped axle **5.9** and the CD **1.1** do not allow the CD **1.1** to thread from the narrower end of the cavity. Alternatively, if inclusion does occur through threading of the CD **1.1** from the narrower end, it may be that the CD **1.1** is localised in proximity of the amino group of the monocapped axle **5.9** such that capping of the inclusion complex is limited by steric hindrance, resulting in the formation of only the single isomeric rotaxane **5.5**.

Figure 5.5. Crystal structure of the rotaxane **5.5** displayed in stick style. Solvent molecules are removed for clarity. Black = carbon, white = hydrogen, blue = nitrogen and red = oxygen.

5.3 X-Ray Crystal Packing of Unsymmetrically Capped [2]Rotaxane

X-Ray crystallography also gives crystal packing information which reveals that the rotaxane **5.5** forms molecular fibres along a single axis through π–π interactions between the 3,5-dimethylaniline blocking group and the trinitrophenyl blocking group of adjacent rotaxanes (**Figure 5.6**). The CDs of the rotaxane **5.5** are aligned head-to-tail with alternating rows of CDs facing opposite directions to form centrosymmetric non-polar crystals. The conformation of the rotaxane **5.5** in the solid-state allows π–π interactions through the 3,5-dimethylaniline as well as the trinitrophenyl blocking groups.

(a)

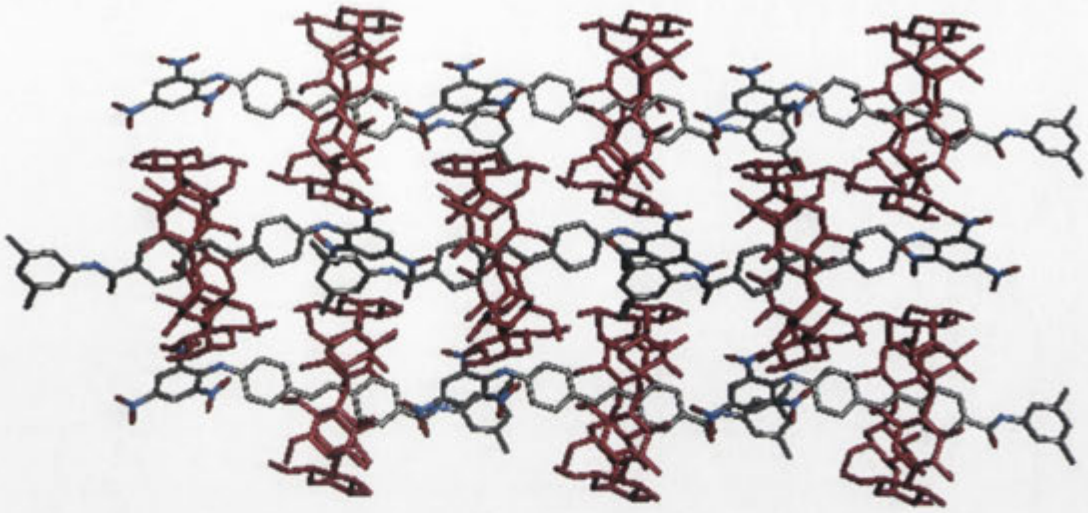

(b)

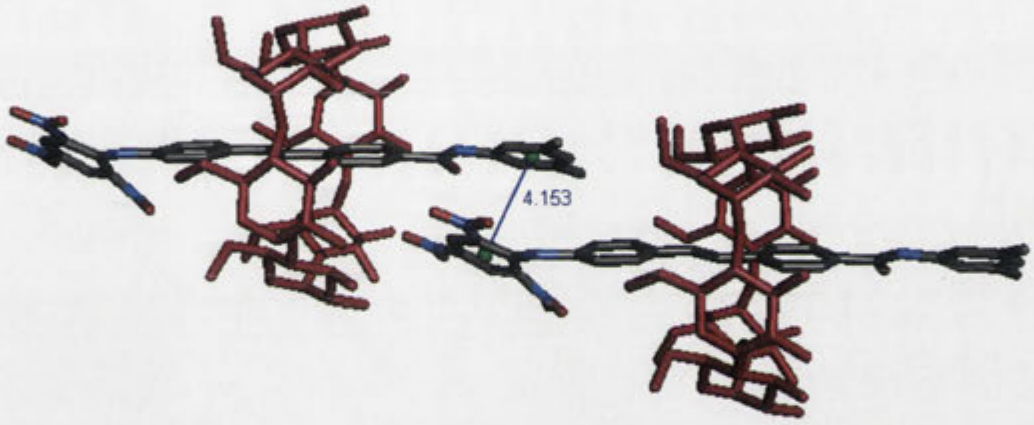

Figure 5.6. Crystal packing of the rotaxane **5.5** showing (a) formation of aligned fibres and (b) the hetero-blocking group π–π interaction. Displayed in stick style. Hydrogen atoms and solvent molecules are removed for clarity.

5.4 Co-crystallisation Using an Unsymmetrically Capped [2]Rotaxane

Given that the trinitrophenyl blocking group of the rotaxane **5.5** shows a π–π interaction with the 3,5-dimethylaniline blocking group of an adjacent species in the solid-state, through π–π interactions of the blocking groups on either end of the rotaxane **5.5**, it seemed likely that the rotaxane **5.5** might incorporate into the crystal lattice of the rotaxane **1.9**. Hence it was of interest to examine whether the rotaxane **5.5** could incorporate into the growing chains of the rotaxane **1.9**, and if so, whether incorporation lead to termination of crystal growth as observed with the rotaxanes **4.1** and **4.2** in the work described in Chapter 4. Accordingly, an experiment was designed to observe the crystal growth from four solutions containing the rotaxane **5.5** (0, 10,

50 or 100 μM) and 100 μM of the rotaxane **1.9**. The solutions were left to stand for 4 days while being monitored using an optical microscope fitted with a polarising lens (**Figure 5.7**). Inspection of the crystals grown from a solution of the rotaxane **1.9** (100 μM) gave long needles that are on average 0.90 mm in length (**Table 5.1** Entry 1). The length of the crystals grown decreased with increasing concentration of the rotaxane **5.5**. When the crystals were grown form a solution of the rotaxane **1.9** (100 μM) and the rotaxane **5.5** (100 μM), the length of the needles decreased to 0.45 mm on average (**Table 5.1** Entry 4). An inverse correlation between the crystal length and the concentration of the rotaxane **5.5** indicates that the rotaxane **5.5** interferes with the crystal growth of the rotaxane **1.9** and terminates needle elongation as seen with the rotaxanes **4.1** and **4.2**.

To investigate if the rotaxane **5.5** incorporates in the crystal lattice of the rotaxane **1.9**, crystals were collected by centrifugation, dissolved in MeOH and analysed using HPLC to measure the relative proportions of the rotaxanes **1.9** and **5.5** (**Table 5.1**). To compare the areas under the peaks that are due to the rotaxanes **1.9** and **5.5** in the HPLC chromatogram, the isosbestic point of the two rotaxanes **1.9** and **5.5** was first measured by injecting an equimolar solution of the two rotaxanes **1.9** and **5.5** onto the HPLC. The areas under the peaks in the HPLC chromatogram were then integrated at the isosbestic point (332 nm) to estimate the percentage compositions. When 10 μM of the rotaxane **5.5** was present in the mixture that was left to stand, the area under the peak corresponding to the rotaxane **5.5** was 0.7% of the total peak area (**Table 5.1**, Entry 2). When 100 μM of the rotaxane **5.5** was present in the mixture that was left to stand, the area under the peak corresponding to the rotaxane **5.5** increased to 5.0% in total (**Table 5.1**, Entry 4). The percentage composition of the rotaxane **5.5** is inversely proportional to crystal length. Although it may be possible for the rotaxane **5.5** to incorporate into the growing chains of the rotaxane **1.9** through both trinitrophenyl as well as 3,5-dimethylaniline blocking groups, termination of crystal growth through incorporation suggests that the rotaxane **5.5** does not fit in the crystal lattice of the rotaxane **1.9** perfectly. As the rotaxane **5.5** continues to incorporate, crystal growth is eventually terminated as the crystal has too many crystal lattice defects to continue its growth.

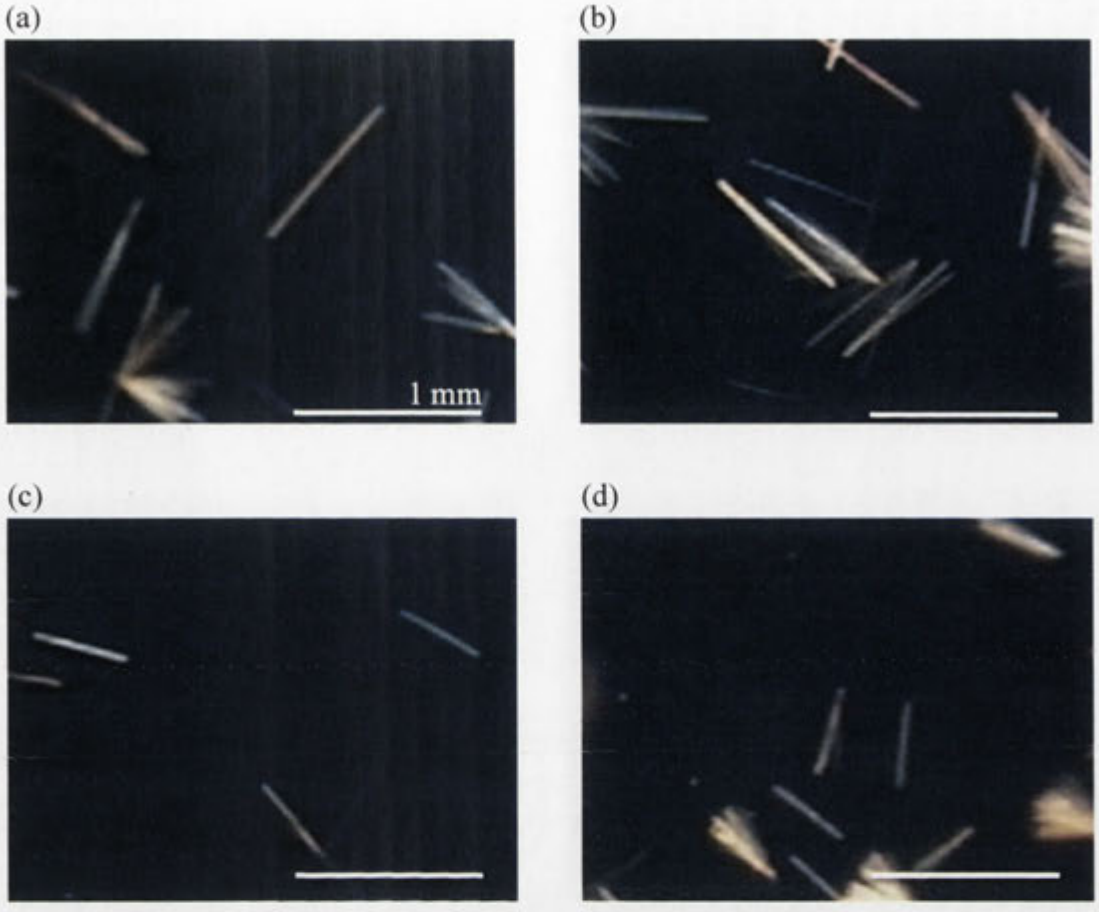

Figure 5.7. Optical microscope images of crystals grown after 4 days from solutions of (a) 100 μM of the rotaxane **1.9**, (b) 100 μM of the rotaxane **1.9** and 10 μM of the rotaxane **5.5**, (c) 100 μM of the rotaxane **1.9** and 50 μM of the rotaxane **5.5** and (d) 100 μM of the rotaxane **1.9** and 100 μM of the rotaxane **5.5**.

Entry	Concentration of the rotaxane **1.9** (μM)	Concentration of the rotaxane **5.5** (μM)	Average length of crystals (mm)	Number of rotaxanes aligned along the molecular fibre of the grown crystals	Composition of the rotaxane **5.5** in the grown crystals (%)
1	100	0	0.90	410000	0
2	100	10	0.80	360000	0.7
3	100	50	0.55	250000	3.9
4	100	100	0.45	200000	5.0

Table 5.1. Analysis of lengths and compositions of crystals shown in **Figure 5.7**.

5.5 Conclusion and Future Directions

The unsymmetrically capped rotaxane **5.5** was designed using a crystal engineering approach where the blocking groups can be used as synthons to guide intermolecular

self-assembly and regulate the formation of fibrous structures. The crystals of the rotaxane **1.9** have extended conjugation along the crystal fibres through π–π interactions of the blocking groups that are co-planar to the axles, however, when the rotaxane **5.5** incorporates into the crystals of the rotaxane **1.9**, extended conjugation would be limited as the trinitrophenyl blocking groups of the rotaxane **5.5** are expected to be out-of-plane of the axle. As a result, further to regulating self-assembly of rotaxanes, this opens up the possibility of using the unsymmetrically capped rotaxane **5.5** to explore regulating the degree of extended conjugation within molecular fibres of the rotaxane **1.9**. Only two different types of blocking groups have been studied, however, crystal growth experiments of the rotaxane **1.9** with the rotaxanes **4.1**, **4.2** and **5.5** suggest that regulation of crystal growth can be extended to other types of blocking groups. Additionally, it would be interesting to investigate the crystal growth regulation of not only the rotaxane **1.9** but also other rotaxanes that form fibres through π–π interactions. These preliminary experiments with the rotaxane **5.5** illustrate that crystal engineering using CD-based rotaxanes is a versatile approach towards regulating self-assembly and understanding molecular level interactions in the solid-state. Based on the understanding of self-assembly in the solid-state, it is likely that the work can also be further extended to the solution phase to regulate aggregates in solution and lyotropic liquid crystalline materials.

CHAPTER 6 - Results and Discussion
Synthesis of Rotaxanes to Preserve the Fluorescence of Paramagnetic Profluorescent Nitroxides

6.1 Synthesis and Conformational Analysis

As described in the Introduction, the objective of the work described in this Chapter was to prepare the rotaxanes **1.33**, **1.34**, **1.35** and **1.36** in an attempt to prevent *trans-cis* isomerisation, and consequently sustain the fluorescence of the corresponding dumbbells **1.37** and **1.38**. The rotaxanes **1.33** and **1.34** were prepared following a procedure adapted from Maniam.[135] Although only the isolation of the single isomer **1.34** was reported by Maniam, theoretically, there are two isomers differing in the orientation of the CD with respect to the dumbbell that could form.[134,165-169] The profluorescent nitroxide axle **6.1** was equilibrated with excess α-CD **1.1** and two molar equivalents of TEA in water. Then DMT-MM was added, followed by 2,6-dimethylaniline **2.4** (**Scheme 6.1**). Only one new spot was detected by TLC, however, two components that presumably co-eluted on TLC were separated by HPLC (**Figure 6.1**). ESI mass spectrometry of each component showed a protonated molecular ion at *m/z* 1413 and the desired rotaxanes **1.33** and **1.34** were isolated in yields of 19% and 21% through this single synthetic procedure.

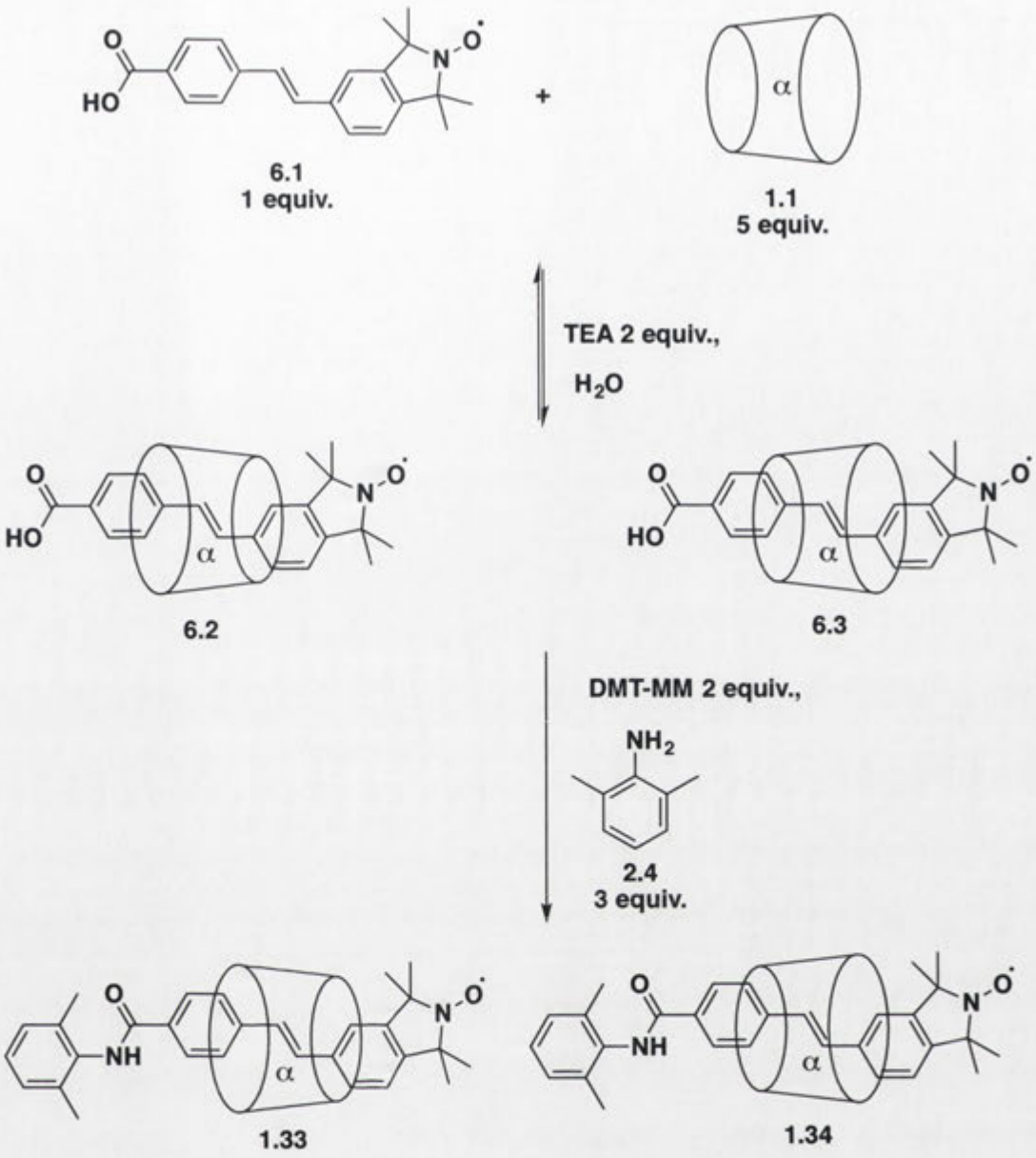

Scheme 6.1. Synthesis of the stilbenylnitroxide-based rotaxanes **1.33** and **1.34**.

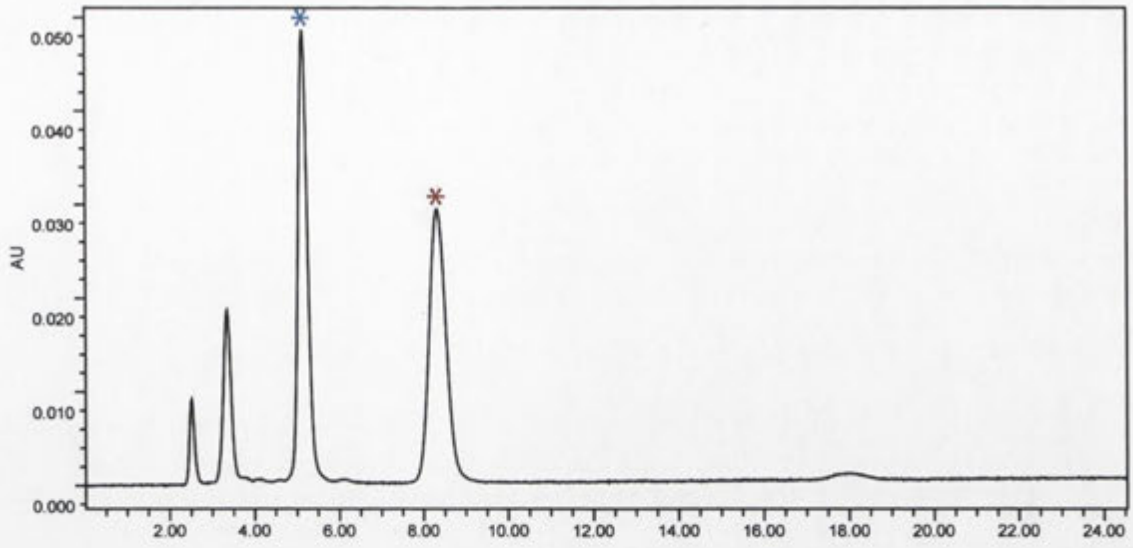

Figure 6.1. Chromatogram obtained through reverse phase HPLC of the crude product mixture formed as outlined in **Scheme 6.1**.

Figure 6.2 shows the ^{1}H NMR spectrum of the sample corresponding to the HPLC peak indicated by the blue asterisk in **Figure 6.1**. Preliminary observation of the spectrum suggests this sample is the orientational isomer of the rotaxane **1.34**, as it differs from the spectrum of the rotaxane **1.34** reported by Maniam.[135] Indeed, this sample was assigned as the rotaxane **1.33** by NMR analysis as described in the following pages. Initially the proton signals could not be assigned as they are broad due to the paramagnetic nature of the rotaxane **1.33**. Hence, the rotaxane **1.33** was reduced to the hydroxylamine **6.5** using ascorbic acid **6.4** (**Scheme 6.2**).[90] **Figure 6.3** shows the ^{1}H NMR spectrum of the hydroxylamine **6.5** showing well resolved signals for analysis. The ^{1}H NMR spectrum confirms the presence of the components, showing resonances of the CD, styrylisoindoline and arylamino protons. In order to verify the rotaxane formation and the orientation of the CD with respect to the dumbbell, 2D NMR analysis of the rotaxane **1.33** was also carried out on the reduced form **6.5**.

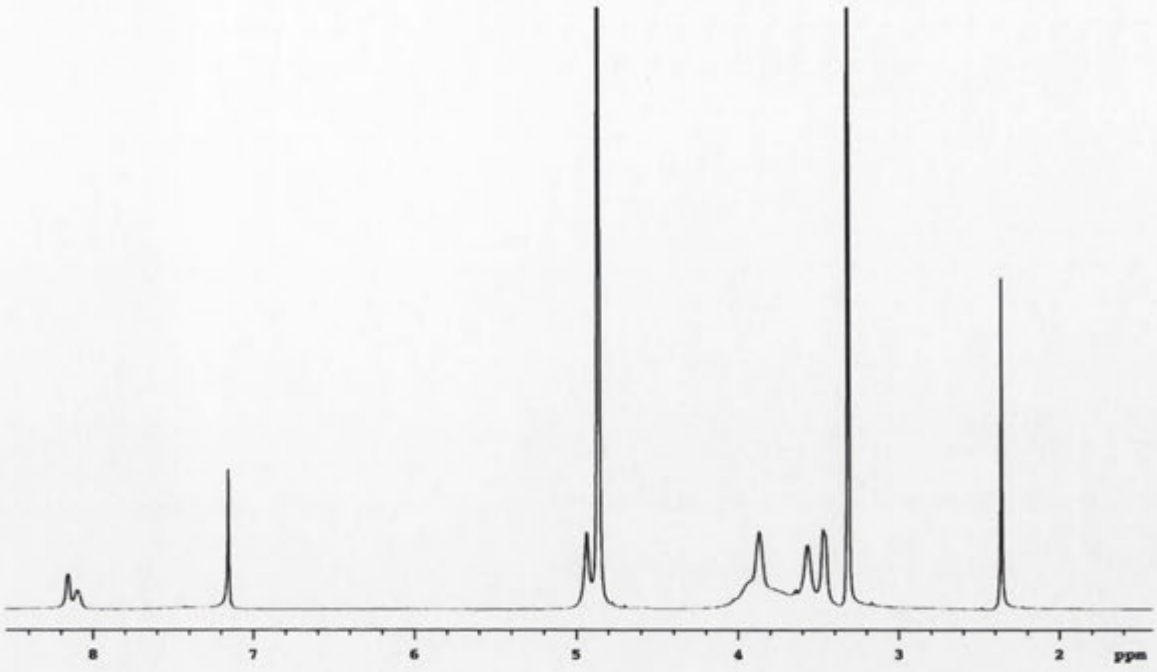

Figure 6.2. 500 MHz ^{1}H NMR spectrum of the rotaxane **1.33** in CD_3OD.

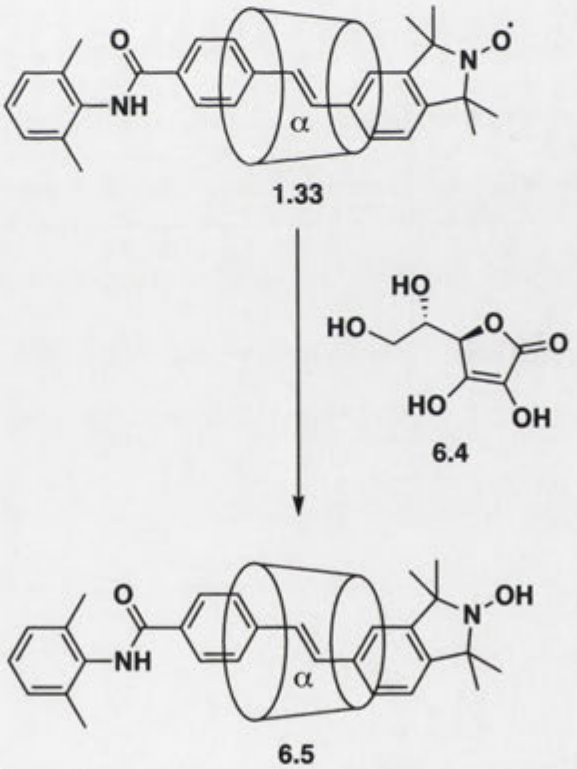

Scheme 6.2. Reduction of the rotaxane **1.33** to the hydroxylamine **6.5** using ascorbic acid **6.4**.

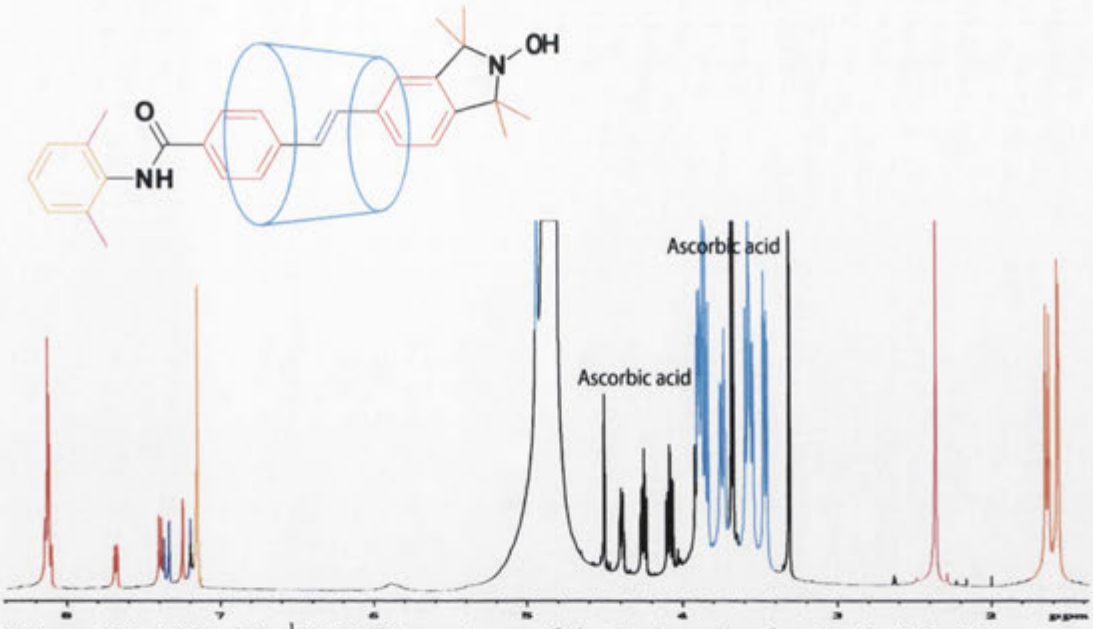

Figure 6.3. 500 MHz ^{1}H NMR spectrum of the hydroxylamine **6.5** in CD_3OD.

The general protocol used in Chapter 2 to determine the position of the CD along the axle and the conformation of CD-based [2]rotaxanes was followed for the rotaxane **6.5**.[170] **Figure 6.4** shows a section of the DQF-COSY NMR spectrum of the rotaxane **6.5**, where the CD proton cross-peaks are found. The most downfield CD resonance at δ4.93 is assigned to the CD-C1 anomeric protons. A ^{1}H-^{1}H correlation between these protons and those giving rise to the signal at δ3.46 is seen, and the latter is therefore assigned to the CD-C2 protons. Likewise, there is a cross-peak between the resonance at δ3.46 (CD-C2) and the resonance at δ3.86 which is therefore attributed to the CD-C3 protons. This resonance at δ3.86 (CD-C3) also shows a cross-peak with the resonance at δ3.57 which is therefore assigned to the CD-C4 protons. Again, the resonance at δ3.57 (CD-C4) also shows a cross-peak with the resonance at δ3.89 which is therefore assigned to the CD-C5 protons. Finally, the resonances at δ3.74 and 3.59 corresponding to the CD-C6 protons show cross-peaks with each other.

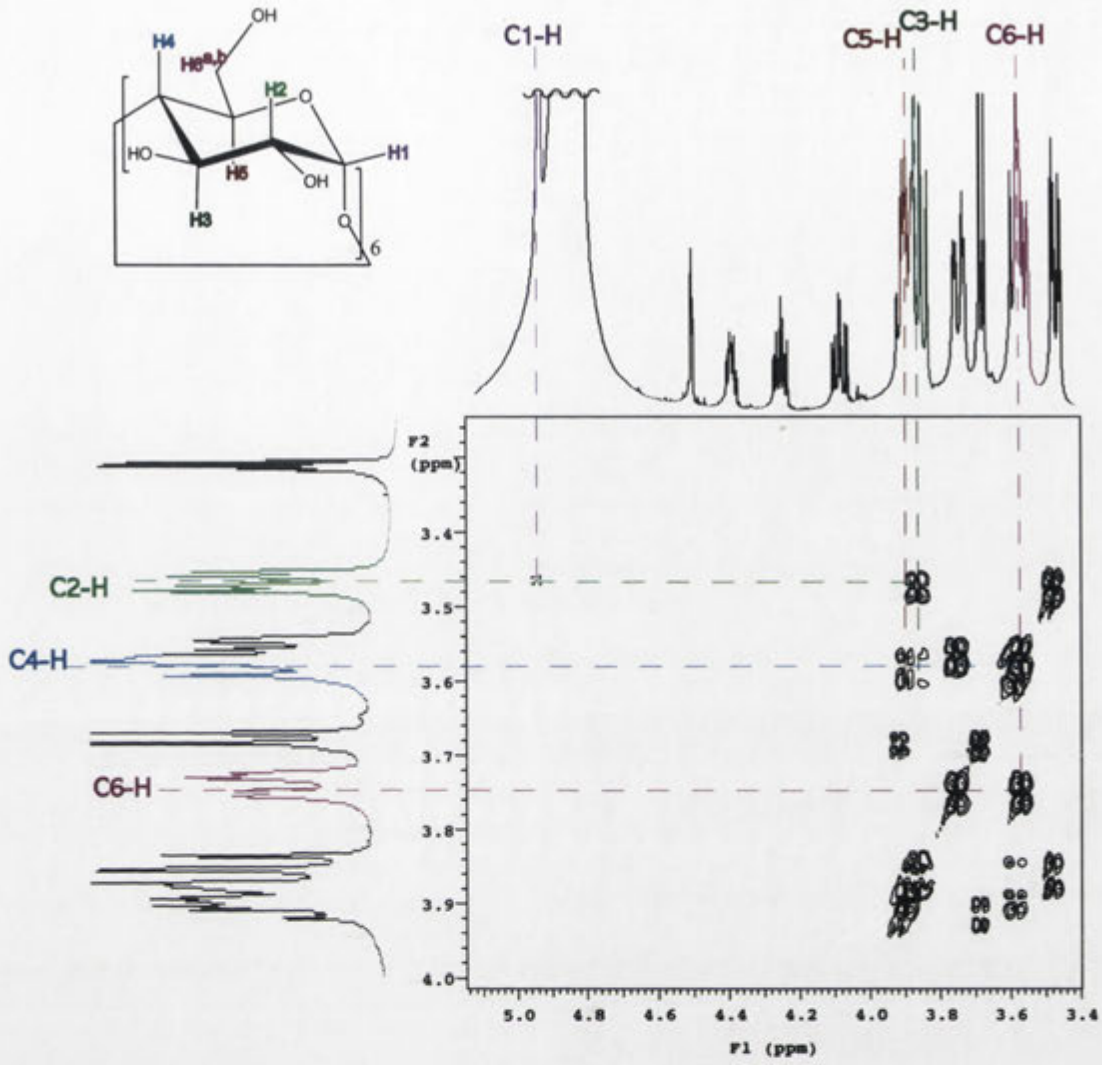

Figure 6.4. A section of the 500 MHz 2D DQF-COSY NMR spectrum of the rotaxane **6.5** in CD_3OD showing cross-peaks between CD proton signals.

The structural assignment can then be completed by analysis of the nuclear Overhauser effect (NOE) interactions in the ROESY NMR spectrum. **Figure 6.5** shows a section of the 2D ROESY NMR spectrum with cross-peaks for the aromatic protons. Since the signal at δ8.10, which integrates for two protons, shows a cross-peak with the olefinic proton signal at δ7.18, these two signals are assigned as the aromatic protons E and olefinic proton G respectively. Likewise, the signal at δ7.68, which integrates for one proton, shows a cross-peak with the olefinic proton signal at δ7.36. Therefore, these signals are assigned as the aromatic proton I and olefinic proton F respectively. The signal at δ8.13, which integrates for two protons and has the same coupling constant as the signal at δ8.10 (protons E) is assigned as the aromatic protons D. The doublet at δ7.39 with the same coupling constant as the

resonance of proton I is assigned to the resonance of proton J, while the singlet at δ7.25 is assigned to resonance of proton H.

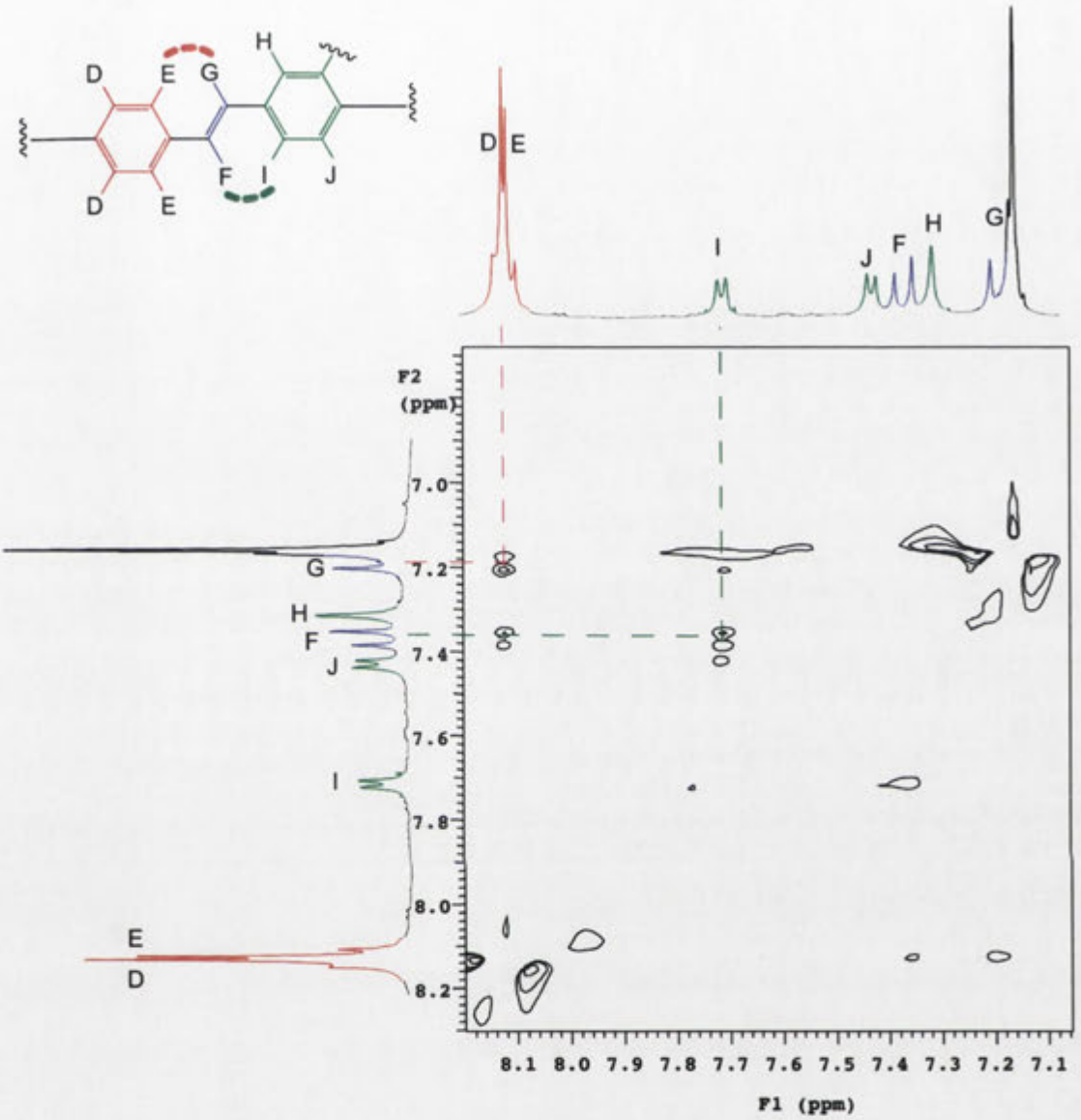

Figure 6.5. A section of the 500 MHz 2D ROESY NMR spectrum of the rotaxane **6.5** in CD_3OD showing cross-peaks between aromatic proton signals.

Figure 6.6 shows a section of the 2D ROESY NMR spectrum with axle and aniline aromatic proton resonance cross-peaks with those of methyl and CD protons. The presence of the NOE cross-peaks labelled NOE1 and NOE2 indicates the resonances at δ1.64 and 1.62 correspond to the methyls of the isoindoline moiety in proximity to the aromatic proton H (protons K and L), and the resonances at δ1.57 and 1.56 correspond to those in proximity to the aromatic proton J (protons M and N). The resonance of aniline protons A and B appears at δ7.16. The presence of the NOE cross-peaks labelled NOE3 and NOE4 indicates that the resonance at δ2.36

corresponds to the methyls of the 2,6-dimethylaniline moiety (protons C). Looking at the cross-peaks between the aromatic and CD protons, the CD orientation can be assigned. Protons H, I and J show NOEs with the CD-C5 and CD-C6 protons, hence they are next to the narrow end of the CD as shown in **Figure 6.6**. Overall, from the structural assignment of the hydroxylamine **6.5**, the analogous nitroxide can be assigned as the rotaxane **1.33**, which is the orientational isomer of the rotaxane **1.34** previously reported by Maniam.[135]

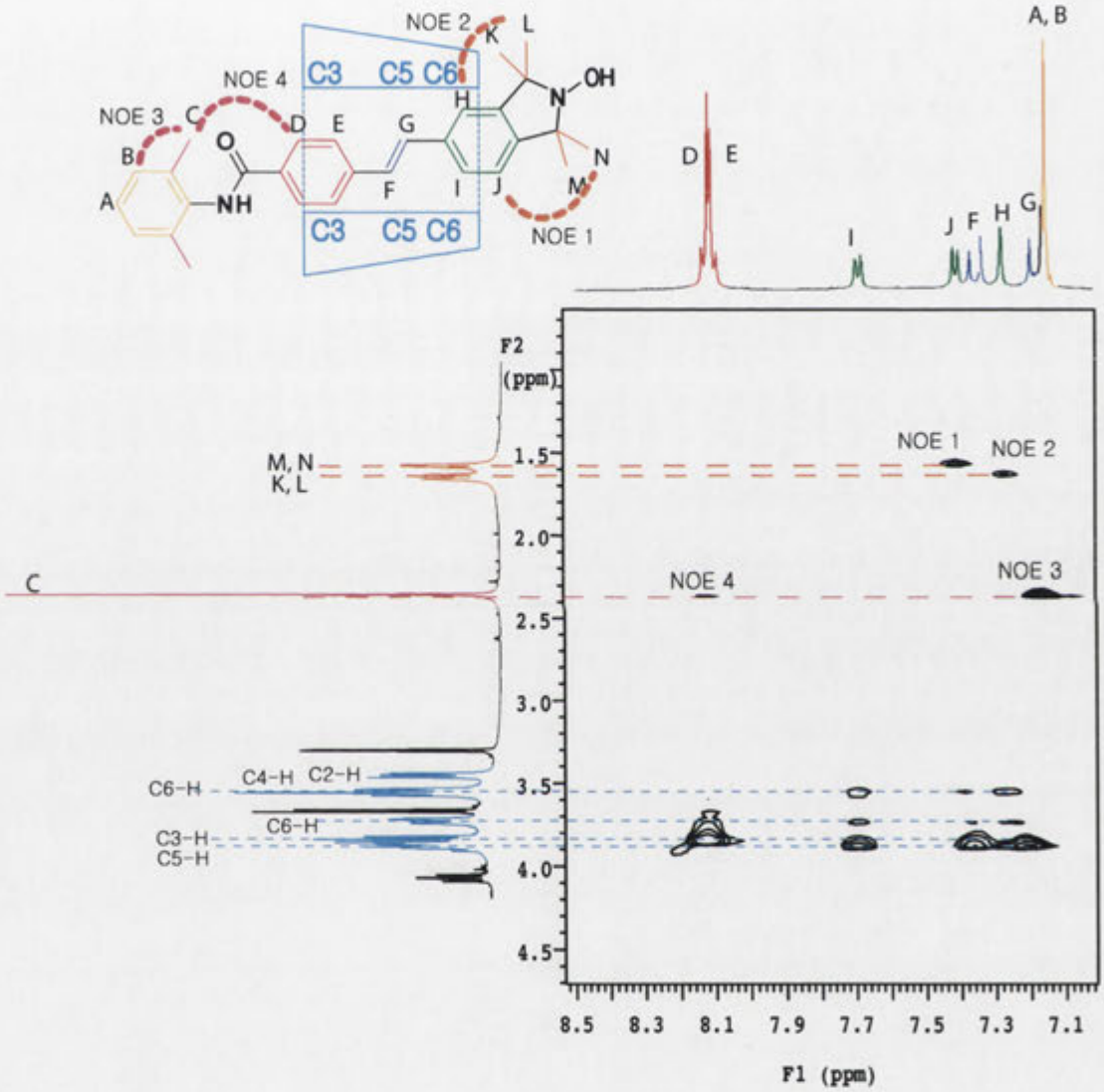

Figure 6.6. A section of the 500 MHz 2D ROESY NMR spectrum of the rotaxane **6.5** in CD_3OD showing axle and aniline aromatic proton resonance cross-peaks with those of methyl and CD protons.

Figure 6.7 shows the ^1H NMR spectrum of the sample corresponding to the HPLC peak indicated by the pink asterisk in **Figure 6.1**. This sample was reduced as shown in **Scheme 6.3**. **Figure 6.8** shows the ^1H NMR spectrum of this sample in the reduced

form. The spectral data shown in **Figure 6.7** and **Figure 6.8** are consistent with those of the rotaxane **1.34** and the corresponding hydroxylamine **6.6** reported by Maniam.[135]

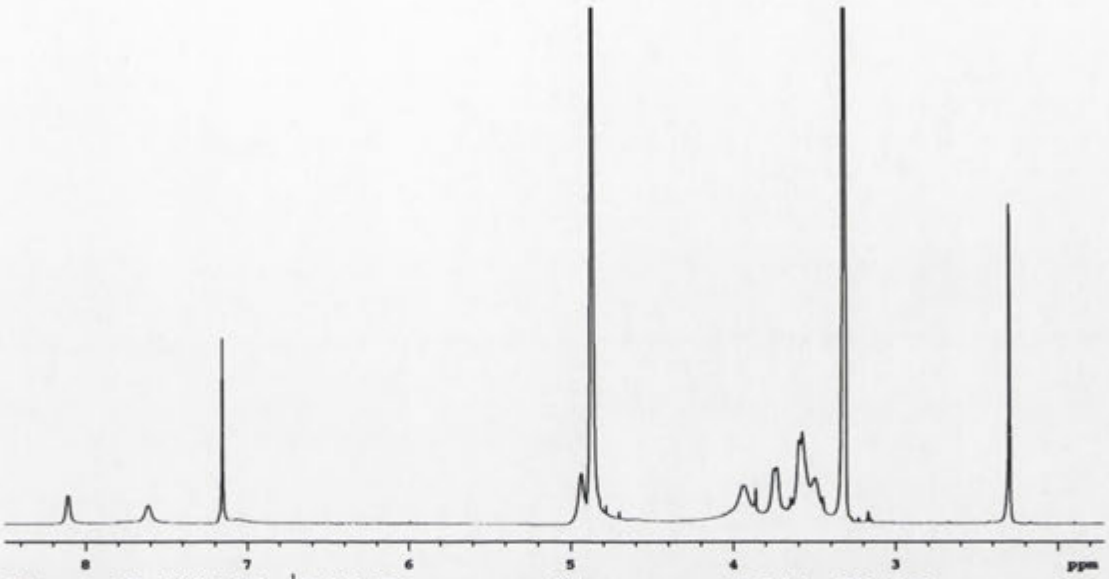

Figure 6.7. 500 MHz ^{1}H NMR spectrum of the rotaxane **1.34** in CD_3OD.

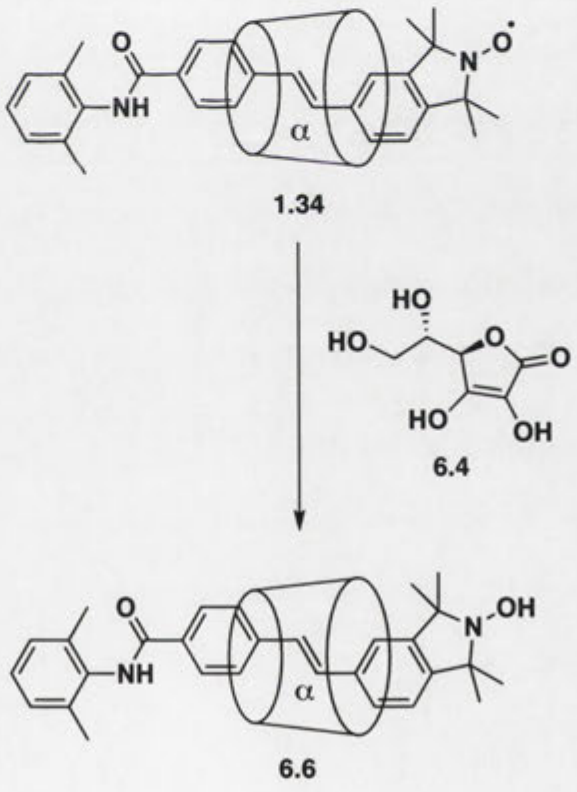

Scheme 6.3. Reduction of the rotaxane **1.34** to the hydroxylamine **6.6** using ascorbic acid **6.4**.

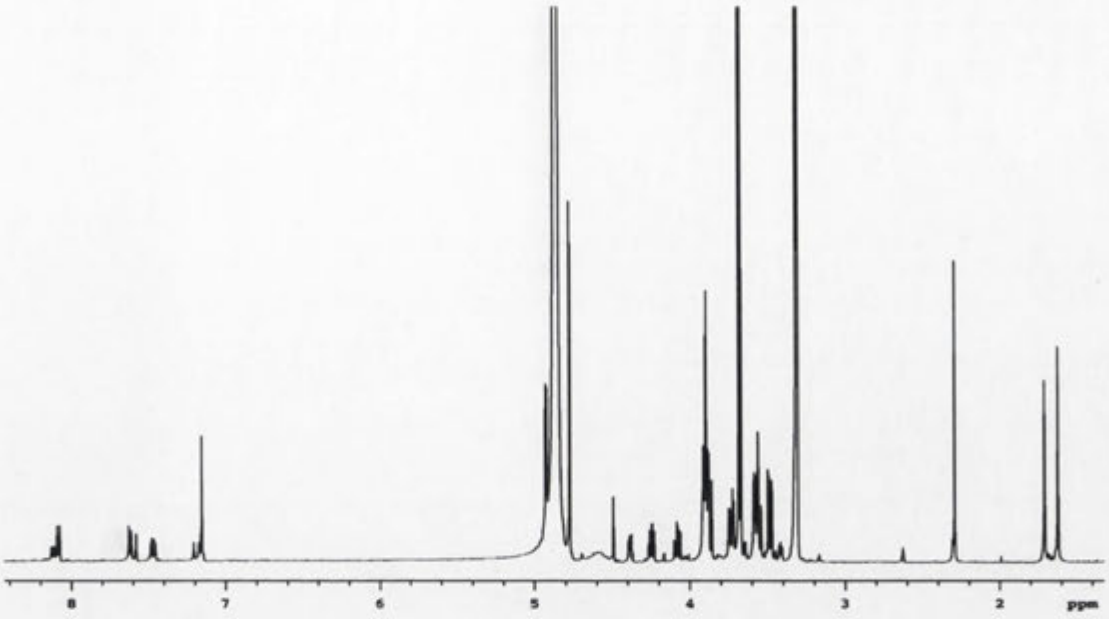

Figure 6.8. 500 MHz ^{1}H NMR spectrum of the hydroxylamine **6.6** in CD_3OD.

Following the successful synthesis of the rotaxanes **1.33** and **1.34**, the analogous rotaxanes **1.35** and **1.36** with 3,5-dimethylaniline blocking groups were also prepared using a similar procedure.[135] The stilbenylnitroxide axle **6.1** was equilibrated with excess α-CD **1.1** and two molar equivalents of TEA in water. Then DMT-MM was added, followed by 3,5-dimethylaniline **2.2** (**Scheme 6.5**). TLC of the reaction mixture showed a component with a different R_f value to α-CD **1.1**, yet showing both the UV absorbance of an aromatic compound and the pink colouration characteristic of a CD on exposure to acidic naphthalene-1,3-diol.[138] Although only one new spot was detected by TLC, two components that presumably co-eluted on TLC were separated by HPLC. ESI mass spectrometry of each component showed a protonated molecular ion at *m/z* 1413 and the desired rotaxanes **1.35** and **1.36** were isolated in yields of 30% and 29%.

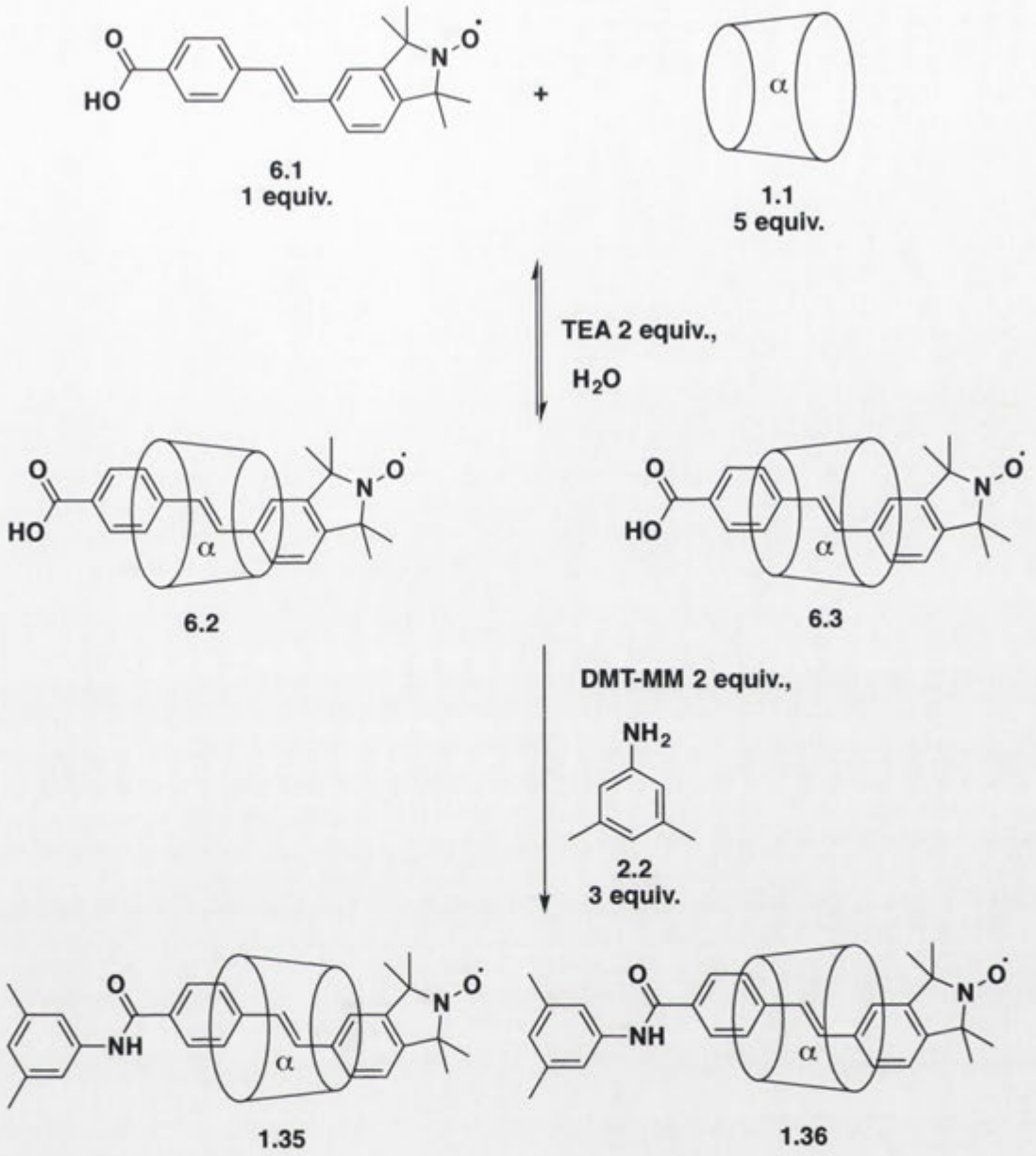

Scheme 6.4. Synthesis of the nitroxide-based rotaxanes **1.35** and **1.36**.

Two fractions, each containing a rotaxane isomer, were collected through HPLC. The first eluting fraction was assigned as the rotaxane **1.35** and the later fraction as the rotaxane **1.36** by NMR analysis as described below. **Figure 6.9** shows the ^{1}H NMR spectrum of the first eluting fraction collected through HPLC. NMR analysis was carried out in the reduced form **6.7** as shown in **Figure 6.10**.

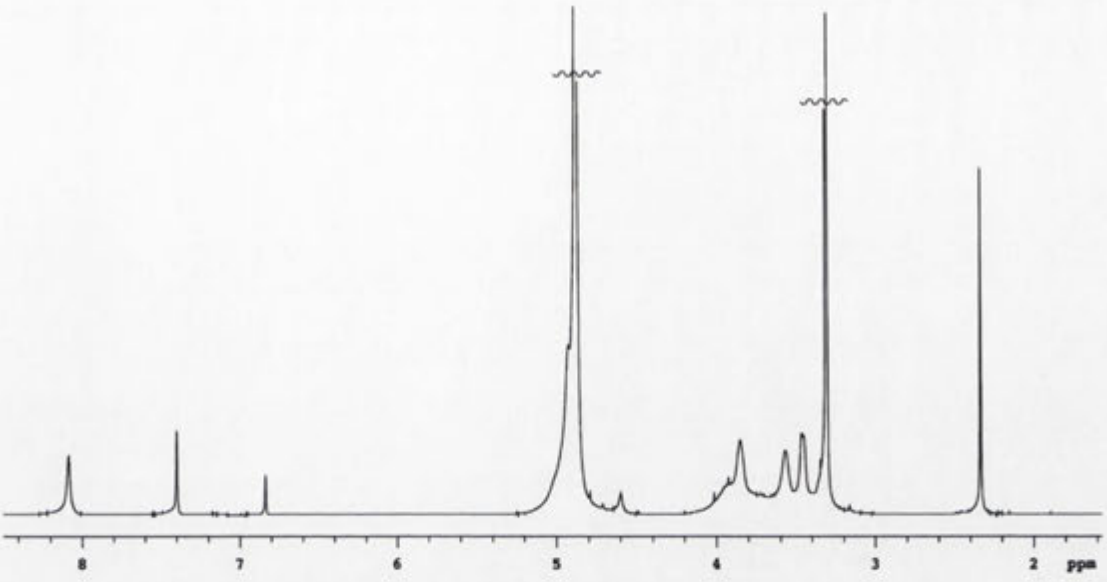

Figure 6.9. 500 MHz ^{1}H NMR spectrum of the rotaxane **1.35** in CD_3OD.

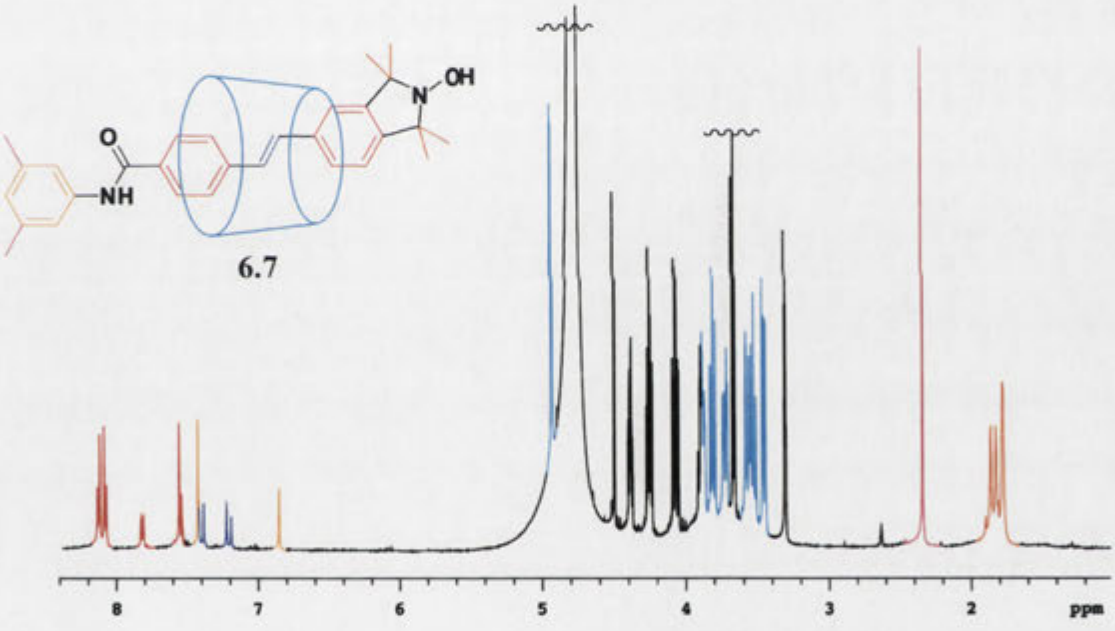

6.7

Figure 6.10. 500 MHz ^{1}H NMR spectrum of the hydroxylamine **6.7** in CD_3OD.

To unambiguously determine the orientation of the CD with respect to the dumbbell and assign the structure of the rotaxane **6.7**, 2D NMR analysis was carried out following the protocol described for the rotaxane **6.5**. The CD proton resonances were assigned using the DQF-COSY NMR spectrum shown in **Figure 6.11**. The most downfield CD resonance at δ4.93 is assigned to the CD-C1 anomeric protons. A ^{1}H-^{1}H correlation between these protons and those giving rise to the signal at δ3.46 is seen, and the latter is therefore assigned to the CD-C2 protons. Likewise, there is a

cross-peak between the resonance at δ3.46 (CD-C2) and the resonance at δ3.81 which is therefore attributed to the CD-C3 protons. This resonance at δ3.81 (CD-C3) also shows a cross-peak with the resonance at δ3.53 which is therefore assigned to the CD-C4 protons. Again, the resonance at δ3.53 (CD-C4) also shows a cross-peak with the resonance at δ3.90 which is therefore assigned to the CD-C5 protons. Finally, the resonances at δ3.72 and 3.58 corresponding to the CD-C6 protons show cross-peaks with each other.

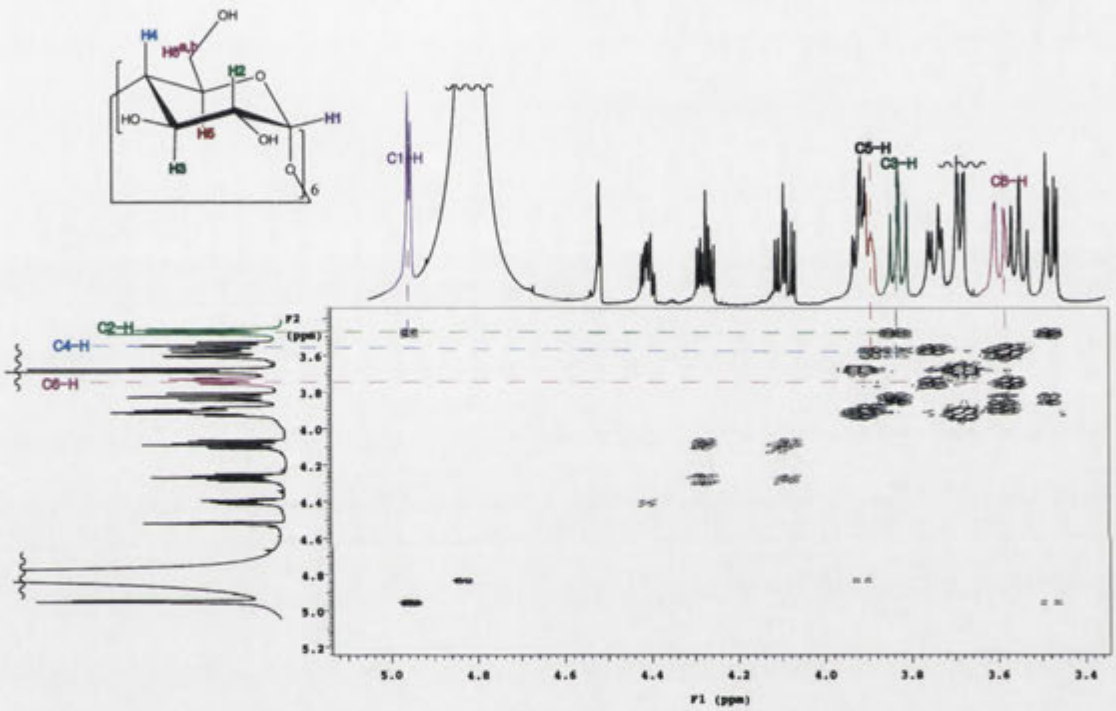

Figure 6.11. A section of the 500 MHz 2D DQF-COSY NMR spectrum of the rotaxane **6.7** in CD_3OD showing cross-peaks between CD proton signals.

Assignments were continued by examining a section of the 2D ROESY NMR spectrum with cross-peaks for the aromatic protons shown in **Figure 6.12**. Since the signal at δ8.13, which integrates for two protons, shows a cross-peak with the olefinic proton signal at δ7.22, these two signals are assigned as the aromatic protons E and olefinic proton G respectively. Likewise, the signal at δ7.82, which integrates for one proton, shows a cross-peak with the olefinic proton signal at δ7.40. Therefore, these signals are assigned as the aromatic proton I and olefinic proton F respectively. The signal at δ8.08, which integrates for two protons and has the same coupling constant as the signal at δ8.13 (protons E) is assigned as the aromatic protons D. The doublet at δ7.55 with the same coupling constant as the resonance of proton I can be assigned to

the resonance of proton J, while the singlet at δ7.56 can be assigned to resonance of proton H.

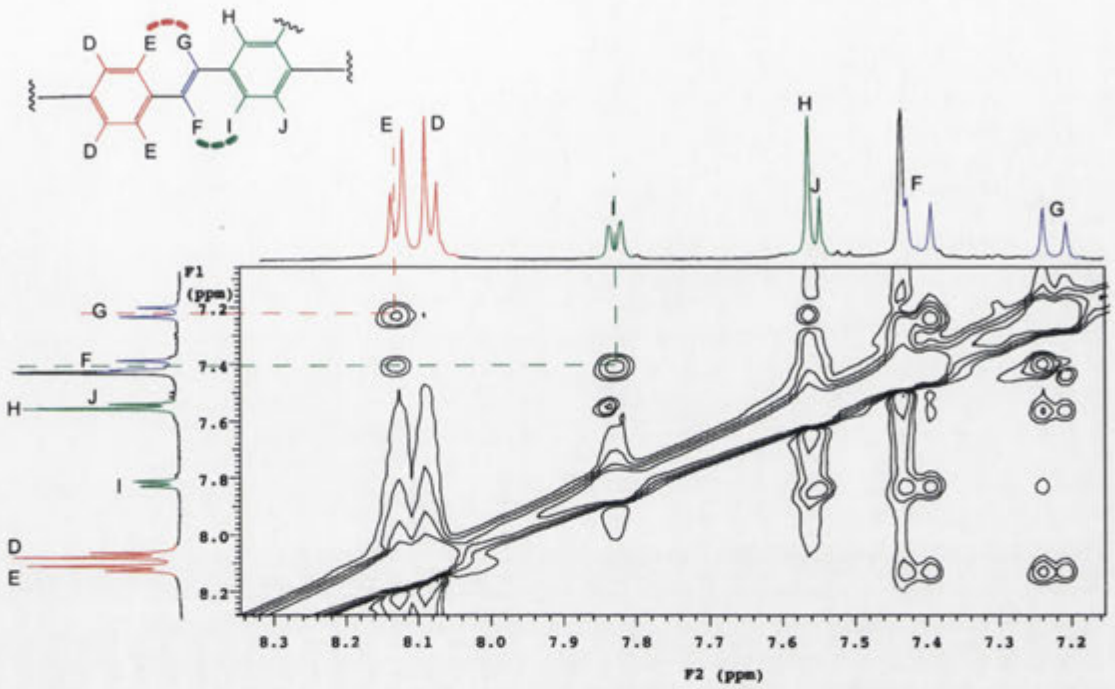

Figure 6.12. A section of the 500 MHz 2D ROESY NMR spectrum of the rotaxane **6.7** in CD_3OD showing cross-peaks between aromatic proton signals.

Figure 6.13 shows a section of the 2D ROESY NMR spectrum with axle and aniline aromatic proton resonance cross-peaks with those of methyl and CD protons. The presence of the NOE cross-peak labelled NOE1 indicates the resonances at δ1.78 correspond to the methyls of the isoindoline moiety in proximity to the aromatic proton J (protons M and N). Likewise, the presence of the NOE cross-peak labelled NOE2 indicates the resonances at δ1.87 and 1.83 correspond to the methyls of the isoindoline moiety in proximity to the aromatic proton H (protons K and L). The resonances of aniline protons C appear at δ7.48 and the aniline proton A at δ6.85. The presence of the NOE cross-peaks labelled NOE3 and NOE4 indicates that the resonance at δ2.35 corresponds to the methyls of the 3,5-dimethylaniline moiety (protons B). Looking at the cross-peaks between the aromatic and CD protons, the CD orientation can be assigned. As protons D and E show the strongest NOEs with the CD-C3 protons, they are next to the wider end of the CD. Protons H, I and J show NOEs with CD-C5 and CD-C6 protons, hence they are next to the narrow end of the CD as shown in **Figure 6.13** and the structure is assigned as the rotaxane **6.7**. From

the structural assignment of the hydroxylamine **6.7**, the analogous nitroxide can be assigned as the rotaxane **1.35**.

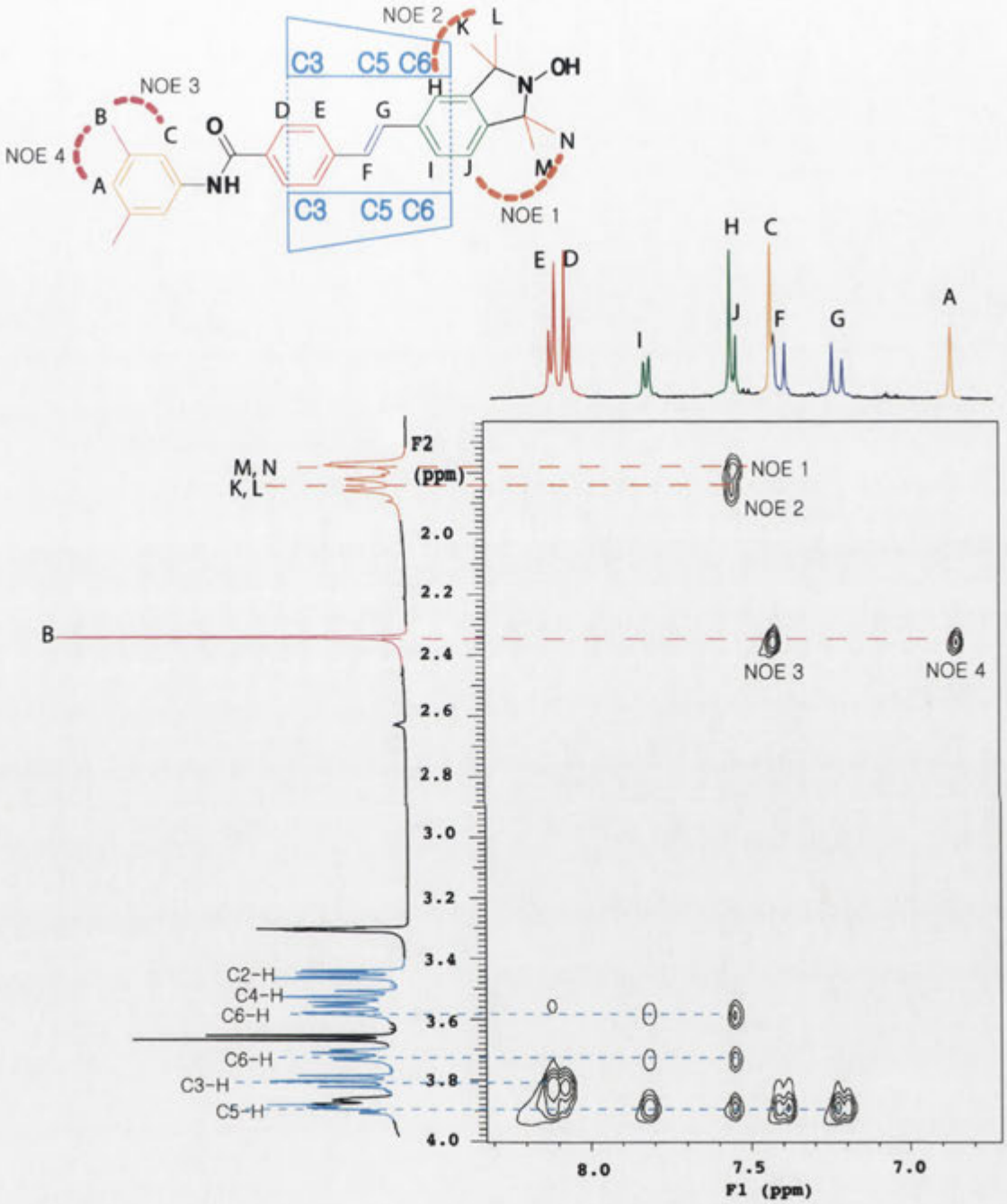

Figure 6.13. A section of the 500 MHz 2D ROESY NMR spectrum of the rotaxane **6.7** in CD_3OD showing axle and aniline aromatic proton resonance cross-peaks with those of methyl and CD protons.

Figure 6.14 shows the ^1H NMR spectrum of the second eluting fraction collected through HPLC. NMR analysis was carried out in the reduced form **6.8** (**Figure 6.15**).

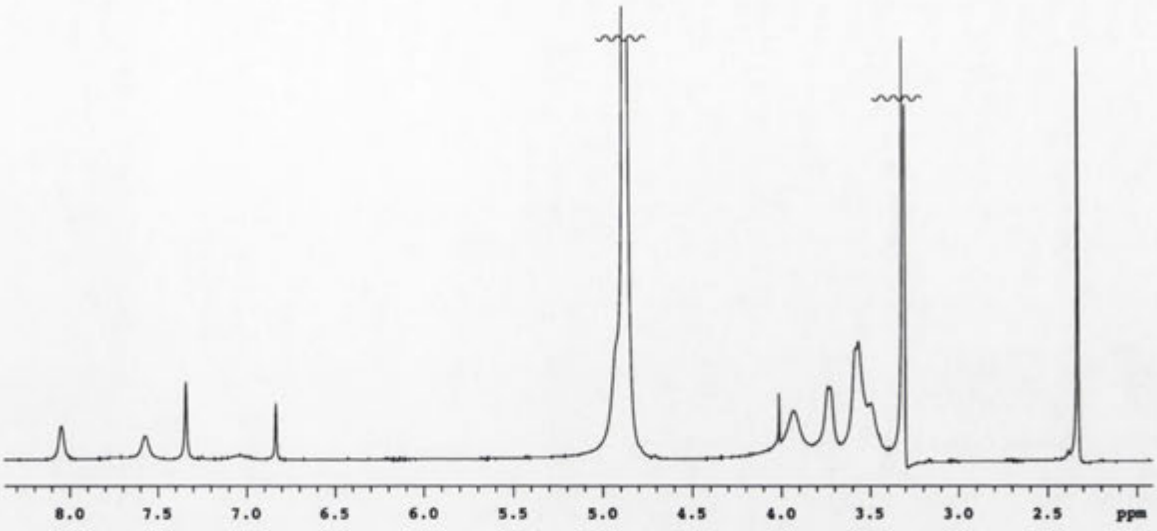

Figure 6.14. 500 MHz ^{1}H NMR spectrum of the rotaxane **1.36** in CD_3OD.

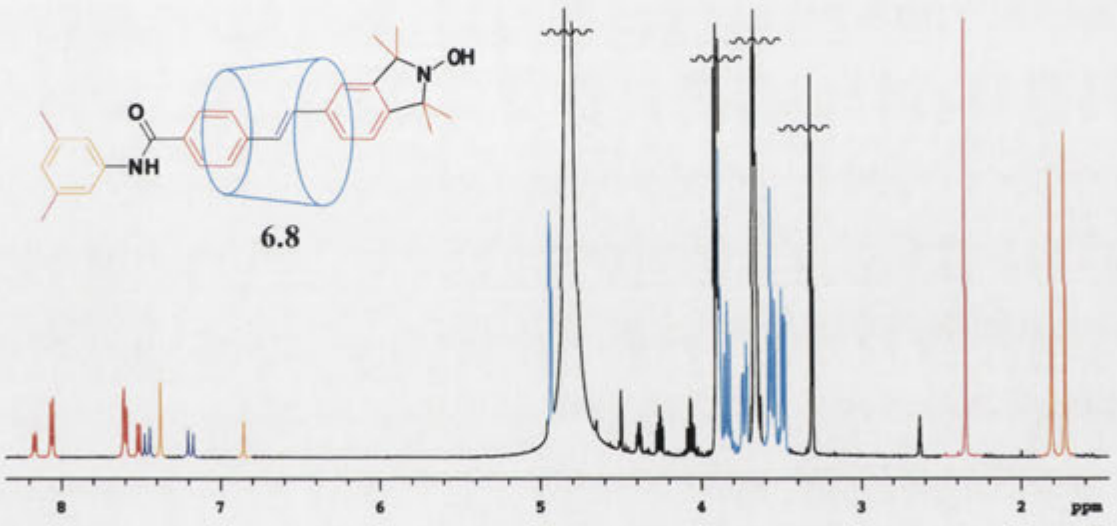

Figure 6.15. 500 MHz ^{1}H NMR spectrum of the hydroxylamine **6.8** in CD_3OD.

Following the standard protocol carried out with the rotaxanes **6.5** and **6.7**, the proton resonances of the rotaxane **6.8** were assigned. First, the CD proton resonances were assigned in the same manner as described above using the DQF-COSY NMR spectrum shown in **Figure 6.16**. The resonance of the CD-C1 anomeric protons is assigned at δ4.94. A ^{1}H-^{1}H correlation between these protons and those giving rise to the signal at δ3.50 is seen, and the latter is therefore assigned to the CD-C2 protons. Likewise, there is a cross-peak between the resonance at δ3.50 (CD-C2) and the resonance at δ3.81 which is therefore attributed to the CD-C3 protons. This resonance

at δ3.81 (CD-C3) also shows a cross-peak with the multiplet at δ3.57 which is therefore assigned to the CD-C4 protons. Again, the resonance at δ3.57 (CD-C4) also shows a cross-peak with the resonance at δ3.88 which is therefore assigned to the CD-C5 protons. Finally, the resonances at δ3.72 and 3.57 corresponding to the CD-C6 protons show cross-peaks with each other.

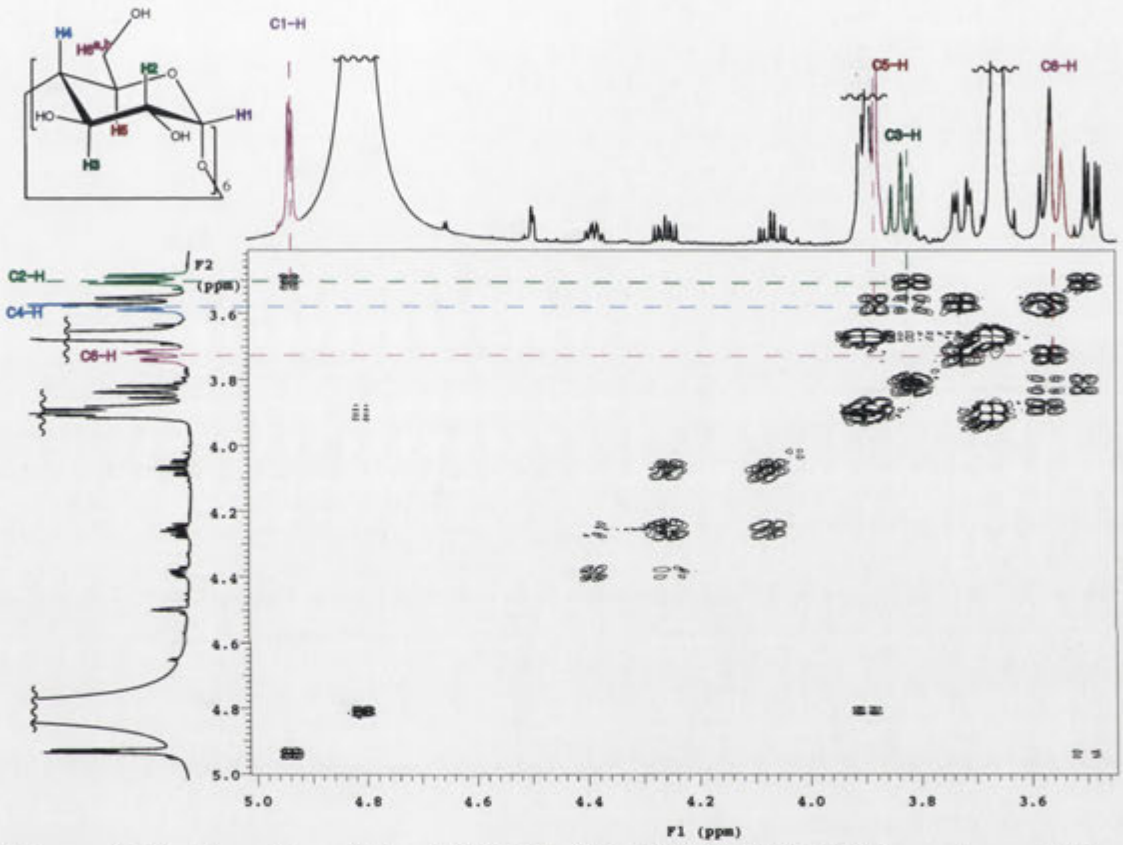

Figure 6.16. A section of the 500 MHz 2D DQF-COSY NMR spectrum of the rotaxane **6.8** in CD_3OD showing cross-peaks between CD proton signals.

Next the aromatic region was assigned using the 2D ROESY NMR spectrum as shown in **Figure 6.17**. Since the signal at δ7.60, which integrates for two protons, shows a cross-peak with the olefinic proton signal at δ7.46, these two signals are assigned as the aromatic protons E and olefinic proton G respectively. Likewise, the signal at δ8.21, which integrates for one proton, shows a cross-peak with the olefinic proton signal at δ7.21. Therefore, these signals are assigned as the aromatic proton I and olefinic proton F respectively. The signal at δ8.05, which integrates for two protons and has the same coupling constant as the signal at δ7.60 (protons E) is assigned as the aromatic protons D. The doublet at δ7.56 with the same coupling

constant as the resonance of proton I can be assigned to the resonance of proton J, while the singlet at δ7.64 can be assigned to resonance of proton H.

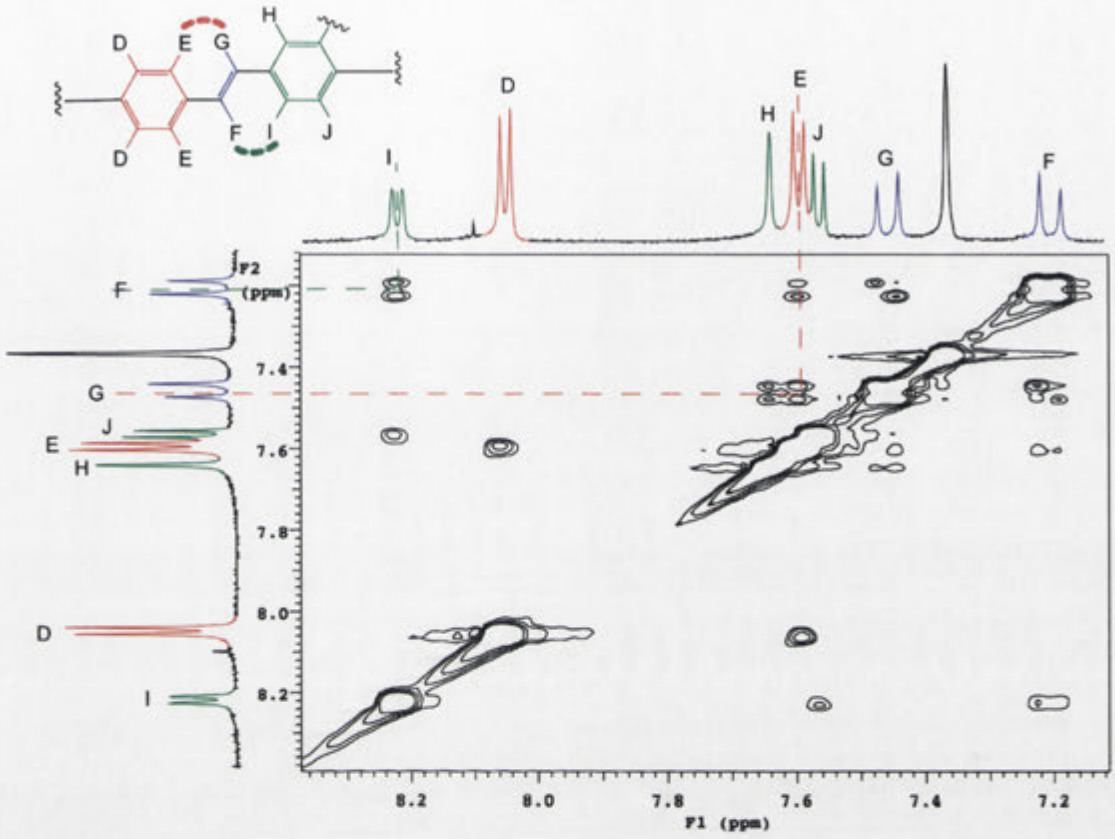

Figure 6.17. A section of the 500 MHz 2D ROESY NMR spectrum of the rotaxane **6.8** in CD_3OD showing cross-peaks between aromatic proton signals.

Finally, **Figure 6.18** shows a section of the 2D ROESY NMR spectrum with axle and aniline aromatic proton resonance cross-peaks with those of methyl and CD protons. The presence of the NOE cross-peak labelled NOE1 indicates that the resonances at δ1.88 correspond to the methyls of the isoindoline moiety in proximity to the aromatic proton H (protons K and L). Likewise, the NOE cross-peak labelled NOE2 indicates the resonances at δ1.88 correspond to the methyls of the isoindoline moiety in proximity to the aromatic proton J (protons M and N). The resonances of the aniline protons C appear at δ7.40 and the aniline proton A at δ6.85. The presence of the NOE cross-peaks labelled NOE3 and NOE4 indicate that the resonance at δ2.34 corresponds to the methyls of the 3,5-dimethylaniline moiety (protons B). Looking at the cross-peaks between the aromatic and CD protons, the CD conformation can be assigned. Protons H, I and J show NOEs with the CD-C3 protons, hence they are next

to the wider end of the CD. Protons E show NOEs with CD-C5 and CD-C6 protons, hence they are next to the narrow end of the CD as shown in **Figure 6.18**, and the structure is assigned as the rotaxane **6.8**. Thus by inference, the analogous nitroxide is assigned as the rotaxane **1.36**, which is the orientational isomer of the rotaxane **1.35** described above.

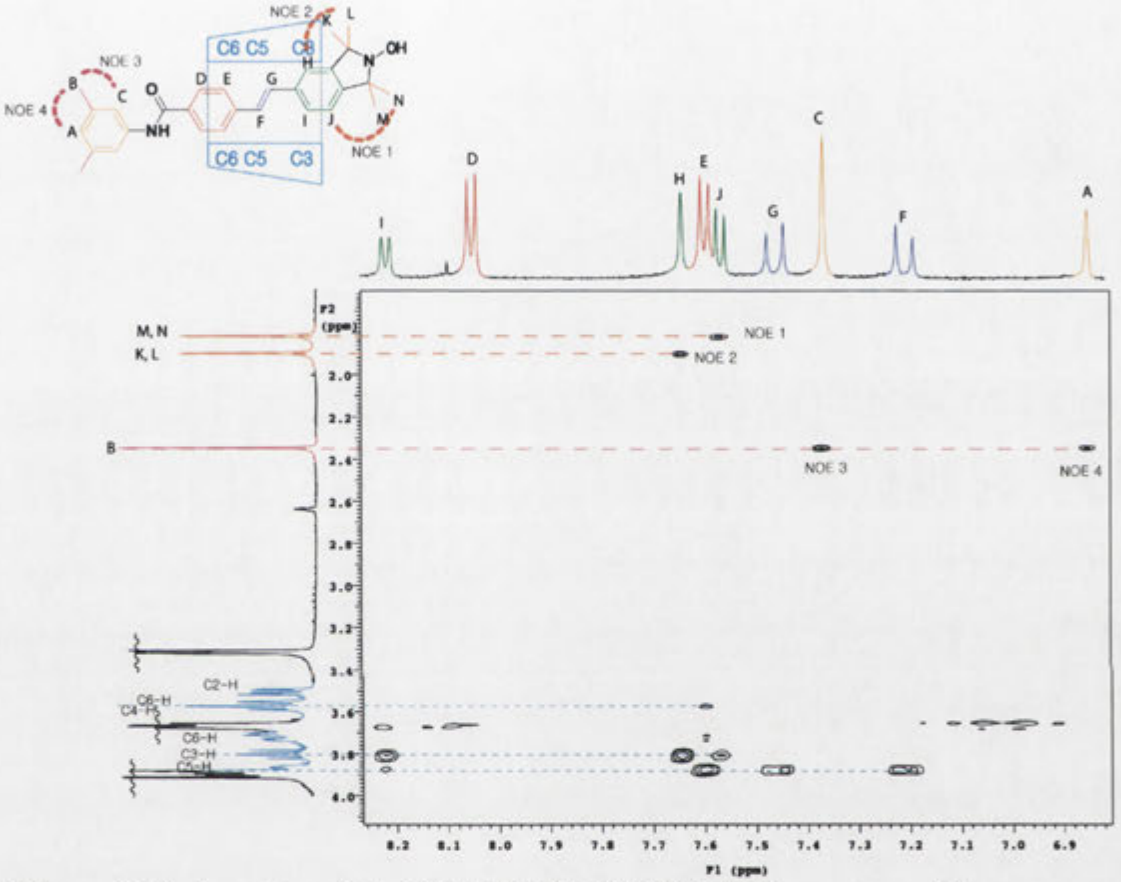

Figure 6.18. A section of the 500 MHz 2D ROESY NMR spectrum of the rotaxane **6.8** in CD_3OD showing axle and aniline aromatic proton resonance cross-peaks with those of methyl and CD protons.

An interesting observation from the 1D ^1H NMR spectra of the rotaxanes **1.33**, **1.34**, **1.35** and **1.36** is that, while the paramagnetic nature of the nitroxide group caused broadening of stilbene proton resonance peaks, those of the aniline moiety remained sharp. Conceivably this could be due to the lack of through space interaction between the free radical and the aniline blocking group, or it might be attributable to the lack of conjugation between the nitroxide containing axle and the aniline blocking group. As discussed in Chapter 4, the conformational analysis of the rotaxanes **1.9**, **4.1**, **4.2** and **1.18** in solution by UV/visible spectroscopy suggests that the 2,6-dimethylaniline blocking groups are twisted out-of-plane of the axle while the 3,5-dimethylaniline

blocking groups are co-planar to the axle. Hence the 2,6-dimethylaniline blocking groups of the rotaxanes **1.33** and **1.34** are most probably rotated out-of-the plane of the free radical containing axle, resulting in discontinued conjugation to the aniline moieties. On the other hand, the 3,5-dimethylaniline blocking groups of the rotaxanes **1.35** and **1.36** can be envisaged to be co-planar and hence fully conjugated with the free radical containing axle. Therefore, the sharpness of the aniline aromatic and methyl proton resonance peaks appears to be independent of the conjugation between the aniline blocking group and the axle. Instead, as the aniline protons are the furthest from the free radical through space, the nature of the lack of line broadening is conceivably due to distance.[89]

To compare the photoisomerisation behaviour of the rotaxanes **1.33** and **1.35** with the analogous compound without the CD, the dumbbell **1.37** was prepared following a procedure adapted from Maniam.[135] The stilbenylnitroxide axle **6.1** and BOP was added to DMF, followed by the addition of 2,6-dimethylaniline **2.4** and TEA (**Scheme 6.4**). The product was isolated in a yield of 47% through reverse phase HPLC. The identity of the dumbbell **1.37** was confirmed using ^{1}H NMR spectroscopic and mass spectrometric data which were found to be in agreement with those reported previously.[135]

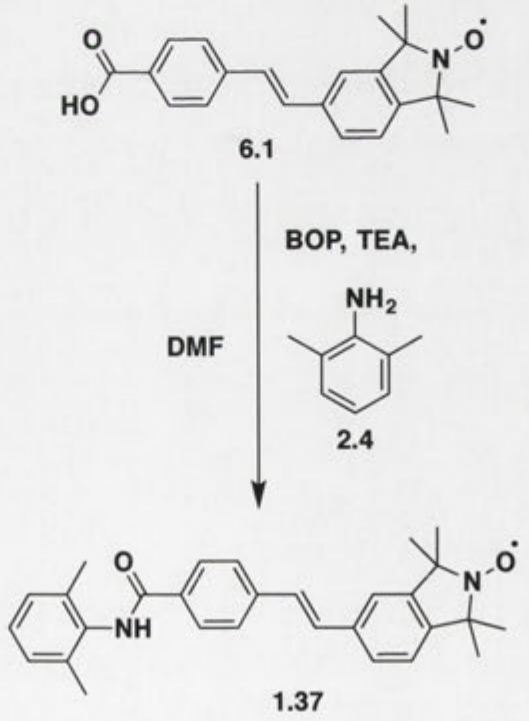

Scheme 6.7. Synthesis of the dumbbell **1.37**.

The analogous dumbbell **1.38** with 3,5-dimethylaniline in place of 2,6-dimethylaniline was also prepared following an analogous procedure. The stilbenylnitroxide axle **6.1** and BOP was added to DMF, followed by 3,5-dimethylaniline **2.2** and TEA (**Scheme 6.9**). ESI mass spectrometry showed an ion at *m/z* 441, which corresponds to the protonated molecular ion, and the product was isolated in a yield of 82% through reverse phase HPLC.

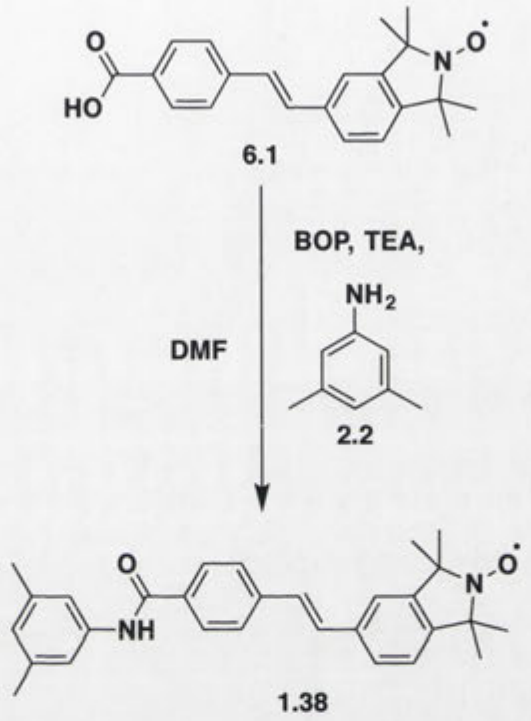

Scheme 6.8. The synthesis of the dumbbell **1.38**.

NMR analysis was carried out in the reduced form **6.9** (**Figure 6.19**). The ^{1}H NMR spectrum confirmed the presence of the components, showing resonances of the styrylisoindoline and arylamino protons.

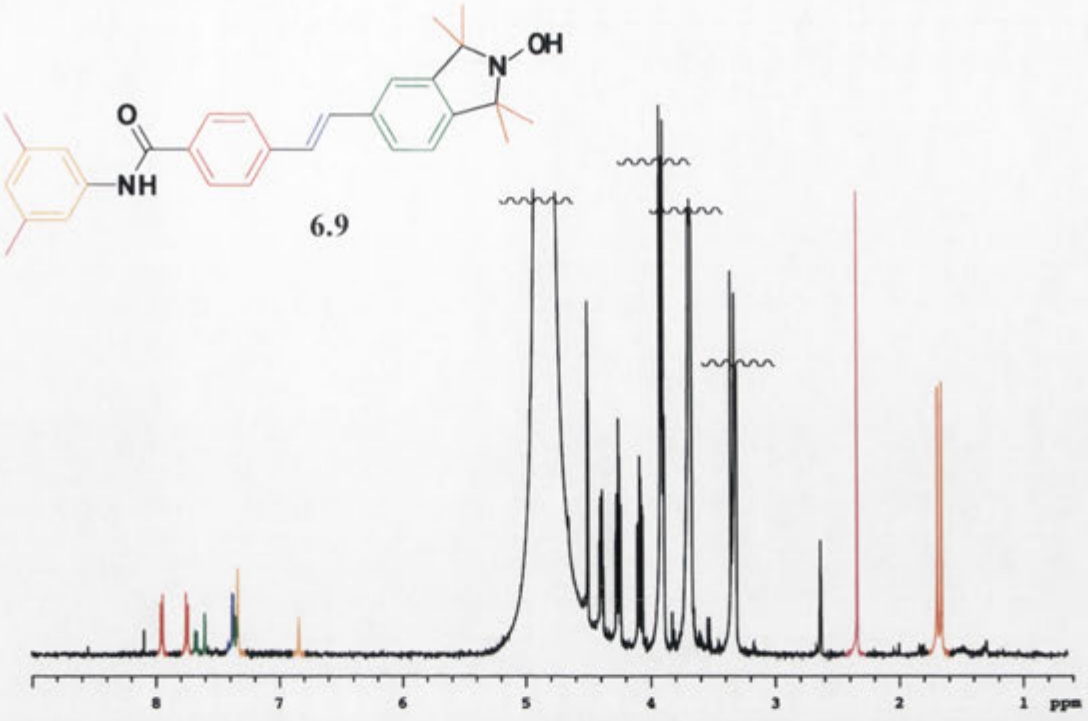

Figure 6.19. 500 MHz ^{1}H NMR spectrum of the hydroxylamine **6.9** in CD_3OD.

Having prepared the compounds **1.33**, **1.34**, **1.35**, **1.36**, **1.37** and **1.38**, investigating their photoisomerisation behaviour using UV/visible spectroscopy and HPLC analysis was the next objective.

CHAPTER 7 - Results and Discussion
Photoisomerisation of Paramagnetic Profluorescent Nitroxides

7.1 Photoisomerisation Studies Using UV/visible Spectroscopy and HPLC Analysis

Having prepared the profluorescent rotaxanes **1.33**, **1.34**, **1.35** and **1.36**, and the corresponding dumbbells **1.37** and **1.38**, the next objective was to study their photoisomerisation. Unlike the dumbbells **1.37** and **1.38**, which are virtually insoluble in water, the CDs make the rotaxanes **1.33**, **1.34**, **1.35** and **1.36** water-soluble. However, for consistency in experimental conditions, each compound was dissolved in an ACN/water mixture to prepare 70 μM solutions. Aliquots (3.5 mL) of each solution were transferred to a cuvette and the photoisomerisation was monitored at intervals during exposure to 300 nm light using UV/visible spectroscopy. A photoreactor equipped with a UV-B fluorescent lamp was used for irradiation.

The UV/visible spectra of the dumbbell **1.37** with a 2,6-dimethylaniline blocking group show an absorption band at 324 nm. This is typical for a *trans*-stilbene moiety with symmetry-allowed π–π transition[171,172] (**Figure 7.1** (a)). Upon irradiation, a decrease in absorbance at 324 nm and a corresponding increase in absorbance at 232 nm corresponding to the *cis*-stilbene moiety are observed. The photostationary state was reached after 10 min of irradiation. While the decrease in absorbance at 324 nm reflects the photoisomerisation of the *trans*-stilbene moiety to the *cis*-stilbene moiety, it is not a direct measure of the amount of *trans*-isomer present in solution as the *cis*-stilbene moiety also absorbs at 324 nm, but with a lower molar absorbance.

When the dumbbell **1.37** is protected by α-CD, the UV/visible spectra of the isomeric rotaxanes **1.33** (**Figure 7.1** (b)) and **1.34** (**Figure 7.1** (c)) both show *trans-cis* isomerisation over 10 min as described above. The significantly smaller change in absorbance upon irradiation of the isomeric rotaxanes **1.33** and **1.34** indicates that the *trans-cis* isomerisation is restricted compared to the unprotected dumbbell **1.37**.

The analogous compounds with 3,5-dimethylaniline blocking groups show similar behaviour where the dumbbell **1.38** photoisomerises readily (**Figure 7.1** (d)) as per

the dumbbell **1.37**, while the isomeric rotaxanes **1.35** and **1.36** show restricted *trans-cis* isomerisation as per the rotaxanes **1.33** (**Figure 7.1** (e)) and **1.34** (**Figure 7.1** (f)).

(a)

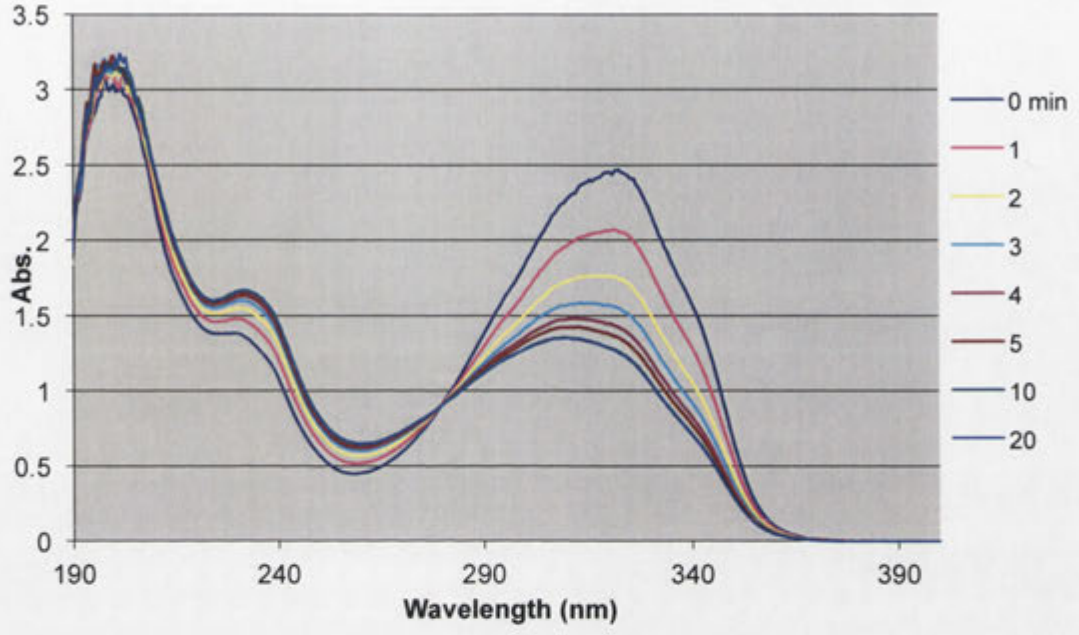

(b)

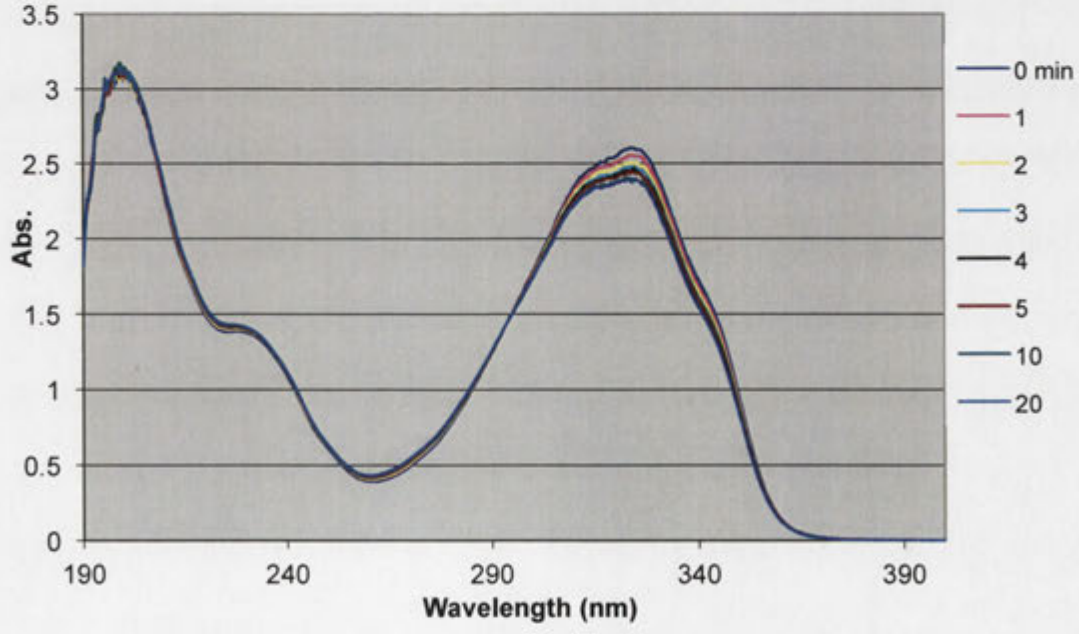

(c)

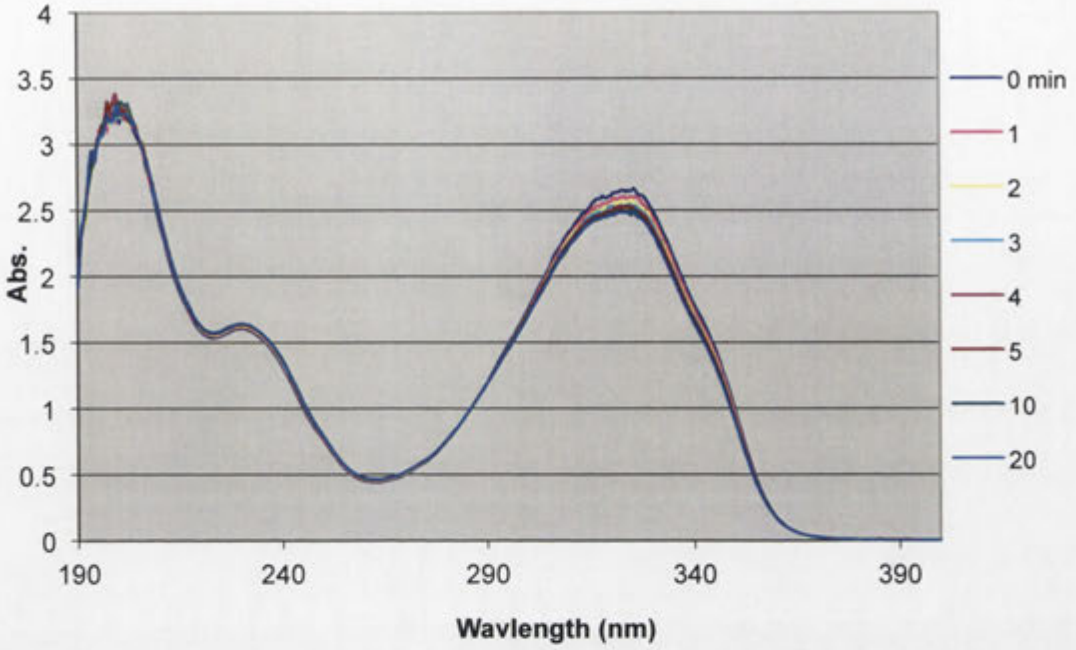
4
3.5
3
2.5
2
1.5
1
0.5
0
Abs.
190
240
290
340
390
Wavlength (nm)
0 min
1
2
3
4
5
10
20

(d)

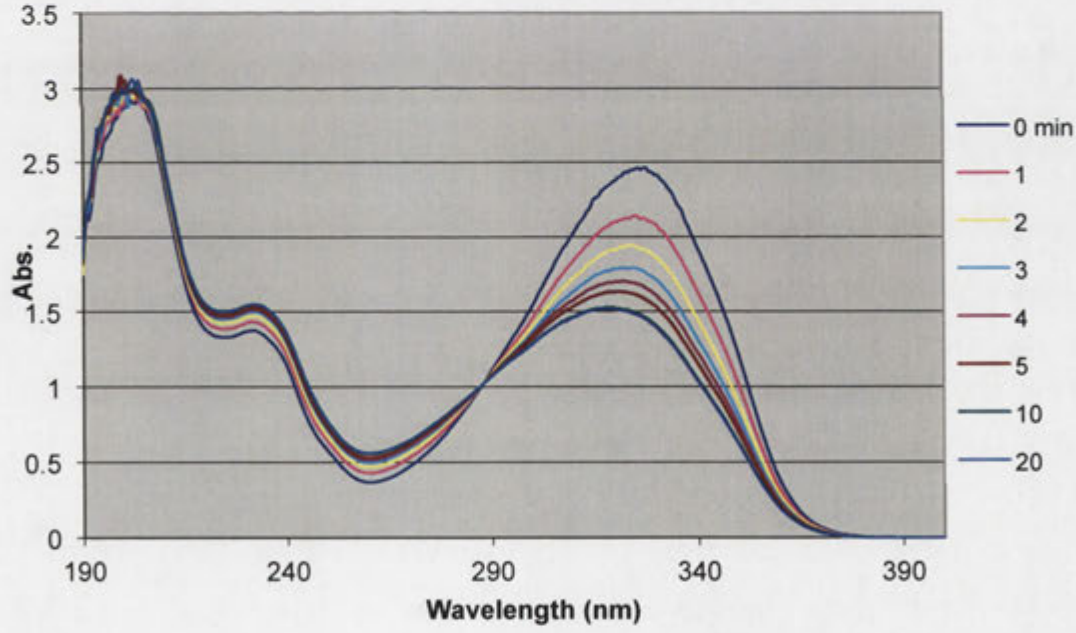
3.5
3
2.5
2
1.5
1
0.5
0
Abs.
190
240
290
340
390
Wavelength (nm)
0 min
1
2
3
4
5
10
20

(e)

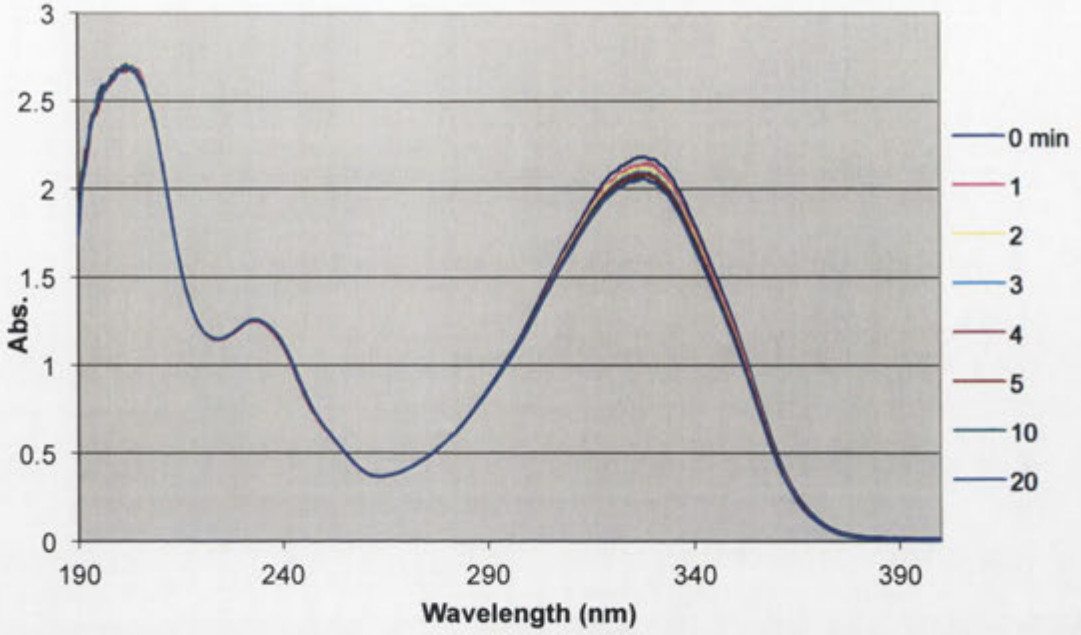

(f)

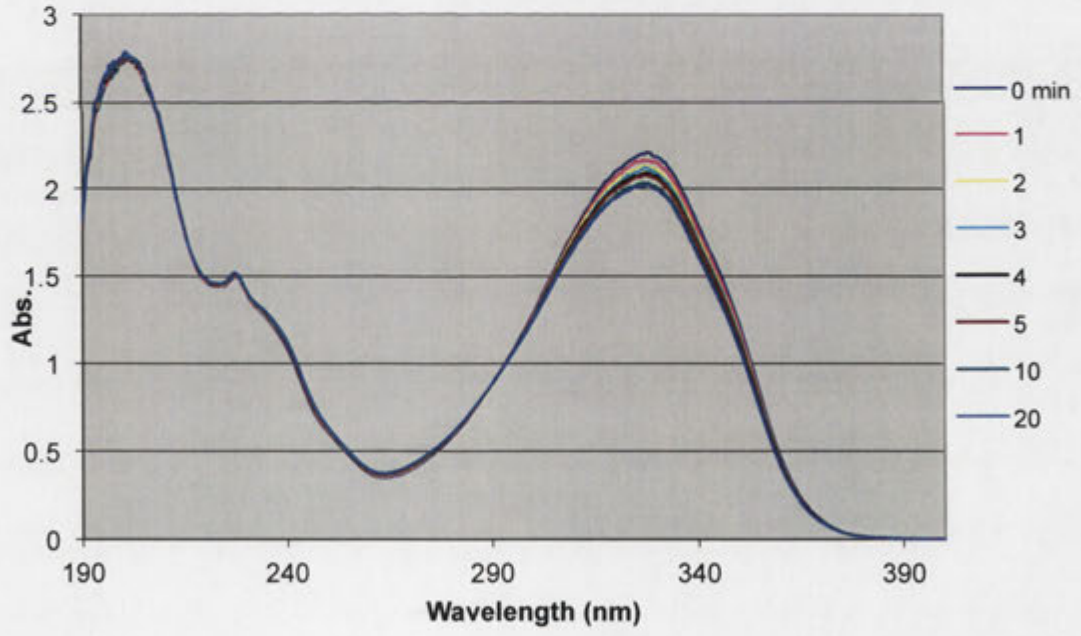

Figure 7.1. UV/visible spectra of 70 μM solutions of (a) the dumbbell **1.37**, (b) the rotaxane **1.33**, (c) the rotaxane **1.34**, (d) the dumbbell **1.38**, (e) the rotaxane **1.35** and (f) the rotaxane **1.36** in ACN/water monitored at time intervals during exposure to 300 nm light.

To determine and quantify the amount of *cis* and *trans* isomers present in solution, the photoisomerisation of the dumbbells **1.37** and **1.38** alone and when they are included

in α-CD in the form of the rotaxanes **1.33**, **1.34**, **1.35** and **1.36** was also monitored using HPLC. Compounds were first dissolved in ACN/water. Then, aliquots (300 μL) of each solution were sealed and bubbled with nitrogen to maintain an inert atmosphere before being exposed to light at 300 nm at time intervals. Aliquots (20 μL) of the irradiated solution were sampled and subject to HPLC analysis after each time interval. In each case, the HPLC chromatogram was monitored at the isosbestic UV absorbance point. At the isosbestic point, the molar absorptivity of the *cis* and *trans* isomers is the same. Therefore the relative proportions of each isomer present can be quantified by comparing the area underneath each peak.

When monitoring the HPLC chromatogram at the isosbestic point (280 nm) of the dumbbell **1.37**, the peak at 7.9 min corresponding to the dumbbell **1.37** decreased upon irradiation, which was accompanied by an increase in a peak at 8.6 min over time. Mass spectrometric analysis showed that the mass of the material that eluted at 8.6 min has the same mass as the dumbbell **1.37**. The UV/visible profile of this material showed absorption bands at 232 and 293 nm, which correspond to the absorbance of a *cis*-stilbene moiety.[172] Hence, the peak at 8.6 min is assigned to the *cis* isomer of the dumbbell **1.37**. After 10 min of irradiation, peak intensities no longer changed, indicating that the photostationary state was reached. This is consistent with the time required for the photostationary state to be reached with the UV/visible studies as shown above. The solution at the photostationary state contained 30% of the *trans* and 70% of the *cis* isomer (**Figure 7.2**).

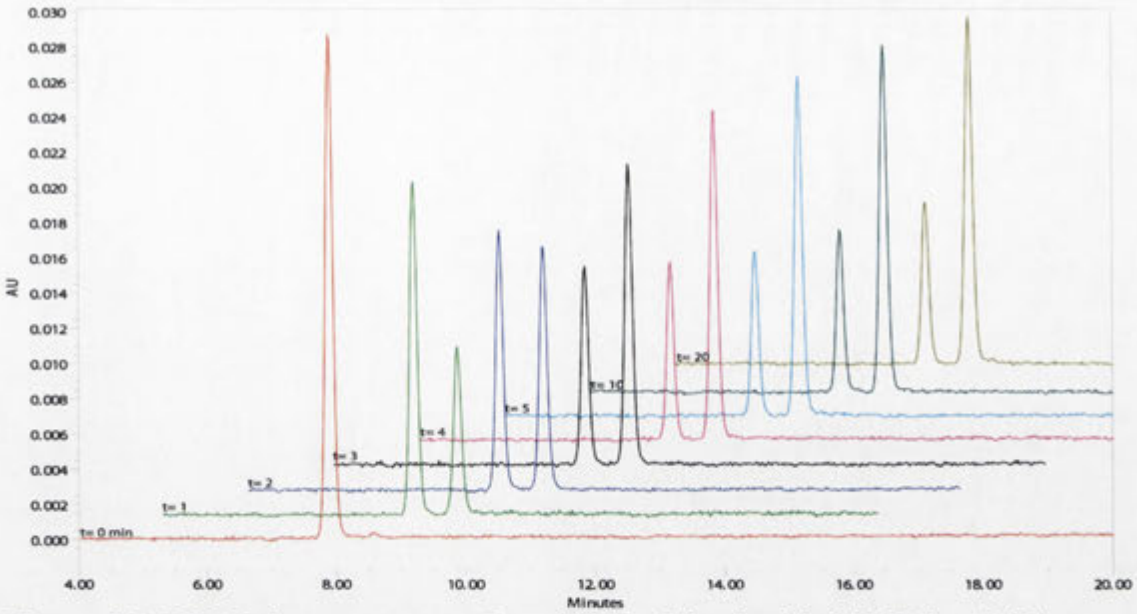

Figure 7.2. HPLC chromatograms of a solution of the dumbbell **1.37** in ACN/water monitored at time intervals during exposure to 300 nm light (monitored at 280 nm). Each chromatogram is offset for clarity.

Likewise, the HPLC chromatograms of the mixtures obtained after irradiation of a solution of the rotaxane **1.33** showed a decrease in the peak at 5.7 min corresponding to the rotaxane **1.33**, which was accompanied by an increase in a peak at 7.2 min. Following the analysis above, the material that eluted at 7.2 min has the same mass as the rotaxane **1.33** and the absorbance of a *cis*-stilbene moiety. Hence the peak at 7.2 min is assigned to the *cis* isomer of the rotaxane **1.33**. The solution at the photostationary state contained 84% of the *trans* and 16% of the *cis* isomer (**Figure 7.3**).

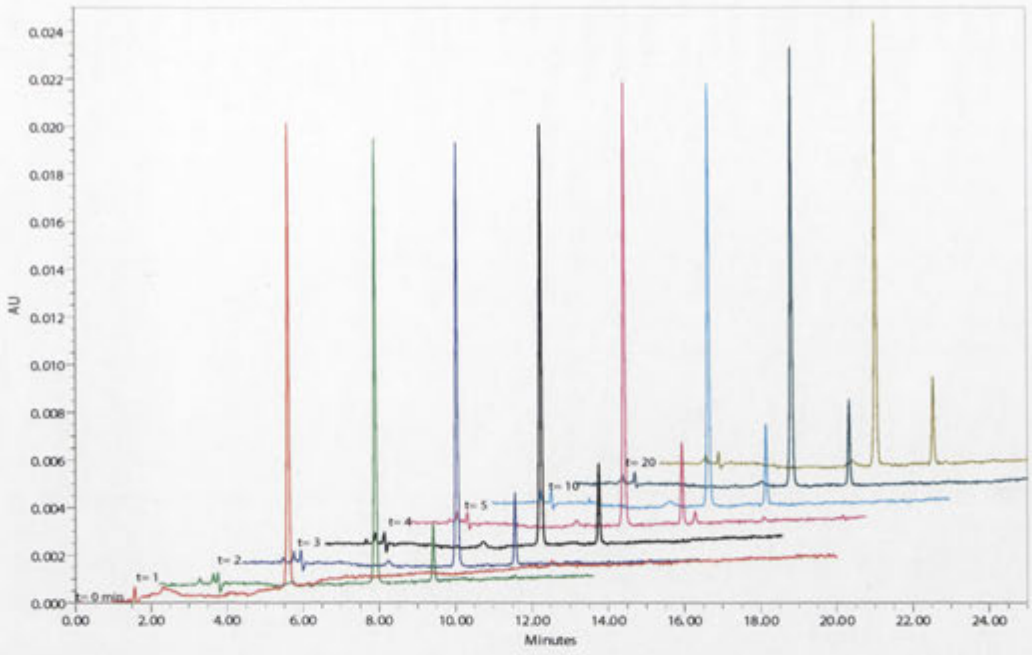

Figure 7.3. HPLC chromatograms of a solution of the rotaxane **1.33** in ACN/water monitored at time intervals during exposure to 300 nm light (monitored at 290 nm). Each chromatogram is offset for clarity.

Figure 7.4 shows a section of the HPLC chromatograms of the mixtures obtained after irradiation of a solution of the rotaxane **1.34**. The peak at 6.8 min corresponding to the rotaxane **1.34** decreased upon irradiation, which was accompanied by an increase in a peak at 6.6 min over time. Again, the peak at 6.6 min is assigned to the *cis* isomer of the rotaxane **1.34** from mass spectrometric data and UV/visible analysis. The solution at the photostationary state contained 87% of the *trans* and 13% of the *cis* isomer.

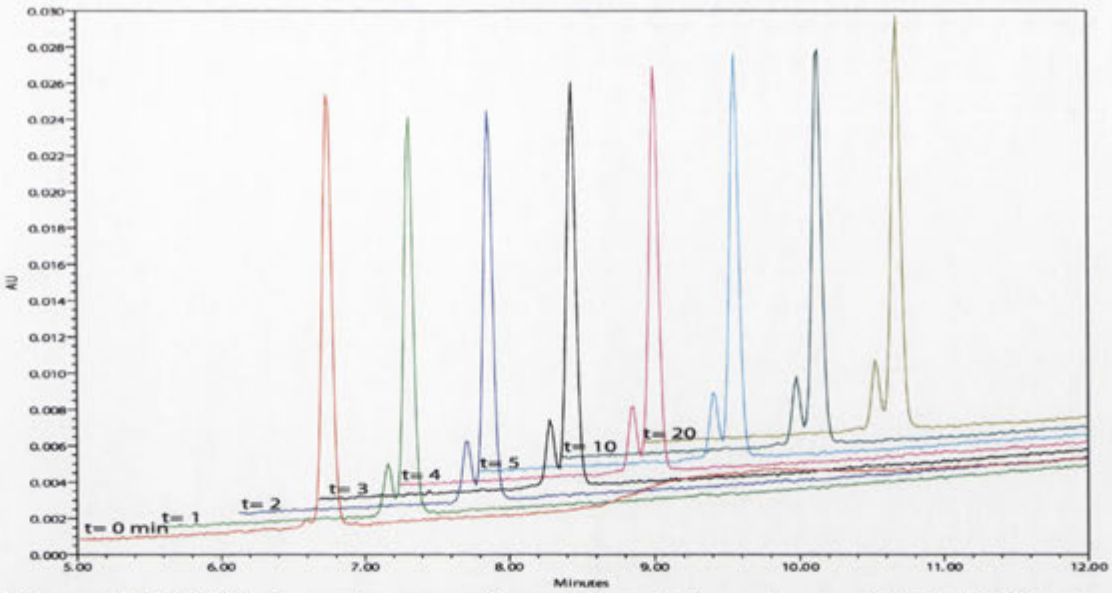

Figure 7.4. HPLC chromatograms of a solution of the rotaxane **1.34** in ACN/water monitored at time intervals during exposure to 300 nm light (monitored at 290 nm). Each chromatogram is offset for clarity.

Upon irradiation of the dumbbell **1.38** solution, the peak at 12.5 min corresponding to the dumbbell **1.38** decreased, while a peak at 13.1 min increased (**Figure 7.5**). The peak at 13.1 min is assigned to the *cis* isomer of the dumbbell **1.38** using the procedure above. The solution at the photostationary state contained 40% of the *trans* and 60% of the *cis* isomer.

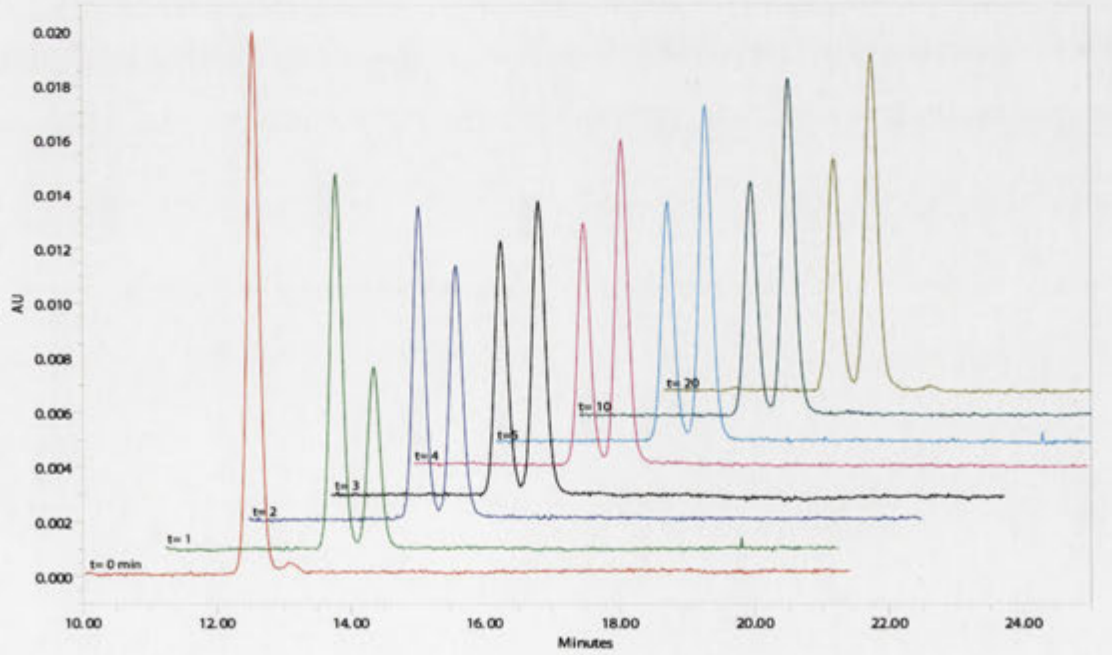

Figure 7.5. HPLC chromatograms of a solution of the dumbbell **1.38** in ACN/water monitored at time intervals during exposure to 300 nm light (monitored at 288 nm). Each chromatogram is offset for clarity.

In the HPLC chromatograms of the mixtures obtained after irradiation of a solution of the rotaxane **1.35** (**Figure 7.6**), a decrease in the peak corresponding to the rotaxane **1.35** at 7.6 min was observed, as well as an increase in a peak corresponding the *cis* isomer of the rotaxane **1.35** at 10.3 min. The solution at the photostationary state contained 88% of the *trans* and 12% of the *cis* isomer.

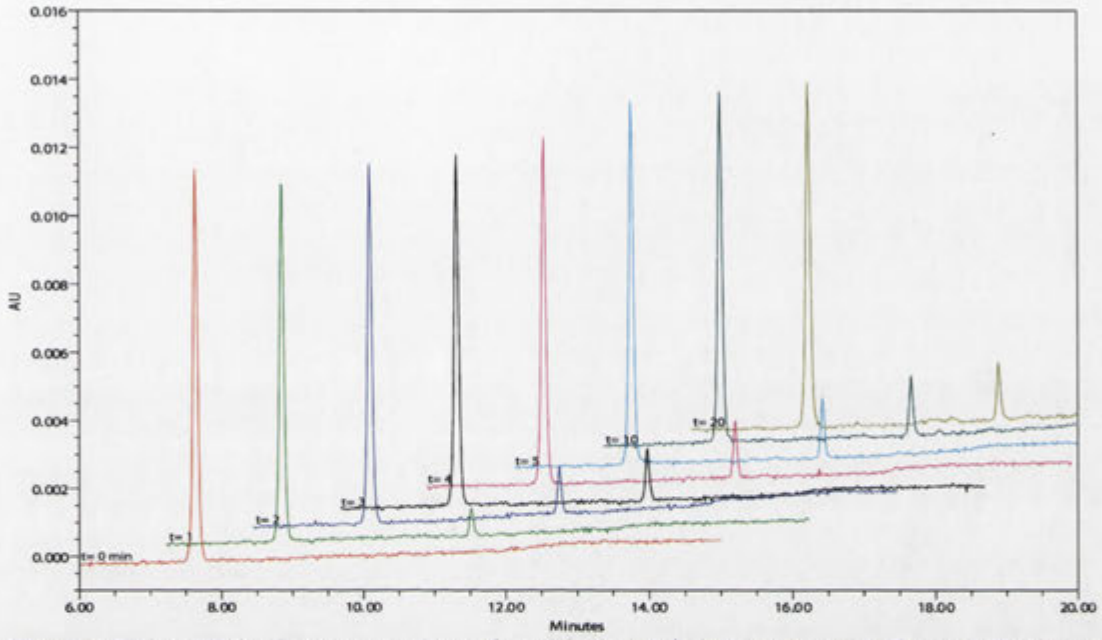

Figure 7.6. HPLC chromatograms of a solution of the rotaxane **1.35** in ACN/water monitored at time intervals during exposure to 300 nm light (monitored at 290 nm). Each chromatogram is offset for clarity.

Finally, a section of the HPLC chromatograms of the mixtures obtained after irradiation of a solution of the rotaxane **1.36** is shown in **Figure 7.7**. The peak at 9.6 min corresponding to the rotaxane **1.36** decreased upon irradiation, which was accompanied by an increase in a peak for the *cis* isomer of the rotaxane **1.36**. The solution at the photostationary state contained 88% of the *trans* and 12% of the *cis* isomer.

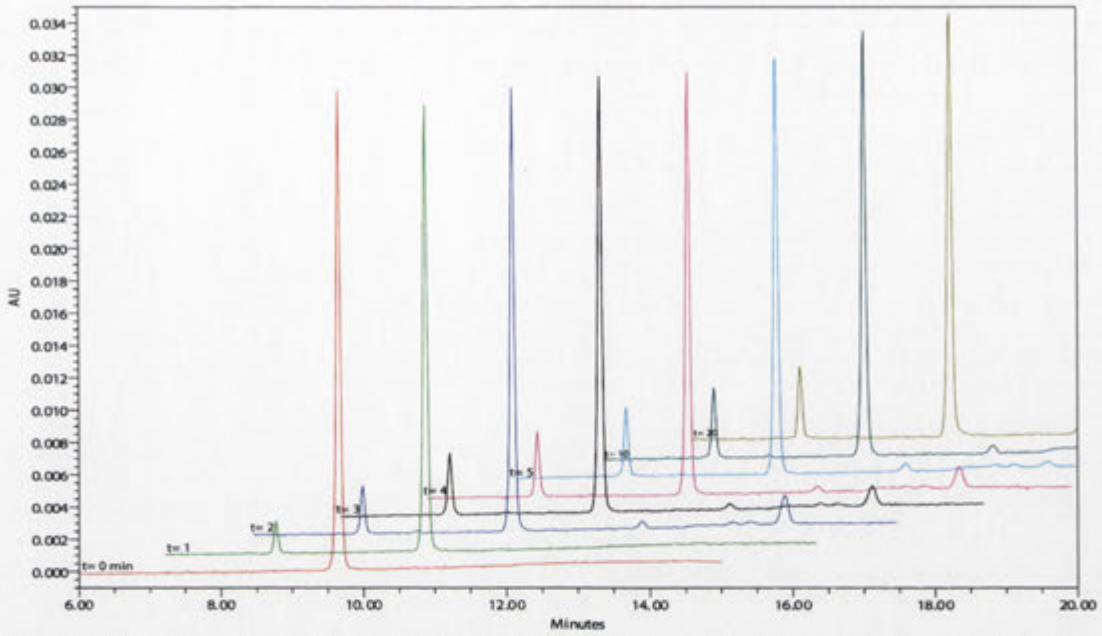

Figure 7.7. HPLC chromatograms of a solution of the rotaxane **1.36** in ACN/water monitored at time intervals during exposure to 300 nm light (monitored at 290 nm). Each chromatogram is offset for clarity.

Through formation of CD-based rotaxanes, the profluorescent probes of all four of the rotaxanes **1.33**, **1.34**, **1.35** and **1.36** are better preserved than the dumbbells **1.37** and **1.38**. At the photostationary state, the CDs limit *trans-cis* isomerisation of the dumbbells **1.37** and **1.38** to 16% or less. Given that the fluorescence of *cis*-stilbenes is less than 1% of that from *trans*-stilbenes,[111] the profluorescent properties of the rotaxanes **1.33**, **1.34**, **1.35** and **1.36** are preserved by at least 84%. In comparison, the dumbbells **1.37** and **1.38** show up to 70% *trans-cis* isomerisation. When profluorescent probes are used to detect free radicals in material, sufficient exposure would be required for the profluorescent probes to reach their photostationary state. Consequently, the composition of *trans* and *cis* isomers present in irradiated mixtures is likely to vary depending on the amount of *trans-cis* isomerisation that occurred. Based on up to 16% *trans-cis* isomerisation observed with the rotaxanes **1.33**, **1.34**, **1.35** and **1.36**, the amount of the profluorescent probes of rotaxanes preserved in material is expected to vary between 84-100%. Those of dumbbells are expected vary between 30-100% based on up to 70% *trans-cis* isomerisation observed with the dumbbells **1.37** and **1.38**. Hence detection of free radicals using the rotaxanes **1.33**, **1.34**, **1.35** and **1.36** is advantageous, as the error associated is less than a quarter of that using the dumbbells **1.37** and **1.38**.

The photoisomerisation studies by HPLC analysis are consistent with the UV/visible studies that show restricted *trans-cis* isomerisation when the stilbene moiety is protected by the CD. The restricted *trans-cis* isomerisation is presumably because the size of the α-CD cavity is not large enough to accommodate a *cis*-stilbene moiety, and the length of the dumbbell is not sufficient for the α-CD to shift away from the stilbene moiety such that *trans-cis* isomerisation can occur.[26]

The dumbbell **1.37** isomerises somewhat more extensively than the dumbbell **1.38**. According to the UV/visible spectra of the dumbbells **1.37** and **1.38**, the molar absorptivity of the *trans*-dumbbell **1.37** is stronger than the *trans*-dumbbell **1.38** at 300 nm. As a result, the rate of *trans-cis* isomerisation is greater for the dumbbell **1.37**. On the other hand, the molar absorptivity of the *cis*-dumbbell **1.37** is weaker than the dumbbell **1.38** at 300 nm. Hence the rate of *cis-trans* isomerisation is smaller for the dumbbell **1.37**. This results in a photostationary state containing a lower concentration of the *trans* isomer and higher concentration of the *cis* isomer for the dumbbell **1.37** such that the overall rate of *trans-cis* isomerisation is equal to the rate of *trans-cis* isomerisation.

The amount of *trans-cis* isomerisation is similar between the isomeric rotaxanes **1.33** and **1.34**. The small difference may be attributable to the slight difference in the location of the CDs on the dumbbells, which may affect their abilities to photoisomerise. The amount of *trans-cis* isomerisation is the same for the isomeric rotaxanes **1.35** and **1.36**. The rotaxanes with a 2,6-dimethylaniline blocking group **1.33** and **1.34**, and the rotaxanes with a 3,5-dimethylaniline blocking group **1.35** and **1.36** show similar amounts of *trans-cis* isomerisation. This suggests that when the dumbbells **1.37** and **1.38** are protected in α-CD in the form of rotaxanes, the two different blocking groups have little effect on the photoisomerisation as the CDs restrict isomerisation.

7.2 Retention of the Profluorescent Probe Under Extreme Conditions

Given that protecting the stilbene moieties in CDs in the form of rotaxanes restricts photoisomerisation, the profluorescent probes of the rotaxanes **1.33**, **1.34**, **1.35** and **1.36** are better preserved than the dumbbells **1.37** and **1.38** at their photostationary

states. For detection of free radicals in cells, in pollution and for monitoring material degradation, profluorescent probes may be exposed to intense UV irradiation or used for monitoring degradation over a long period of time. Hence it was of interest to study whether the profluorescent probes of the rotaxanes **1.33**, **1.34**, **1.35** and **1.36** would still be preserved even under more extreme conditions such as longer exposure and more intense irradiation. Due to time constraints, it was not feasible to monitor the profluorescent probes over extended periods of time. Hence to simulate long term exposure in an accelerated manner, solutions of the compounds **1.33**, **1.34**, **1.35**, **1.36**, **1.37** and **1.38** were irradiated with UV light over 24 h using the method described above. Each solution was subject to HPLC analysis before and after irradiation for 24 h while chromatograms were obtained at the wavelengths identical to the above (isosbestic points) and the relative proportions of each material present in solution were measured by peak area.

Figure 7.8 (a) shows the HPLC chromatograms of the dumbbell **1.37** solution before irradiation, and the mixture obtained after irradiation. After irradiation, the peak at 7.9 min corresponding to the *trans* isomer decreased, while the intensity of two major peaks at 8.6 min corresponding to the *cis* isomer, and 9.0 min increased. *cis*-Stilbenes are known to undergo electrocyclisation to give dihydrophenanthrenes, which can oxidise to form phenanthrenes.[146,147] Mass spectrometric analysis of the irradiated solution showed an ion at *m/z* 440, which corresponds to the *trans*- and *cis*-dumbbells **1.37**, as well as an ion at *m/z* 438, which is two mass units smaller than that of the *trans*- and *cis*-dumbbells **1.37**. The UV/visible profile of this material showed an absorption band at 258 nm, which corresponds to the absorbance of a phenanthrene moiety.[173] Hence, the peak at 9.0 min is assigned to the phenanthrene **7.1**. There are minor peaks unaccounted for, which presumably result from decomposition due to intense irradiation. The solution contained 19% of the *trans* isomer and 45% of the *cis* isomer. From the chromatogram shown in **Figure 7.8** (a), the amount of the phenanthrene **7.1** present in solution cannot be obtained without the molar absorptivity of the compound at the measured wavelength. Hence an estimate was made by assuming that phenanthrenes have the same molar absorptivity as *cis* and *trans*-stilbenes at the isosbestic point of the latter two. Based on this assumption, the amount of the phenanthrene **7.1** in solution is 33% by peak area, which leaves 3% of materials unaccounted for.

The HPLC chromatogram of the mixture obtained after irradiation of the rotaxane **1.33** solution showed the peak at 5.7 min corresponding to the *trans* isomer decreased, which was accompanied by an increase in a peak at 7.2 min corresponding to the *cis* isomer and other unknown peaks (**Figure 7.8** (b)). The irradiated solution consisted of 70% of the *trans* isomer and 14% of the *cis* isomer, leaving 16% of materials unaccounted for.

The mixture obtained after irradiation of the rotaxane isomer, the rotaxane **1.34**, showed the peak at 6.8 min corresponding to the *trans* isomer decreased and an increase in a peak at 8.1 min corresponding to the *cis* isomer as well as other unknown peaks (**Figure 7.8** (c)). Overall, the resulting solution was made up of 70% of the *trans* isomer and 12% of the *cis* isomer, leaving 18% of materials unaccounted for.

Similar to the dumbbell **1.37**, the mixture obtained after irradiation of the dumbbell **1.38** showed the peak at 12.5 min corresponding to the *trans* isomer decreased, which was accompanied by an increase in two major peaks at 13.1 min corresponding to the *cis* isomer, and 14.1 min (**Figure 7.8** (d)). The peak at 14.1 min is assigned to the phenanthrene **7.2** from mass spectrometric data and UV/visible analysis as above. Based on the assumption that phenanthrenes have the same molar absorptivity as *trans*- and *cis*-stilbenes, a solution containing 30% of the *trans* isomer, 36% of the *cis* isomer, 31% of the phenanthrene **7.2** and 3% of materials that are unaccounted for resulted.

The HPLC chromatogram of the mixture obtained after irradiation of the rotaxane **1.35** showed the peak at 7.6 min corresponding to the *trans* isomer decreased, which was accompanied by an increase in peaks at 10.3 min corresponding to the *cis* isomer and others at higher retention times (**Figure 7.8** (e)). Consequently a solution containing 60% of the *trans* isomer, 8% of the *cis* isomer, and 32% of materials that are unaccounted for resulted.

The HPLC chromatogram of the mixture obtained after irradiation of the rotaxane isomer, the rotaxane **1.36**, showed the *trans* isomer peak at 9.6 min decreased, and increase in peaks at 7.6 min corresponding to the *cis* isomer as well as other retention

times (**Figure 7.8** (f)). After irradiation, the solution contained 69% of the *trans* isomer and 13% of the *cis* isomer leaving 18% of materials unaccounted for.

(a)

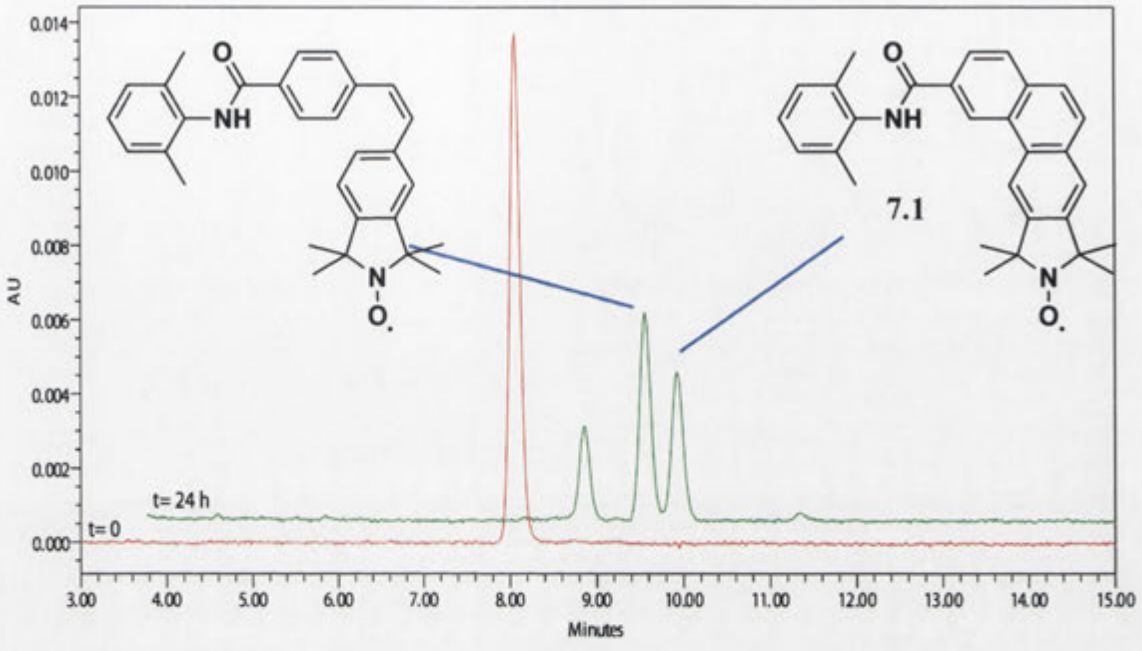

(b)

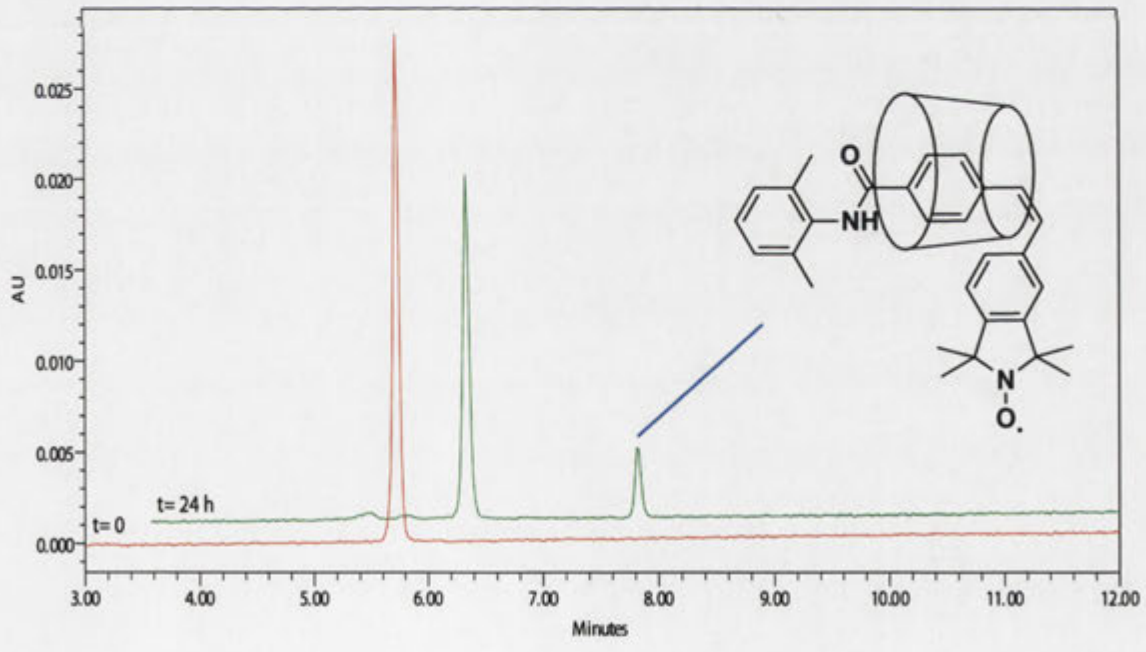

(c)

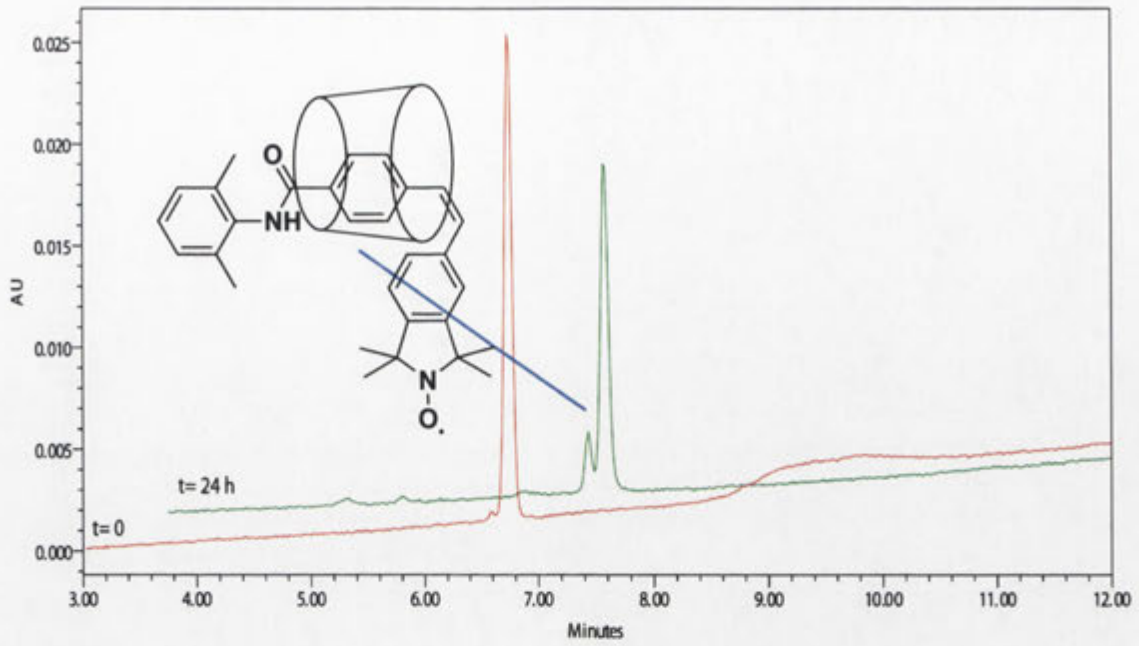
0.025
0.020
0.015
0.010
0.005
0.000
AU
O
NH
N
O.
t= 24 h
t= 0
3.00
4.00
5.00
6.00
7.00
8.00
9.00
10.00
11.00
12.00
Minutes

(d)

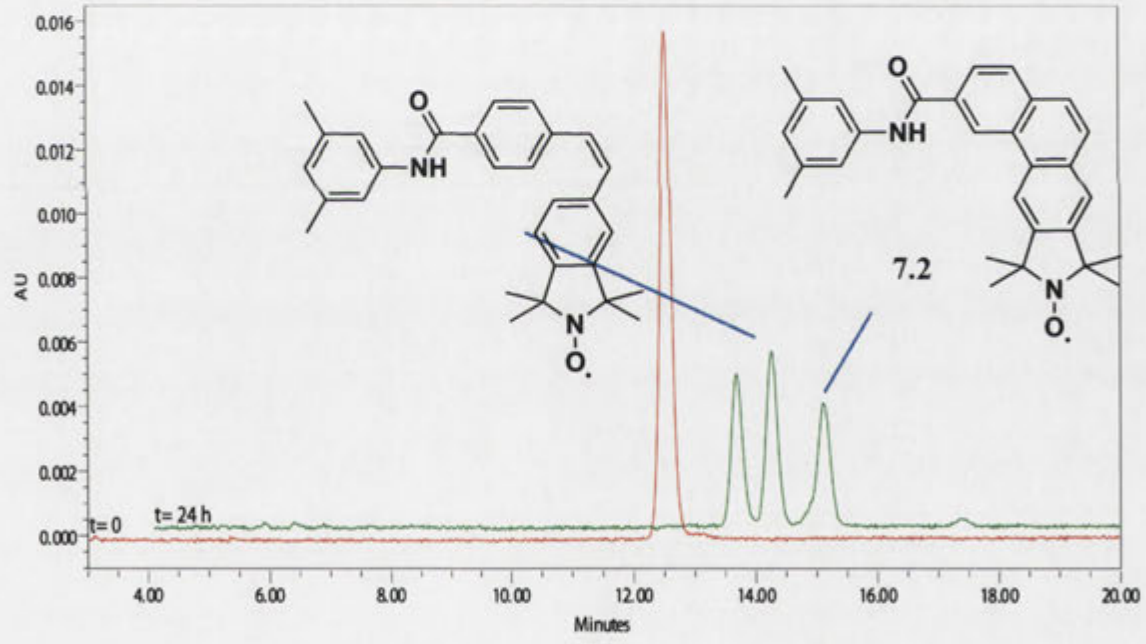
0.016
0.014
0.012
0.010
0.008
0.006
0.004
0.002
0.000
AU
O
NH
N
O.
7.2
t= 0
t= 24 h
4.00
6.00
8.00
10.00
12.00
14.00
16.00
18.00
20.00
Minutes

(e)

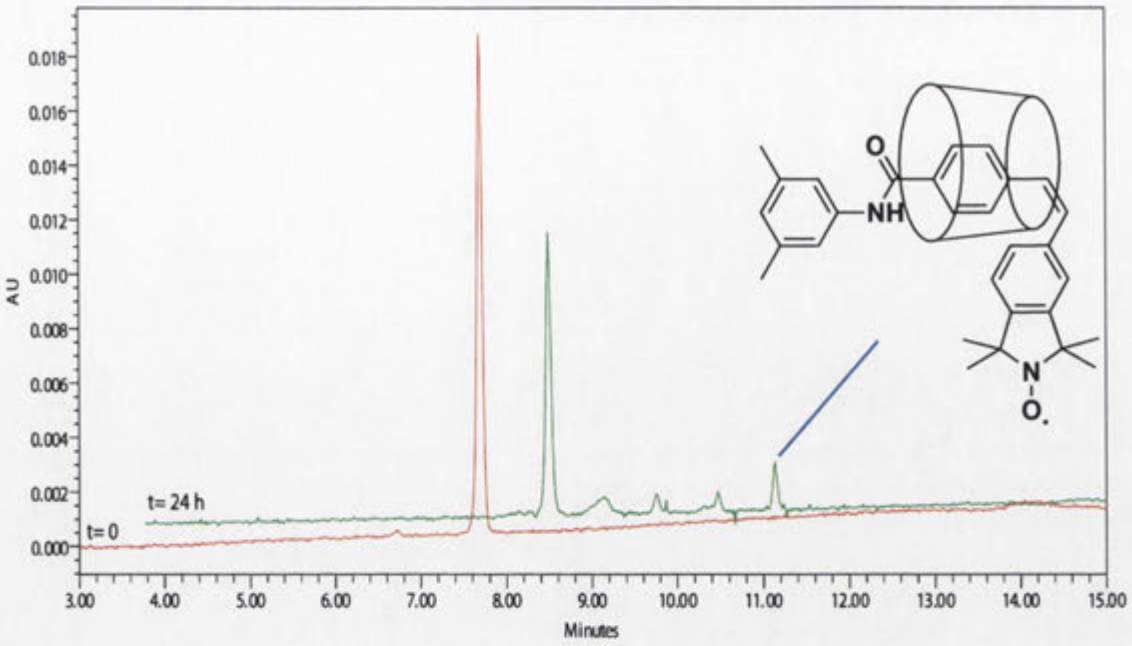

(f)

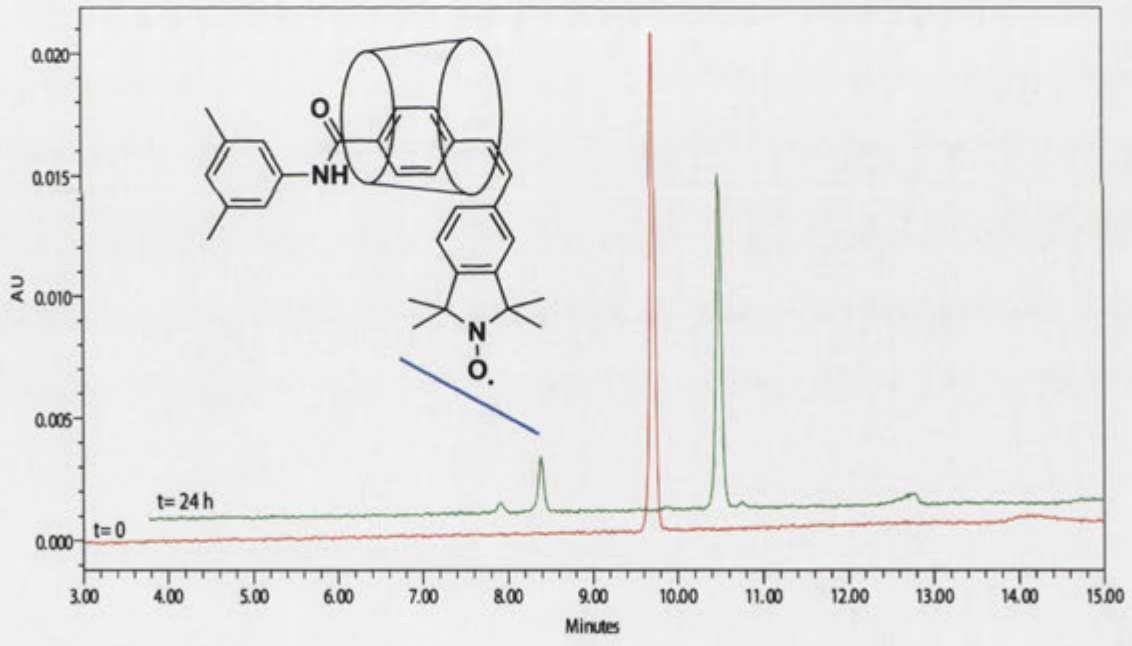

Figure 7.8. HPLC chromatograms of 20 μM solutions of (a) the dumbbell **1.37**, (b) the rotaxane **1.33**, (c) the rotaxane **1.34**, (d) the dumbbell **1.38**, (e) the rotaxane **1.35** and (f) the rotaxane **1.36** in ACN/water before irradiation, and after exposure to 300 nm light for 24 h (obtained at the isosbestic point of *trans* and *cis* isomers of the related compound). Each chromatogram is offset for clarity.

Overall, the profluorescent probes of the rotaxanes **1.33**, **1.34**, **1.35** and **1.36** are better preserved compared to the dumbbells **1.37** and **1.38** even after extended exposure to UV light. Furthermore, oxidised by-products were not detected when the stilbene

moieties are protected by the CD cavity. The oxidised by-products are formed *via* conversion of *trans*-stilbenes to their *cis* isomers, which can then undergo cyclisation and oxidation to form phenanthrenes. One possible explanation for the lack of phenanthrene formation from the rotaxanes **1.33**, **1.34**, **1.35** and **1.36** could be the lower conversion to their *cis* isomers. Due to the small quantities of *cis* isomers forming, the subsequent cyclisation and oxidation products may not be forming in detectable amounts. Another possible explanation may be the limited size of an α-CD which may prevent the phenyl rings of *cis*-stilbenes from being in the same plane, which is required for the cyclisation. Although the profluorescent probes of the rotaxanes **1.33**, **1.34**, **1.35** and **1.36** are better preserved compared to the dumbbells **1.37** and **1.38**, more non-specific decomposition was detected in the irradiated mixtures of the rotaxanes **1.33**, **1.34**, **1.35** and **1.36**. As observed in the UV/visible spectra above, *trans*-stilbenes have a higher molar absorptivity than *cis*-stilbenes at 300 nm. Hence when more material remains in the form of *trans*-stilbenes as observed with the rotaxanes **1.33**, **1.34**, **1.35** and **1.36**, extended irradiation at 300 nm may cause further non-specific decomposition that gives rise to peaks of unaccounted materials.

Under natural circumstances entailing a broader spectrum and lower intensity of light, non-specific decomposition is less likely. As a result, the fluorescent probes of the rotaxanes **1.33**, **1.34**, **1.35** and **1.36** are expected to be better preserved, and consequently, the vast majority of the rotaxanes **1.33**, **1.34**, **1.35** and **1.36** would each be present as a single species. On the other hand, it is probable that the dumbbells **1.37** and **1.38** would undergo *trans-cis* isomerisation and irreversible phenanthrene formation under natural circumstances causing loss of fluorescent probes. When a single species with known profluorescent properties abstracts free radicals and causes fluorescence, radical degradation can be monitored accurately by measuring the fluorescence emission. In comparison, when a mixture of profluorescent compounds are present, the species present in the mixture and the profluorescent properties of each species are required for quantitative analysis of radical degradation. The amount of *trans-cis* isomerisation, cyclisation and phenanthrene formation of the dumbbells **1.37** and **1.38** can be expected to vary depending on the duration, intensity and type of irradiation as well as the penetration of irradiated light to the matrix that contains the

profluorescent probes and the amount of oxygen present that could oxidise dihydrophenanthrenes to phenanthrenes. The number of variables makes it difficult to predict the species present in a given mixture. Therefore it would be advantageous to use the rotaxanes **1.33**, **1.34**, **1.35** and **1.36** rather than the dumbbells **1.37** and **1.38** for monitoring free radicals.

7.3 Conclusion

The profluorescent probes of the dumbbells **1.37** and **1.38** were preserved through formation of the CD-rotaxanes **1.33**, **1.34**, **1.35** and **1.36** making them advantageous for fluorescence detection. In addition, through formation of the CD-rotaxanes **1.33**, **1.34**, **1.35** and **1.36**, the hydrophobic stilbene moieties of the dumbbells **1.37** and **1.38** are encapsulated in the cavity of CDs. As a result, the profluorescent probes that are otherwise virtually insoluble in water are now water-soluble. This enables the fluorescent probes to be used under physiological conditions and in *in vivo* studies. In this study, samples were exposed to intense irradiation compared to intensities natural light would provide. Under natural circumstances, the rotaxanes **1.33**, **1.34**, **1.35** and **1.36** are expected to be predominantly preserved, while the dumbbells **1.37** and **1.38** will undergo decomposition.

For the rotaxanes **1.33**, **1.34**, **1.35** and **1.36** to be used to monitor radical degradation, the profluorescent properties of the dumbbells **1.37** and **1.38** must be maintained. To study if the profluorescent properties of the dumbbells **1.37** and **1.38** are preserved when they are insulated in CDs in the form of the rotaxanes **1.33**, **1.34**, **1.35** and **1.36**, preliminary work has been carried out to measure the fluorescence of the nitroxides **1.33**, **1.34**, **1.35**, **1.36**, **1.37** and **1.38** in their reduced hydroxylamine forms. Upon reduction, each of the nitroxides **1.33**, **1.34**, **1.35**, **1.36**, **1.37** and **1.38** showed similar fluorescence. Therefore the rotaxanes **1.33**, **1.34**, **1.35** and **1.36** are suitable for use as profluorescent probes. Future work to determine the profluorescent behaviour of the products of irradiation of the rotaxanes **1.33**, **1.34**, **1.35** and **1.36**, and the dumbbells **1.37** and **1.38** is beyond the scope of this work. When a mixture of species is present, the fluorescence is not exclusively due to the fluorescence of the *trans*-stilbene moiety. Instead, each species may affect the overall fluorescence of the mixture. To measure the fluorescence due to the profluorescent probes, determining the composition of the species present after irradiation and the fluorescence quantum

yields of each species is required. Nonetheless, due to the profluorescent probes of the rotaxanes **1.33**, **1.34**, **1.35** and **1.36** being preserved, the fluorescent properties of these compounds are also preserved. Consequently, CD-based rotaxanes with profluorescent nitroxides can be used for monitoring radical degradation.

Since CDs have many hydroxyl groups that can be functionalised, they can be covalently attached to polymers.[174-176] Hence preparation of CD-based rotaxanes can be a useful method to incorporate the profluorescent probes into polymers to monitor degradation. Furthermore, CD-based rotaxane formation is a promising method to change the reactivity of compounds that can be exploited as CD guests and preserve the properties of CD guests, making this method ideal for material science applications.

CHAPTER 8 - Experimental

8.1 General

NMR spectroscopy was conducted using a Varian Inova 500 MHz spectrometer operating at 500 MHz for ^{1}H NMR and 125.7 MHz for ^{13}C NMR spectroscopy, a Varian Mercury 300 MHz spectrometer operating at 300 MHz for ^{1}H NMR and 75.5 MHz for ^{13}C NMR spectroscopy, or a Bruker Avance 800 MHz spectrometer operating at 200 MHz for ^{13}C NMR spectroscopy. δ_H And δ_c values are reported in parts per million (ppm), while *J* values are given in Hz. CD_3OD was referenced at δ = 3.31 for ^{1}H and 49.0 for ^{13}C NMR spectroscopy. DMSO-d_6 was referenced at δ = 2.50 for ^{1}H and 39.5 for ^{13}C NMR spectroscopy. CD_2Cl_2 was referenced at δ = 5.32 for ^{1}H and 54.0 for ^{13}C NMR spectroscopy. $CDCl_3$ was referenced at δ = 77.2 for ^{13}C NMR spectroscopy. Acetone was referenced at δ = 2.05 for ^{1}H NMR spectroscopy.

Low resolution (LR) electrospray ionisation (ESI) mass spectra were recorded using a Micromass-Waters LC-ZMD single quadrupole liquid chromatograph mass spectrometer. LR mass spectral data are reported as mass-to-charge ratios (*m/z*). Assignments and percentage abundances are reported where in parentheses. High resolution (HR) ESI mass spectra were recorded using a Waters LCT premier^{TM} XE orthogonal acceleration time-of-flight (oa-TOF) mass spectrometer, while HR electron impact (EI) mass spectra were recorded using a Micromass VG AutoSpec M mass spectrometer. HR mass spectral data are reported as mass-to-charge ratios (*m/z*).

Thin layer chromatography (TLC) was performed on Merck Silica gel 60 F_{254} TLC plates, visualised with a 254 nm UV lamp and by treatment with a naphthalene-1,3-diol solution (0.1% w/v) in ethanol:water:H_2SO_4 (200:157:43 v/v/v) followed by heating.[138]

Elemental analyses were performed by the Australian National University Microanalytical Service. Melting points were recorded using an SRS OptiMelt Automated Melting Point System.

Analytical high performance liquid chromatography (HPLC) was performed with a Waters 2695 Separation Module with a Waters 2996 Photodiode Array Detector running with Empower 2 software. Semi-preparative and preparative HPLC were

performed with a Waters 600 Controller with a Waters 717 plus Autosampler and a Waters 2996 Photodiode Array Detector running with Empower Pro Empower 2 software. Eluting fractions were collected using a Waters Fraction Collector III. Preparative HPLC was carried out using a Grace Alltima C18 5 μm, 22 × 250 mm with a Grace Alltima C18 10 μm, 33 mm guard column or a Waters XBridge Prep C18 5 μm, 19 × 150 mm column. A Phenomenex Luna 5 μm C18(2) 100 Å, 10 × 250 mm column was used for semi-preparative HPLC. A YMC Pack ODS-AQ 3 μm, 150 × 3.0 mm column was used for analytical HPLC. A prepacked ODS column [LiChroprep RP-18, size B (25 × 310 mm), Merck] was used for low-pressure RP column chromatography. Waters clear glass snap neck total recovery vials (12 × 32 mm) or Grace shell vials (8 × 30 mm) were used for analytical HPLC.

UV/visible spectrophotometric studies were conducted using a Shimadzu UV-2450 UV/visible spectrophotometer with a Shimadzu CPS-temperature controller running with UV Probe Version 2.10 software. A Luzchem photoreactor was used to irradiate samples using UV-B fluorescent lamps (8 W) for 300 nm irradiation.

Crystal data collections were undertaken using a Nonius Kappa CCD diffractometer. The structures were solved by Dr Anthony C. Willis at the Research School of Chemistry, Australian National University. Further refinements were undertaken by Prof. Peter J. Steel at University of Canterbury. Discovery Studio 3.1 was used to visualise crystal structures.

Microscope images were obtained using an OLYMPUS SZ40 binocular optical microscope fitted with a cross-polarising lens. Scanning electron microscope (SEM) images were obtained by the Research School of Biological Science Electron Microscopy Unit, using a Zeiss UltraPlus FESEM microscope.

α-CD **1.1** (99.1% purity) was purchased from Nihon Shokuhin Kako Co., Japan and dried overnight under vacuum at 60 °C to constant weight before use. Azobenzene-4,4'-dicarboxylic acid **2.1**, azobenzene-4,4'-dicarbonyl dichloride **4.3** and 2,4,6-trinitrobenzene-1-sulfonic acid sodium salt dihydrate **5.3** were purchased from Tokyo Kasei Kogyo Co. Ltd., Japan. Stilbene-4,4'-dicarboxylic acid **1.9** was purchased from

Alfa Aesar, USA. TEA, DMT-MM, 3,5-dimethylaniline **1.8**, 2,6-dimethylaniline **1.10**, PPh_3, 4-vinylaniline **5.7**, 4-iodobenzoic acid **5.8** and palladium(II) acetate were purchased from Aldrich, USA. BOP was purchased from Merck, Germany. The acid **6.1** was prepared by Prof. Steven Bottle's group, Queensland University of Technology, Brisbane. Water was purified using an ELGA Purelab Classic UV system.

8.1.1 Procedure to Prepare Buffer Solutions

0.2 M Sodium Carbonate Buffer (pH 10.0, 0.2 M)

A solution of 100 mL of 0.2 M sodium carbonate buffer (pH 10.0) was prepared by adding $NaHCO_3$ (1.13 g) and Na_2CO_3 (0.69 g) to a 100 mL volumetric flask, adjusting the pH with either HCl or NaOH and adding water to make 100 mL.

0.5 M Sodium Phosphate Buffer (pH 7.0)

A solution of 1.0 L of 0.5 M sodium phosphate buffer (pH 7.0) was prepared by adding $NaH_2PO_4.2H_2O$ (78.0 g) to a 1.0 L volumetric flask, adjusting the pH with NaOH and adding water to make 1.0 L.

8.1.2 Procedure to Record NMR Spectra of Free Radical Species

For NMR spectroscopic analysis in Section **8.6**: Ascorbic acid **6.4** was added to DMSO-d_6 until it no longer dissolved. 3 Drops of saturated ascorbic acid in DMSO-d_6 were added to NMR sample solutions (*ca.* 700 μL) before the mixture was shaken. The resulting solution was left to stand for 3 days to ensure that paramagnetic nitroxide radicals were fully reduced to their corresponding diamagnetic hydroxylamines.

8.2 Experimental for Chapter 2

[*trans*-4,4'-Bis(3,5-dimethylphenylaminocarbonyl)azobenzene]-[α-cyclodextrin]-[2]rotaxane 1.9

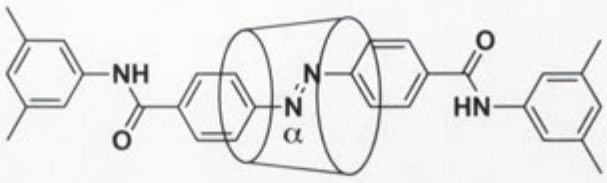

A mixture of the azobenzene **2.1** (100 mg, 3.7×10^{-4} mol) and α-CD **1.1** (3.0 g, 3.1×10^{-3} mol) in 0.2 M sodium carbonate buffer (pH 10, 25 mL) was equilibrated for 2 h at room temperature. DMT-MM (1.6 g, 5.6×10^{-3} mol) and 3,5-dimethylaniline **2.2** (180 mg, 1.5×10^{-3} mol) were added to the reaction mixture and stirred overnight at room temperature. Water (70 mL) was added to the reaction mixture and the mixture was washed with EtOAc (3 × 100 mL). The aqueous layer was concentrated under reduced pressure. The resulting mixture was dissolved in MeOH and purified by HPLC. The fractions containing the product **1.9** were concentrated and lyophilised to give the title compound **1.9** (16 mg, yield 3%) as orange powder.

Physical and spectral properties were consistent with those reported previously.[135]

TLC (5:4:3:2 v/v/v/v *i*-propanol:ethanol:water:acetic acid) R_f 0.80.

Melting point 306-308 °C (dec.) [lit.[135] 307-308 °C (dec.)].

^{1}H NMR (500 MHz, CD_3OD) δ_H 8.65 (2H, d, *J* 8.5, Azo-H), 8.26 (2H, d, *J* 8.5, Azo-H), 8.20 (2H, d, *J* 8.5, Azo-H), 8.04 (2H, d, *J* 8.5, Azo-H), 7.46 (2H, s, aniline-H), 7.37 (2H, s, aniline-H), 6.87 (1H, s, aniline-H), 6.86 (1H, s, aniline-H), 4.88 (6H, d, *J* 3.0, CD-C1-H), 3.83-3.80 (6H, m, CD-C5-H), 3.75-3.72 (12H, m, CD-C3-H and CD-C6-H), 3.58 (6H, m, CD-C6-H), 3.51 (6H, apparent t, *J* 9.0, CD-C4-H), 3.43 (6H, dd, *J* 3.0, 9.5, CD-C2-H), 2.36 (6H, s, Me), 2.34 (6H, s, Me).

Mass spectrum (ESI, positive ion mode) *m/z* (%) 1450 [($M+H^+$), 35], 1472 [($M+Na^+$), 100].

HPLC (Preparative) t_R 5.8 min [column: Waters XBridge Prep C18 5 μm, 19 × 150 mm; 10 mL/min MeOH/H_2O 50:50 isocratic, detection wavelength: 352 nm].

[*trans*-4,4'-Bis(2,6-dimethylphenylaminocarbonyl)stilbene]-[α-cyclodextrin]-[2]rotaxane 1.10

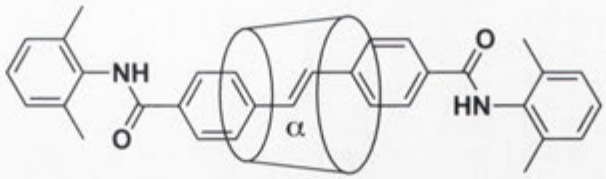

The stilbene **2.3** (50 mg, 1.9×10^{-4} mol) was suspended in a saturated solution of α-CD **1.1** in water (25 mL) and TEA (57 mg, 5.6×10^{-4} mol) was then added to the mixture to solubilise the stilbene **2.3**. The mixture was sonicated to allow equilibration for 2 h at room temperature. DMT-MM (206 mg, 7.4×10^{-4} mol), 2,6-dimethylaniline **2.4** (113 mg, 9.3×10^{-4} mol) and TEA (57 mg, 5.6×10^{-4} mol) were added to the reaction mixture and stirred overnight at room temperature. After another addition of DMT-MM (206 mg, 7.4×10^{-4} mol), the reaction mixture was stirred overnight. Water (70 mL) was added to the reaction mixture and the mixture was washed with EtOAc (3 × 100 mL). The aqueous layer was concentrated under reduced pressure. The resulting mixture was dissolved in MeOH and purified by HPLC. The fractions containing the product **1.10** were concentrated and lyophilised to give the title compound **1.10** (11 mg, yield 14%) as colourless powder.

Physical and spectral properties were consistent with those reported previously.[177]

TLC (5:4:3 v/v/v *n*-butanol:ethanol:water) R_f 0.74.

Melting point 275-277 °C (dec.) [lit.[177] 275 °C (dec.)].

^{1}H NMR (500 MHz, CD_3OD) δ_H 8.14 (4H, s, stilbene-H), 8.10 (2H, d, *J* 8.5, stilbene-H), 7.72 (2H, d, *J* 8.5, stilbene-H), 7.50 (1H, d, *J* 16.5, olefinic-H), 7.35 (1H, d, *J* 16.5, olefinic-H), 7.16 (6H, apparent s, aniline-H), 4.94 (6H, d, *J* 3.5, CD-C1-H), 3.91-3.87 (12H, m, CD-C3-H and CD-C5-H), 3.75 (6H, dd, *J* 3.5, 12.0, CD-C6-H), 3.61 (6H, dd, *J* 1.5, 12.0, CD-C6-H), 3.57 (6H, t, *J* 9.0, CD-C4-H), 3.47 (6H, dd, *J* 3.5, 10.0, CD-C2-H), 2.35 (6H, s, Me), 2.30 (6H, s, Me).

Mass spectrum (ESI, positive ion mode) *m/z* (%) 1448 [($M+H^+$), 90], 1470 [($M+Na^+$), 30].

HPLC (Preparative) t_R 9.2 min [column: Waters XBridge Prep C18 5 μm, 19 × 150 mm; 10 mL/min MeOH/H_2O 30:70 isocratic, detection wavelength: 334 nm].

[*trans*-4,4'-Bis(3,5-dimethylphenylaminocarbonyl)stilbene]-[α-cyclodextrin]-[2]rotaxane 1.17

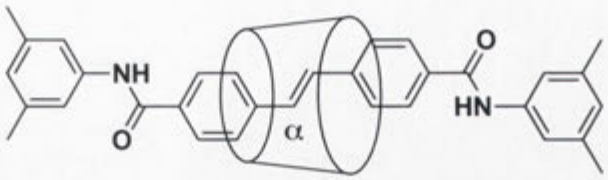

The stilbene **2.3** (100 mg, 3.7×10^{-4} mol) was suspended in water (25 mL) and TEA (110 mg, 1.1×10^{-3} mol) was then added to the mixture to solubilise the stilbene **2.3**. α-CD **1.1** (1.8 g, 1.9×10^{-3} mol) was added and the mixture was sonicated to allow equilibration for 2 h at room temperature. DMT-MM (1.6 g, 5.6×10^{-3} mol), 3,5-dimethylaniline **2.2** (180 mg, 1.5×10^{-3} mol) and TEA (110 mg, 1.1×10^{-3} mol) were added to the reaction mixture and stirred for 2 h at room temperature. After another addition of DMT-MM (1.6 g, 5.6×10^{-3} mol), the reaction mixture was stirred overnight. Water (70 mL) was added to the reaction mixture and the mixture was washed with EtOAc (3 × 100 mL). The aqueous layer was concentrated under reduced pressure. The resulting mixture was dissolved in MeOH and purified by HPLC. The fractions containing the product **1.17** were concentrated and lyophilised to give the title compound **1.17** (8 mg, yield 2%) as colourless powder. Crystals of the rotaxane **1.17** were obtained through slow evaporation of MeOH/water over a period of several weeks.

TLC (5:4:3 v/v/v *n*-butanol:ethanol:water) R_f 0.80.

Melting point 290-291 °C (dec.).

^{1}H NMR (500 MHz, CD_3OD) δ_H 8.12 (2H, d, *J* 8.0, stilbene-H), 8.08 (2H, d, *J* 8.0, stilbene-H), 8.04 (2H, d, *J* 8.0, stilbene-H), 7.67 (2H, d, *J* 8.0, stilbene-H), 7.48 (1H, d, *J* 16.0, olefinic-H), 7.39 (2H, s, aniline-H), 7.34 (2H, s, aniline-H), 7.32 (1H, d, *J* 16.0, olefinic-H), 6.84 (2H, apparent s, aniline-H), 4.94 (6H, d, *J* 3.0, CD-C1-H), 3.90 (6H, m, CD-C5-H), 3.87 (6H, m, CD-C3-H), 3.75 (6H, dd, *J* 3.5, 12.0, CD-C6-H), 3.60 (6H, m, CD-C6-H), 3.57 (6H, m, CD-C4-H), 3.47 (6H, dd, *J* 3.0, 10.0, CD-C2-H), 2.34 (6H, s, Me), 2.33 (6H, s, Me).

^{13}C NMR (125.7 MHz, CD_3OD) δc 168.9 and 167.8 (C=O), 140.6, 140.1, 139.6(4), 139.5(7), 136.6, 136.0, 134.0, 133.3, 131.7, 130.4, 129.6, 129.2, 129.1, 127.8, 127.3, 127.3, 120.2, 104.0, 83.3, 75.1, 73.9, 73.8, 61.5, 21.5 (Me, two coincident resonances).

Mass spectrum *m/z* (ESI-HR, positive ion mode) Found 1469.5372 [(M+Na^+), $C_{68}H_{90}N_2O_{32}$+Na^+]. Requires 1469.5374.

Elemental analysis Found C, 50.22; H, 6.31; N, 1.41%. $C_{68}H_{90}N_2O_{32}\cdot 9.5H_2O$ requires C, 50.45; H, 6.80; N, 1.73%.

X-ray crystallographic data are presented in Appendix 1.

HPLC (Semi-preparative) t_R 16.5 min [column: Phenomenex Luna 5 μm C18(2) 100 Å, 10 × 250 mm; 3 mL/min MeOH/H_2O 50:50 isocratic, detection wavelength: 337 nm].

[*trans*-4,4'-Bis(2,6-dimethylphenylaminocarbonyl)azobenzene]-[α-cyclodextrin]-[2]rotaxane 1.18

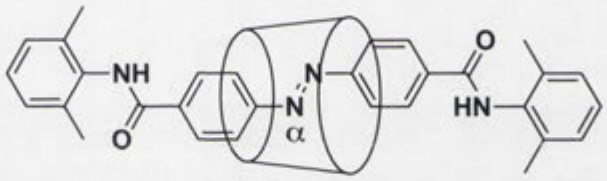

A mixture of the azobenzene **2.1** (50 mg, 1.9×10^{-4} mol) and α-CD **1.1** (540 mg, 5.5×10^{-4} mol) in 0.5 M sodium phosphate buffer (pH 7.0, 10 mL) was equilibrated for 2 h at room temperature. DMT-MM (1.5 g, 5.6×10^{-3} mol) and 2,6-dimethylaniline **2.4** (90 mg, 7.4×10^{-4} mol) were added to the reaction mixture and stirred overnight at room temperature. Water (100 mL) was added to the reaction mixture and the mixture was washed with EtOAc (5 × 100 mL). The aqueous layer was concentrated under reduced pressure and the residue was dissolved in water (10 mL), which was then subjected to low-pressure RP chromatography. Elution with water (1 L) and gradient elution from 5% MeOH to 30% MeOH were applied to obtain the crude product of **1.18**. The resulting solution was concentrated under reduced pressure and further purified using the HPLC. The fractions containing the product **1.18** were concentrated and lyophilised to give the title compound **1.18** (21 mg, yield 8%) as orange powder. Crystals of rotaxane **1.18** were obtained through slow evaporation of MeOH/water over a period of several days.

TLC (5:4:3 v/v/v *n*-butanol:ethanol:water) R_f 0.78.

Melting point 250-251 °C (dec.).

^{1}H NMR (500 MHz, CD_3OD) δ_H 8.67 (2H, d, *J* 8.5, Azo-H), 8.32 (2H, d, *J* 8.5, Azo-H), 8.27 (2H, d, *J* 8.5, Azo-H), 8.09 (2H, d, *J* 8.5, Azo-H), 7.17 (6H, apparent s,

aniline-H), 4.91 (6H, d, *J* 3.5, CD-C1-H), 3.82 (6H, apparent d, *J* 9.0, CD-C5-H), 3.77 (6H, m, CD-C3-H), 3.74 (6H, m, CD-C6-H), 3.60 (6H, apparent d, *J* 12.0, CD-C6-H), 3.51 (6H, apparent t, *J* 9.0, CD-C4-H), 3.43 (6H, dd, *J* 3.5, 10.0, CD-C2-H), 2.39 (6H, s, Me), 2.32 (6H, s, Me).

^{13}C NMR (125.7 MHz, CD_3OD) δc 168.6 and 167.9 (C=O), 155.1, 154.8, 139.2, 138.6, 137.5, 137.2, 135.7, 135.6, 130.2, 129.5, 129.2, 129.1, 128.6(9), 128.6(7), 126.4, 124.5, 103.9, 83.3, 75.0, 73.7, 73.4, 61.7, 18.9 and 18.5 (Me).

Mass spectrum *m/z* (ESI-HR, positive ion mode) Found 1471.5281 [$(M+Na^+)$, $C_{66}H_{88}N_4O_{32}+Na^+$]. Requires 1471.5279.

Elemental analysis Found C, 50.62; H, 6.40; N, 3.37%. $C_{66}H_{88}N_4O_{32}\cdot 6.5H_2O$ requires C, 50.59; H, 6.51; N, 3.58%.

X-ray crystallographic data are presented in Appendix 1.

HPLC (Preparative) t_R 14.9 min [column: Grace Alltima C18 5 μm, 22 × 250 mm with Grace Alltima C18 10 μm, 33 mm guard column; 10 mL/min MeOH/H_2O 40:60 isocratic, detection wavelength: 340 nm].

8.3 Experimental for Chapter 3

8.3.1 Procedure to Obtain SEM and Optical Microscope Images Described in Section 3.2

(a) SEM Images

Crystals for SEM were obtained by evaporating aliquots (*ca.* 1 mL) of solutions of the rotaxanes **1.9**, **1.10**, **1.17** and **1.18** with concentrations ranging from approximately 10 to 100 μM. Dried crystals were mounted on adhesive carbon tape and each sample was coated with conductive gold-palladium at 15 mA for 4 min before scanning.

(b) Optical Microscope Images

Lyophilised samples of the rotaxanes **1.9**, **1.10**, **1.17** and **1.18** were added to water (5 mL) while being heated until they did not dissolve further. Each mixture was filtered before the solutions were cool to room temperature to give supersaturated solutions. Aliquots (*ca.* 300 μL) of the resulting solutions were transferred to quartz cuvettes* and sealed. These solutions were left to stand in a 25 °C constant temperature room and monitored until crystals did not grow further. An optical microscope fitted with a polarising lens was used to monitor crystal growth.

*Pathlength 1mm, chamber volume 350 mL, fitted with a PTFE stopper. The sealed cuvettes provided a flat surface where crystals can grow whilst being monitored under the microscope. Polarising lens prevents unpolarised light from passing. As crystals polarise light, they are more clearly observed, as the polarised light contrasts the black background.

8.3.2 Procedure to Monitor Crystal Growth Behaviour Described in Section 3.3

(a) Time Dependent Crystal Growth: A 250 μM stock solution of the rotaxane **1.9** was prepared by adding the rotaxane **1.9** (1.81 mg) to water (5 mL), heating the mixture in a water bath set to 95 °C and cooling to room temperature. An aliquot (*ca.* 300 μL) of the resulting solution was transferred to a cuvette (as specified in Section **8.3.1**), sealed and left to stand in a 25 °C constant temperature room. Crystals were monitored using an optical microscope fitted with a polarising lens after 2 and 90 h.

(b) Concentration Dependent Crystal Growth: The 250 μM stock solution of the rotaxane **1.9** prepared as described in the Section above was diluted to 25 μM by combining 0.5 mL of the stock solution with 4.5 mL of water, followed by heating in a water bath set to 95 °C and cooling to room temperature. Aliquots (*ca.* 300 μL) of the stock solution (250 μM) and the diluted solution above (25 μM) were transferred to respective cuvettes (as specified in Section **8.3.1**) and sealed. The solutions were left to stand in a 25 °C constant temperature room. Crystals were observed after 90 h using an optical microscope fitted with a polarising lens.

(c) Temperature Dependent Crystal Growth: Aliquots (*ca.* 300 μL) of the stock solution (250 μM) of the rotaxane **1.9** were transferred to respective cuvettes (as specified in Section **8.3.1**), sealed and the two samples were incubated at 4 °C and 18 °C for 72 h. Crystals grown at 18 °C were observed with an optical microscope fitted with a polarising lens. Those at 4 °C were monitored without a polarising lens as the crystals were too fine to be observed otherwise.

(d) Sonication Experiment: A mixture containing crystals of the rotaxane **1.9** was sonicated for 30 min at room temperature. The mixture was observed before and after sonication using an optical microscope fitted with a polarising lens.

8.4 Experimental for Chapter 4

8.4.1 Synthesis

[*trans*-4-(2,6-Dimethylphenylaminocarbonyl)-4'-(3,5-dimethylphenylaminocarbonyl)azobenzene]-[α-cyclodextrin]-[2]rotaxanes 4.1 and 4.2

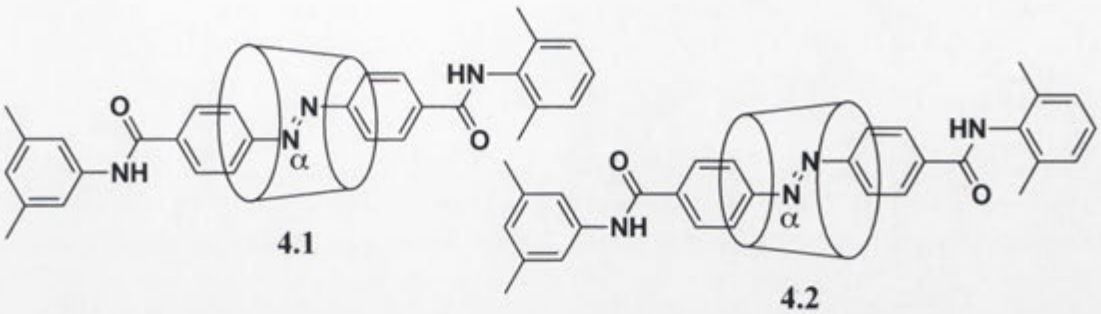

The asymmetrically substituted axle **4.4** (15 mg, 4.0×10^{-5} mol) was suspended in water (3 mL) and TEA (73 mg, 7.2×10^{-4} mol) was added, followed by α-CD **1.1** (117 mg, 1.2×10^{-4} mol), and the mixture was stirred overnight at room temperature. DMT-MM (44 mg, 1.6×10^{-4} mol) and 2,6-dimethylaniline **2.4** (45 mg, 3.6×10^{-4} mol) were added and the mixture was stirred for 4 h before further addition of DMT-MM (44 mg, 1.6×10^{-4} mol). After that mixture was stirred overnight, more DMT-MM (44 mg, 1.6×10^{-4} mol) was added twice at 24 h intervals. Water (70 mL) was then added to the reaction mixture and the mixture was washed with EtOAc (3 × 70 mL). The combined organic layers were extracted with water (70 mL) and the aqueous extract was washed with EtOAc (70 mL). The combined aqueous solutions were concentrated under reduced pressure. The residue was dissolved in MeOH and subjected to HPLC. Respective fractions containing the isomeric products **4.1** and **4.2** were concentrated and lyophilised to give the title compounds **4.1** (20 mg, yield 34%) and **4.2** (13 mg, yield 22%) as orange powders. Crystals of the rotaxanes **4.1** and **4.2** were obtained through slow evaporation of MeOH over a period of several weeks.

For compound **4.1**:

TLC (5:4:3 v/v/v *n*-butanol:ethanol:water) R_f 0.55.

Melting point 245-247 °C (dec.).

^{1}H NMR (500 MHz, CD_3OD) δ_H 8.65 (2H, d, *J* 8.5, Azo-H), 8.27 (2H, d, *J* 8.5, Azo-H), 8.26 (2H, d, *J* 8.5, Azo-H), 8.07 (2H, d, *J* 8.5, Azo-H), 7.45 (2H, s, aniline-H), 7.17 (3H, apparent s, aniline-H), 6.87 (1H, s, aniline-H), 3.83 (6H, m, CD-C5-H), 3.77 (6H, m, CD-C3-H), 3.72 (6H, m, CD-C6-H), 3.59 (6H, m, CD-C6-H), 3.50 (6H,

m, CD-C4-H), 3.42 (6H, dd, *J* 3.5, 10, CD-C2-H), 2.35 (6H, s, Me), 2.31 (6H, s, Me).

^{13}C NMR (125.7 MHz, CD_3OD) δc 168.3 and 167.9 (C=O), 155.1, 154.6, 140.1, 139.6, 139.4, 138.6, 137.2, 135.6, 130.2, 129.4, 129.2, 128.7, 127.5, 126.4, 124.5, 120.3, 103.9, 83.2, 75.0, 73.8, 73.4, 61.7, 21.5 and 18.5 (Me).

Mass spectrum (ESI-HR, positive ion mode) *m/z* Found 1471.528 [($M+Na^+$), $C_{66}H_{88}N_4O_{32}+Na^+$]. Requires 1471.527.

Elemental analysis Found C, 51.73; H, 6.62; N, 3.56%. $C_{66}H_{88}N_4O_{32}\cdot 5H_2O$ requires C, 51.49; H, 6.42; N, 3.64%.

X-ray crystallographic data are presented in Appendix 1.

HPLC (Preparative) t_R 4.6 min [column: Waters XBridge Prep C18 5 μm, 19 × 150 mm; 10 mL/min MeOH/H_2O (0.1% TFA) gradient - 50-70% MeOH, 0-20 min, detection wavelength: 346 nm].

For compound **4.2**:

TLC (5:4:3 v/v/v *n*-butanol:ethanol:water) R_f 0.60.

Melting point 245-248 °C (dec.).

^{1}H NMR (500 MHz, CD_3OD) δ_H 8.66 (2H, d, *J* 8.5, Azo-H), 8.32 (2H, d, *J* 8.5, Azo-H), 8.20 (2H, d, *J* 8.5, Azo-H), 8.05 (2H, d, *J* 8.5, Azo-H), 7.37 (2H, s, aniline-H), 7.17 (3H, apparent s, aniline-H), 6.86 (1H, s, aniline-H), 3.81 (6H, m, CD-C5-H) 3.77 (6H, m, CD-C3-H), 3.74 (6H, m, CD-C6-H), 3.59 (6H, m, CD-C6-H), 3.51 (6H, m, CD-C4-H) 3.43 (6H, m, CD-C2-H), 2.39 (6H, s, Me), 2.34 (6H, s, Me).

^{13}C NMR (125.7 MHz, CD_3OD) δc 168.6 and 167.5 (C=O), 154.9, 154.8, 139.6, 139.5, 139.4, 139.1, 137.5, 135.7, 130.2, 129.4, 129.1, 128.7, 127.5, 126.4, 124.3, 120.1, 103.9, 83.3, 75.0, 73.7, 73.3, 61.7, 21.5 and 18.9 (Me).

Mass spectrum (ESI-HR, positive ion mode) *m/z* Found 1449.543 [($M+H^+$), $C_{66}H_{88}N_4O_{32}+H^+$]. Requires 1449.546.

Elemental analysis Found C, 52.96; H, 6.99; N, 3.88%. $C_{66}H_{88}N_4O_{32}\cdot 4.5CH_3OH$ requires C, 53.13; H, 6.70; N, 3.52%.

X-ray crystallographic data are presented in Appendix 1.

HPLC (Preparative) t_R 5.9 min [column: Waters XBridge Prep C18 5 μm, 19 × 150 mm; 10 mL/min MeOH/H_2O (0.1% TFA) gradient - 50-70% MeOH, 0-20 min, detection wavelength: 346 nm].

***trans*-4'-(2,6-Dimethylphenylaminocarbonyl)azobenzene-4-carboxylic acid 4.4 and *trans*-4,4'-bis(2,6-Dimethylphenylaminocarbonyl)azobenzene 4.5**

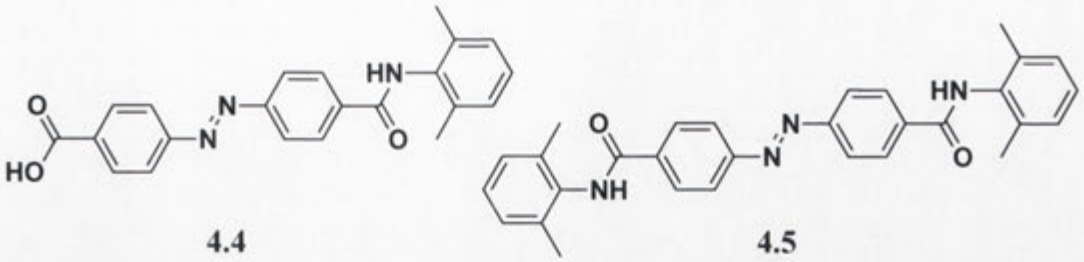

4.4 **4.5**

Under dry nitrogen atmosphere, azobenzene-4,4'-dicarbonyl dichloride **4.3** (200 mg, 6.5×10^{-4} mol) was dissolved in dry DCM (10 mL) and a solution of 2,6-dimethylaniline **2.4** (63 mg, 5.2×10^{-4} mol) in dry DCM (60 mL) was added dropwise over 30 min while the temperature was maintained at $\leq$ -5 °C using an ice bath with sodium chloride. TEA (80 mg, 7.9×10^{-4} mol) was added to the reaction mixture, which was then stirred at room temperature for 1 h, before additional 2,6-dimethylaniline **2.4** (32 mg, 2.6×10^{-4} mol) dissolved in dry DCM (5 mL) was added dropwise. The reaction mixture was stirred for further 2 h at room temperature, and then concentrated under reduced pressure. THF/water (150 mL, 2:1 v/v) was added to the residue and the mixture was sonicated at 50 °C for 1 h. The resulting solution was concentrated under reduced pressure. That residue was chromatographed over silica gel column, which was eluted with a MeOH-DCM solvent gradient. The di-capped byproduct **4.5** was eluted with 1-3% MeOH in DCM, followed by the mono-capped product **4.4** with 5% MeOH in DCM. The fractions containing each material were combined and concentrated under reduced pressure to give the title compounds **4.4** (103 mg, yield 42%) and **4.5** (87 mg, yield 28%) as orange powders.

For compound **4.4**:

TLC (5:95 v/v MeOH:DCM) R_f 0.16.

Melting point 289-290 °C (dec.).

^{1}H NMR (300 MHz, Acetone-d_6) δ_H 8.29 (2H, d, *J* 8.5, Azo-H), 8.26 (2H, d, *J* 8.5, Azo-H), 8.09 (4H, m, Azo-H), 7.13 (3H, apparent s, aniline-H), 2.28 (6H, s, Me).

^{13}C NMR (75.5 MHz, $CDCl_3$) δc 167.9 and 166.1 (C=O), 154.7, 154.0, 136.4, 135.5, 133.7, 132.7, 130.6, 128.3, 127.9, 127.3, 122.9, 122.6, 17.9 (Me).

Mass spectrum (EI-HR) *m/z* Found 373.143 [($M^{+\cdot}$), $C_{22}H_{19}N_3O_3^{+\cdot}$]. Requires 373.143.

Elemental analysis Found C, 71.00; H, 5.36; N, 11.39%. $C_{22}H_{19}N_3O_3$ requires C, 70.76; H, 5.13; N, 11.25%.

For compound **4.5**:

TLC (5:95 v/v MeOH:DCM) R_f 0.70.

Melting point 227-229 °C (dec.).

^{1}H NMR (300 MHz, DMSO-d_6) δ_H 10.01 (2H, s, NH), 8.24 (4H, d, *J* 8.5, Azo-H), 8.09 (4H, d, *J* 8.5, Azo-H), 7.15 (6H, apparent s, aniline-H), 2.22 (12H, s, Me).

^{13}C NMR (75.5 MHz, DMSO-d_6) δc 164.2 (C=O), 153.4, 136.9, 135.5, 135.0, 128.9, 127.7, 126.8, 122.7, 18.0 (Me).

Mass spectrum (EI-HR) *m/z* Found 476.221 [($M^{+\cdot}$), $C_{30}H_{28}N_4O_2^{+\cdot}$]. Requires 476.221.

8.4.2 Determination of the Solubility of [2]Rotaxanes

8.4.2.1 Procedure to Obtain the Solubility Plot Described in Section 4.6

A 100 μM stock solution of the rotaxane **1.9** was prepared by adding the rotaxane **1.9** (4.35 mg) to water (30 mL) and heating the mixture to 80 °C in a water bath to dissolve. The stock solution cooled to ambient temperature. Solutions of the rotaxane **1.9** (5, 10, 20 and 50 μM) were prepared as described in the following. The stock solution was diluted to 50 μM by combining water (9 mL) with the stock solution (9 mL). The stock solution also was diluted to 20 μM by combining water (6 mL) with the stock solution (24 mL). The 20 μM solution was then diluted to 10 μM by combining water (15 mL) with the 20 μM solution (15 mL). Finally, the 10 μM solution was diluted to 5 μM by combining water (15 mL) with the 10 μM solution (15 mL). All solutions (5, 10, 20, 50 and 100 μM) were heated at 80 °C in a water bath, placed in three separate vials (5 mL each) and incubated at 80 °C, 50 °C, and 10 °C. The UV/visible spectra of the supernatants were monitored during incubation over 7 days, after which time no further change in absorbance was observed. Absorbance at 350 nm was plotted against moles of the rotaxane **1.9**/litre of water as shown in **Figure 4.14**.

8.4.2.2 Procedure to Monitor Crystallisation Described in Section 4.6

A 100 μM solution of the rotaxane **1.9** was prepared by adding the rotaxane **1.9** (1.45 mg) to water (10 mL) and heating the mixture to 80 °C in a water bath. The UV/visible spectra of the supernatant were obtained over 12 days during incubation at 30 °C.

8.4.3 Procedure to Study Crystal Growth Inhibition Described in Section 4.7

8.4.3.1 Procedure for Co-crystallisation

Lyophilised solids which contain both crystalline and amorphous solids were used to prepare solutions required for experiments to regulate crystal growth. Prior to crystallisation experiments, mixtures containing rotaxanes were heated at a higher temperature to form supersaturated solutions.

The stock mixture of the rotaxane **1.9** (200 μM) was prepared by adding the rotaxane **1.9** (1.45 mg) to water (5 mL), heating the mixture in a water bath set to 95 °C and cooling to ambient temperature. The stock mixture of respective inhibitor rotaxanes was also prepared as above. The stock mixtures of the rotaxanes **1.9** and inhibitor rotaxanes were not completely clear solutions, as they are above the saturation concentration. However, they were mixed thoroughly before 200 μM solution of the rotaxane **1.9** (500 μL) was combined with solutions of the respective inhibitor rotaxane (500 μL) and heated in a water bath set to 95 °C. The resulting solutions were cooled to 25 °C in a constant temperature room, transferred to cuvettes, sealed and monitored using an optical microscope fitted with a polarising lens at this temperature.

8.4.3.2 Procedure to Determine the Relative Proportions of Rotaxanes in Grown Crystals

To measure the relative proportions of the rotaxane **1.9** and respective inhibitor rotaxanes present in grown crystals prepared, crystals were collected and analysed by HPLC. Firstly, assayed samples were transferred to 1.5 mL microcentrifuge tubes and centrifuged for 1 min at 13,200 rpm to collect crystals. They were resuspended in water (1 mL) to remove excess rotaxane in the solution and centrifuged for another 1 min at 13,200 rpm. Collected crystals were dissolved in MeOH (*ca.* 500 μL) and aliquots (50 μL) of each sample were subject to HPLC. HPLC chromatograms were

obtained at the isosbestic point of the relevant rotaxanes and the percentage composition of the two rotaxanes was estimated by integrating the areas underneath each peak.

8.4.3.3 Crystal Growth Inhibition Study Using the Rotaxane 4.1

Co-crystallisation of the rotaxanes **4.1** and **1.9** was carried out as described in Section **8.4.3.1**. The stock mixture of the rotaxane **4.1** (200 μM) was prepared by adding the rotaxane **4.1** (1.45 mg) to water (5 mL) and heating the mixture in a water bath set to 95 °C, then cooling to ambient temperature. Solutions (20 and 100 μM) of the rotaxane **4.1** were prepared using the 200 μM stock mixture of the rotaxane **4.1** and water. The rotaxane **4.1** (0, 20, 100 or 200 μM) and the rotaxane **1.9** (200 μM) were combined. The final concentrations of the rotaxane **4.1** were 0, 10, 50 or 100 μM respectively and all four solutions contained 100 μM of the rotaxane **1.9**. The resulting solutions were monitored for 3.5 days. HPLC analysis was carried out as described in Section **8.4.3.2** to measure the relative proportions of the rotaxanes **1.9** and **4.1** present in grown crystals.

HPLC t_R 5.5 min (rotaxane **4.1**), 7.3 min (rotaxane **1.9**) [column: Phenomenex Luna 5 μm C18(2) 100 Å, 250 × 10 mm; 3 mL/min H_2O/ACN 60:40 isocratic, detection wavelength: 349 nm].

8.4.3.4 Crystal Growth Inhibition Study Using the Rotaxane 4.2

Co-crystallisation of the rotaxanes **4.2** and **1.9** was carried out as described in Section **8.4.3.1**. The stock mixture of the rotaxane **4.2** (400 μM) was prepared by adding the rotaxane **4.2** (2.90 mg) to water (5 mL) and heating the mixture in a water bath set to 95 °C, then cooling to ambient temperature. Solutions (200 and 300 μM) of the rotaxane **4.2** were prepared using 400 μM stock mixture of the rotaxane **4.2**. The rotaxane **1.9** (200 μM) and the rotaxane **4.2** (0, 200, 300 or 400 μM) were combined. The final concentration of the rotaxane **4.2** were 0, 100, 150 or 200 μM respectively and all four solutions contained 100 μM of the rotaxane **1.9**. The resulting solutions were monitored for 36 days. HPLC analysis was carried out as described in Section **8.4.3.2** to measure the relative proportions of the rotaxanes **1.9** and **4.2** present in grown crystals.

HPLC t_R 18.7 min (rotaxane **4.2**), 27.0 min (rotaxane **1.9**) [column: Waters XBridge

Prep C18 5 μm, 19 × 150 mm; 10 mL/min H_2O/ACN 50:50 isocratic, detection wavelength: 349 nm].

8.4.3.5 Crystal Growth Inhibition Study Using the Rotaxane 1.18

Co-crystallisation of the rotaxanes **1.18** and **1.9** was carried out as described in Section **8.4.3.1**. The stock mixture of the rotaxane **1.18** (200 μM) was prepared by adding the rotaxane **1.18** (1.45 mg) to water (5 mL) and heating the mixture in a water bath set to 95 °C, then cooling to ambient temperature. Solutions (20 and 100 μM) of the rotaxane **1.18** were prepared using the 200 μM stock mixture of the rotaxane **1.18** and water. The rotaxane **1.18** (0, 20, 100 or 200 μM) and the rotaxane **1.9** (200 μM) were combined. The final concentrations of the rotaxane **1.18** were 0, 10, 50 or 100 μM respectively and all four solutions contained 100 μM of the rotaxane **1.9**. The resulting solutions were monitored for 10 days. HPLC analysis was carried out as described in Section **8.4.3.2** to measure the relative proportions of the rotaxanes **1.9** and **1.18** present in grown crystals.

HPLC t_R 7.3 min (rotaxane **1.9**) [column: Phenomenex Luna 5 μm C18(2) 100 Å, 250 × 10 mm; 3 mL/min H_2O/ACN 60:40 isocratic, detection wavelength: 346 nm].

8.5 Experimental for Chapter 5

8.5.1 Synthesis

[*trans*-4-(3,5-Dimethylphenylaminocarbonyl)-4'-(2,4,6-trinitrophenylamino)stilbene]-[α-cyclodextrin]-[2]rotaxane 5.5

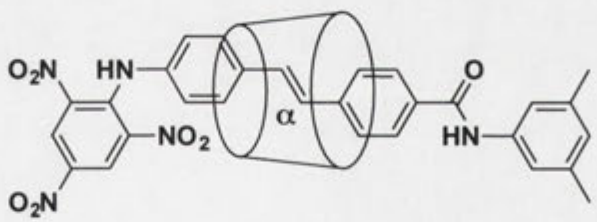

A mixture of the *trans*-4-(3,5-dimethylphenylaminocarbonyl)-4'-aminostilbene **5.9** (5 mg, 1.5×10^{-5} mol) and α-CD **1.1** (568 mg, 5.8×10^{-4} mol) in 0.2 M sodium carbonate buffer (pH 10.0, 40 mL) was equilibrated for 2 h at room temperature. Dihydrate of 2,4,6-trinitrobenzene-1-sulfonic acid sodium salt **5.3** (10 mg, 2.8×10^{-5} mol) was added and the mixture was stirred for 24 h at room temperature. The resultant solution was washed with EtOAc (5 × 100 mL). The aqueous layer was

concentrated under reduced pressure and then subjected to HPLC. The fractions containing the product **5.5** were concentrated and lyophilised to give the title compound **5.5** (3 mg, yield 13%) as orange powder. Crystals of rotaxane **5.5** were obtained through slow evaporation of MeOH/water over a period of several weeks.

TLC (5:4:3 v/v/v *n*-butanol:ethanol:water) R_f 0.79.

Melting point 245-246 °C (dec.).

^{1}H NMR (500 MHz, CD_3OD) δ_H 9.90 (1H, s, NH), 9.10 (2H, s, trinitrophenyl-H), 8.08 (2H, d, *J* 8.5, stilbene-H), 8.05 (2H, d, *J* 8.5, stilbene-H), 7.45 (2H, d, *J* 8.0, stilbene-H), 7.38 (2H, s, aniline-H), 7.32 (1H, d, *J* 16.0, olefinic-H), 7.27 (2H, d, *J* 8.0, stilbene-H), 7.20 (1H, d, *J* 16.0, olefinic-H), 6.84 (1H, s, aniline-H), 4.93 (6H, d, *J* 3.5, CD-C1-H), 3.87 (6H, apparent d, *J* 9.0, CD-C5-H), 3.86 (6H, apparent t, *J* 9.0, CD-C3-H), 3.75 (6H, dd, *J* 3.5, 12.0, CD-C6-H), 3.64 (6H, apparent d, *J* 12.0, CD-C6-H), 3.58 (6H, apparent t, *J* 9.0 CD-C4-H), 3.45 (6H, dd, *J* 3.5, 9.0, CD-C2-H), 2.33 (6H, s, Me).

^{13}C NMR (200 MHz, CD_3OD) δc 168.9, 141.0, 140.6(1), 140.5(7), 139.5(8), 139.5(6), 139.5, 137.8, 136.2, 134.8, 130.4, 129.6, 129.0, 128.9, 128.7, 128.0, 127.3, 122.9, 120.2, 104.0, 83.2, 75.1, 73.9, 73.8, 61.5, 21.5.

Mass spectrum *m/z* (ESI-HR, positive ion mode) Found 1526.4847 [$(M+H^+)$, $C_{65}H_{83}N_5O_{37}+H^+$]. Requires 1526.4845.

X-ray crystallographic data are presented in Appendix 1.

HPLC (Preparative) t_R 14.6 min [column: Waters XBridge Prep C18 5 μm, 19 × 150 mm; 10 mL/min $MeOH/H_2O$ 30:70 isocratic, detection wavelength: 333 nm].

4-(4'-Aminostilbene) carboxylic acid 5.8

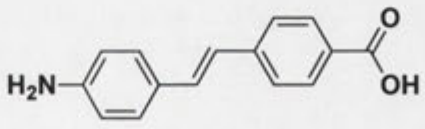

4-Vinylaniline **5.6** (590 mg, 5.0×10^{-3} mol) and 4-iodobenzoic acid **5.7** (1.1 g, 4.4×10^{-3} mol) were dissolved in DMF (6 mL) and TEA (6 mL). PPh_3 (12 mg, 4.6×10^{-5} mol) and palladium(II) acetate (10 mg, 4.5×10^{-5} mol) were added and the solution was then refluxed for 48 h. The reaction mixture was concentrated under reduced pressure. EtOAc (300 mL) was added to the solid residue, and insoluble precipitate was removed by filtration. The product was extracted with 2 M HCl (3 × 100 mL)

from the filtrate, and the aqueous layer containing the product was neutralised with aqueous NaOH solution. Precipitate was formed, and it was collected though centrifugation. The precipitate was washed with water (2 × 40 mL) and Et_2O (40 mL) before drying under vacuum to give the desired compound **5.8** (194 mg, yield 18%). Physical and spectral properties were consistent with those reported previously.[164]

TLC (5:2 v/v EtOAc:Hexane) R_f 0.80.

Melting point 293-296 °C (dec.) [lit.[164] 292-300 °C (dec.)].

^{1}H NMR (300 MHz, DMSO-d_6) δ_H 7.79 (2H, d, *J* 7.5, stilbene-H), 7.40 (2H, d, *J* 7.5, stilbene-H), 7.28 (2H, d, *J* 7.5, stilbene-H), 7.06 (1H, d, *J* 16.0, olefinic H), 6.89 (1H, d, *J* 16.0, olefinic H), 6.56 (2H, d, *J* 7.5, stilbene-H), 5.30 (2H, s, NH_2).

Mass spectrum *m/z* (ESI-HR, negative ion mode) Found 238.0868 [(M-H$^-$), $C_{15}H_{13}NO_2$-H]. Requires 238.0868.

***trans*-4-(3,5-Dimethylphenylaminocarbonyl)-4'-aminostilbene 5.9**

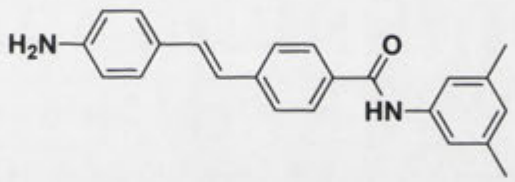

Under dry nitrogen atmosphere, the stilbene **5.8** (100 mg, 4.2 × 10^{-4} mol) and BOP (279 mg, 6.3 × 10^{-4} mol) were dissolved in 3,5-dimethylaniline **2.2** (12 mL, 9.6 × 10^{-2} mol) and stirred overnight at room temperature before further addition of BOP (279 mg, 6.3 × 10^{-4} mol). After the mixture was stirred for 48 h at room temperature, more BOP (93 mg, 2.1 × 10^{-4} mol) was added and stirred overnight at room temperature. The crude reaction mixture was passed through a silica gel column using hexane-Et_2O solvent gradient (0-100% Et_2O) to remove unreacted 3,5-dimethylaniline **2.2**. The product mixture was recovered by flushing this column with MeOH. The crude product mixture was purified by silica gel chromatography with EtOAc-hexane solvent gradient. The title compound **5.9** was eluted with 20-100% EtOAc. The fractions containing the desired compound **5.9** were combined, concentrated and further purified by HPLC (22 mg, yield 15%).

TLC (5:2 v/v Hexane:EtOAc) R_f 0.51.

Melting point 190-195 °C (dec.).

^{1}H NMR (300 MHz, CD_2Cl_2) δ_H 7.82 (2H, d, *J* 8.1, stilbene-H), 7.81 (1H, s, NH),

7.58 (2H, d, *J* 8.1, stilbene-H), 7.36 (2H, d, *J* 8.4, stilbene-H), 7.28 (2H, s, aniline-H), 7.15 (1H, d, *J* 16.0, olefinic-H), 6.96 (1H, d, *J* 16.0, olefinic H), 6.81 (1H, s, aniline-H), 6.68 (2H, d, *J* 8.4, stilbene-H), 3.89 (2H, s, NH_2), 2.33 (6H, s, Me).

^{13}C NMR (125.7 MHz, CD_2Cl_2) δc 165.6 (C=O), 147.8, 142.1, 139.3, 138.6, 133.6, 131.6, 128.6, 128.0, 127.6, 126.7, 126.6, 123.9, 118.4, 115.5 and 21.7 (Me).

Mass spectrum *m/z* (ESI-HR, positive ion mode) Found 343.1810 [($M+H^+$), $C_{23}H_{22}N_2O+H^+$]. Requires 343.1810.

Elemental analysis Found C, 78.54; H, 6.52; N, 7.77%. $C_{23}H_{22}N_2O \cdot 0.5H_2O$ requires C, 78.59; H, 6.61; N, 7.97%.

HPLC (Preparative) t_R 44.6 min [column: Grace Alltima C18 5 μm, 22 × 250 mm with a Grace Alltima C18 10 μm, 33 mm guard column; 10 mL/min ACN/H_2O 57:43 isocratic, detection wavelength: 333 nm].

8.5.2 Procedure to Determine the Relative Proportions of the Rotaxane 5.5 in the Crystals of the Rotaxane 1.9

Co-crystallisation of the rotaxanes **5.5** and **1.9** were carried out according to the procedure described in Section **8.4.3.1**. The stock mixture of the rotaxane **5.5** (200 μM) was prepared by adding the rotaxane **5.5** (1.53 mg) to water (5 mL) and heating the mixture in a water bath set to 95 °C, then cooling to ambient temperature. Solutions (20 and 100 μM) of the rotaxane **5.5** were prepared using the 200 μM stock mixture of the rotaxane **5.5** and water. The rotaxane **5.5** (0, 20, 100 or 200 μM) and the rotaxane **1.9** (200 μM) were combined. The final concentrations of the rotaxane **5.5** were 0, 10, 50 or 100 μM respectively and all four solutions contained 100 μM of the rotaxane **1.9**. The resulting solutions were monitored for 4 days. HPLC analysis was carried out as described in Section **8.4.3.2** to measure the relative proportions of the rotaxanes **1.9** and **5.5** present in grown crystals.

HPLC t_R 9.9 min (rotaxane **5.5**), 10.9 min (rotaxane **1.9**) [column: YMC Pack ODS-AQ 3 μm, 150 × 3.0 mm; 0.7 mL/min H_2O/ACN gradient- 5-30% ACN, 0-10 min, detection wavelength: 332 nm].

8.6 Experimental for Chapter 6

[*trans*-*N*-(2,6-Dimethylphenyl)-4-(2-(1,1,3,3-tetramethylisoindolin-2-yl)oxyl-5-yl) vinyl)benzamide]-[α-cyclodextrin]-[2]rotaxanes 1.33 and 1.34

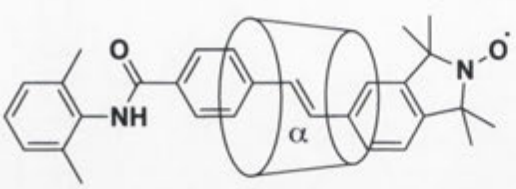

1.33

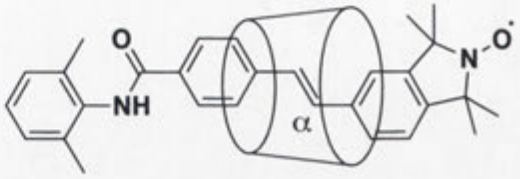

1.34

The stilbene **6.1** (25 mg, 7.4×10^{-5} mol) was suspended in water (25 mL) and TEA (15 mg, 1.5×10^{-4} mol) was added to the mixture to dissolve. α-CD **1.1** (360 mg, 3.7×10^{-4} mol) was added to the mixture, and the mixture was sonicated to give a clear solution. Following equilibration of the mixture for 2 h at room temperature, DMT-MM (410 mg, 1.5×10^{-4} mol) and 2,6-dimethylaniline **2.4** (27 mg, 2.2×10^{-4} mol) were added to the mixture and stirred for 17 h at room temperature. The resultant mixture was concentrated under reduced pressure. The residue was then suspended in 20 mL water, and centrifuged to remove precipitate. The solid residue was washed with water (3 × 20 mL) and centrifuged to separate solids. All soluble fractions were combined, and subjected to HPLC. The fractions containing the desired isomeric products **1.33** and **1.34** were concentrated and lyophilised to give the title compounds **1.33** (20 mg, yield 19%) and **1.34** (22 mg, yield 21%) as colourless powders. Purified samples showed decomposition. Therefore, small-scale purification was carried out by analytical HPLC, where fractions containing the pure compounds were collected under light shielded conditions and lyophilised immediately to prevent isomerisation after purification.

For compound **1.33**:

TLC (5:4:3 v/v/v *n*-butanol:ethanol:water) R_f 0.57.

Melting point 222-225 °C (dec.).

^{1}H NMR (500 MHz, CD_3OD containing ascorbic acid **6.4**, see Section **8.1.2**) δ_H 8.13 (2H, d, *J* 8.5, Ar-H), 8.10 (2H, d, *J* 8.5, Ar-H), 7.68 (1H, d, *J* 7.5, Ar-H), 7.39 (1H, d, *J* 7.5, Ar-H), 7.36 (1H, d, *J* 16.5, olefinic-H), 7.25 (1H, s, Ar-H), 7.18 (1H, d, *J* 16.5, olefinic-H), 7.16 (3H, apparent s, aniline-H), 4.93 (6H, d, *J* 3.5, CD-C1-H), 3.92-3.83 (12H, m, CD-C3-H and CD-C5-H), 3.74 (6H, dd, *J* 3.0, 12.0, CD-C6-H), 3.59-3.55 (12H, m, CD-C4-H and CD-C6-H), 3.46 (6H, dd, *J* 3.5, 10.0, CD-C2-H), 2.36 (6H, s,

Me), 1.64 (3H, s, Me), 1.62 (3H, s, Me), 1.57 (3H, s, Me), 1.56 (3H, s, Me).

Mass spectrum *m/z* (ESI-HR, positive ion mode) Found 1412.5630 [($M+H^+$), $C_{65}H_{91}N_2O_{32}+H^+$]. Requires 1412.5633.

Elemental analysis Found C, 49.90; H, 6.92; N, 1.95%. $C_{65}H_{91}N_2O_{32}\cdot 8H_2O$ requires C, 50.15; H, 6.94; N, 1.80%.

HPLC (Preparative) t_R 5.4 min [column: Waters XBridge Prep C18 5 μm, 19 × 150 mm; 10 mL/min MeOH/H_2O 25:75 isocratic, detection wavelength: 324 nm].

HPLC (Analytical) t_R 5.7 min [column: YMC Pack ODS-AQ 3 μm, 150 × 3.0 mm; 0.7 mL/min H_2O/ACN gradient- 5-30% ACN, 0-10 min, detection wavelength: 324 nm].

For compound **1.34**:

Physical and spectral properties were consistent with those reported previously.[135]

TLC (5:4:3 v/v/v *n*-butanol:ethanol:water) R_f 0.57.

Melting point 253-257 °C (dec.) [lit.[135] 248-250 °C (dec.)].

^{1}H NMR (500 MHz, CD_3OD containing ascorbic acid **6.4**, see Section **8.1.2**) δ_H 8.12 (1H, d, *J* 8.0, Ar-H), 8.08 (2H, d, *J* 8.0, Ar-H), 7.62 (2H, d, *J* 8.0, Ar-H), 7.58 (1H, s, Ar-H), 7.47 (1H, d, *J* 8.0, Ar-H), 7.47 (1H, d, *J* 16.0, olefinic-H), 7.19 (1H, d, *J* 16.0, olefinic-H), 7.15 (3H, apparent s, aniline-H), 4.92 (6H, d, *J* 3.5, CD-C1-H), 3.91-3.88 (12H, m, CD-C3-H and CD-C5-H), 3.90 (6H, dd, *J* 3.5, 12.5, CD-C6-H), 3.59-3.54 (12H, m, CD-C4-H and CD-C6-H), 3.48 (6H, dd, *J* 3.5, 10.0, CD-C2-H), 2.30 (6H, s, Me), 1.71 (6H, br s, Me), 1.62 (6H, br s, Me).

Mass spectrum (ESI, positive ion mode) *m/z* (%) 1413 [($M+H^+$), 20], 1435 [($M+Na^+$), 100].

HPLC (Preparative) t_R 8.3 min [column: Waters XBridge Prep C18 5 μm, 19 × 150 mm; 10 mL/min MeOH/H_2O 25:75 isocratic, detection wavelength: 324 nm].

HPLC (Analytical) t_R 6.8 min [column: YMC Pack ODS-AQ 3 μm, 150 × 3.0 mm; 0.7 mL/min H_2O/ACN gradient- 5-30% ACN, 0-10 min, detection wavelength: 324 nm].

[*trans*-*N*-(3,5-Dimethylphenyl)-4-(2-(1,1,3,3-tetramethylisoindolin-2-yl)oxyl-5-yl) vinyl)benzamide]-[α-cyclodextrin]-[2]rotaxanes 1.35 and 1.36

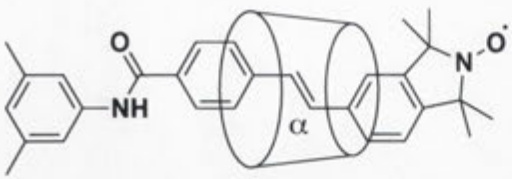

1.35

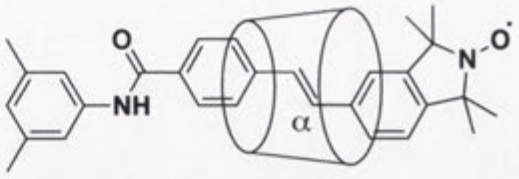

1.36

The stilbene **6.1** (25 mg, 7.4×10^{-5} mol) was suspended in water (25 mL) and TEA (15 mg, 1.5×10^{-4} mol) was added to the mixture to dissolve. α-CD **1.1** (360 mg, 3.7×10^{-4} mol) was added to the mixture, and the mixture was sonicated to give a clear solution. Following equilibration of the mixture for 2 h at room temperature, DMT-MM (410 mg, 1.5×10^{-4} mol) and 3,5-dimethylaniline **2.2** (27 mg, 2.2×10^{-4} mol) were added to the mixture and stirred for 14 h at room temperature. The resultant mixture was concentrated under reduced pressure. The residue was then suspended in 20 mL water, and centrifuged to remove precipitate. The solid residue was washed with water (3 × 20 mL) and centrifuged to separate solids. All soluble fractions were combined, and subjected to HPLC. The fractions containing the desired isomeric products **1.35** and **1.36** were concentrated and lyophilised to give the title compounds **1.35** (31 mg, yield 30%) and **1.36** (30 mg, yield 29%) as colourless powders. Purified samples showed decomposition. Therefore, small-scale purification was carried out using the procedure described for the compounds **1.33** and **1.34**.

For compound **1.35**:

TLC (5:4:3 v/v/v *n*-butanol:ethanol:water) R_f 0.68.

Melting point 223-225 °C (dec.).

^{1}H NMR (500 MHz, CD_3OD containing ascorbic acid **6.4**, see Section **8.1.2**) δ_H 8.13 (2H, d, *J* 8.0, Ar-H), 8.08 (2H, d, *J* 8.0, Ar-H), 7.82 (1H, d, *J* 8.5, Ar-H), 7.56 (1H, s, Ar-H), 7.55 (1H, d, *J* 8.5, Ar-H), 7.48 (2H, s, aniline-H), 7.40 (1H, d, *J* 16.0, olefinic-H), 7.22 (1H, d, *J* 16.0, olefinic-H), 6.85 (1H, s, aniline-H), 4.93 (6H, d, *J* 3.5, CD-C1-H), 3.90 (6H, m, CD-C5-H), 3.81 (6H, dd, *J* 10.0, CD-C3-H), 3.72 (6H, dd, *J* 3.5, 12.0, CD-C6-H), 3.58 (6H, dd, *J* 3.5, 12.0, CD-C6-H), 3.53 (6H, apparent t, *J* 9.0, CD-C4-H), 3.46 (6H, dd, *J* 3.5, 10.0, CD-C2-H), 2.35 (6H, s, Me), 1.87 (3H, s, Me), 1.83 (3H, s, Me), 1.78 (6H, s, Me).

Mass spectrum *m/z* (ESI-HR, positive ion mode) Found 1434.5464 [(M+Na$^+$),

$C_{65}H_{91}N_2O_{32}$+Na^+]. Requires 1434.5453.

Elemental analysis Found C, 49.89; H, 6.60; N, 1.88%. $C_{65}H_{91}N_2O_{32}\cdot 9H_2O$ requires C, 49.57; H, 6.99; N, 1.78%.

HPLC (Preparative) t_R 6.9 min [column: Waters XBridge Prep C18 5 μm, 19 × 150 mm; 10 mL/min MeOH/H_2O 35:65 isocratic, detection wavelength: 328 nm].

HPLC (Analytical) t_R 7.6 min [column: YMC Pack ODS-AQ 3 μm, 150 × 3.0 mm; 0.7 mL/min H_2O/ACN gradient- 5-30% ACN, 0-10 min, detection wavelength: 328 nm].

For compound **1.36**:

TLC (5:4:3 v/v/v *n*-butanol:ethanol:water) R_f 0.68.

Melting point 207-211 °C (dec.).

^{1}H NMR (500 MHz, CD_3OD containing ascorbic acid **6.4**, see Section **8.1.2**) δ_H 8.21 (1H, d, *J* 8.0, Ar-H), 8.05 (2H, d, *J* 8.5, Ar-H), 7.64 (1H, s, Ar-H), 7.60 (2H, d, *J* 8.5, Ar-H), 7.56 (1H, d, *J* 8.0, Ar-H), 7.46 (1H, d, *J* 16.5, olefinic-H), 7.37 (2H, s, aniline-H), 7.21 (1H, d, *J* 16.5, olefinic-H), 6.85 (1H, s, aniline-H), 4.94 (6H, d, *J* 3.5, CD-C1-H), 3.88 (6H, m, CD-C5-H), 3.81 (6H, m, CD-C3-H), 3.72 (6H, dd, *J* 3.5, 12.0, CD-C6-H), 3.57 (12H, m, CD-C6-H and CD-C4-H), 3.50 (6H, dd, *J* 3.5, 10.0, CD-C2-H), 2.34 (6H, s, Me), 1.88 (6H, s, Me), 1.80 (6H, s, Me).

Mass spectrum *m/z* (ESI-HR, positive ion mode) Found 1434.5457 [(M+Na^+), $C_{65}H_{91}N_2O_{32}$+Na^+]. Requires 1434.5453.

Elemental analysis Found C, 49.73; H, 6.57; N, 1.80%. $C_{65}H_{91}N_2O_{32}.9H_2O$ requires C, 49.57; H, 6.99; N, 1.78%.

HPLC (Preparative) t_R 15.4 min [column: Waters XBridge Prep C18 5 μm, 19 × 150 mm; 10 mL/min MeOH/H_2O 35:65 isocratic, detection wavelength: 328 nm].

HPLC (Analytical) t_R 9.6 min [column: YMC Pack ODS-AQ 3 μm, 150 × 3.0 mm; 0.7 mL/min H_2O/ACN gradient- 5-30% ACN, 0-10 min, detection wavelength: 328 nm].

***trans*-*N*-(2,6-Dimethylphenyl)-4-(2-(1,1,3,3-tetramethylisoindolin-2-yl)oxyl-5-yl) vinyl)benzamide 1.37**

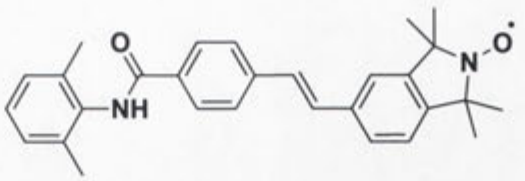

The acid **6.1** (20 mg, 6.0×10^{-5} mol) and BOP (39 mg, 9.0×10^{-5} mol) were dissolved in anhydrous DMF (2 mL) under dry nitrogen atmosphere. 2,6-Dimethylaniline **2.4** (7 mg, 6.0×10^{-4} mol) and TEA (9 mg, 9.0×10^{-4} mol) were added to the solution and stirred overnight at room temperature. The reaction mixture was subjected to HPLC. The fractions containing the product **1.37** were concentrated and dried under vacuum to give the title compound **1.37** (12 mg, yield 47%). Purified samples showed decomposition. Therefore, small-scale purification was carried out using the procedure described for the compounds **1.33** and **1.34**.

Physical and spectral properties were consistent with those reported previously.[135]

Melting point 226-228 °C (dec.).

^{1}H NMR (300 MHz, DMSO-d_6 containing ascorbic acid **6.4**, see Section **8.1.2**) δ_H 9.78 (1H, s, NH), 8.01 (2H, d, *J* 8.4, Ar-H), 7.74 (2H, d, *J* 8.4, Ar-H), 7.57 (1H, s, Ar-H), 7.53 (1H, d, *J* 7.5, Ar-H), 7.43 (1H, d, *J* 16.5, olefinic-H), 7.34 (1H, d, *J* 16.5, olefinic-H), 7.26 (1H, d, *J* 7.5, Ar-H), 7.12 (3H, apparent s, aniline-H), 2.18 (6H, s, Me), 1.40 (6H, br s, Me), 1.37 (6H, br s, Me).

Mass spectrum *m/z* (ESI-HR, positive ion mode) Found 440.2466 [$(M+H^+)$, $C_{29}H_{31}N_2O_2+H^+$]. Requires 440.2464.

HPLC (Analytical) t_R 7.9 min [column: Phenomenex Luna 5 μm C18(2) 100 Å, 250 × 4.6 mm; 1 mL/min H_2O/ACN 30:70 isocratic, detection wavelength: 324 nm].

***trans*-*N*-(3,5-Dimethylphenyl)-4-(2-(1,1,3,3-tetramethylisoindolin-2-yl)oxyl-5-yl) vinyl)benzamide 1.38**

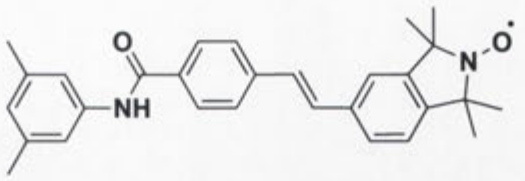

The acid **6.1** (20 mg, 6.0×10^{-5} mol) and BOP (39 mg, 9.0×10^{-5} mol) were dissolved in anhydrous DMF (2 mL) under dry nitrogen atmosphere. 3.5-Dimethylaniline **2.2** (7 mg, 6.0×10^{-4} mol) and TEA (9 mg, 9.0×10^{-4} mol) were added to the solution and stirred overnight at room temperature. The reaction mixture was subjected to HPLC. The fractions containing the product **1.38** were concentrated and dried under vacuum (22 mg, yield 82%). Purified samples showed decomposition. Therefore, small-scale purification was carried out using the procedure described for the compounds **1.33** and **1.34**.

Melting point 238-240 °C (dec.)

^{1}H NMR (500 MHz, CD_3OD containing ascorbic acid **6.4**, see Section **8.1.2**) δ_H 7.95 (2H, d, *J* 8.5, Ar-H), 7.73 (2H, d, *J* 8.5, Ar-H), 7.67 (1H, d, *J* 8.0, Ar-H), 7.60 (1H, s, Ar-H), 7.39 (1H, d, *J* 16.5, olefinic-H), 7.35 (1H, d, *J* 16.5, olefinic-H), 7.35 (1H, d, *J* 8.0, Ar-H), 7.33 (2H, s, aniline-H), 6.83 (1H, s, aniline-H), 2.33 (6H, s, Me), 1.69 (6H, br s, Me), 1.65 (6H, br s, Me).

Mass spectrum *m/z* (ESI-HR, positive ion mode) Found 440.2464 [$(M+H^+)$, $C_{29}H_{31}N_2O_2+H^+$]. Requires 440.2464.

HPLC (Preparative) t_R 22.0 min [column: Waters XBridge Prep C18 5 μm, 19 × 150 mm; 10 mL/min ACN/H_2O 70:30 isocratic, detection wavelength: 328 nm].

HPLC (Analytical) t_R 12.5 min [column: Phenomenex Luna 5 μm C18(2) 100 Å, 250 × 4.6 mm; 1 mL/min H_2O/ACN 30:70 isocratic, detection wavelength: 328 nm].

8.7 Experimental for Chapter 7

8.7.1 Calibration

In order to determine the concentration of the solutions prepared from small quantities of purified samples dissolved in ACN/water mixture, a calibration curve was used.

To determine the calibration curves, stock solutions (70 μM) were prepared for each of the rotaxanes **1.33**, **1.34**, **1.35**, and **1.36** (2.0 mg) in ACN/water (v/v 2:1, 20 mL). Stock solutions (70 μM) were also prepared for each of the dumbbells **1.37** and **1.38** (1.5 mg) in ACN/water (v/v 2:1, 50 mL). The stock solutions prepared were then diluted to 10, 20, 40, 60 and 70 μM. Aliquots (5 μL) of each solution were subjected to HPLC and the area underneath the peaks were measured and plotted against concentration to give calibration curves as shown in **Figure 8.1** and **Figure 8.2**.

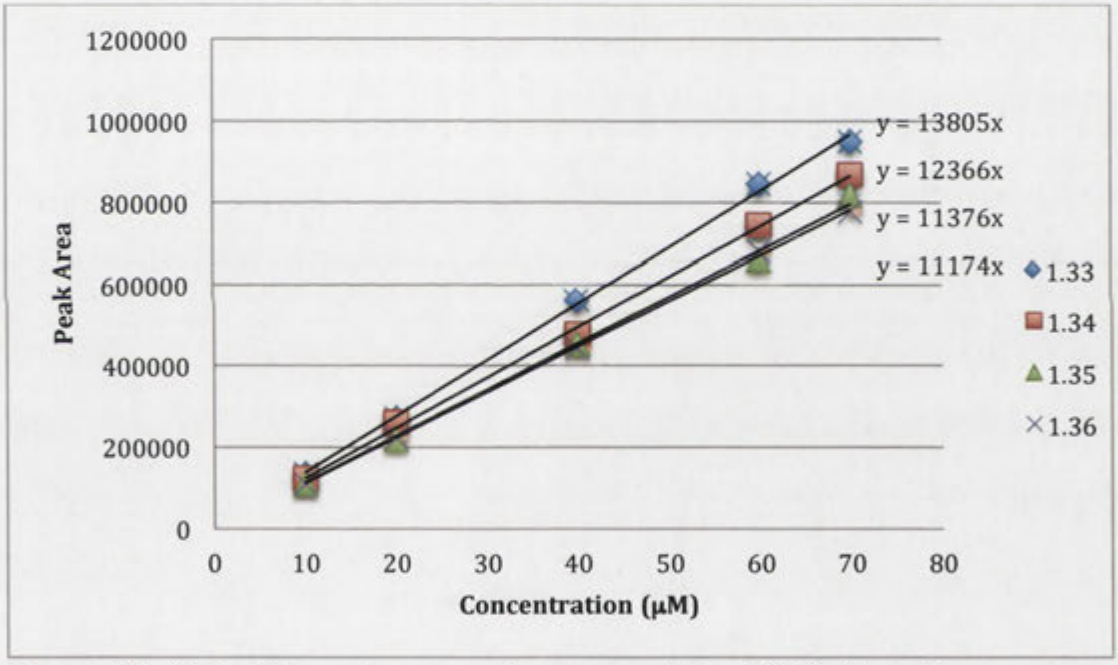

Figure 8.1. Plot of the peak area on the reverse phase HPLC chromatogram versus concentration to obtain calibration curves for the rotaxanes **1.33**, **1.34**, **1.35**, and **1.36**.

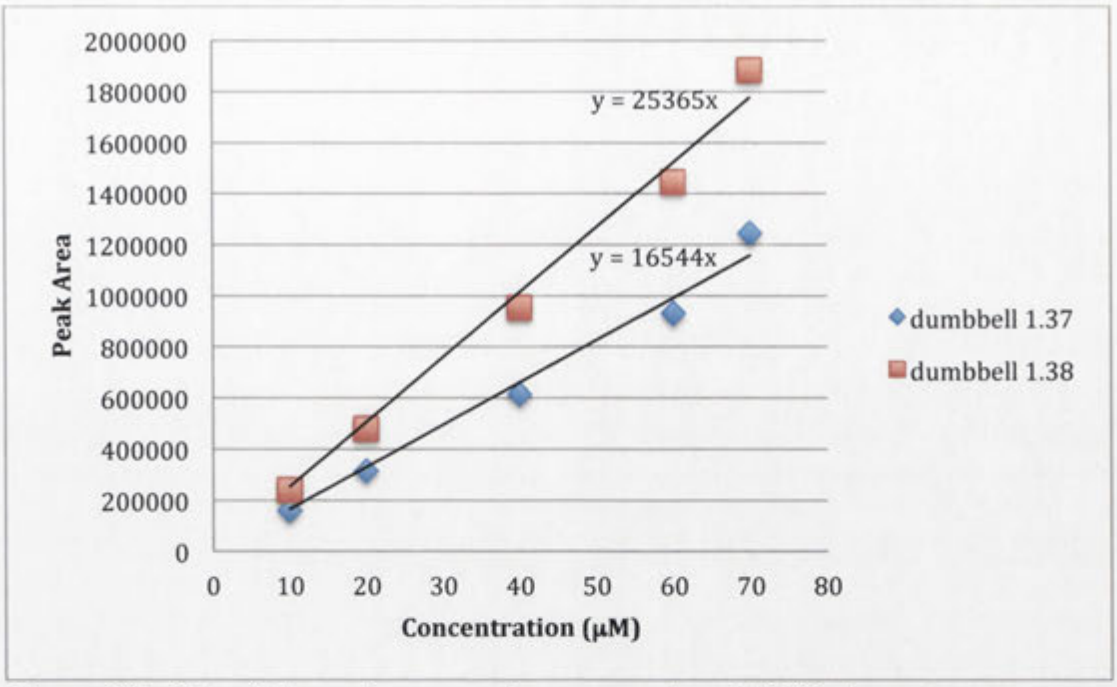

Figure 8.2. Plot of the peak area on the reverse phase HPLC chromatogram versus concentration to obtain calibration curves for the dumbbells **1.37** and **1.38**.

8.7.2 Photoirradiation and Monitoring

For UV/visible analysis: Solutions (70 μM) were prepared for each of the rotaxanes **1.33**, **1.34**, **1.35**, and **1.36** (2.0 mg) in ACN/water (v/v 2:1, 20 mL). Solutions (70 μM) were prepared for each of the dumbbells **1.37** and **1.38** (1.5 mg) in ACN/water (v/v 2:1, 50 mL). Aliquots (3 mL) of the solutions were sealed in quartz cuvettes. Prior to photoirradiation, UV/visible spectra of respective compounds were recorded. Then, the solutions were irradiated with one 300 nm UV-B lamp (8 W) in the photoreactor. The solutions were removed at 1, 2, 3, 4, 5, 10 and 20 min from the reactor to record UV/visible spectra.

For HPLC analysis: Samples further purified by analytical HPLC were reconstituted using 300 μL of ACN/water (v/v 2:1). Prior to analyses, concentration of respective solutions were determined using calibration curves in Section **8.7.1**. Once the concentrations were determined, each solution concentration was adjusted to 20 μM by adding appropriate amount of solvent. Aliquots (300 μL) of respective solutions were placed in HPLC shell vials (8 × 30 mm) and sealed. These solutions were then irradiated with one 300 nm UV-B lamp (8 W) in the photoreactor. Aliquots (20 μL) of the irradiated solutions were placed in HPLC total recovery vials (12 × 32 mm) at 1,

2, 3, 4, 5, 10, 20 min and 24 h, and loaded into the HPLC carousel (maintained at 4 °C and dark) to inject 5 μL of the sample and monitor the progress of the reaction.

References

(1) Feynman, R. P. *Engineering and Science* **1960**, *23*, 22.

(2) Schulz, M. *Nature* **1999**, *399*, 729.

(3) Thompson, S. E.; Parthasarathy, S. *Materials Today* **2006**, *9*, 20.

(4) Lehn, J. M. *Angewandte Chemie-International Edition in English* **1988**, *27*, 89.

(5) Watson, J. D.; Crick, F. H. C. *Nature* **1953**, *171*, 964.

(6) Mandl, C. P.; Konig, B. *Angewandte Chemie-International Edition* **2004**, *43*, 1622.

(7) Hernandez, J. V.; Kay, E. R.; Leigh, D. A. *Science* **2004**, *306*, 1532.

(8) Anelli, P. L.; Spencer, N.; Stoddart, J. F. *Journal of the American Chemical Society* **1991**, *113*, 5131.

(9) Bottari, G.; Dehez, F.; Leigh, D. A.; Nash, P. J.; Perez, E. M.; Wong, J. K. Y.; Zerbetto, F. *Angewandte Chemie-International Edition* **2003**, *42*, 5886.

(10) Bissell, R. A.; Cordova, E.; Kaifer, A. E.; Stoddart, J. F. *Nature* **1994**, *369*, 133.

(11) Jimenez, M. C.; Dietrich-Buchecker, C.; Sauvage, J. P. *Angewandte Chemie-International Edition* **2000**, *39*, 3284.

(12) Colquhoun, H. M.; Zhu, Z. X.; Williams, D. J. *Organic Letters* **2003**, *5*, 4353.

(13) Petitjean, A.; Khoury, R. G.; Kyritsakas, N.; Lehn, J. M. *Journal of the American Chemical Society* **2004**, *126*, 6637.

(14) Easton, C. J.; Lincoln, S. F. *Modified cyclodextrins : scaffolds and templates for supramolecular chemistry*; Imperial College Press: River Edge, N. J., **1999**.

(15) Brinker, U.; Mieusset, J.-L. *Molecular encapsulation : organic reactions in constrained systems*; Wiley: Chichester, West Sussex, **2010**.

(16) Atwood, J. L.; Davies, J. E. D.; MacNicol, D. D. *Inclusion compounds*; Academic Press: London ; Orlando, **1984**.

(17) Szejtli, J. *Chemical Reviews* **1998**, *98*, 1743.

(18) Saenger, W. *Angewandte Chemie-International Edition in English* **1980**, *19*, 344.

(19) Breslow, R.; Dong, S. D. *Chemical Reviews* **1998**, *98*, 1997.

(20) Easton, C. J.; Lincoln, S. F.; Barr, L.; Onagi, H. *Chemistry-a European*

Journal **2004**, *10*, 3120.

(21) Szejtli, J. *Journal of Inclusion Phenomena and Molecular Recognition in Chemistry* **1992**, *14*, 25.

(22) Wenz, G. *Angewandte Chemie-International Edition in English* **1994**, *33*, 803.

(23) Schill, G. *Catenanes, rotaxanes, and knots*; Academic Press: New York, **1971**.

(24) Sauvage, J.-P., Deitrich-Buchecker, C. *Molecular Catenanes, Rotaxanes and Knots: A Journey Through the World of Molecular Topology*; Wiley-VCH: Weinheim, **1999**.

(25) Wenz, G.; Han, B. H.; Muller, A. *Chemical Reviews* **2006**, *106*, 782.

(26) Stanier, C. A.; Alderman, S. J.; Claridge, T. D. W.; Anderson, H. L. *Angewandte Chemie-International Edition* **2002**, *41*, 1769.

(27) Girek, T. *Journal of Inclusion Phenomena and Macrocyclic Chemistry* **2012**, *74*, 1.

(28) Yamauchi, K.; Miyawaki, A.; Takashima, Y.; Yamaguchi, H.; Harada, A. *Journal of Organic Chemistry* **2010**, *75*, 1040.

(29) Cacialli, F.; Wilson, J. S.; Michels, J. J.; Daniel, C.; Silva, C.; Friend, R. H.; Severin, N.; Samori, P.; Rabe, J. P.; O'Connell, M. J.; Taylor, P. N.; Anderson, H. L. *Nature Materials* **2002**, *1*, 160.

(30) Onagi, H.; Carrozzini, B.; Cascarano, G. L.; Easton, C. L.; Edwards, A. J.; Lincoln, S. F.; Rae, A. D. *Chemistry-a European Journal* **2003**, *9*, 5971.

(31) Stanier, C. A.; O'Connell, M. J.; Clegg, W.; Anderson, H. L. *Chemical Communications* **2001**, 493.

(32) Terao, J.; Tang, A.; Michels, J. J.; Krivokapic, A.; Anderson, H. L. *Chemical Communications* **2004**, 56.

(33) Hunter, C. A.; Sanders, J. K. M. *Journal of the American Chemical Society* **1990**, *112*, 5525.

(34) Hunter, C. A. *Angewandte Chemie-International Edition in English* **1993**, *32*, 1584.

(35) Cockroft, S. L.; Hunter, C. A.; Lawson, K. R.; Perkins, J.; Urch, C. J. *Journal of the American Chemical Society* **2005**, *127*, 8594.

(36) Jouaiti, A.; Hosseini, M. W.; Kyritsakas, N. *Chemical Communications* **2002**, 1898.

(37) Cieslinski, M. M.; Steel, P. J.; Lincoln, S. F.; Easton, C. J. *Supramolecular Chemistry* **2006**, *18*, 529.

(38) Maniam, S.; Cieslinski, M. M.; Lincoln, S. F.; Onagi, H.; Steel, P. J.; Willis, A. C.; Easton, C. J. *Organic Letters* **2008**, *10*, 1885.

(39) Rau, H. *Angewandte Chemie-International Edition in English* **1973**, *12*, 224.

(40) Venkataramana, G.; Sankararaman, S. *European Journal of Organic Chemistry* **2005**, 4162.

(41) Priestly, P. J., Wojotowicz, P.S., Sheng, P.; Wojtowicz, P. S.; Sheng, P. *Introduction to Liquid Crystals*; Plenum Press: New York, **1975**.

(42) Gennes, P. G. d.; Prost, J. *The physics of liquid crystals*; 2nd ed.; Clarendon Press, Oxford University Press: Oxford, New York, **1993**.

(43) Desiraju, G. R. *Journal of American Chemical Society* **2013**, *135*, 9952.

(44) Desiraju, G. R. *Angewandte Chemie-International Edition in English* **1995**, *34*, 2311.

(45) Dulmage, W. J.; Lipscomb, W. N. *Acta Crystallographica* **1951**, *4*, 330.

(46) Langley, P. J.; Hulliger, J.; Thaimattam, R.; Desiraju, G. R. *New Journal of Chemistry* **1998**, *22*, 1307.

(47) Desiraju, G. R. *Journal of Chemical Sciences* **2010**, *122*, 667.

(48) Mahapatra, S.; Azim, Y.; Desiraju, G. R. *Journal of Molecular Structure* **2010**, *976*, 200.

(49) Thakur, T. S.; Kirchner, M. T.; Blaser, D.; Boese, R.; Desiraju, G. R. *Crystengcomm* **2010**, *12*, 2079.

(50) Vogelsberg, C. S.; Garcia-Garibay, M. A. *Chemical Society Reviews* **2012**, *41*, 1892.

(51) Manor, P. C.; Saenger, W. *Journal of the American Chemical Society* **1974**, *96*, 3630.

(52) Saenger, W.; Lindner, K. *Angewandte Chemie-International Edition in English* **1980**, *19*, 398.

(53) Chacko, K. K.; Saenger, W. *Journal of the American Chemical Society* **1981**, *103*, 1708.

(54) Maclennan, J. M.; Stezowski, J. J. *Biochemical and Biophysical Research Communications* **1980**, *92*, 926.

(55) Hingerty, B.; Saenger, W. *Journal of the American Chemical Society* **1976**, *98*, 3357.

(56) Lindner, K.; Saenger, W. *Carbohydrate Research* **1982**, *107*, 7.

(57) Tokuoka, R.; Abe, M.; Fujiwara, T.; Tomita, K.; Saenger, W. *Chemistry Letters*

1980, 491.

(58) Saenger, W.; Mcmullan, R. K.; Fayos, J.; Mootz, D. *Acta Crystallographica Section B-Structural Science* **1974**, *30*, 2019.

(59) Harata, K. *Bulletin of the Chemical Society of Japan* **1979**, *52*, 2451.

(60) Lindner, K.; Saenger, W. *Carbohydrate Research* **1982**, *99*, 103.

(61) Mcmullan, R. K.; Saenger, W.; Fayos, J.; Mootz, D. *Carbohydrate Research* **1973**, *31*, 37.

(62) Harata, K. *Bulletin of the Chemical Society of Japan* **1976**, *49*, 1493.

(63) Tokuoka, R.; Abe, M.; Matsumoto, K.; Shirakawa, K.; Fujiwara, T.; Tomita, K. *Acta Crystallographica Section B-Structural Science* **1981**, *37*, 445.

(64) Saenger, W.; Noltemeyer, M. *Chemische Berichte-Recueil* **1976**, *109*, 503.

(65) Saenger, W.; Beyer, K.; Manor, P. C. *Acta Crystallographica Section B-Structural Science* **1976**, *32*, 120.

(66) Harata, K. *Bulletin of the Chemical Society of Japan* **1977**, *50*, 1416.

(67) Harata, K. *Bulletin of the Chemical Society of Japan* **1990**, *63*, 2481.

(68) Harata, K. *Carbohydrate Research* **1989**, *192*, 33.

(69) Harata, K.; Uekama, K.; Otagiri, M.; Hirayama, F. *Bulletin of the Chemical Society of Japan* **1982**, *55*, 3904.

(70) Kamitori, S.; Hirotsu, K.; Higuchi, T.; Fujita, K.; Yamamura, H.; Imoto, T.; Tabushi, I. *Journal of the Chemical Society-Perkin Transactions 2* **1987**, 7.

(71) Di Blasio, B.; Pavone, V.; Nastri, F.; Isernia, C.; Saviano, M.; Pedone, C.; Cucinotta, V.; Impellizzeri, G.; Rizzarelli, E.; Vecchio, G. *Proceedings of the National Academy of Sciences* **1992**, *89*, 7218.

(72) Anderson, S.; Anderson, H. L. *Angewandte Chemie-International Edition in English* **1996**, *35*, 1956.

(73) Anderson, S.; Aplin, R. T.; Claridge, T. D. W.; Goodson, T.; Maciel, A. C.; Rumbles, G.; Ryan, J. F.; Anderson, H. L. *Journal of the Chemical Society-Perkin Transactions 1* **1998**, 2383.

(74) Buston, J. E. H.; Young, J. R.; Anderson, H. L. *Chemical Communications* **2000**, 905.

(75) Taylor, P. N.; O'Connell, M. J.; McNeill, L. A.; Hall, M. J.; Aplin, R. T.; Anderson, H. L. *Angewandte Chemie-International Edition* **2000**, *39*, 3456.

(76) Craig, M. R.; Hutchings, M. G.; Claridge, T. D. W.; Anderson, H. L. *Angewandte Chemie-International Edition* **2001**, *40*, 1071.

(77) Michels, J. J.; O'Connell, M. J.; Taylor, P. N.; Wilson, J. S.; Cacialli, F.; Anderson, H. L. *Chemistry-a European Journal* **2003**, *9*, 6167.

(78) Breuer, E.; Aurich, H. G.; Nielsen, A. *Nitrones, Nitronates and Nitroxides*; Wiley: New York, **1989**.

(79) Kokorin, A. I. *Nitroxides - Theory, Experiment and Applications*; InTech, **2012**.

(80) Fraser, D. M.; Louro, S. R. W.; Horvath, L. I.; Miller, K. W.; Watts, A. *Biochemistry* **1990**, *29*, 2664.

(81) Borbat, P. P.; Costa-Filho, A. J.; Earle, K. A.; Moscicki, J. K.; Freed, J. H. *Science* **2001**, *291*, 266.

(82) Mason, R. P. *Free Radical Biology and Medicine* **2004**, *36*, 1214.

(83) Krishna, M. C.; Samuni, A. *Oxygen Radicals in Biological Systems, Pt D* **1994**, *234*, 580.

(84) Hawker, C. J.; Bosman, A. W.; Harth, E. *Chemical Reviews* **2001**, *101*, 3661.

(85) Studer, A. *Chemistry-a European Journal* **2001**, *7*, 1159.

(86) Blough, N. V.; Simpson, D. J. *Journal of the American Chemical Society* **1988**, *110*, 1915.

(87) Gerlock, J. L.; Zacmanidis, P. J.; Bauer, D. R.; Simpson, D. J.; Blough, N. V.; Salmeen, I. T. *Free Radical Research Communications* **1990**, *10*, 119.

(88) Green, S. A.; Simpson, D. J.; Zhou, G.; Ho, P. S.; Blough, N. V. *Journal of the American Chemical Society* **1990**, *112*, 7337.

(89) Blinco, J. P.; Fairfull-Smith, K. E.; Morrow, B. J.; Bottle, S. E. *Australian Journal of Chemistry* **2011**, *64*, 373.

(90) Keddie, D. J.; Johnson, T. E.; Arnold, D. P.; Bottle, S. E. *Organic & Biomolecular Chemistry* **2005**, *3*, 2593.

(91) Micallef, A. S.; Blinco, J. P.; George, G. A.; Reid, D. A.; Rizzardo, E.; Thang, S. H.; Bottle, S. E. *Polymer Degradation and Stability* **2005**, *89*, 427.

(92) Pou, S.; Huang, Y. I.; Bhan, A.; Bhadti, V. S.; Hosmane, R. S.; Wu, S. Y.; Cao, G. L.; Rosen, G. M. *Analytical Biochemistry* **1993**, *212*, 85.

(93) Toniolo, C.; Crisma, M.; Formaggio, F. *Biopolymers* **1998**, *47*, 153.

(94) Hideg, E.; Kalai, T.; Hideg, K.; Vass, I. *Biochemistry* **1998**, *37*, 11405.

(95) Bottle, S. E.; Chand, U.; Micallef, A. S. *Chemistry Letters* **1997**, 857.

(96) Bottle, S. E.; Micallef, A. S. *Organic & Biomolecular Chemistry* **2003**, *1*, 2581.

(97) Matko, J.; Ohki, K.; Edidin, M. *Biochemistry* **1992**, *31*, 703.

(98) Keddie, D. J.; Fairfull-Smith, K. E.; Bottle, S. E. *Organic & Biomolecular Chemistry* **2008**, *6*, 3135.

(99) Fairfull-Smith, K. E.; Blinco, J. P.; Keddie, D. J.; George, G. A.; Bottle, S. E. *Macromolecules* **2008**, *41*, 1577.

(100) Micallef, A. S.; Bott, R. C.; Bottle, S. E.; Smith, G.; White, J. M.; Matsuda, K.; Iwamura, H. *Journal of the Chemical Society-Perkin Transactions 2* **1999**, 65.

(101) Busfield, W. K.; Engelhardt, L. M.; Healy, P. C.; Jenkins, I. D.; Thang, S. H.; White, A. H. *Australian Journal of Chemistry* **1986**, *39*, 357.

(102) Walker, J. R.; Fairfull-Smith, K. E.; Anzai, K.; Lau, S.; White, P. J.; Scammells, P. J.; Bottle, S. E. *Medchemcomm* **2011**, *2*, 436.

(103) Morrow, B. J.; Keddie, D. J.; Gueven, N.; Lavin, M. F.; Bottle, S. E. *Free Radical Biology and Medicine* **2010**, *49*, 67.

(104) Stevanovic, S.; Miljevic, B.; Eaglesham, G. K.; Bottle, S. E.; Ristovski, Z. D.; Fairfull-Smith, K. E. *European Journal of Organic Chemistry* **2012**, 5908.

(105) Stevanovic, S.; Ristovski, Z. D.; Miljevic, B.; Fairfull-Smith, K. E.; Bottle, S. E. *Chemical Industry & Chemical Engineering Quarterly* **2012**, *18*, 653.

(106) Miljevic, B.; Fairfull-Smith, K. E.; Bottle, S. E.; Ristovski, Z. D. *Atmospheric Environment* **2010**, *44*, 2224.

(107) Moghaddam, L.; Blinco, J. P.; Colwell, J. M.; Halley, P. J.; Bottle, S. E.; Fredericks, P. M.; George, G. A. *Polymer Degradation and Stability* **2011**, *96*, 455.

(108) Yan, G. P.; Fairfull-Smith, K. E.; Smith, C. D.; Hanson, G. R.; Bottle, S. E. *Journal of Porphyrins and Phthalocyanines* **2011**, *15*, 230.

(109) Colwell, J. M.; Khan, J. H.; Will, G.; Fairfull-Smith, K. E.; Bottle, S. E.; George, G. A.; Trueman, A. *Light Weight Metal Corrosion and Modeling for Corrosion Prevention, Life Prediction and Assessment* **2010**, *138*, 137.

(110) Kubicki, A. A. *Chemical Physics Letters* **2003**, *373*, 471.

(111) Lewis, G. N.; Magel, T. T.; David, L. *Journal of the American Chemical Society* **1940**, *62*, 2973.

(112) Nakamura, T.; Takeuchi, S.; Suzuki, N.; Tahara, T. *Chemical Physics Letters* **2008**, *465*, 212.

(113) Tzeli, D.; Theodorakopoulos, G.; Petsalakis, I. D.; Ajami, D.; Rebek, J.

Journal of the American Chemical Society **2012**, *134*, 4346.

(114) Okazaki, M.; Kuwata, K. *Journal of Physical Chemistry* **1985**, *89*, 4437.

(115) Ebel, C.; Ingold, K. U.; Michon, J.; Rassat, A. *Tetrahedron Letters* **1985**, *26*, 741.

(116) Karoui, H.; Rockenbauer, A.; Pietri, S.; Tordo, P. *Chemical Communications* **2002**, 3030.

(117) Karoui, H.; Tordo, P. *Tetrahedron Letters* **2004**, *45*, 1043.

(118) Ionita, G.; Chechik, V. *Chemical Communications* **2010**, *46*, 8255.

(119) Ionita, G.; Chechik, V. *Physical Chemistry Chemical Physics* **2010**, *12*, 6956.

(120) Ionita, G.; Caragheorgheopol, A.; Caldararu, H.; Jones, L.; Chechik, V. *Organic & Biomolecular Chemistry* **2009**, *7*, 598.

(121) Franchi, P.; Pedulli, G. F.; Lucarini, M. *Journal of Physical Chemistry A* **2008**, *112*, 8706.

(122) Rossi, S.; Bonini, M.; Lo Nostro, P.; Baglioni, P. *Langmuir* **2007**, *23*, 10959.

(123) Sueishi, Y.; Tobisako, H.; Kotake, Y. *Bulletin of the Chemical Society of Japan* **2007**, *80*, 894.

(124) Demisheva, I. V.; Livshits, V. A.; Alfimov, M. V. *Russian Chemical Bulletin* **2006**, *55*, 2174.

(125) Lucarini, M.; Luppi, B.; Pedulli, G. F.; Roberts, B. P. *Chemistry-a European Journal* **1999**, *5*, 2048.

(126) Krumkacheva, O.; Tanabe, M.; Yamauchi, S.; Fedin, M.; Marque, S. R. A.; Bagryanskaya, E. *Applied Magnetic Resonance* **2012**, *42*, 29.

(127) Ionita, G.; Maganu, M.; Caproiu, M. T.; Ionita, P. *Journal of Inorganic and Organometallic Polymers and Materials* **2009**, *19*, 228.

(128) Ionita, G.; Florent, M.; Goldfarb, D.; Chechik, V. *Journal of Physical Chemistry B* **2009**, *113*, 5781.

(129) Chechik, V.; Ionita, G. *New Journal of Chemistry* **2007**, *31*, 1726.

(130) Chechik, V.; Ionita, G. *Organic & Biomolecular Chemistry* **2006**, *4*, 3505.

(131) Ionita, G.; Chechik, V. *Organic & Biomolecular Chemistry* **2005**, *3*, 3096.

(132) Mezzina, E.; Fani, M.; Ferroni, F.; Franchi, P.; Menna, M.; Lucarini, M. *Journal of Organic Chemistry* **2006**, *71*, 3773.

(133) Franchi, P.; Fani, M.; Mezzina, E.; Lucarini, M. *Organic Letters* **2008**, *10*, 1901.

(134) Casati, C.; Franchi, P.; Pievo, R.; Mezzina, E.; Lucarini, M. *Journal of the*

American Chemical Society **2012**, *134*, 19108.

(135) Maniam, S. Ph.D Thesis, The Australian National University, **2007**.

(136) Kunishima, M.; Kawachi, C.; Monta, J.; Terao, K.; Iwasaki, F.; Tani, S. *Tetrahedron* **1999**, *55*, 13159.

(137) Kunishima, M.; Kawachi, C.; Hioki, K.; Terao, R.; Tani, S. *Tetrahedron* **2001**, *57*, 1551.

(138) Onagi, H.; Easton, C. J.; Lincoln, S. F. *Organic Letters* **2001**, *3*, 1041.

(139) Inoue, Y. *Annual Reports on NMR Spectroscopy* **1993**, *27*, 59.

(140) Saka, W.; Yamamoto, Y.; Inoue, Y.; Chujo, R.; Takahashi, K.; Hattori, K. *Bulletin of the Chemical Society of Japan* **1990**, *63*, 3175.

(141) Melton, L. D.; Slessor, K. N. *Carbohydrate Research* **1971**, *18*, 29.

(142) Connors, K. A. *Chemical Reviews* **1997**, *97*, 1325.

(143) Rong, D.; Dsouza, V. T. *Tetrahedron Letters* **1990**, *31*, 4275.

(144) Gavezzotti, A.; Filippini, G. *Journal of the American Chemical Society* **1995**, *117*, 12299.

(145) Nangia, A. *Accounts of Chemical Research* **2008**, *41*, 595.

(146) Mallory, F. B.; Wood, C. S.; Gordon, J. T. *Journal of the American Chemical Society* **1964**, *86*, 3094.

(147) Waldeck, D. H. *Chemical Reviews* **1991**, *91*, 415.

(148) Dugave, C.; Demange, L. *Chemical Reviews* **2003**, *103*, 2475.

(149) Yager, K. G.; Barrett, C. J. *Journal of Photochemistry and Photobiology a-Chemistry* **2006**, *182*, 250.

(150) Kang, L. T.; Fu, H. B.; Cao, X. Q.; Shi, Q. A.; Yao, J. N. *Journal of the American Chemical Society* **2011**, *133*, 1895.

(151) Braga, D.; d'Agostino, S.; Dichiarante, E.; Maini, L.; Grepioni, F. *Chemistry-an Asian Journal* **2011**, *6*, 2214.

(152) Harrison, I. T.; Harrison, S. *Journal of the American Chemical Society* **1967**, *89*, 5723.

(153) Alonzo, D. E.; Zhang, G. G. Z.; Zhou, D. L.; Gao, Y.; Taylor, L. S. *Pharmaceutical Research* **2010**, *27*, 608.

(154) Matteucci, M. E.; Paguio, J. C.; Miller, M. A.; Williams, R. O.; Johnston, K. P. *Molecular Pharmaceutics* **2009**, *6*, 375.

(155) Elgindy, N.; Elkhodairy, K.; Molokhia, A.; Elzoghby, A. *European Journal of Pharmaceutics and Biopharmaceutics* **2010**, *74*, 397.

(156) Wang, Z. X.; Zhang, X. P.; Deng, Y. J.; Wang, T. *Journal of Inclusion Phenomena and Macrocyclic Chemistry* **2007**, *57*, 349.

(157) Ni, N.; Tesconi, M.; Tabibi, E. S.; Gupta, S.; Yalkowsky, S. H. *International Journal of Pharmaceutics* **2001**, *226*, 39.

(158) Kasraian, K.; Deluca, P. P. *Pharmaceutical Research* **1995**, *12*, 484.

(159) Kasraian, K.; Deluca, P. P. *Pharmaceutical Research* **1995**, *12*, 491.

(160) Priestly, P. J., Wojotowicz, P.S., Sheng, P. *Introduction To Liquid Crystals*; Plenum Press: New York, **1975**.

(161) de Gennes, P. G., Prost, J. *The Physics of Liquid Crystals*; 2nd ed.; Clarendon Press: Oxford, **1993**.

(162) Beletskaya, I. P.; Cheprakov, A. V. *Chemical Reviews* **2000**, *100*, 3009.

(163) Easton, C. J.; Lincoln, S. F.; Meyer, A. G.; Onagi, H. *Journal of the Chemical Society-Perkin Transactions 1* **1999**, 2501.

(164) Kanaya, A.; Takashima, Y.; Harada, A. *Journal of Organic Chemistry* **2011**, *76*, 492.

(165) Park, J. W.; Song, H. J. *Organic Letters* **2004**, *6*, 4869.

(166) Park, J. W.; Song, H. J.; Chang, H. J. *Tetrahedron Letters* **2006**, *47*, 3831.

(167) Zhao, Y. L.; Dichtel, W. R.; Trabolsi, A.; Saha, S.; Aprahamian, I.; Stoddart, J. F. *Journal of the American Chemical Society* **2008**, *130*, 11294.

(168) Isnin, R.; Kaifer, A. E. *Journal of the American Chemical Society* **1991**, *113*, 8188.

(169) Buston, J. E. H.; Marken, F.; Anderson, H. L. *Chemical Communications* **2001**, 1046.

(170) Schneider, H. J.; Hacket, F.; Rudiger, V.; Ikeda, H. *Chemical Reviews* **1998**, *98*, 1755.

(171) Beale, R. N.; Roe, E. M. F. *Journal of the Chemical Society* **1953**, 2755.

(172) Beveridg.Dl; Jaffe, H. H. *Journal of the American Chemical Society* **1965**, *87*, 5340.

(173) Wu, M. L.; Nie, M. Q.; Wang, X. C.; Su, J. M.; Cao, W. *Spectrochimica Acta Part a-Molecular and Biomolecular Spectroscopy* **2010**, *75*, 1047.

(174) Harada, A.; Furue, M.; Nozakura, S. *Macromolecules* **1976**, *9*, 701.

(175) Seo, T.; Kajihara, T.; Iijima, T. *Makromolekulare Chemie-Macromolecular Chemistry and Physics* **1987**, *188*, 2071.

(176) Suh, J. H.; Lee, S. H.; Zoh, K. D. *Journal of the American Chemical Society*

1992, *114*, 7916.

(177) Cieslinski, M. M. PhD Thesis, The Australian National Univeristy, **2005**.